Imperial College London
Department of Earth Science and Engineering

Design tools for the optimal exploitation of tidal-stream renewable energy

Zoe Louise Goss

Supervised by
Prof. Matthew D. Piggott
Prof. Colin J. Cotter

Submitted in part fulfilment of the requirements for the degree of
Doctor of Philosophy in Earth Science and Engineering of
the Diploma of Imperial College, June 2021

Copyright Declaration

Zoe Louise Goss

Department of Earth Science and Engineering

Imperial College London

June 2021

Declaration of Originality

I declare that this thesis titled, **Design tools for the optimal exploitation of tidal-stream renewable energy**, and the work presented in it are my own, performed under the supervision of Matthew Piggott and Colin Cotter at the Department of Earth Science and Engineering, Imperial College London. All published and unpublished material used in the thesis has been given full acknowledgement. This thesis has not been previously submitted in whole or in part for a degree or any other qualification at this University or any other institution.

Zoe Louise Goss

Department of Earth Science and Engineering

Imperial College London

June 2021

Abstract

Tidal stream power generation is attractive for a number of reasons. However, this will only be deployed on a commercial scale, in arrays of tens to hundreds of turbines, if these arrays can be shown to be viable from economic, engineering and environmental perspectives. With limited experience from real arrays and constraints on the size of lab-based experiments, advanced numerical tools are needed to both predict and maximise power yield. These tools can be used to prove viability of new sites and aid array design in this fledgling industry. Holistic economic models are needed to aid the industry's move from demonstrator arrays to commercially sized arrays that can compete at a lower subsidy level.

This thesis investigates economic models for evaluating the performance of arrays and different cost reduction methods, which may help to bring the cost of tidal energy in line with other sustainable energy sources. A methodology to optimise array design with respect to complex economic models is presented. This method builds an emulator of the trade-off curve between total yield and number of turbines, generated from a computationally expensive set of optimisation loops. It enables far more robust analysis of the implications of changes to the economic models than is possible through direct optimisation alone.

A tool is created to investigate further cost reductions that could be obtained through the assessment of a range of different turbine rotor sizes and rated capacities, as well as other array design specifications. The tool is used to make preliminary assessments of array design choices, while adhering to practical constraints such as sea bed depth and steepness, along with legal constraints such as consents on the number of turbines and spacing between them. The tool developed can be applied to early-stage assessments and narrowing down the scope of array design specifications.

Acknowledgements

I would like to give thanks to my supervisor Matthew Piggott for inspiration, ideas, detailed feedback and arranging key opportunities for me, without which this PhD would not have been possible, and to my co-supervisor Colin Cotter for his support and teachings through the Mathematics of Planet Earth CDT.

I have so much appreciation for the support given by my coworkers and friends within the Applied Modelling & Computation Group. Thank you for brightening my days with coffee discussions, pub trips and girls' nights. Thank you Stephan Kramer for your patience in answering the small questions and expertise in answering the big ones. Thank you Danny Coles for arranging and supervising my amazing opportunity for at SIMEC Atlantis and to you and Athanasias Angeloudis for welcoming me to Edinburgh and supporting me throughout the final stages.

I would like to thank my colleagues at SIMEC Atlantis for inspiring me by showing tidal developers in action and giving my work the motivation and direction to tackle the real challenges faced by the industry. Particular thanks goes to Fraser Johnson, Rowan Boswood and Anna Dunbar for their kind supervision and patience, and to Sophie Smith for coordinating this opportunity for me through the National Productivity Investment Fund.

Thank you to my amazing family and friends who kept me company, especially during a time where company was hard to come by! And thank you to my partner Pete, who helped me in countless ways.

List of Figures

List of Tables

Contents

Chapter 1

Introduction

1.1 Overview of ocean energy

The threats of climate change on biodiversity and human welfare become clearer each year. [13]. Concern over these effects has led to global efforts to reduce greenhouse gas emissions. One of the most effective ways to curb climate change is to decarbonise our energy supply. In the Climate Change Act of 2008, the UK government committed to a legally binding target of reducing carbon emissions by 80% by 2050. To do so the UK's electricity generation (and fuel for transport and heat) must become almost entirely carbon free by then[14].

In 2010, 67% of global electricity came from fossil fuels and 33% from low-carbon sources, of which renewables accounted for 20.1% and nuclear energy for 12.9%. A decade later low-carbon sources accounted for 39.1% of 2020's global electricity supply, with renewables providing for 29% and nuclear 10.1% [15]. With globally increasing energy demand, and fuel for heating and transport still predominantly relying on fossil fuels, this transition to clean energy sources needs to rapidly accelerate.

Diversifying the energy mix is a crucial strategy for achieving energy security and can help reduce the carbon intensity of a country's electrical grid in a sustainable and robust way [16]. Energy security includes the availability and affordability of different energy sources, and the social impact of their generation. Diversification through introducing different types of energy resource into the energy generation mix and increasing the share of energy generated from each type, helps to avoid a sole dependence on a single energy resource [17]. Diverse energy portfolios are less

susceptible to market fluctuations and disruptions to the supply of one particular energy source, for example weather-driven periods of non-availability. Investing in a variety of clean energy sources can help preserve reliability and affordability, but so far hydro, wind and solar have been dominant.

The need to rapidly expand the clean energy sector and diversify its sources, provides motivation to invest in relatively unexplored forms of sustainable energy. This has driven technological advances to help harness the vast quantities of kinetic and potential energy in the oceans [18]. Marine energy is an emergent sector in the sustainable power industry, with demonstrator deployments of wave and tidal showing the potential for this industry to succeed and expand, the latter with a higher technology readiness level [19].

Marine energy generation involves harnessing the energy from the sea to generate electricity. There are three main types of ocean energy; wave, tidal range and tidal stream. Wave energy is generated by converting the kinetic or potential energy of the oscillations of waves into electrical power. The key difference between tidal range and tidal stream is whether the head difference, i.e. gravitational potential energy, or the momentum of the currents, i.e. kinetic energy, is converted into electrical power. The differences are discussed below, but this thesis focuses on horizontal axis tidal stream turbine arrays, which have a relatively high level of technical readiness compared to other marine sources and have many parallels with offshore wind farms.

The tidal resource is especially great in the UK, with a department for Business, Energy & Industrial Strategy (BEIS) study finding the UK to have around 50% of Europe's total tidal energy resource. BEIS estimated that wave and tidal energy have the potential to meet up to 20% of the UK's electricity demand, through an installed capacity of 30–50 GW. The Carbon Trust's 2011 Tidal Current Resource and Economics report [18] suggested a total of 20.6 TWh per year could practically be extracted from 30 key tidal stream sites in the UK, amounting to 6% of the UK's 2019 electricity demand of 346 TWh [20]. The Crown Estate [21] estimates the total theoretical wave resource is 69TWh/year (27GW installed capacity), tidal stream is 95 TWh/year (32GW installed capacity) tidal barrages 96 TWh/year (45GW installed capacity), tidal lagoons 25 TWh/year (14GW installed capacity), with the majority of the UK's wave resource being in Scottish waters. Tidal stream resources are more distributed around the UK in Scottish, Welsh, English and Northern Irish waters. The Bristol Channel and Severn Estuary contain the greatest tidal range resources in the UK.

Investigations by the World Energy Council found that marine energy has huge resource potential globally, but that high cost is a barrier to global deployment [19]. Electricity generation is essential for transport, manufacturing, and daily life, and affordable energy is crucial for improving equality and reaching the UN's sustainable development goals. In order to aid the faster transition from fossil fuels to renewable energy, the costs of these new forms of renewable energy need to fall substantially. This thesis investigates the many routes through which the overall cost of tidal energy can be reduced, from optimal design of tidal arrays, such as optimising the location of turbines within an array, choosing the best design parameters for an array and taking advantage of cost reductions that arise from greater experience and moving to larger scale projects.

1.1.1 Wave energy

Winds blowing over the surface of the sea cause waves to form. The kinetic and potential energy of these waves can be harnessed and converted into electricity. The magnitude of these waves depends on the wind speeds, duration and distance over which it blows (called the *fetch*). The bathymetry of the seafloor and the tidal currents below the sea surface can also either disperse of amplify the energy in the waves. Friction from the seabed dissipates the wave energy, so greater resource is found further offshore in deeper waters. The long fetch of the Atlantic Ocean creates a favourable resource at the Western coasts of Europe, with Europe having one of the highest wave powers in the world, at an estimated 33 to 76 kW/m of wave crest [22]. The UK is estimated to have a total theoretical wave energy resource of 69TWh/year from an installed rated capacity of 27GW [21], the majority of this resource is in Scottish waters, with significant resources also off the coasts of southwest England and Wales.

Wave energy converters (WEC) have yet to converge on a common design and many of these variants are currently being tested at demonstrator sites, or through models developed in labs. Some of the most common variants are described below, but they are not focused on in this thesis because the high levels of uncertainty in the design mean the industry is not yet at an appropriate stage for wave arrays to be optimised on a large scale (hundreds of MW to GW scale). However, many of the economic modelling and layout optimisation methods developed in this thesis could be adapted and applied to the wave industry in the future.

1.1.2 Tidal range

Tidal range technologies make use of the head difference between high tide and low tide, converting the gravitational potential energy of the tides into usable electricity. There are limited locations suitable for tidal range generation and 90% of the world's potential tidal range resource is distributed among just five countries; Australia (1760 TWh/year), Canada (1357 TWh/year), the UK (734 TWh/year), France (732 TWh/year), and the US (619 TWh/year) [23].

There is greater convergence in the design of tidal range generators than wave energy devices. The basic concept, of a containing wall holding back a mass of water to convert its gravitational potential energy into electricity by building up a head difference between the two sides of the wall and then releasing the water through turbines within it, remains the same between different types of tidal range technologies. The main difference between each design paradigm is how the wall is constructed to hold back the water. Figure 1.1 shows diagrams of the main categories of tidal range devices.

Tidal barrages (Figure 1.1a) are constructed from a dam which spreads across the entire width of an estuary. Turbines are placed within the retaining wall and power is generated when a head difference is built up on either side of the wall and the water is released through the turbines.

Tidal lagoons operate in a very similar way to tidal barrages, except the retaining wall forms a basin, in which a head difference is built up. They do not stretch across the whole width of the estuary. This has the advantage of potentially reducing overall construction costs and also reducing environmental impact. Tidal lagoons can be single-basin (Figure 1.1c) or multi-basin (Figure 1.1d). Multiple basin designs can used to reduce the periods of non-generation time and reduce variability in the supply, but come at the cost of notable reductions in the overall energy output [24].

So-called bunded tidal lagoons (Figure 1.1b) bridge the gap between tidal barrages and lagoons, in that they do not fully obstruct an estuary, but the lagoon is partly bounded by a retaining wall and partly by the coastline. The environmental impact is therefore not as damaging as a barrage that blocks the whole estuary, but it can require less expensive infrastructure than an offshore lagoon that is bounded from all sides.

Tidal range projects are to an extent flexible over when they can generate power, by delaying the time at which the water is released through the embedded turbines.

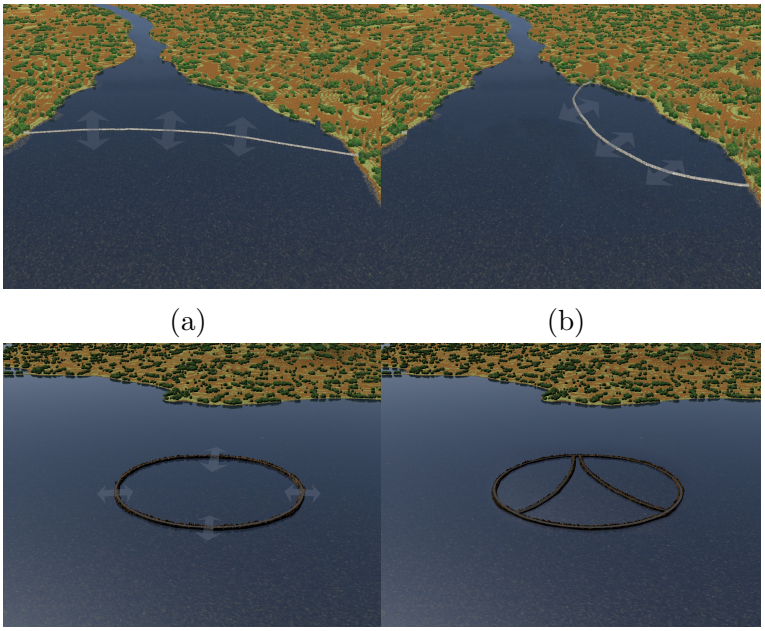

Figure 1.1: Different types of tidal range technologies. (a) Tidal barrage (b) Bunded tidal lagoon (c) Single-basin offshore tidal lagoon (d) Multi-basin offshore tidal lagoon. Images courtesy of www.aquaret.com

The operation of tidal range projects can be optimised with flexible scheduling and pumping to maximise the energy generation [25]. An advantage of tidal range projects is that they may also provide flood protection, additional to their energy generation capabilities [26].

The world's first tidal barrages were installed in the 1960s, and a few are still operational today. The La Rance facility in France began operating in 1966 and still generates up to 600 GWh per year to date. Ecological evaluation of the facility showed that the isolation of the estuary during the construction phase was particularly damaging to the environment [27]. The construction of tidal barrages is a costly infrastructure challenge and very few barrages have been deployed in recent years. Tidal lagoons are a relatively new technology, that have yet to be deployed, but proponents of the technology hope the capital costs and potential damage will be much lower than for barrages. The strategic case for a small "pathfinder" tidal lagoon project (of <500MW) was assessed and supported in the UK's 2016 "Hendry Review", with positive comparison made to the long-term costs of nuclear [28].

1.1.3 Tidal stream

Tidal stream turbines convert the momentum of tidal currents into electricity. They convert the kinetic energy of the moving water into mechanical work, and use this to drive a generator and output electricity. Tidal stream turbines generate electricity in very similar methods to wind turbines. Like in wind, devices can be vertical axis tidal turbines (VATT, Figure 1.2b) or, more commonly, horizontal axis tidal turbines (HATT, Figure 1.2a). Alternative devices that have been investigated include Reciprocating hydrofoils, Venturi effect ducted turbines, Archimedes screws and Tidal kites, but only HATT devices have been deployed for commercial tidal power generation [29], and therefore these are the devices investigated in this thesis.

Reciprocating hydrofoils (Figure 1.2c) are comprised of a hydrofoil attached to an arm, that oscillated due to the lift caused by the tidal stream currents and converts that oscillating motion to electricity. Venturi effect devices (Figure 1.2d) funnel tidal flow through a ducted turbines, where either the water drives the turbine directly or is used to create a pressure differential and drive an air turbine. Archimedes screws (Figure 1.2e) consist of a helical corkscrew, that surrounds a central shaft. As the water moves through the spiral it turns the turbines. Tidal kites (Figure 1.2f) have turbines mounted below their wings and are tethered to the seabed, in a design that has many parallels to wind energy kites that a number of firms are investigating. They pass through a figure-of-eight motion, creating higher relative flow speeds.

HATT designs bear many similarities with conventional wind turbine designs, and many lessons from the more established wind industry can be applied to tidal stream turbines. To generate significant amounts of energy, and benefit from the economies that come from sharing costs of ocean infrastructure among multiple devices, tidal stream turbines must be deployed in arrays of multiple turbines, much like traditional wind farms. The aspirations of the industry is to deploy arrays on an industrial scale, with 10's to 100's of turbines together in a tidal site. This will help benefit from economies of scale and volume, and produce more significant amounts of energy.

Tidal stream turbines typically consist of a rotor nacelle assembly (RNA), comprised of (typically 2–4) composite blades attached to a steel nacelle, a drivetrain within the nacelle, which sets the torque and speeds for the generator, a generator which converted the rotational energy of the hub to electrical energy, a support structure which holds the turbine in place. Interarray cabling is used to links the turbines to their substations. Currently these substations are located onshore, but future

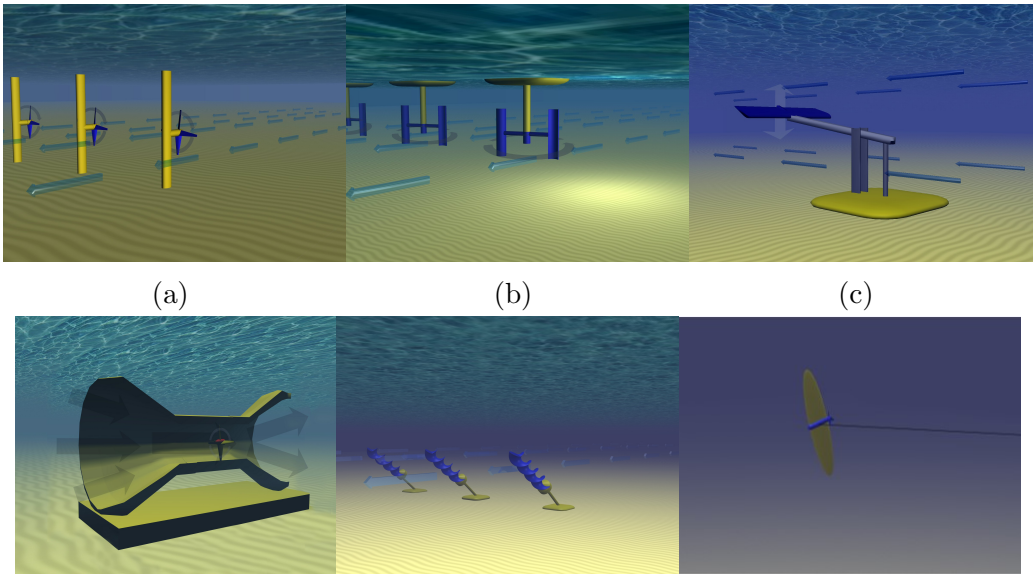

(a) (b) (c)

(d) (e) (f)

Figure 1.2: The different types of tidal stream device. (a) Horizontal axis tidal turbine (b) Vertical axis tidal turbine (c) Reciprocating hydrofoil (d) Venturi effect ducted turbine (e) Archimedes screw (f) Tidal kite. Images courtesy of www.aquaret.com

arrays are likely to use subsea substations that can connect up to around seven turbines, with a higher capacity cable collecting the power from the substation and transmitting it to shore [30]. This shortens the overall cabling routes and will decrease the costs. An onshore plant then transfers the electricity either directly to customers or distributors.

1.2 Introduction to the tidal stream energy industry

The industry is at a potential tipping point, where the technological success of prototype devices and demonstrator arrays, and the financial success of the first commercial-scale arrays could determine whether investors have confidence to support future projects or not, resulting in either an expansion or decline of the whole industry. Success of the sector could have economical benefits to the UK, through job creation and exportation of expertise, to greater energy autonomy, where domestic generation reduces vulnerability to global energy price variations. This section discusses the potential resource available in the UK and worldwide, and reviews the current state of the tidal stream energy industry.

1.2.1 Total resource in the UK and worldwide

The UK is particularly well suited for tidal generation, with a technical resource supply of 29.0TWh/year (with a pessimistic and optimistic estimate of 16.4 and 38.4TWh/year, respectively)[18], thanks to its bathymetry and coastline features which accelerate tidal currents in many locations. This could provide approximately 11% of the UK's annual electricity demand of 346TWh/year. The UK is estimated to have 10-–15% of the global harvestable tidal resource [31], making development of the tidal industry an attractive prospect in the UK.

The UK's most concentrated areas of tidal stream resource are located in the Irish Sea, the English Channel and the Pentland Firth. Draper et al. estimated that 4.2 GW of power could be extracted from the Pentland Firth [32], a strait between mainland Scotland and the Orkney Islands and contains fast tidal currents of over 5 m/s and a mean undisturbed flow velocity of 2.7m/s [33]. A recent study by Coles et al. [34] assessed the energy resource of different tidal sites around the Channel Islands and concluded that the Alderney Race contains the majority of the Channel Islands resource, with a maximum potential of 5.1 GW. The next largest resources within the Channel Islands are the Casquets with 0.47 GW and the Big Roussel with 0.24 GW. In the Irish Sea peak velocities reach 3.7m/s [35] and the regions with the highest tidal stream resource, including Anglesey and Ramsey Sound, have a total practical resource of 1 GW [36].

Globally, there are notable tidal stream and range sites in Canada, Argentina, France, Ireland, Russia, Australia and China [29]. It is estimated that up to 5.7 GW could be extracted from the Minas Passage in the Bay of Fundy [37], 1.3 GW could be extracted from the Johnstone Strait [38], and 0.087 GW could be extracted from Masset Sound [39], in Canada.

Estimates for a realistic extractable tidal-stream power potential in France are 5.4 GW, the highest potential site being Raz Blanchard (known as the Alderney Race in the UK) [40]. China has a theoretical potential of over 8.2 GW [41]. However, it should be noted that estimates on a global scale may not be consistent, due to variations in assumptions on the geographical, technical and environmental constraints that limit a country's potential resource.

1.2.2 Current state of the global tidal energy industry

The tidal energy industry is very rapidly evolving, with many world firsts being achieved in the last decade, but it is also very volatile. Many tidal energy companies have risen and dissolved in the time taken to deliver this thesis, with others merging into other more stable tidal energy companies.

Ocean Energy Europe, a non-profit organisation representing many professionals engaged in ocean energy research and industry, report on their key findings from 2020 that 27.9 MW tidal stream has been installed in Europe since 2010, with 10.1MW currently in the water [42]. This makes up the majority of the 36.3MW cumulative installation worldwide. Progress has not been linear, however, with only 260kW added in 2020 and only 1.52MW added in 2019 to the tidal capacity in Europe. This was low compared to 3.7MW in 2018 and 2.5MW in 2017 [43], however there are many larger scale arrays planned for the early 2020s. Most notably, leases have been secured for the expansion of the MeyGen project to 86MW and the installation of a 12MW array in the Alderney Race (with plans to install up to 3GW in the Race and surrounding regions in the future). In 2020, the EU Offshore Renewables Strategy published a target to install 100MW of ocean energy by 2025. Currently there is 11.2MW operating in the water, 10.1MW of which is tidal energy and 1.1MW is wave [42]. The UK currently leads the world for tidal energy deployments, however there is promising resource and plans in France, Canada, China and the USA [44].

In 2008 the world's first commercial-scale grid-connected tidal stream turbine began exporting energy to the grid [45]. The SeaGen generator was a dual-rotor (each 16m diameter), 1.2MW rated device, installed and operated by Marine Current Turbines in the Strangford Narrows in Northern Ireland. Its predecessor was the demonstrator SeaFlow project that was a single rotor 300kW turbine installed in Lynmouth, North Devon, but not connected to the grid. In 2015 Marine Current Turbines was sold to SIMEC Atlantis Energy, who carried out the decommissioning stage of the project from 2016 to 2019. Small numbers of demonstrator turbines have been installed around the world since then.

Currently there are a small number of tidal stream arrays around the world, all in the pre-commercial stage. Nova Innovation deployed the world's first fully functional, commercial, grid-connected offshore tidal array in Bluemull Sound in 2016–17, called the Shetland Tidal Array, consisting of three 9m diameter 100kW tidal turbines. Alongside some Tesla lithium ion batteries, the Shetland Tidal Array supplied baseload power to the Shetland grid. They added a fourth turbine to the

array in 2020 and at the time of writing have plans to increase the array size to six turbines, as part of the EnFAIT project. The MeyGen project phase 1A, in the Pentland Firth, Scotland, was the second array installed and is the highest capacity tidal stream array in the world at the time of writing, consisting of four 16m diameter 1.5MW turbines, with plans and consent to expand to 86MW for phase 1C. In 2018 MeyGen set a world record for monthly production from a tidal stream, array, of 1400MWh [43]. In 2019 the European tidal stream sector exported close to 15 GWh, led by Meygen and the EnFAIT projects [44]. Many valuable lessons have been learnt from both these groundbreaking projects, as they demonstrate the technical feasibility and potential for commercial viability of tidal stream. Other arrays recently deployed include Verdant Power's RITE Project, which consists of three 35kW, 5m diameter turbines attached to a tri-frame installed in October 2020 in the East River, New York. Sustainable Marine have announced plans to deploy the world's first floating tidal energy array, providing up to 9MW of clean power generation. The Pempa'q In-stream Tidal Energy Project will be situated in the Bay of Fundy, Nova Scotia, Canada and the first phase will consist of three 420kW PLAT-I 6.40 floating tidal energy platforms and will have a total capacity of 1.26MW. The first of these platforms, on which six 4m diameter, 70kW rated rotors are mounted, was installed in February 2021, and is shown in Figure 1.6.

Prior to these arrays being installed, there were notable laboratory experiments with arrays of turbines at a tank-scale (with 270mm diameter rotors) [46]. These experiments were only carried out on relatively small numbers of turbines (3 to 5) and there is limited ability to expand the size of these arrays to model industrial scale deployments, due to limitations on tank size. Many demonstrator projects are deployed at testing facilities around the UK and Europe, that allow full-scale individual prototype devices to be constructed nearby and operated in their waters. Popular sites to test individual turbines include the Nigg Energy Park in Highland, Scotland and the European Marine Energy Centre (EMEC) test site at the Fall of Warness, Orkney, whose clients include Magallanes, Orbital and Verdant Power. Nigg Energy Park is a facility used by turbine developers, shown in Figure 1.3, such as SIMEC Atlantis and Marine Current Turbines, to conduct vessel operations, foundation and turbine fabrication, assembly and testing. These testing centres are vital for assessing the technological feasibility and operational performance of individual turbines. However, little can be learnt about the interactions between multiple devices and the impact on overall array yield at these sites. Therefore accurate computational modelling of array performance is essential for aiding the design of the future stages of large-scale tidal stream arrays.

(a) (b)

Figure 1.3: Photos courtesy of SIMEC Atlantis, showing the AR1500 turbine (a) inside the Nigg Energy Park warehouse during assembly and (b) en route to testing.

More wave and tidal power is currently being tested in the UK's waters than the rest of the world combined [43]. Additional benefits to expanding clean energy generation through the tidal stream sector, include employment opportunities and revenue, especially in the UK which is at the forefront of the global tidal industry. The UK is well positioned to capture a high percentage of the growing tidal-stream energy market, with its favourable resource and current dominance of device developers. The UK's high levels of resource mean that it could be a world leader for the tidal energy industry, with successful array expansions here driving the uptake of tidal arrays worldwide. In February 2021, SIMEC Atlantis announced the successful installation and first 10MWh of energy generated by the first tidal turbine installed in Japan, demonstrating a widening worldwide interest in tidal energy and the potential for UK experts in the field to collaborate on international projects. The device installed in the Naru Strait, off Japan's Goto Islands, depicted in Figure 1.4, will initially be operating at a capped output of 500kW, while performance and environmental data collection, and device validation are undertaken. The Goto Islands have an estimated extractable resource of 50–107MW [47], thus if this project is proven to be successful and satisfies the regulators requirements it could be the first of many tidal projects in the region.

The future role of marine energy in the UK's energy system remains uncertain due to its currently high costs and relatively low levels of certainty over how rapidly those costs will fall in the future [48]. The Low Carbon Innovation Coordination Group (LCICG) predicted future deployment scenarios could range from almost no additional marine energy to over 20GW in the UK by 2050 [48]. They argued that the cost of marine energy would need to reduce by around 50–75% by 2025, for it to compete with offshore wind power and other generation technologies. They

(a) (b)

Figure 1.4: Photos courtesy of SIMEC Atlantis, showing the (a) transportation vessel and (b) installation of a AR500 (500kW) turbine in the Naru Strait off Japan's Goto Islands.

estimated the costs of the first arrays would be of the order of £350–400/MWh for wave and £200–300/MWh for tidal. There is a need to move from demonstrator arrays to commercial-scale arrays that can compete at a lower subsidy level, and eventually operate alongside more established technologies such as offshore wind.

1.2.3 Variations in horizontal axis tidal stream turbine design

This thesis investigates array optimisation and economic modelling of such commercial-scale tidal arrays made up of many horizontal axis tidal stream turbines. The impact of varying the rotor diameter, rated power and hub height is investigated in Chapter 5, but it is always assumed the design used will be for a single-rotor HATT with a monopile foundation. Much like in the offshore wind industry, tidal stream design is typically converging on variations of HATTs, with the most notable differences between devices being the rated power, diameter, and mounting. These modelling techniques are adaptable and as alternative devices are tested and gain more experience, similar assessments could be applied to these too.

Tidal turbines typically require depths of 30m or more, but that can vary with the size of the turbines and the tip-to-surface spacing required. Unlike wind turbines, where the upper limit to the rotor diameter is determined by cost and engineering requirements, the upper limit to tidal turbine diameters and their hub height is often constrained by the depths of the waters. Tidal devices deployed to date have varied greatly in rotor diameter, from Verdant Power's 5m diameter river based turbines, to SIMEC Atlantis's 16m diameter turbines deployed in MeyGen Phase

1A. Multi-rotor and floating devices typically have much smaller rotor diameters. There is a substantial difference between the rated power (100kW to 1.5MW) and the rotor diameter (9m to 16m) of the turbines used the the world's first two tidal arrays. Currently the world's largest single-rotor turbine is the AR2000 by SIMEC Atlantis, a 2MW rated device which accommodates rotors of 20–24m. The AR2000 has been developed although it is yet to be deployed but is expected to be used in future phases of the MeyGen project. Future iterations of SIMEC Atlantis turbines may be up to 3MW rated power and 26m in diameter or more [49].

Choosing these turbine specifications will depend on the trade-off between costs and power generation desired. This trade-off will vary greatly depending on the flow and other conditions at the tidal site. Smaller turbines allow vessels to pass overhead easier and are easier to install and maintain because they can be transported on smaller local vessels. Higher rated turbines generate more power in higher flow velocities, but if the flow rarely exceeds the rated speed of a device there is little benefit in increasing its rating. Greater diameter turbines generate more power below rated speeds but many tidal sites may not have deep enough waters for increased rotor diameters and, due to conservation of mass, flow tends to be faster in shallower waters. Chapter 5 investigates the choice of these turbine specifications in greater detail.

The wind energy industry have converged on horizontal axis turbine designs with three blades. The fewer blades the lower the drag, so more than three blades creates too much flow resistance. 2-bladed turbines also cost less due to using fewer materials, being a more convenient shape to transport and install, and they make the rotor lighter. However, using just one or two turbine blades lead to stability issues and increases the stresses of the components of the turbines. In 3-bladed turbines when one blade is vertical the other two are at angles, creating a more constant angular momentum. 2-bladed turbines spin faster and are therefore louder. It has been found that in practice 2-bladed rotors incur a 3% loss relative to 3-bladed designs, and 1-bladed designs incur a 7-13% loss [50]. A 4-bladed rotor has marginal efficiency increases relative to 3-bladed ones, but not enough to justify the cost of manufacturing an extra blade. As the number of blades is decreased the dynamic loads on the turbine increase [51], so 3-bladed designs have largely been settled on as a good balance between increased efficiency, reduced loads and reduced weight, and the expense of the rotor.

A similar consensus has yet to be reached in the tidal stream industry. Only two tidal stream arrays have begun operating to date, with the Nova Innovation array in

Bluemull sound consisting of three 2-bladed turbines and the SIMEC Atlantis array in Pentland Firth consisting of four 3-bladed turbines. OpenHydro (now liquidated) developed a 6m diameter device composed of 16 ducted fins and and open centre to allow marine life to pass through. Greater experience of testing the devices in the water may lead to developers converging on either 2 or 3-bladed devices as a standard, with the trade-off between the greater costs of more blades vs the stability and efficiency yet to be fully explored and subject to change as the costs are expected to fall with increased deployment.

Turbines may have a fixed axis (usually allowing for bidirectional generation) or they may yaw to face the dominant direction of the tides. If there is a significant difference between the orientation of the turbine and the direction of the flow this may reduce the power output. However, the ocean environments tidal turbines are installed in are harsh, and fixed axis devices may be more robust to the extreme loads. Yawing is assumed in this work, such that turbines are always assumed to face the flow, but further work should investigate the impact of angle changes.

There are many different mounting options available for tidal stream turbines. Both the EnFAIT project and MeyGen Phase 1A, use turbines with a gravity-based support structure, like those shown in Figures 1.5a and 1.5b. The Nova innovation turbines use a steel-tripod gravity-based foundation which have a footprint of 13.5 x 12.2 m, and a weight in water of 80 tonnes. The SIMEC Atlantis turbines in MeyGen 1A use a gravity-base weighing over 1000 tonnes. An advantage of gravity bases are that they require no drilling into the seabed, keeping installation relatively simple. Furthermore, this in principle allows the layout of the turbines to be adjusted after installation, something the the EnFAIT project hopes to take advantage of to optimise the interactions between turbines when the array is expanded to six turbines. Downsides of gravity-based foundations include being extremely heavy to transport and having large footprint on the seafloor, which can restrict the number of suitable locations if the seabed is not flat enough.

An alternative to gravity-bases are fixed drilled pylons, called *monopiles*, as shown in Figure 1.5d. Monopile foundations can reduce the amount of steel required by 90% compared to gravity-based foundations, thus cutting the overall costs, and are currently the design intended for use in MeyGen 1C [52]. This is a popular design in the wind industry, with monopile foundations used in 96% of offshore wind turbines [2]. Their footprint is far smaller than gravity-based foundations, allowing for greater flexibility in the micro-siting of turbines. Their cross-sectional area is also much smaller than the tripod gravity-based foundations currently used,

so the turbine support structure will introduce less drag to the flow.

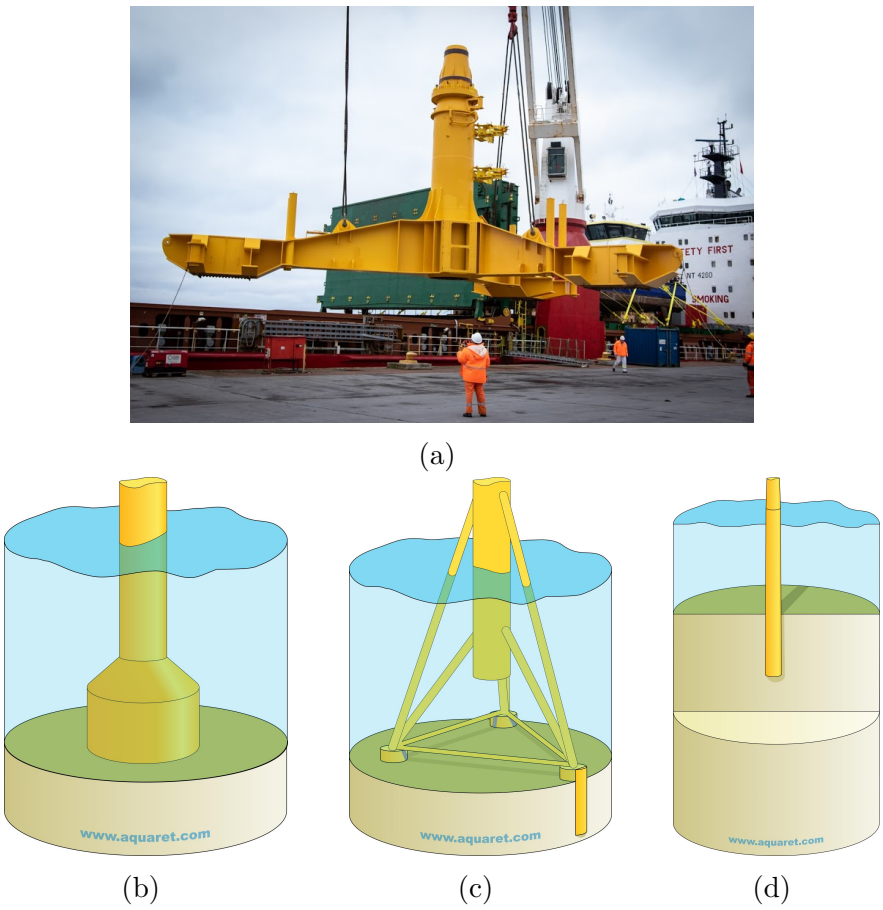

Figure 1.5: Examples of the different types of bed-mounted turbine foundations. (a) A gravity base foundation being installed, photo courtesy of SIMEC Atlantis. Diagrams of (b) a gravity base foundation, (c) a piled steel jacket attached to a monopile, and (d) a drive monopile foundation. Diagrams courtesy of www.aquaret.com.

Tidal turbines are not just seabed-mounted, however. Numerous companies are looking into floating tidal turbines, which typically are attached by steel arms to a barge and lowered into the water below. In April 2021 Orbital Marine Power Ltd launched the Orbital O2 in the Port of Dundee, the installation shown in Figure 1.6a. At 2MW rated capacity across the two rotors, it is the world's most powerful tidal stream device currently in operation. The device consists of a 74m long barge with twin 20m diameter rotors at the end of two retractable leg structures, each rated 1MW. The retractable legs allow for easy access for installation, minimise the downtime of the devices and reduce installation and operational costs. The PLAT-I 6.40 platforms from the world's first floating tidal energy array, the Pempa'q Instream Tidal Energy Project, have a similar design, except six rotors are mounted to the rear of the device, shown in Figure 1.6b. Advantages of the floating array include that it can be towed to the site for low cost installation and the turbines can

be easily accessed for maintenance, and the platform uses a turret configuration to allow it to passively align the turbines with the flow.

(a) (b)

Figure 1.6: Examples of different floating tidal stream devices. (a) The installation of a barge-mounted dual-rotor O2 device, photo courtesy of Orbital Marine Power. (b) The first of the six-rotor PLAT-I 6.40 floating tidal energy platforms in the Pempa'q In-stream Tidal Energy Project, in the Bay of Fundy, Nova Scotia, Canada.

1.2.4 Characteristics of tidal energy

In many ways the tidal stream arrays studied in this thesis are similar to offshore wind farms. It is assumed in this thesis that the devices deployed will generally be horizontal-axis three-bladed turbines, and that to generate significant amounts of power and achieve economical efficiency, they will be deployed in offshore arrays formed of many devices. This section discusses the characteristics of extracting energy from the tides rather than the wind, both advantageous and disadvantageous, that distinguish tidal stream energy from wind and other forms of renewable power.

Predictable, cyclic, non-dispatchable generation

Grid operators need to be able to meet the electric demand by matching it with a load supplied from various energy sources. Meeting this demand and balancing out the effects of intermittent energy sources requires energy that is *dispatchable*, meaning its output can be adjusted up or down on demand. Hydro, diesel generators and natural gas, are all examples of dispatchable energy resources. The extent to which an energy source may be considered dispatchable may depend on the time scales, for example capacitors and hydroelectric facilities can be fully ramped up within a mater of seconds, natural gas turbines can generally be ramped up in minutes, to respond to fluctuations in energy demand. By contrast biomass, nuclear and coal energy have limited flexibility, taking hours to ramp up, and are typically used to

provide *baseload power* – the minimum amount of power an electrical grid requires at any given time – rather than respond to demand variations. A *baseload power* generator refers to one that can operate continuously at its rated capacity, except during times of scheduled or unscheduled maintenance. *Baseload power* generators do not need to meet the same fast and flexible requirements as *dispatchable* ones.

Stochastic renewable energy sources, such as wind and solar, are unpredictable, unreliable and unsuitable for providing a region's baseload power and can cause problems for electrical distribution networks and power supply management [53]. Tidal energy is one of the few types of renewable energy generation that is highly predictable over long timescales, so daily power generation variations are known well in advance, allowing for better grid scheduling and security, and possible use as a baseload power provider [54, 55]. This predictable nature increases its value in the future electricity market [56]. This is particularly important as stochastic renewable technologies, such as wind and solar, contribute an increasingly significant component of the power market, and reliable reserve capacity is needed to maintain supply during weather-driven periods of non-availability. [31] Resource assessments can require significant amounts of computational power and input data, but they are largely accurate years into the future, once carried out, provided there are no additional disturbances to the flow not modelled (such as the presence of coastal infrastructures or other tidal arrays [57, 34]).

Most forms of renewable energy generation, including wind, solar, wave and tidal, are *variable* in their output, meaning that the output cannot be explicitly controlled by the generator operator and instead fluctuate with their resource. For example, the upper limit of how much wind power a wind farm can generate at any given time depends on the time-varying wind speed and a solar array's maximum generation depends on the sunlight intensity, affected by factors such as time of day and cloud cover. The only control operators typically have is a reduction in power output, i.e. *curtailment*, which can be necessary if supply exceeds the demand and the energy grid's storage capacity is full. As grid penetration of variable renewable generators increases, either significantly more storage capacity needs to be installed, or operators will need to curtail their generation more often. To help plan energy distribution and storage more effectively, countries are dependent on weather forecasts and yield predictions, many of which are stochastic, especially over shorter timescales.

Tidal energy is *cyclic* rather than *stochastic* in nature, which is a major benefit to grid operators over *intermittent* energy sources [58, 59, 60, 61, 62]. Tidal energy in

the UK sees approximately four power generation cycles per day, everyday. This cyclic nature is much more suitable for combination with energy storage solutions than wind or solar, that may have long periods of peak generation, where storage systems get filled and excess power must be curtailed, and long periods of no generation, where storage systems deplete and are not recharged, so carbon intensive dispatchable energy source must be used. This effect was demonstrated on a small scale by comparing a tidal-battery-oil hybrid system to a wind-battery-oil hybrid system for the power supply to Alderney [62]. Coles et al. demonstrated that a tidal-hybrid system curtails less energy than a wind-hybrid system (0.2 GWh/year to 1.9GWh/year) and successfully displaces more of the islands carbon intensive and expensive imported-oil for backup generation (78% displaces, compared to 67% for wind). This may help reduce the gap between the cost of tidal and wind energy in island hybrid systems, and is likely to have applications in other island locations. For example, Nova Innovation have recently secured funding for a second tidal array, which will consist of five 100kW turbines and help the island of Ynys Enlli, Wales switch from dependency on expensive diesel generation. On a grid-level, other studies have shown that tidal stream energy, combined with energy storage mechanisms, could help supply a country's baseload power, and that even relatively small storage capacities could be effective [59, 60, 61].

Periods of high wind in nearby regions often coincide with one another, therefore it is anticipated that as the market penetration of wind energy increases its value will decrease, and similarly with solar. Hirth [56] found that the variability of solar and wind power causes their market value to fall as the penetration of variable renewable increases. He found that at 30% penetration, wind power is worth only 50—80% of a constant power source. This is because sudden drops in renewable energy supply require dispatchable energy sources, such as gas and coal, to be kept online and ready to respond but remain predominantly idle. This effect, combined with energy policy that puts precedent on using renewable sources first, can result in negative energy prices on highly sunny and/or windy days. This effect of decreased market value can be avoided in the tidal industry through smart deployment of array locations.

Because the tides are out of phase in different parts of the UK coasts, while one location is in slack tide other locations can be generating energy. It has been shown that it is possible to take advantage of the tidal phase difference across different parts of the country to help smooth out the total power produced over daily timescales. [63, 58] The extent to which production can be flattened depends on the balance of the size of tidal farms in different regions around the country. If one

site dominates the production, for example the Pentland Firth or Alderney Race, each with more substantial plans for large scale arrays than other regions, then there will still be a high level of intermittency over the sum of the UK's tidal power generation. Furthermore, neap tides have far lower resource available than spring tides, regardless of the location, so it is impossible to completely flatten out the tidal generation on larger time-scales with tidal stream alone [64]. However, other studies have shown that it is possible to combine tidal stream with hydraulic pumped storage to smooth fluctuations in the daily cycle, making tidal-hybrid systems suitable for providing baseload power [58]. A study by Vennell and Adcock even showed it is theoretically possible to vary the timing of peak power production in some tidal stream sites but up to a few hours, by manipulating the inertia of tidal flow [65]. However, in practice with realistically size tidal stream farms, it will only be possible to vary the time of peak power generation by very small amounts.

Marine conditions loads and visual impact

Tidal turbines are typically placed in regions of high flow to maximise power, however this means they experience high forces and significant stress to their hardware. High levels of turbulence in the flow can cause structural fatigue. The higher the power generation per turbine, the higher the structural loads this turbine must endure. This creates a need for more robust turbines which generally goes hand in hand with higher construction costs. Conversely tidal arrays located in lower flow areas may reduce their costs to offset the power reduction, by using more lightly built turbines [66].

Sites with high tidal flow often tend to be remote and provide difficult conditions to install and maintain the turbines from, sometime with narrow windows when offshore operations can be performed. Simec Atlantis reported in their lessons learnt from the first few years of MeyGen 1A's operation that many maintenance vessels were not suitable for planned works because they could not hold their position in the peak tidal flows experienced during the neap tide window [67].

Because tidal turbines are underwater they cause less visual pollution than wind turbines, have lower environmental/ecological impact due to slower rotor speeds, and are space saving; due to the higher density of water tidal turbines can generate the same amount of power as a much larger wind turbine. They also have a reduced acoustic impact on local residents than wind farms. Bed mounted tidal turbines typically sit low enough in the water column that vessels can pass overhead (with

a minimum clearance requirement of 8m from the highest blade tip to the lowest astronomical tide often imposed) so they do not impact on local shipping activities, although they may prevent certain types of fishing. The floating tidal devices currently being deployed around the world, however, will likely require local vessels to adjust their routes.

Environmental impact

The presence of a tidal energy generation plant can result in changes to the local environment. Some of these changes may be positive, for example it was argued in the proposals for Swansea bay Lagoon and Ramsey Harbour in the Isle of Man that bird life could benefit and the lagoon breakwater walls could help provide a habitat for lobster and crab, and hatcheries for sea bass, herring and pollock [68]. But generally there is concern about substantial negative impact on the environment. Environmental impact may occur during the construction, operation of decommissioning stages of a tidal project. Operational impact includes changes to the salinity, sediment and nutrient transport, disruption of the movement of marine life and their habitats.

Environmental changes may occur locally, within the tidal stream array boundaries or the basin of a lagoon or barrage, but they may also occur further afield. Tidal range projects may have far reaching changes to the tidal levels in the surrounding regions. Tidal stream projects may alter the speed of the flow in the surrounding area, near and afar. These changes in flow and elevation can cause environmental disturbances in the surrounding regions of a tidal energy generator.

Tidal stream energy has notably lower environmental impact than constrained forms of tidal energy, because a solid barrier is not place in the ocean. The presence of the turbines causes significant changes to the local flow, with a decrease in the flow through the entire site, decelerated flow passing through the turbine swept area and accelerated flow at the free surface and near the sea bed. Turbulence is significantly increased downstream of the turbines. The regional scale impact depends greatly on how many turbines are in the array and the coastal features in the region. For example, if a large-scale array is installed in a strait between an island and a landmass, the flow on the far side of the island is likely to accelerate. It is important to study whether the changes in velocity in nearby regions are of environmental or ecological significance, for example if they are the habit of species that is sensitive to a change in the flow. However, even large-scale tidal stream arrays

have a significantly lower impact on the regional dynamics than tidal barrages.

However, due to limited operational experience with tidal lagoons and tidal stream arrays, the environmental impacts are not fully understood, at present. Much research is ongoing to identify the environmental and ecological impact of these generators [69, 70, 71, 72]. Chapter 2 discusses ways in which environmental and ecological impact can be taken into account when optimising the design of tidal stream arrays.

1.3 Tidal theory

The tide is defined as the rise and fall of the surface of the ocean, and it is driven by the gravitational forces of celestial bodies acting on the Earth in a rotating system [73]. Take a simplified model of our solar system, considering just the Moon and the Sun (the two celestial bodies which exert the greatest gravitational force on Earth), and the Earth approximated by an oceanic planet with no land. The variable gravitational pull of the Moon and the Sun on the Earth causes the ocean surface to bulge toward each body, and the sea level to rise and fall. This variable gravitational force also causes a simultaneous bulge on the opposite side of the Earth to each of the celestial bodies. Throughout the Earth's rotation the bulges of the lunar and solar tide point directly towards and away from the Moon and the Sun, respectively.

The M2 tidal constituent is the leading component (within a so-called harmonic decomposition) of the sea level fluctuations due to the gravitational force of the Moon on the Earth. The M2 constituent is the highest magnitude of all of the tidal forcings, due to the assumptions that define it and the Moon's greater proximity to Earth, and has a period of 12 hours, 25 minutes and 14 seconds, half of the time it takes for the Earth to complete a full rotation relative to the Moon, due to the bulges on both sides.

The S2 constituent is the analogue of M2 due to the Sun and the Earth alone, and has a period of 12 hours, half the time taken for a complete rotation of the Earth relative to the Sun. This is the second greatest magnitude constituent, with solar tides being roughly half the magnitude of lunar tides.

Further tidal constituents account for the astronomical pattern the Moon makes around the Earth, and the Earth makes around the Sun.

(a) *Spring tides* occur when the Sun, Moon and Earth are aligned, with the Moon either on the same side as or directly opposite the Sun.

(b) *Neap tides* occur when the Sun and the Moon are $\pi/2$ or $3\pi/2$ out of phase.

Figure 1.7: A simplified representation of the Earth (E), as a rotating planet covered in water and the Sun (S) and the Moon (M) as celestial bodies exerting a gravitational pull on the Earth. The solar tides (S2 constituent) shown in light blue, and lunar tides (M2 constituent) are shown in dark blue.

As the Moon completes its 29.5 day cycle around the Earth, the relative angle between the M2 and the S2 forces changes. When the Sun, Earth and Moon are aligned, as shown in Figure 1.7a, the solar and lunar tides are in phase and their forces are compounded together, resulting in the high magnitude *spring tide*. Figure 1.7a shows the Moon and the Sun on opposite sides of Earth, but the same effect is felt when they are on the same side of Earth as each other. If the Sun and the Moon are out of phase by either $\pi/2$ or $3\pi/2$, as shown in Figure 1.7b, the solar tides act against the lunar tides, resulting in the lower magnitude *neap tides*. The spring-neap cycle occurs each half orbit of the Moon around the Earth, i.e. every 14.75 days.

In reality the Earth is not a water covered perfect sphere; landmasses and ocean bathymetry interact with the tides to create horizontal tidal currents. The Coriolis effect causes water to rotate clockwise within basins in the southern hemisphere and anticlockwise within basins in the northern hemisphere. The period of these rotations is determined by the dominant tidal constituents in the region. These are called *amphidromic systems*, and can be of many different sizes. *Amphidromic*

points are the centres around which the water moves.

When two large bodies of water are connected by a relatively narrow strait, the tides in each of the two bodies of water may be out of phase to some degree, resulting in unequal surface elevation between each end of the strait, called a *head difference*. This head difference induces a tidal current in the strait. Shallow seas or features that compress the flow, tend to create optimal locations for tidal stream arrays with sufficiently high local velocities.

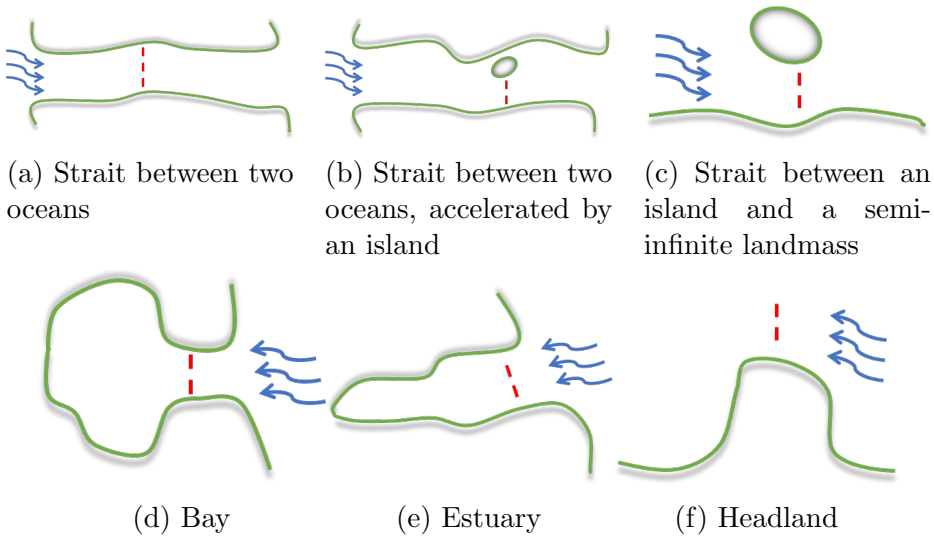

(a) Strait between two oceans

(b) Strait between two oceans, accelerated by an island

(c) Strait between an island and a semi-infinite landmass

(d) Bay

(e) Estuary

(f) Headland

Figure 1.8: Different classes of generic coastal sites suitable for tidal energy extraction, as identified by [1].

Figure 1.8 shows diagrams of the main different types of tidal site identified by Draper et al. [1]. The categorisation of coastal features that accelerate the flow includes bays, estuaries (for example the Severn Estuary, the greatest tidal range potential in the UK), headlands, flow in a strait between two oceans (for example Saltstraumen, Norway, with the fastest tidal currents on Earth, of up to 11m/s [74], or the Pentland Firth, home to the world's most powerful tidal stream array to date) and flow in a strait between an island and a semi-infinite landmass (for example the Alderney Race, the greatest tidal stream potential in the UK, of up to 5.1GW [34]).

Most locations experience two high tides and two low tides a day, called a *semidiurnal* tidal cycle. Other areas only have one high and one low tide a day, called *diurnal tides*, and others have *mixed semidiurnal tides*, where the two high and two low tides a day differ in height due to the compounded effect of a semidiurnal and diurnal tide in the region. Without the presence of landmasses, all locations on Earth would experience equally proportioned semidiurnal tides, but the continents block the westward movement of the tidal bulges, establishing more complicated patterns.

The Gulf of Mexico is an example of a diurnal location, the US West Coast a mixed semidiurnal location and the UK coasts experience semidiurnal tides. Diurnal tides are not typically powerful enough for tidal energy extraction [68]. Tidal currents are usually bidirectional (subject to local conditions) fluctuating in the *ebb* (tidal currents flowing seaward) and *flood* (tidal currents flowing inland) directions.

Although the M2 and S2 tidal constituents are the greatest in magnitude, the effects of many other constituents superimposed together determine the actual tidal elevation. Lunar and solar declination (the change in the angle of each body in relation to Earth's equator), lunar perigee (the part of the Moon's elliptical orbit that is closest to Earth, with a monthly period), solar perihelion (the part of Earth's elliptical orbit that is closest to the Sun, in December, with a half-year period)) and gravitational influences from other celestial bodies can all impact the tides. An accurate tidal model will force the free surface elevation with the constituents that have the greatest magnitude impact in that region. In the models of the UK tides discussed in this thesis the diurnal forcings Q1, O1, P1 and K1 are modelled, along with the semidiurnal M2, S2, N2 and K2, and the shallow water constituent M4, and their forcing is implemented via the open-source *Uptide*[1] package using data extracted from the OSU Tidal Prediction Software (OTPS) [75]. Diurnal constituents all have periods of approximately 24 hours (with Q1 being the greatest at 26.8 hours) and semidiurnal constituents have periods of approximately 12 hours.

Accurate tidal models rely on knowledge of the constituents present in the region, the bathymetry and the levels of bed friction. Other factors that can effect the amplitude of tidal currents include meteorological mechanisms; wind effects, storm surges and barometric pressure. Typically the magnitude of these effects is small relative to forces due to celestial motion and topography of the oceans. These factors have a more significant impact on the stress and fatigue that the turbines undergo than the overall yield, with weather-driven turbulence increasing the loading on some components. Furthermore, they have a greater impact at the top layers of the ocean, whereas tidal devices typically sit lower in the water column where the magnitude of the currents is largely determined by more predictable forces.

[1] https://github.com/stephankramer/uptide

1.4 Hydrodynamic modelling of tidal stream sites

This section describes the impact that tidal turbines have on the surrounding flow by firstly considering the *actuator disc method* as a simple representation of how wakes form. Installing arrays of tidal-stream turbines creates local and global blockage, and the effects this has on the surrounding flow and the yield needs to be considered. Modelling all these effects in large-scale arrays is a very computationally expensive multi-scale problem, so a two-dimensional model of tidal flows and arrays is commonly used, including in this work.

1.4.1 Theoretical actuator disc model

Modelling entire turbines, their rotating blades and their fixed support structure, would require time-varying 3D modelling at a high resolution and thus would be very computationally expensive. This computational expense increases further as the tidal industry looks to expand and needs to model large-scale arrays with tens to hundreds of turbines. Therefore approximations that mimic the effect that a tidal turbine has on the flow and produce reliable power predictions are desirable. One of the most commonly used models, which can be used to develop understanding of tidal power production but does not require consideration of the moving parts is the *Actuator Disc Method* (ADM).

Actuator disc theory (also known as momentum theory) is used to model the momentum extraction of a turbine, independently of detailed rotor characteristics. The turbines are represented as an infinitesimally-thin *actuator disc*, a porous disc with the same swept area and orientation (ideally perpendicular to the flow), that removes momentum from the flow. The ADM calculates the momentum loss of the flow as a function of the thrust force exerted on the turbine. A pressure drop over the disc creates a thrust force on the turbine and extracts momentum, and therefore energy.

Consider a control volume, defined by the streamtube (cross-sections with a fixed mass flow rate, surrounded by streamlines) which passes through the rotor swept area, as shown in Figure 1.9. As flow passes through a tidal turbine, momentum is lost, $\mathbf{u}_1 \geqslant \mathbf{u}_2$, the flow slows and therefore by conservation of mass, the streamtube expands $A_1 \leqslant A_2$, where A_1 is the area of the streamtube at $\mathbf{u}_1$ and A_2 is the area of the streamtube at $\mathbf{u}_2$. Conversely, the bypass flow is contracted and accelerated as it bypasses the turbine rotors, $\mathbf{u}_1 \leqslant \mathbf{u}_{\text{bypass}}$.

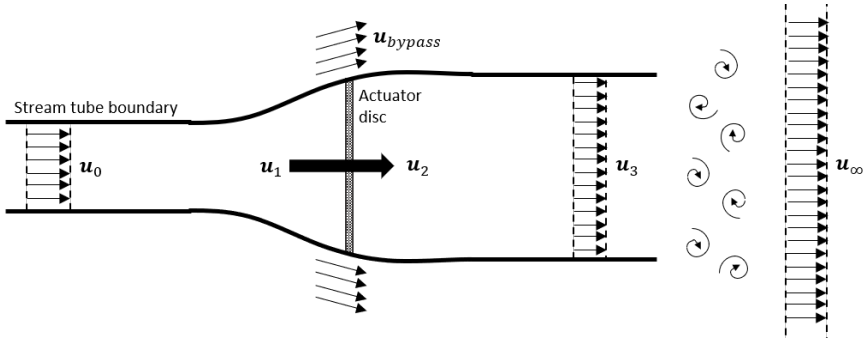

Figure 1.9: A single turbine represented as an infinitesimally thin actuator disc. The turbine extracts momentum and slows the flow, causing the streamtube to expand and the bypass flow to be accelerated. Sufficiently downstream turbulent mixing between the wake and bypass flow lead to wake regeneration.

The near-wake region is the region immediately behind a turbine, where turbulence is caused by flow passing through the individual blades. The average velocity in the wake is lower than that in the undisturbed flow, and the turbulence is greater. Wake structure in this region depends on the shape of the turbine blades. This requires a higher level of modelling such as computational fluid dynamics (CFD). The far-wake region is defined as the region where the wake is fully developed, i.e. the minimum velocity is found at the turbine centre line. It can extend over twenty turbine diameters downstream [76]. Wake structure in this region is dependent on the turbine (or actuator disc) diameter.

The idealised stream tube approximation, where the mass flow rate is conserved, relies on the assumption of laminar flow. This is no longer valid further downstream of the rotor where turbulent eddies arise due to the obstruction of the flow and create a *mixing zone*. Turbulence within the mixing layer transfers momentum from the accelerated bypass flow to the decelerated flow through the rotor, causing the wake to regenerate with increasing distance from the turbine. The regeneration causing the flow behind the turbine to return to similar levels as the flow between turbines, shown as u_∞ in Figure 1.9, is called *wake recovery*. Far enough downstream behind the turbine the wake is fully mixed and the presence of the turbine can no longer be detected, i.e. a uniform velocity is reached between bypass flow and the flow that passed through the rotor.

The ADM assumes that the flow is inviscid, incompressible, irrotational and the boundaries are far from the turbines. It also assumes that both the flow and the thrust are uniform across the disc area. In practice this is not the case because the friction causes the flow to increase logarithmically with height, and closer to

the surface gets impacted by wind and waves. However, at the heights that tidal turbines are deployed (with constraints imposing a minimum distance from the seabed to the bottom tip and the top tip to the lowest astronomical tide) the flow remains relatively uniform across the rotor's swept area. As a consequence of not modelling the rotating hub of a turbine, there is no swirl generated in ADM [77]. These differences are anticipated to mostly affect the near-wake region, and have been shown to only affect the region less than four diameters downstream for wind energy [78], so these simplifications may be unsuitable for detailed wake modelling and loads assessment, but is practical for yield assessment, especially if there is sufficient spacing allowed between rows of turbines.

Length scales in hydrodynamic modelling

Modelling tidal turbines is an inherently multi-scale problem. Each of the length-scales is coupled to its adjacent scales, making modelling complex. Adcock et al.'s review of tidal hydrodynamic modelling identified the key length scales when modelling tidal stream energy generation [68]. Blade scale models (10^{-3}m to 10^{1}m) look at the lift and drag that results from flow around the turbine blades. Modelling at this length scale has been well developed within the wind industry. Turbine scale (10^{-2}m to 10^{2}m) looks at the flow around and performance of a single turbine. Array scale models (10^{-1}m to 10^{4}m) look at the interaction of multiple turbines. Site scale (10^{0}m to 10^{5}m) looks at spatial and temporal variations of flow at a tidal site, modelling the interaction of turbines in an array with the flow. Regional scale models (10^{1}m to 10^{6}m) look at the dynamics which drive the strong tidal flows, and the large scale effects of tidal arrays on the hydrodynamics in the surrounding region.

Turbine scale modelling is used for the design of turbines themselves, for example for determining optimum blade shape and size. At this level of detail accurate calculation of the loads on the blades and (in some applications) the support structure is important. In these applications a high resolution 3D Navier-Stokes CFD model is needed. An example of such a model tailored the application of tidal energy is *Fluidity* [79], in which adaptive unstructured meshes are used to capture turbulent eddies and resolve the wake. This type of modelling is very expensive to run, especially if trying to model more than one tidal turbine. *Fluidity* was applied to tidal turbines in [80] where a single turbine and a row of 3 turbines were simulated using 3D CFD. Mesh optimisation helped reduce the computational cost, but it was still modelled on a relatively small domain and the turbines were approximated as

actuator discs rather than fully resolved. To fully capture the resource in a real tidal location the coastal features of the surrounding regions must also be modelled.

At farm scale 3D modelling generally becomes too expensive, so hydrodynamic processes must be approximated with either an analytical wake model superimposed on top of the ambient flow or using shallow water approximations. Superimposing wake models is relatively computationally cheap because a numerical model of ambient flow needs to be calculated only once, then just the analytical model is altered for each different array design. This comes at the cost of losing information on the interaction between turbines, but due to its cheapness global optimisation algorithms can be used with it. Using the non-linear shallow water equations to solve the flow is more computationally expensive and therefore needs to be combined with local gradient-based algorithms rather than expensive global algorithms such as genetic algorithms. However, because the resultant flow rather than the ambient flow is used, the array design and hydrodynamics are fully coupled [81].

Regional resource assessments or models of multifarm interactions [57] cover too large a domain to routinely model individual turbines. Instead farms can be represented as a continuous bottom friction function representing the turbine density [82]. The allows for a coarser mesh resolution, and the number of turbines does not need to be explicitly defined which prevents expensive nested optimisation loops.

The hierarchy of models that can be used for tidal turbine modelling range from low fidelity to high fidelity; at a multi-farm to farm scale a continuum approach solving the non-linear shallow water equations can be used [82], at the farm scale either individual turbines with a prescribed wake model or individual turbines solved using the non-linear shallow water equations can be used, at a device scale turbines can be modelled with actuator disc or fully resolved, with the flow represented using the 3D Navier-Stokes equations and associated solvers. A balance needs to be made between reducing the computational expense while increasing the accuracy of the models. This thesis seeks to expand upon the options for farm-scale modelling within this hierarchy, by finding computationally cheaper ways to assess the economic impact of array design choices, such as the number of turbines or their diameter and power rating.

1.4.2 Numerical shallow water model

Many hydrodynamic models of multi-tidal-turbine arrays use the depth-averaged shallow water equations, rather than the full 3D Navier-Stokes equations to solve the flow [38, 83, 81, 84]. Full 3D modelling of the flow is very computationally expensive and can severely limit the number of turbines that can be modelled and the size of the domain simulated, thus limiting its suitability for array optimisation and large-scale array yield analysis. The dynamics in the oceans where tidal turbines are deployed can often be described as shallow, i.e. where the key length scales of dynamics are far greater than the depth scales, $L \gg h$. Despite the British Channel having an average depth of about 120m, the horizontal length scales are much greater than the vertical ones. The most promising tidal array locations have even shallower depths of around 30–40m.

The shallow water equations are a set of partial differential equations derived as a two-dimensional approximation to the Navier-Stokes equations, under the assumption that the length scales of the body of water modelled are far greater than the vertical scales. Shallow water dynamics applied to oceanic problems describe a fluid bounded from below by a rigid surface i.e. the seabed and from above by a free surface. The total depth locally is described as $h(\mathbf{x}) = H + \eta_s(\mathbf{x}, t) - \eta_b(\mathbf{x})$, where H is the average depth, which is constant across the domain, η_s is the local elevation perturbation relative to the average sea surface height and η_b is the local deviation of the sea bed height from its averaged value, both varying spatially with $\mathbf{x} = [x, y]$. This configuration is depicted in Figure 1.10.

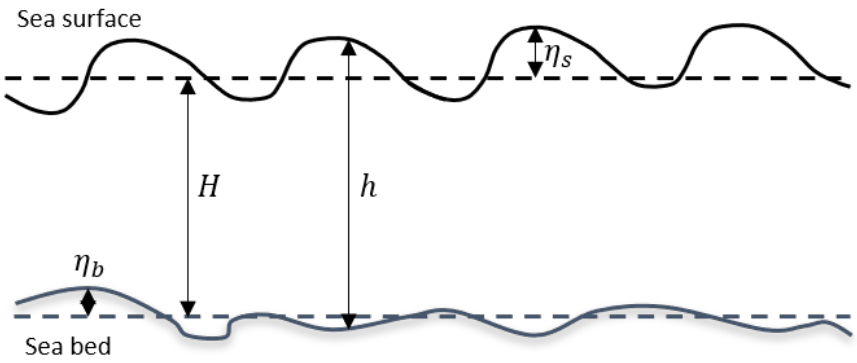

Figure 1.10: Definitions of the sea surface height, η_s, the sea bed height, η_b, the total local depth, h, and the average depth, H.

The Navier-Stokes equations are found as a consequence of the physical principles of the conservation of mass and momentum. Applying these two principles to a

control volume of incompressible, Newtonian fluid and combining them results in the continuity and momentum equation pair

$$\begin{aligned} \nabla \cdot \mathbf{u} &= 0 \\ \frac{\partial \mathbf{u}}{\partial t} + (\mathbf{u} \cdot \nabla)\mathbf{u} &= -\frac{1}{\rho}\nabla p + \nu \nabla^2 \mathbf{u} + \mathbf{F_b}\,, \end{aligned} \tag{1.1}$$

where $\mathbf{u} = [u, v, w]$ is the velocity of the fluid and ρ is the water density, p is the pressure, $\nu \equiv \mu/p$ is the kinematic viscosity, where μ is the dynamic viscosity, and $\mathbf{F_b}$ represents the external body forces per unit mass, such as gravity.

The shallow water equations can be obtained by depth-integrating the Navier-Stokes equations. This is derived by invoking the hydrostatic approximation, where

$$\frac{\partial p}{\partial z} = -\rho g\,, \tag{1.2}$$

i.e. the gravitational term is balanced by the pressure term in a balance known as *hydrostasy*. The hydrostatic approximation is valid when the vertical acceleration of the fluid is small relative to gravity, i.e. $Dz/Dt \gg g$, which is nearly always the case in the atmosphere and ocean [85]. Hydrostasy is then used as an approximation to the vertical component of the momentum equation.

Combining this approximation with depth-integration, and substituting in gravity and Coriolis forces to $\mathbf{F_b}$, produces the nonlinear shallow water continuity and momentum equations, given here in their non-conservative form

$$\begin{aligned} \frac{\partial \eta}{\partial t} + \nabla \cdot (h\mathbf{u}) &= 0, \\ \frac{\partial \mathbf{u}}{\partial t} + \mathbf{u} \cdot \nabla \mathbf{u} - \nu \nabla^2 \mathbf{u} + f\mathbf{u}^{\perp} + g\nabla\eta + C_d \frac{|\mathbf{u}|\mathbf{u}}{h} &= 0. \end{aligned} \tag{1.3}$$

η is the free surface perturbation, t is time, h is the total water depth, $\mathbf{u} = [u, v]$ is the 2D depth-averaged velocity vector, ν is the kinematic viscosity of the fluid, $f\mathbf{u}^{\perp}$ is the Coriolis forcing, g is acceleration due to gravity, and C_d is a dimensionless quadratic drag coefficient for seabed friction. Wind and wave conditions, and atmospheric pressure are not considered in this thesis, because it is assumed their effect will be minimal at the tidal-turbine hub heights considered. These effects may be more important to model if this work is applied at a later date to arrays of floating tidal turbines, rather than bed mounted ones.

The shallow water equations cannot be solved analytically, and instead are solved

using a finite element discretisation to predict the time-evolution of the elevation, $\eta(x, y)$, and the depth-averaged velocity across the whole domain, $\mathbf{u}(x, y) = [u, v]$. A set of initial conditions and boundary conditions are required to solve them. An initial velocity and elevation is given over the domain, typically $\mathbf{u}(t = 0) = \mathbf{0}$ and $\eta(t = 0) = 0$, then a spin-up period is allowed before any measurements are taken. Boundary conditions are imposed on each portion of the boundary, Γ. Examples of conditions imposed on the coastline include no normal flow, $\mathbf{u}.\mathbf{n} = 0$ on Γ, or no-slip $\mathbf{u} = 0$ on Γ. The open boundaries, typically at the entrance and exit of the channel or strait modelled, are forced with Dirichlet boundary conditions on elevation, $\eta = \eta^D$, with spatially varying time series data reconstructed from tidal constituent data available in tidal atlases.

In this thesis, an open-source coastal ocean modelling tool called *Thetis* is employed to solve the shallow water equations. *Thetis* can be used for tidal array simulation, performance assessment, and array design through optimisation of turbine locations, known as *micrositing*. *Thetis* allows for the use of structured and unstructured meshes, and is built using the *Firedrake* finite element framework. *Thetis* can be used for both 2D depth averaged models or full 3D models, but in this thesis is only used for the former, due to computational expense limitations, particularly when combined with iterative optimisation requiring multiple runs of the model.

The domain is split up into a finite number of cells, called *elements*. The elements are typically triangular and form an unstructured mesh in the following work, unless otherwise specified. The shallow water equations are solved on this discretised domain, using one of the finite element families supported in *Thetis*. The degree of the finite element pair, n, is specified for the $\mathbf{u}$ space and η space, with the options including equal order Discontinuous Galerkin (P(n)DG-P(n)DG), Raviart-Thomas DG (RT(n+1)-P(n)DG), P1DG-P2CG, and Brezzi-Douglas-Marini DG (BDM(n+1)-P(n)DG). Temporal discretisation is performed via the Crank-Nicolson method, such that

$$\begin{aligned} \frac{\partial \mathbf{u}}{\partial t} &\rightarrow \frac{\mathbf{u}^{n+1} - \mathbf{u}^n}{\triangle t} \\ \mathbf{u} &\rightarrow \frac{1}{2}(\mathbf{u}^{n+1} + \mathbf{u}^n) \\ \eta &\rightarrow \frac{1}{2}(\eta^{n+1} + \eta^n)\,. \end{aligned} \tag{1.4}$$

An advantage of the unstructured meshes used in *Thetis*, is the greater flexibility in the way the elements can be connected, allowing the resolution to vary across the

domain. As described in Section 1.4.1, modelling tidal arrays is a highly multi-scale problem and far away coastal features can impact on the flow, so being able to tailor a coarse mesh in afar regions and a finer mesh at the coastline and within the farm area improves the trade-off between accuracy and computational expense.

1.5 Blockage effects in tidal stream arrays

The presence of turbines can have tangible effects on the flow both downstream and upstream, in both the near-field and potentially far-reaching too. This interaction results in a system where the hydrodynamics are coupled with the array design, and therefore yield estimates need to be based on the disturbed flow, with the turbines modelled, rather than the ambient flow. Bryden et al. [86] found that in a simple channel 10% energy extraction of the natural energy flux resulted in a 3% flow speed reduction and 20% extraction resulted in a 6% speed reduction, therefore models that do not simulate the effects of energy extraction on the flow tend to overestimate the array yield. Blockage effects can be seen on a turbine scale and an array scale, known as *local* and *global* blockage respectively. For numerical and analytical models of tidal arrays to be accurate, they must take into account both of these blockage effects.

The extent of the blockage has a significant effect on the flow hydrodynamics, and it is often quantified as a ratio of the percentage of the channel's cross-sectional area that the turbines take up. The local blockage ratio for a turbine within a row of turbines which have a tip-to-tip lateral spacing of s and diameter of $\emptyset$ at an average depth, H, can be found from

$$B_L = \frac{\frac{1}{4}\pi\emptyset^2}{(s+\emptyset)H}\,. \tag{1.5}$$

Whereas the global blockage can be more complex to quantify, especially for irregular channels and turbine layouts that are not strict rows with even spacings.

Local blockage occurs on an individual turbine scale. It encompasses the deceleration of the flow through a single turbine, the acceleration of the flow around it and the increase in water pressure immediately upstream of the turbine. Local blockage can be exploited to boost the turbine output, through staggering turbines in such a way that subsequent rows are in the path of accelerated flow that bypasses the previous rows rotors [87, 88, 89, 83]. Garrett and Cummins [90] found that higher blockage

is generally preferable, where turbines form rows or *fences* that stretch across the width of a channel, with higher blockage rations allowing for a greater C_P/C_T ratio for a given thrust coefficient. If local blockage isn't accounted for in the array design, however, and turbines are placed in the wake of upstream devices, then the array yield suffers.

Additional to local blockage, which can be easily described by models such as ADM and has been well studied within the wind industry, tidal turbines have to take particular account of global blockage. When deployed on a commercial level, the added drag of large-scale tidal arrays will have a significant and far-reaching impact on the surrounding ambient flow field. Effects of global blockage include a reduction in flow speed through the array and downstream of it, and an increase in flow speed either side of the array, and an increase in free surface elevation upstream of the array. For example, a study on large-scale array designs in the Alderney Race showed that array-scale blockage could cause a reduction in flow speeds in the array of up to 2.5m/s, increased flow speeds either side of the array of up to 1m/s and a reduction in the mean volume flux through the Alderney Race of 8% [91]. Global blockage has been observed and studied to some extent in the wind industry [92, 93] but it can have a more significant impact on the yield of tidal arrays because water is incompressible and the turbines have a relatively large rotor diameter compared to the vertical length scales of the flow (typically approximately half the water depth [94]) and can therefore have a more significant hydrodynamic influence on the surrounding flow.

It is vital to take into account both local and global blockage effects at the array design stage because blockage can cause a diminishing return on the power generated by additional turbines. Global blockage causes there to be a threshold value; the maximum amount of power that can be extracted from a region before adding more turbines increases the blockage by so much that the total power of the array decreases [33, 95]. Because the tidal turbines are expensive, these diminishing returns result in an economic limit to the extractable power, at a much lower number of turbines than the physical limit to the extractable power.

Not only should the array size and layout be designed to account for blockage effects, but the design of turbine rotors must account for its effect on wake recovery too. Schluntz and Willden [96] found that the power coefficient of turbines can be improved if they are designed appropriately for the blockage conditions they will operate in. Rotors in high blockage conditions should be designed with an increased solidity (dependent on the number of blades and local chord), however these rotors

then perform poorly in unblocked flow conditions, so suitable turbine design will be site-dependent.

1.6 Resource assessment and tidal array design

In order to generate industrial amounts of energy, tidal turbines should be deployed in arrays comprising of up to hundreds of turbines. However, the world's first large-scale commercial array is yet to be installed. This means that there is extremely limited practical experience on how to find the best size and layout of turbines within these arrays and therefore reliable models are necessary instead. These arrays will only be developed, and a new UK-based industry formed, if they can be shown to be economically viable. Optimisation of the array location, its size and its precise configuration is essential to achieve this, with sophisticated numerical models required to assist array developers in these tasks.

The physical maximum power that can be extracted from a channel is sometimes referred to as the *potential*. The potential is found from a balance between increasing an array's gross drag coefficient (by effectively increasing the number of turbines in attempt to increase power production) and the associated reduction in the free-stream velocity which reduces power production [33]. In order to exploit the majority of a channel's potential the turbines must spread across most of the channel's cross-section [97].

Power generation of tidal arrays are determined by the number of turbines within the array (with sizes ranging from less than 10 turbines in small-scale demonstrator projects to plans to go up to the GW scale with hundreds of turbines), the array design (the location of the individual turbines and the resulting interaction with the flow), the design of the turbines themselves (their rated power, diameter and power coefficients all determining the power curve) and the tidal resource available in the region. Location of the turbines within an array can have a significant impact on the amount of power that can be extracted, with Funke et al. finding up to 38% increases in power generation for optimised array layouts compared to regular or staggered array layouts [81]. This section introduces some computational tools that can be used to aid the array design.

First let us consider a simple optimisation objective, of maximising power alone, by selecting a suitable number of turbines and their locations. The optimisation

functional of interest is therefore the time averaged power generation of the whole array, $J = P_{\text{avg}}(\mathbf{u}, n_t)$, where P_{avg}, is found by integrating over a representative time period. Chapter 2 proposes methods of extending upon this approach so that the number of turbines is chosen to optimise the economic performance of the array, rather than maximising the overall power generation.

1.6.1 Yield estimates for tidal-stream arrays

The power of an individual turbine can be calculated from

$$P = \frac{1}{2}\rho C_p A_T ||\mathbf{u}||^3, \tag{1.6}$$

where ρ is the density of the water, C_p is the power coefficient, A_T is the swept area of the turbine, and $\mathbf{u}$ is the speed of the flow. The power coefficient varies with $\mathbf{u}$, such that

$$C_P(\mathbf{u}) = \begin{cases} C_p^*, & \mathbf{u_{cutin}} < \mathbf{u} < \mathbf{u_{rated}} \\ C_p^* \dfrac{\mathbf{u}_{\text{rated}}^3}{\mathbf{u}^3}, & \mathbf{u_{rated}} < \mathbf{u} < \mathbf{u_{cutout}} \\ 0, & \text{otherwise} \end{cases} \tag{1.7}$$

where C_P^* is the power coefficient below rated speed. The cut in speed is the minimum speed required to generate enough momentum to turn the rotor and generate power, the rated speed is the speed at which the turbine reaches its rated capacity, and the cut out speed is the speed at which the blades are pitched away from the currents and power generation is stopped, to protect the turbine from damage. The power coefficient of the turbine is a dimensionless number, which represents the efficiency of the turbine; the proportion of the available power in the water passing through the rotor swept area over the power converted into electricity. The power coefficient depends on the flow velocity and the design characteristics of the turbine, such as blade shape and control features, but it is typically around 0.4 for tidal turbines [98].

1.6.2 Optimisation to tidal-stream array design

As can be seen in (1.6), below rated small changes in velocity can have substantial impacts on the power generated. Therefore the total power generated throughout the array is highly sensitive to the location of individual turbines, with respect to

the regions of highest tidal current and with respect to one another. This process is called *micro-siting*. This is an important step developers must take once macro-siting (deciding the region to extract power from and agreeing a lease area in which the turbines can be installed e.g. [99]) is carried out. This thesis focuses on optimisation tools for the micro-siting stage, assuming that a site has already been leased to the developer and the outer array boundaries are already known.

Manual optimisation, applying understanding of turbine wakes and accelerated bypass flow, can be used to achieve substantial gains in array power. For example, Divett et al. [83] tested 4 layouts and showed that staggered layouts could generate 54% more power than non staggered. However, this was just for an idealised channel model where the flow was relatively constant throughout. Deciding the optimal location for turbines becomes much more complex when realistic bathymetry and coastline features create time and spatially varying flow patterns. Commercial-scale array optimisation of large numbers of turbines results in increasingly important and complex interactions of local and global blockage, which are harder to intuitively design for than staggering rows to avoid local wakes alone.

Many decisions need to be made at the array design stage, from the number and locations of many turbines to possible choices in the turbine design such as rated power and rotor diameter. Manual optimisation is impractical over such a large parameter space, with complex non-linear interactions between parameter choices, and high levels of uncertainty in many of the variables. Specially designed computational tools can overcome this problem, and can be repeated to find an optimal design that is robust to uncertainty. This work suggests design paradigms which are efficient and scalable with the size of the array and the number of array features to optimise. It attempts to acknowledge the limitations of each tool developed and place them within a hierarchy, of tools that are most appropriate for each stage of the array design and decision making process.

Global optimisation algorithms, such as genetic algorithms, have been employed in early tidal stream [100] and tidal range [101] energy array designs and have often been used in wind turbine array designs [102, 103]. The algorithms seek to find a globally optimum solution by testing a very large number of different array designs and estimating the power generation for each. The computational expense of testing such a high number severely constrains the type of flow model that can be used, to either simple wake deficit models which do not account for the effects of global blockage, or limited two2-dimensional models with simplified tidal forcing and coarse meshes.

To address these limitations Funke et al. [81] introduced a gradient-based approach to tidal micrositing. Gradient-based algorithms do not necessarily converge tofind global optima, but by their very nature seek out only local optima, however they have been shown to perform well at improving the array design compared to manual approaches, and allow for more complex scaling and linear combinations of optimisation functionals, such as maximising the power while minimising the environmental impact [104] or the cabling costs [105]. The number of flow simulations required to find these optima is substantially reduced compared to brute force or genetic algorithms (typically requiring 10–100 simulations to converge rather than in the order of 10^6) because gradient based algorithms move in the direction of the steepest descent. This means that they can be used in conjunction with a higher fidelity model that is more computationally expensive than genetic algorithms would allow.

Gradient-based approaches are only applicable if it is possible to evaluate the derivative of the functional with respect to the design parameters being optimised (i.e. the number of turbines and their locations). To benefit from the computational economy of the gradient based method, any functional used must have a reasonably efficient derivative, $\frac{dJ}{dd(\mathbf{x})}$, to compute. Section 2.2 discusses ways this can be formulated but they are all relatively simple to compute, except for the Internal Rate of Return, which must be found using a a nonlinear solver such as the Secant method.

Some gradient-based optimisation algorithms are based on finite difference methods, which perturb the model inputs by finite difference in each of the degrees of freedom away from the original point, approximate the gradient from those pieces of information, and move in the steepest direction. Finite difference based methods are reasonably computationally efficient if you only have a few control variables that can be changed. If there are hundreds or thousands of variables you can change (which is the case when you have a spatially varying turbine density value to be optimised) then every optimisation iteration requires hundreds or thousands of gradient calculations, which becomes prohibitively computationally expensive.

Adjoint methods replace the finite difference step with a gradient calculated through the adjoint equations which are relatively computationally cheap. Each iteration of the array optimisation process in *Thetis* has two components. The shallow water equations are solved to evaluate the power that can be extracted by a particular array design, in the so called *forward model*. Solution of the associated adjoint equations are then used to find the sensitivity of that power with respect to the array design parameters, and this information is used to update the array design via a gradient based approach. Solving the adjoint equations takes roughly the same

computational expense as solving the forward model (except in reverse) and just needs to be done per every parameter of interest (normally just the functional), rather than per every control parameter (the turbine density at each node) as would be required for finite difference methods.

This is the optimisation method used in Chapter 3 and 4 of this thesis, greater discussion of its application is provided there.

Continuous versus discrete approach in *Thetis*

In shallow water models, tidal turbines are sometimes represented as a two-dimensional 'bump' of locally increased bottom friction [83, 81, 84]. This approach couples the array design with the hydrodynamic model and therefore accounts for both local and global blockage effects when predicting the array yield. This approach is referred to throughout as the *discrete* case because it 'resolves' each turbine individually. However, due to the simplified representation with no support structure and rotating parts, it does not resolve the details of the turbine and its wake. This can be computationally expensive because it requires a mesh that has an element size at least as small as the turbine diameter, if not an order of magnitude smaller. This is feasible for small arrays but can result in a very high number of elements if the array boundary covers a large area.

Another limitation of this approach is that when optimising the array design with a non-fixed number of turbines, an expensive nested optimisation loop approach must be employed. An inner loop optimises the location of the turbines for a given number of devices, with an outer loop must be employed to vary and determine the optimal number of devices [81, 95]. In [95] the design parameter in the inner loop is $\mathbf{m} = [(x_1, y_1), \ldots, (x_{n_t}, y_{n_t})]$, a vector of turbine locations in Eastings and Northings, and the design parameter in the outer loop is n_t, the number of turbines, which defines the length of vector $\mathbf{m}$.

An alternative approach was developed by Funke et al. [82] to address these concerns. In the *continuous* approach, the turbines are modelled as a continuous spatially-varying turbine density field, $d(x)$, which can be interpreted as the number of turbines per metre squared of seabed. The number of turbines and their "locations" are optimised simultaneously, at a potentially far lower overall computational expense, at the compromise of resolving turbines and their wakes individually [82].

Instead of a series of bump friction functions at the location of each turbine, a

spatially varying turbine density field, $d(\mathbf{x})$, is optimised. Turbines are only allowed to be placed within the predefined farm area, A_f, and are modelled through the inclusion of an additional bottom friction term of the form

$$\frac{c_t}{\rho H}||\mathbf{u}||\mathbf{u}, \tag{1.8}$$

which is added to the left hand side of the Shallow Water Equations (1.3).

The continuous turbine drag coefficient c_t can be found from the density field, $d(x)$, via the relationship;

$$c_t(d(\mathbf{x})) = \frac{1}{2}C_T A_T d(\mathbf{x}), \tag{1.9}$$

where C_T is the turbine thrust coefficient, A_T is the swept area of a turbine.

The turbine density can be integrated over the array area to find the total number of turbines, n_t, such that

$$\int_{A_f} d(\mathbf{x})\, d\mathbf{x} = n_t. \tag{1.10}$$

In the continuous case [82], the average power can be found from the spatially-varying turbine density field, $d(x)$, such that

$$J(\mathbf{u}, \mathbf{m}) = P_{\text{avg}} = \frac{1}{T}\int_0^T \int_{A_f} \rho C_P \frac{1}{2} A_T d(x)\, ||\mathbf{u}||^3\, dx\, dt, \tag{1.11}$$

where T is the time period the hydrodynamic model is run over, A_f is the area of the tidal farm, ρ is the fluid density, C_P is the power coefficient, and $\mathbf{u} = (u, v)$ is the depth averaged velocity.

The basic steps behind both approaches involve; forming the array design as an optimisation problem, using the shallow water equations as the hydrodynamic model and using derivative based methods to solve the optimisation problem. Advantages found by [82] of the continuous approach include flexibility of fixing minimum distances between turbines (through a maximum local density) and changing optimisation functional (cost, profit, power etc), efficiency of simultaneously optimising number of turbines and location and independence of farm size and computational expense and finally accuracy when validated against observations in the Pentland Firth.

1.7 Motivation and scope

This thesis is motivated by the need to increase deployment of all types of sustainable energy, and accelerate the move away from carbon intensive fossil fuels. This will only be carried out if renewable energies can be proven to be economically competitive with more damaging forms of energy. Tidal stream energy could play a key part of the UK's future clean energy mix, but to do so it needs to see significant cost reductions and be deployed in large-scale arrays of up to hundreds of turbines. This thesis sets out to address the following research objectives, to assist the transition to large-scale commercially competitive arrays:

1. Review the choices of financial model that can be used to assess the overall and economic performance of tidal stream arrays, and evaluate their suitability for use within a micro-siting optimisation tool.

2. Collate publicly available cost information on tidal stream arrays to find a reasonable set of input values to the financial model.

3. Develop a tool that allows the optimisation of turbine number and layout, while coupling the hydrodynamics to the array design to take account of global blockage. Ensure the tool is computationally efficient enough to be used to explore the impact of the high degree of uncertainty in the economic inputs.

4. Setup and validate a hydrodynamic model of the Alderney Race, one of the UK's most promising and energetic sites for large-scale tidal stream arrays. Apply the tool here to identify the potential to reduce the cost of tidal energy in this region.

5. Develop a lower-fidelity tool that can be used for fast assessment the impact of different array specifications on annual yield. Demonstrate how this can be useful for narrowing down the scope of options used in the early stages of large-scale array design, by applying it to the case study of the MeyGen expansion from the 6MW Phase 1A to the 86MW Phase 1C.

6. Evaluate how these different tools fit within the various stages of the array design process.

1.8 Thesis outline

Chapter 2 discusses the different choices of economical functional for array design optimisation and presents the results of a data collection study for estimating inputs to financial models of large-scale tidal stream arrays.

Chapter 3 presents the development of a computationally efficient method for optimising tidal-array design, for a non-fixed number of turbines, with respect to economic functionals such as the Levelised Cost of Energy. Chapter 4 applied the method developed int Chapter 3 and applies it to a realistic model of the Alderney Race, to demonstrate the energy extraction potential in the region.

Chapter 5 presents a method for evaluating the impact of varying tidal array design parameters on the predicted yield, and for incorporating practical constraints such as maximum steepness and minimum depths for installation. It is applied to the expansion of the MeyGen array and was carried out in collaboration with SIMEC Atlantis. Chapter 6 summarises the work carried out in this thesis and how each method developed fits within the iterative process of tidal stream array design. It discusses the current limitations of the approaches developed and the avenues for further work to improve upon this.

1.8.1 Publications

Parts of this thesis have been published or submitted for publication. Chapter 2 is hosted on ArXiv [106]. Chapter 3 is published in Applied Energy [107] and includes work from conference papers ([3, 4]). Chapter 4 is published in [108].

Other publications, not explicitly included in this thesis but referred to at times throughout include [109], [57], [110] and [62].

Other contributions include the following presentations:

- Oxford Tidal Energy Workshop, 2018 [109]
- Firedrake, Imperial College, 2018
- SIAM Mathematics of Planet Earth, Philadelphia, 2018
- Renew, Lisbon, 2018 [57]

- Oxford Tidal Energy Workshop, 2019 [3]
- Firedrake, Imperial College, 2019
- EWTEC, Naples, 2019 [4]
- PRIMaRe, Online, 2020

Chapter 2

Literature review of the economics of tidal stream arrays

Abstract

This chapter is adapted from *Economic analysis of tidal stream turbine arrays: a review.* Z. L. Goss, D. S. Coles and M. D. Piggott, published on ArXiv [106], 2021.

The tidal stream energy industry has to date been comprised of small demonstrator projects made up of one to four turbines. However, there are currently plans to expand to commercially sized projects with tens of turbines or more. As the industry moves to large-scale arrays for the first time, there has been a push to develop tools to optimise array design and help bring down costs. This review investigates different methods of modelling the economic performance of tidal-stream arrays, for use within these optimisation tools. Different cost reduction pathways are discussed, from costs falling as the global installed capacity increases, due to greater experience, improved power curves through larger-diameter higher-rated turbines, to economic efficiencies that can be found by moving to large-scale arrays. A literature review is conducted to establish the most appropriate input values for use in economic models. This includes finding a best case, worst case and typical values for costs and other related parameters. The information collated in this review can provide a useful steering for the many optimisation tools that have been developed, especially

when cost information is commercially sensitive and a realistic parameter range is difficult to obtain.

2.1 Introduction & Motivation

Demand for sustainable and reliable energy sources is increasing, and tidal energy could prove an important part of the future energy generation mix, due to its predictable nature. However, tidal energy is a nascent industry compared to more established renewables such as wind and solar. These industries have seen significant costs reductions due to subsidies helping them learn from expensive early demonstrator arrays. These initial subsidies allowed wind and solar to progress to large-scale energy farms with a much lower price of energy. At the time of writing, the UK's largest onshore wind farm now consists of 215 turbines (Whitelee Windfarm) and the largest offshore farm has 189 (the Walney Extension). The maturity of the industry and the economies gained from large numbers of devices has led to the UK seeing a record low price per MWh from offshore wind of £39.65 in their third Contracts for Difference auction, in September 2019, for less established renewable technologies [111].

In order to compete with more established technologies, tools must be developed to predict and help reduce the cost of tidal energy. In order for academically produced tools to be useful for industry, they need to be combined with the economic models and metrics that tidal investors are interested in. The inputs to these models are typically commercially sensitive and are therefore rarely publicly available. While exact values may only be used internally within industry, estimates of the inputs are useful for testing the academically developed tools.

Previous design optimisation studies, such as [82, 81, 105, 112], have optimised not only an array's design, but also the number of turbines in an array. This can be important in order to take advantage of the cost reductions that can be achieved with larger scale arrays, while also balancing against the diminishing returns as the average power generation per device falls with additional turbines. This review formats the cost inputs so they can be used in an economic model with a varying number of turbines and therefore can be used in the functional for a model that optimises both the location and the number of turbines.

This review attempts to summarise the economic models most commonly used by the

tidal energy industry and associated academia and to collate the publicly available cost information to produce appropriately formatted estimates for the inputs into these models. Section 2.2 outlines the most commonly used economic metrics and their advantages and disadvantages. Section 2.3 describes the different mechanisms expected to lead to the reduction in the price per MWh of tidal stream energy. Section 2.4 combines publicly available cost information, yielding data in a format useful for the input into the models described in Section 2.2. Finally, Section 2.5 discusses the uses and the limitations of the information collated in this review.

2.2 Review of economic metrics for evaluating array design

When designing a tidal turbine array the choice of functional to optimise can have a significant impact on the resultant array design. The following sections outline common metrics that are used for evaluating the performance of a tidal array, which could be used as the functional.

2.2.1 Power

Many papers [81, 57, 83] optimise array design for power alone, such that the functional is $J = P_{\text{avg}}$. This can be an effective method of determining a suitable layout, especially if the size of the array is already specified, such as in [81, 83] In such cases the costs are relatively fixed, except for the costs that depend on the individual turbine locations, such as the cabling [105] or distance and depth related installation costs, which are discussed in greater detail in Section 2.2.8. However, in general maximising for power is a reasonable proxy for maximising the economic performance.

Problems in using the power alone as a functional arise, in particular, when the number of turbines is also allowed to vary and becomes a free parameter within the array design optimisation. Earlier work [57, 4] has shown that, when optimising for power alone, the optimal design will feature an impractically high number of turbines, where the overall power generation is at its maximum, but the capacity factor of the array, and therefore its profitability, is relatively low. The optimisation algorithms will keep adding turbines, which slow the flow velocity through the site, until

a point is reached where the blockage is so high that adding any more turbines will decrease the overall power generation. However, the extracted power per additional turbine will diminish long before the threshold where the overall power decreases. Given the high cost of installing devices the optimal economic performance will be achieved at a far lower number of turbines than the optimal power.

2.2.2 Break even power

As established in earlier work [109, 57, 3], adding additional turbines to an array may increase the overall power, but there comes a point where there are diminishing returns for each extra turbine installed, for example due to global blockage effects as well as the array being forced to expand into lower flow areas [113]. From a financial perspective it may be more advantageous to have a smaller array where the average power per device (PPD = Avg Power/n_t) is higher, because tidal turbines are relatively costly to manufacture and install. In recent work [4, 3] a break even power, P_{BE}, is included in the optimisation functional to account for this problem and ensure that turbines are only added if they can generate enough power to cover their installation costs. Varying this parameter changes the trade-off priorities between the objectives of maximising power generation and minimising costs.

The break even power is the average power over all turbines that needs to be generated in order for the array to break even over its lifetime. A formula for choosing a suitable break even power can be found by first using a simplified model for the expected cash flow as the functional, such that

$$\begin{aligned} J &= \text{Revenue} - \text{Cost} \\ &= \sum_{i=0}^{L} (P_{\mathrm{avg}} \times t_i \times T_e) - \sum_{i=0}^{L} \mathrm{Ex}_i, \end{aligned} \tag{2.1}$$

where i is the year the costs are being evaluated over, L is the lifetime of the array in years, P_{avg} is the average power generated by the whole array in MW, t_i is the number of hours of generation in year i, T_e is the electricity tariff, i.e. the price per MWh the electricity generated is sold at, and Ex_i is the sum of all array expenditure incurred in year i. If it is assumed that P_{avg} is independent of the year, a critical average power per device that must be generated by the whole array to break even can be found:

$$P_{\mathrm{BE}} \times n_t \sum_{i=0}^{L} (t_i \times T_e - \mathrm{Ex}_i) = 0, \tag{2.2}$$

$$\iff P_{\mathrm{BE}} = \frac{\sum_{i=0}^{L} \mathrm{Ex}_i}{n_t \times \sum_{i=0}^{L} (t_i \times T_e)}. \tag{2.3}$$

If it is assumed that total expenditure is just a multiple of the number of installed turbines, $\mathrm{Ex}_i = n_t \times \mathrm{Ex}_{t,i}$, then a constant value for P_{BE} can be found which is independent of array design:

$$P_{\mathrm{BE}} = \frac{\sum_{i=0}^{L} \mathrm{Ex}_{t,i}}{\sum_{i=0}^{L} (t_i \times T_e)}. \tag{2.4}$$

In practice, P_{BE} would probably decrease for larger scale arrays, due to economies of volume [12]. More sophisticated models to account for this are discussed below. Since the functional defined in (2.1) is invariant with respect to scaling, it can be seen that optimising with respect to expected cash flow is equivalent to optimising a functional of the form

$$J = P_{\mathrm{avg}} - \frac{\sum_{i=0}^{L} \mathrm{Ex}_{t,i}}{\sum_{i=0}^{L} (t_i \times T_e)}, \tag{2.5}$$

which combined with the aforementioned simplifying assumptions can be reduced to

$$J = P_{\mathrm{avg}} - P_{\mathrm{BE}} \times n_t. \tag{2.6}$$

Therefore for the array to generate a profit the average total power generated by the array must be more than the break even power times the total number of devices. If an appropriate break even power is chosen to reflect all of the costs in (2.1), this choice of functional effectively maximises the profit. It penalises the addition of turbines which do not generate sufficient power to offset their costs, or which due to hydrodynamic changes lead to reductions in the yield of other turbines.

An advantage of using the functional described in (2.6) is that it incorporates financial considerations to the optimisation through the use of just one simple variable, P_{BE}. However, this simplification means that the optimisation process has no flexibility to changes in strike price, annual yield variability, maintenance costs and hours

downtime throughout the many years an array is operating for. It also excludes the effect of economies of volume, where larger-scale arrays would require a lower P_{BE} to break even[12]. Both these limitations mean that, in reality, break even power would be a function of time and the size of the array, rather than a constant as assumed here. This might be an acceptable simplification if the optimal design was robust to changes in P_{BE} that arise from these factors; however, previous studies [3] have shown the optimal design to be very sensitive to even small changes in P_{BE}.

Other papers have used similar or equivalent metrics to the break even power, with varying terminology. Iyer et al. [114] assessed the viability of tidal sites around the UK and used the capacity factor as a simplified indicator of the economic performance of a site, on a per MW basis. They found an average capacity factor of 29.9% (but ranging between 23.3 and 43.6%) across all the sites they investigated in the UK. They noted that this metric has limited usefulness in models where turbine specifications chosen (such as diameter and rated power) are generic rather than tailored to the site being evaluated, therefore under-utilising the resource.

Funke et al. [82] first coined the term break even power, but also called it a cost coefficient. Their definition was very similar to the one given in (2.4), except instead of evaluating about the break even point, they assumed a profit margin, m, was required such that

$$m = \frac{\text{Revenue} - \text{Cost}}{\text{Revenue}} \tag{2.7}$$

and they made the assumption $m = 73\%$. They assumed that the 73% profit margin could be achieved by a 20m diameter turbine if the peak speed was $3.5\,\mathrm{m\,s^{-1}}$, and used this to estimate a break even power of 452 kW. They only tested the optimisation for this one break even power value, but noted that the break even power chosen was expected to have a large impact on the optimal number of turbines.

Funke et al. [82] also noted that the break even power model does not take a discount rate into account. Therefore no financial distinction is made between capital expenditure, i.e. upfront investments such as turbine and installation costs, versus operational expenditure, i.e. maintenance costs incurred years into the future.

A further limitation of using break even power as the functional is that it makes too many simplifying assumptions and has no way to account for economies of scale. An adaptation to the functional to account for this is discussed below. Overall, break even power represents a good early measure while insufficient financial information is available since all you need to know is an aspirational capacity factor. For example, if the developer's financial model finds that an array of 2MW turbines needs to

achieve a 40% capacity factor to be profitable, then the break even power needs to be set to $2000 \times 0.4 = 800$kW. However, once a more complete model of the costs is available a more detailed metric should be used that accounts for all the effects ignored by the above assumptions.

Break even power with economies of volume

When the costs are assumed to increase linearly, as a multiple of the number of turbines, the break even power is independent of the number of turbines and therefore can be used as a constant value, as given in (2.4). In practice that relationship will not reflect the true expenditure and the break even power will likely decrease as n_t increases due to economies of volume. There are a number of ways this impact can be modelled, the simplest of which is to linearly decrease the break even power with the number of turbines, such that $P_{\text{BE:EV}} = P_{\text{BE}} - EV \times n_t$, where EV is a coefficient for economies of volume, and $EV \ll P_{\text{BE}}$. This change can be made to the functional (2.6) so that

$$J = P_{\text{avg}} - (P_{\text{BE}} - EV \times n_t) \times n_t = P_{\text{avg}} - P_{\text{BE}} \times n_t + EV \times n_t^2. \tag{2.8}$$

Using a functional of this format is equivalent to the expenditure instead decreasing quadratically with the number of turbines, such that:

$$P_{\text{BE:EV}} = \frac{\sum_{i=0}^{L} \text{Ex}_{t,i} \times n_t - EV \times n_t^2}{n_t \times \sum_{i=0}^{L} T_e \times t_i} = \underbrace{\frac{\sum_{i=0}^{L} \text{Ex}_{t,i}}{\sum_{i=0}^{L} T_e \times t_i}}_{P_{\text{BE}}} - \underbrace{\frac{\sum_{i=0}^{L} \text{EV}}{\sum_{i=0}^{L} T_e \times t_i}}_{EV} \times n_t. \tag{2.9}$$

Figure 2.1 shows how if the annual expenditure increases linearly with the number of turbines the break even power is fixed, however, if the expenditure declines quadratically with the number of turbines the break even power declines linearly with the number of turbines. Both rely on assumed relationships between the costs and number of turbines but are useful for initial investigations into how bringing costs and economies of volume into the functional effect the optimal array design.

The impact of varying both the P_{BE} and EV parameters are explored in [3]. It was found that as P_{BE} falls, for example due to costs falling in the tidal industry with experience gained, the optimal array design features more turbines and generates

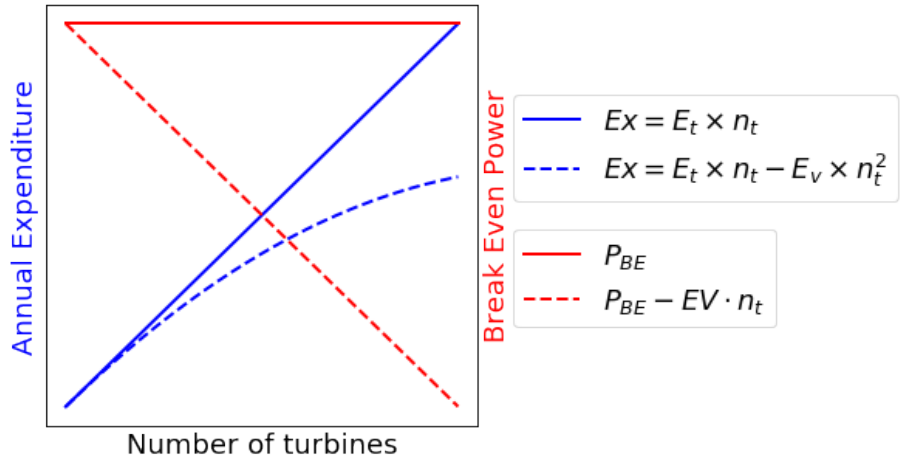

Figure 2.1: A demonstration of how the relationship between expenditure per year and number of turbines in an array corresponds to a fixed or linearly decreasing break even power.

more power overall, but the average power per device drops. It was shown that optimal array properties were more sensitive to changes in the region $300kW \leqslant P_{\mathrm{BE}} \leqslant 500kW$. This was even more notable when including economies of volume too; changing the value of EV had little to no impact on the optimal design for very high or very low values of P_{BE}. For $300kW \leqslant P_{\mathrm{BE}} \leqslant 500kW$ however, it was seen that as EV increased the total power generated and number of turbines increased, and the power generated per device decreased.

2.2.3 Net Present Value

Equation (2.1) describes the sum of all cash flow across an arrays lifetime, however in practice this value is rarely used by investors. Long term investments, such as tidal arrays, rely on discounted cash flow (DCF) analysis to quantify the idea that money today is worth more than money tomorrow to investors. Current funds have the ability to earn interest and become worth more in the future, so investors need to find a way to adjust future cash flow to enable the comparison between costs and revenue in different time periods, in terms of their present day value. The Net Present Value (NPV) is a measure used to find the profit of a project is found by summing all incoming and outgoing cash flows per year, i.e. the revenues minus the costs from each year $i \in [0, L]$, adjusted according to the time value of money by a discount rate, r, such that

$$\begin{aligned} \text{NPV} &= \sum_{i=0}^{L} \frac{\text{Revenue}_i - \text{Cost}_i}{(1+r)^i} \\ &= \sum_{i=0}^{L} \frac{P_{\text{avg}} \times t_i \times T_e - \text{Ex}_i}{(1+r)^i}. \end{aligned} \tag{2.10}$$

Using the NPV as the functional for tidal array optimisation has many advantages. Unlike the previous metrics it takes into account the depreciating time value of money, which is important to investors. It allows for far greater flexibility in the financial modelling than the previous metrics. For example, instead of basing analysis on a time averaged power generation, P_{avg}, it is trivial replace this with a time-varying generation. This can be used to model the impact that the power variation due to the 18.6 lunar nodal cycle [115, 116] has on the economic performance of the array. It could also be used to include the effects of the anticipated degradation of the turbine performance, for example due to biofouling and algae build up [117], and increase in required downtime, due to a higher number of faults with age, as commonly observed in the wind industry [118, 119]. However using an average power generation is very useful while there is still a lot of uncertainty about the planned installation year and fault rates decades into the future.

A disadvantage of using NPV as the functional for tidal array optimisation, is that it is hard to compare between projects of different sizes. A smaller tidal array may have a far higher profit margin but a much lower NPV than a large tidal array. It is hard to interpret directly from the NPV how successful a project is.

Break even analysis

There are a number of different economic metrics which can be derived when applying break even analysis to the Net Present Value formula. Equation (2.10) can be set to zero in order to obtain a value for the so-called break even point of an energy project. Then the resulting equation can be solved for each of the input variables, to determine the parameter value that would need to be achieved for the project to break exactly even over its lifetime. Each of these parameters at break even can be seen as the minimum requirement, and any improvement on these will result in a positive NPV and the project will generate a profit.

The most common metrics are derived by solving for the strike price, to obtain the levelised cost of energy (LCOE), solving for the lifetime, to obtain the payback

period (PP), and solving for the discount rate, to obtain the internal rate of return (IRR).

Discrete versus continuous discounted cash flow analysis

All present value based calculations require summing all the cash flow over a lifetime and discounting them according to the time at which they occurred. The net present value calculation given in (2.10) is setup so that the discount rate is applied on a yearly basis. It is possible to instead apply the discounting on different time intervals, e.g. semiannually, quarterly or monthly, or to use a natural log based formula to apply discounted cash flow analysis continuously.

Using the discrete compounding method, the present value, PV, of a future cash flow, FV, is

$$\mathrm{PV} = \frac{\mathrm{FV}}{(1 + \frac{r}{p})^{pi}}, \tag{2.11}$$

where p is the number of compounding period per year (for example, $p = 1$ for annual compounding or $p = 4$ for quarterly compounding), i is the number of periods into the future that the future cash flow occurs, and r is the annual discount rate.

By comparison the continuous compounding method has no period over which the compounding is applied and can instead be found from

$$\mathrm{PV} = \mathrm{PV} \times e^{-ri}, \tag{2.12}$$

where in this case i is a continuous value for the number of years into the future that the cash flow occurs.

A review into the use of discrete and continuous discount rates by Lewis et al. [120] found, in a literature review of finance and engineering economics journals, that the split between discrete and continuous discounting of future cash flows was fairly even. More mathematical papers tended to use continuous discounting, whereas more applied papers used discrete discounting. In practice many tidal array developers are not likely to have precise knowledge of when exactly costs will be incurred, especially not at the stage of designing an array. Therefore discrete modelling on an annual, or quarterly, basis is sufficient for this application.

2.2.4 Levelised Cost of Energy

The levelised cost of energy (LCOE) is a proxy for the average price of energy, T_e [£/MWh], that an array must receive to break even over its lifetime. It takes into account discounting and is calculated by finding the Net Present Value of the unit-cost of electricity over the lifetime of the array, by setting expression (2.10) to zero and rearranging to find the price of energy;

$$\text{LCOE} = \frac{\text{discounted cost}}{\text{discounted energy}} = \frac{\sum_{i=0}^{L} \frac{\text{Ex}_i}{(1+r)^i}}{\sum_{i=0}^{L} \frac{P_{\text{avg}} \times t_i}{(1+r)^i}}. \tag{2.13}$$

LCOE will be focused on as the main metric for economic optimisation here since many studies and organisation use it as the most established form of estimating the lifetime costs of an energy generation project [121, 122, 123]. It is an effective benchmarking technique for the comparison of multiple energy generation technologies, and in this case multiple array designs. LCOE, IRR and PP are all effectively simplifications of NPV, where an input variable can be removed by instead only investigating the parameters required to break even. Often it is sensible to isolate the variable which has the most uncertainty in it. The price of energy T_e can vary greatly depending on subsidies available to early stage renewable energies, so LCOE predictions often encapsulate less uncertainty than IRR and PP, because an assumption of T_e is not required.

The LCOE is the most commonly used approach for estimating the cost of energy over the lifetime of a project, for both tidal energy and other renewables [121, 122, 123, 12]. Since it is not as sensitive to array size as NPV or other metrics, it enables simple comparison across a range of different projects.

2.2.5 Payback Period

Another metric that can be derived from break even analysis of the Net Present Value formula is the Payback Period (PP), which is the lifetime array must operate for in order to break even. If the planned lifetime of the array is longer than this the array can be considered to be generating profit, if the lifetime of the array is shorted than this it will be making a loss.

The Payback Period can be found by calculating the NPV of every year from 0, until the NPV becomes positive. The critical year, $i_c r$, is the last year before the NPV

becomes positive, i.e. the year before the project breaks even. A payback period can be calculated by estimating how far through the year the project breaks even;

$$\text{Payback Period} = i_{cr} + \frac{\text{NPV}_{cr}}{\text{NPV}_{cr} - \text{NPV}_{cr+1}}. \tag{2.14}$$

2.2.6 Internal rate of return

Finally, (2.10) can be rearranged to find the discount rate at which the project breaks even, call the Internal Rate of Return (IRR). If the IRR is higher than the projected discount rate, then investors can anticipate a profit over the course of the array's lifetime. IRR is harder to calculate because, when trying to find the discount rate at which a project breaks even, $r = \text{IRR}$, the formula can be expanded,

$$0 = (E_0 \times T_e - \text{Ex}_0)(1 + \text{IRR})^L + (E_1 \times T_e - \text{Ex}_1)(1 + \text{IRR})^{L-1} + (E_L \times T_e - \text{Ex}_L), \tag{2.15}$$

but never to a form which can be solved analytically. However, a nonlinear solver such as the Secant method can be applied to find the IRR numerically. Each new iteration, at iteration number $n + 1$, is found from the previous two estimates, such that

$$\text{IRR}_{n+1} = \text{IRR}_n - \text{NPV}_n \times \left(\frac{\text{IRR}_n - \text{IRR}_{n-1}}{\text{NPV}_n - \text{NPV}_{n-1}} \right). \tag{2.16}$$

Solving this is more computationally expensive than finding the NPV, LCOE or PP. While the difference may be negligible if only performing the computation a small number of times for finalised array design, it may become a significant hindrance when used as the functional for a large number of optimisation and adjoint evaluations.

2.2.7 CAPEX versus OPEX

The expenditures in each year, Ex_i, can be split up according to whether they occur before or after the array goes into production. Businesses typically describe all costs involved acquiring assets and setting up the business as Capital Expenditure (or

CAPEX). Vasquez et al. [99] estimated that the capital costs for a tidal stream array break down as 41% device costs, 26% foundations costs, 15% installation costs, 13% cable costs and 5% grid connection costs. By comparison, the MeyGen1A project found that the main contributors to the CAPEX were turbines (39%), onshore balance of plant (BoP, the supporting components and auxiliary systems, 19%), offshore works (13%) and substructures (11%) [67].

In the cash flow model described in (2.1), the CAPEX would typically be

$$\text{CAPEX} = \sum_i \text{Ex}_i, \ \forall i \ \text{ s.t. } \ t_i = 0, \tag{2.17}$$

where t_i is the number of hours of generation in year i i.e. the costs incurred before the array is operational. In more complicated arrays the CAPEX may include the expenses associated with upgrading physical assets, for example in arrays which expand from small demonstrator arrays to larger scale farms, the installation costs are still considered to be CAPEX, even if they are incurred after the first turbines start generating. For simplicity, in this work it will be assumed that all the capital expenditures occur in year $i = 0$ and that the array will start production in year $i = 1$. This is an easy assumption to remove when applied to real tidal arrays, by developers who have full cash flow models of their anticipated costs. CAPEX will be represented in the following models as $\text{CA} \equiv \text{Ex}_0$.

The expenses of normal business operations are called the operational expenditure (or OPEX). OPEX is measured on an annual basis, here starting from year $i = 1$ up to $i = L$, the operational lifetime of the array, and will be represented in the following models as O_i. Typically OPEX includes costs such as rent, payroll, insurance and maintenance. For a tidal farm this may include standard inspections, maintenance, repairs and costs of vessels and staff to perform these tasks. The MeyGen 1A project reported a £1.4m OPEX per year in its four turbine array, with its main components being lease and insurance (32%), unplanned maintenance (21%), planned maintenance (15%) and spare parts (14%) [67].

The final costs to be considered in a tidal energy deployment are the decommissioning costs. These are the costs or removing the turbines, anchoring and cabling from the water and safely ending the operation. There are a number of different ways in which these costs may be covered - from upfront cash security to accrual or insurance[124]. Since these costs could either be incurred through an agreement as part of the CAPEX, or will be delayed to after the final year of operation $i = L + 1$ it is not clear how to include these costs in an academic model at this time. If

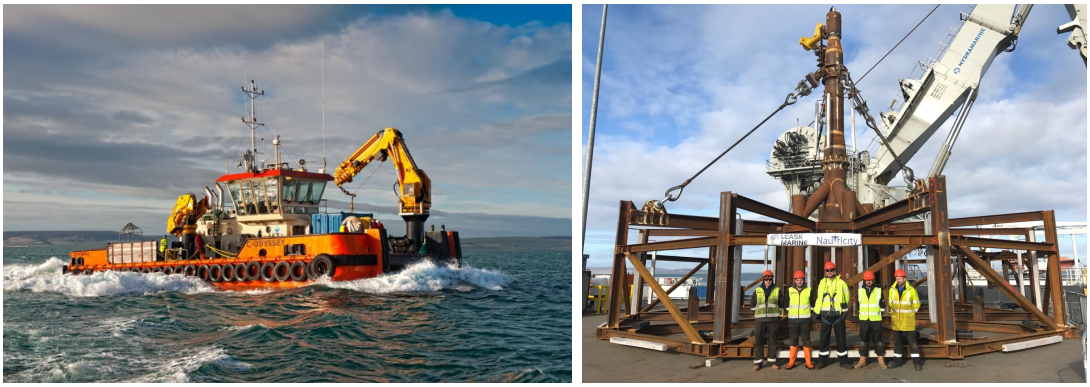

(a) (b)

Figure 2.2: (a) The Leask Marine Ltd. MV C-Odyssey, an example of a multi-cat vessel used for installation and removal of turbines. (b) The Leask Marine Ltd. team after the successful removal of a Nautricity turbine's base with a multi-cat vessel.

incurred in year $i = L + 1$ the costs are likely to have very little impact on metrics based on net present value analysis because the cost will be heavily deprecated due to discounting. Due to minimal present value impact and the large amount of uncertainty about how this will be finances for large-scale tidal stream arrays and limited information to base estimates on how much it will cost, this is not included in the economic assessments in this thesis at this point in time.

An investigation into decommissioning costs by Marine Scotland [124] found that many developers acknowledged that decommissioning had not been an explicit consideration on the design of devices, however a focus on reducing the cost of installation lead to designs which were inherently easier to remove. Technological advances which reduced the decommissioning cost as a by product included devices designed to be towed to (or from) location and devices that could be removed in modules for maintenance. Full decommissioning plans are not enforced by regulators at the marine licensing stage because the design may not be fixed. [124] found that the main cost driver is the cost of the vessels required to remove the infrastructure. Many tidal developers have designed devices to allow installation and removal with low cost multi-cat vessels, for example see Figure 2.2. In demonstrator arrays material costs are low as many parts can be repurposed or stored. As arrays become larger the cost of dismantling and recycling the devices and foundations is likely to increase.

[124] estimated that floating tidal has a decomissioning cost of approximately £100,000 per device, with gravity-base foundations costing £200,000 per device and monopile

foundations costing £500,000 per device. However, it is noted that these estimated could change substantially as design concepts and vessel rates change. Predicting these costs a couple of decades into the future leaves a lot of uncertainty for developers.

2.2.8 Other metrics to consider

Environmental impact

The metrics described in the sections above all focus on the financial performance of a tidal array, however there are many other factors to consider. One of the most important, for ensuring that developments get consent to deploy, is minimising the negative environmental and ecological impact of the array. Tidal energy's sustainable electricity benefits must be shown to outweigh any potential environmental detriments, the extent of which may vary greatly location to location and therefore needs to be appropriately assessed. The ocean environments in which tidal energy is to be installed are already significantly impacted by human activity, with no region complete unaffected by our influence[125]. Marine environments can be highly sensitive to potential effects of installing tidal arrays, including changes in turbidity [126], noise levels [127], and long-established tidal patterns [128].

There have been numerous studies on environmental impact assessment in tidal and other ocean energies [129, 70, 130]. The most significant effects to account for are damage to habitat and health of marine species, and sediment transport. While the problem of assessing the environmental impact of a tidal stream array is well researched, there are limited studies on how to optimise array design whilst accounting for both the economics and the environmental impact. A notable and novel example of using power and environmental impact for multi-objective optimisation is du Feu et al. [112, 104].

[112] uses the extent to which an array alters the flow in the region as a proxy for the environmental concerns and demonstrates a method of finding a Pareto front where there is a trade-off between the conflicting objectives of maximising array yield while minimising the change in the hydrodynamics. This approach is useful for minimising the negative impacts on marine ecosystems because alteration of the tidal flow can affect the dispersion of propagules, material used by marine organisms to propagate between areas and a key part of many marine life-cycles, [69] and there are habitats which are sensitive to flow speed, direction and level of turbidity, for example scallop

nurseries [126]. [112] combined environmental impact assessment at the array design stage by maximising a functional of the form $J = w_p \times P(m) - w_i \times I(m)$, where $P(m)$ is the power generated by the set of turbine locations, m, and $I(m)$ is the impact of those turbines, measured as the array's effect on the ambient flow velocities. The relative importance of each term is modelled by w_p and w_i, the power and impact weights, respectively. However, only a limited set of weighting were tested ($w_p = 1$ and $w_i = 0$, $w_p = 0$ and $w_i = 1$, $w_p = 1$ and $w_i = 1$) and realistic values for the weightings were not discussed. A further limitation of this approach is that the number of turbines was fixed, so varying the number of turbines would allow for greater exploration of the trade-off between power, and therefore profit, and environmental impact.

[104] extended upon the approach of [112], however it optimised the functional $J = w_p \times \text{Profit}(d) - w_h \times H(d)$, where $H(d)$ is a measure of habitat impact, w_h is the relative importance of the habitat impact, and the turbines are instead modelled by a continuous density function, d, which allows for the number of turbines and their locations to be optimised simultaneously. Profit(d) takes the same format as the break even power optimisation described in Section 2.2.2. The habitat impact, $H(d)$, was found through maximum entropy modelling, which was used to generate habitat suitability maps for species that respond to changes in bed-shear stress. The maximum entropy was calculated using MaxEnt, an open-source habitat suitability model [131], and was used to evaluate the impact of a tidal array on the distribution of a specific species at each timestep of the hydrodynamic model. This study investigated the impact of different tidal arrays on two species, the acorn barnacle (Balanus crenatus) and the brown crab (Cancer pagurus), because the former prefers higher flows speeds and tends to react negatively to reductions in bed shear stress and the latter prefers lower flow speeds and reacts positively to reductions in bed shear stress. The relative importance of habitat suitability compared to profit is modelled by the choice of weights of each corresponding term in the functional. The results were demonstrated on four example sites, including the Pentland Firth, location of the world's highest capacity tidal stream array, at the time of writing. While this paper demonstrated a useful method for incorporating the concerns of habitat suitability into the functional, each example site was only demonstrated for one species at a time, either the corn barnacle or the brown crab, and more work needs to be carried out to automate the combination of economics and environmental impact optimisation.

[71] compared the energy extraction of small-scale (five turbine) array designs that

considered environmental constraints compared to those that do not. They found that taking into account environmental constraints decreased the overall power generation of the optimised array design slightly. However, they developed a flexible framework that allowed power maximisation while remaining within the bounds of easily defined constraints to changes in the flow and seabed stress.

The present work does not include environmental impact in the economic analysis and optimisation methods discussed. As demonstrated by the studies discussed above, minimising the environmental impact often leads to a trade-off where the array yield, and therefore profitability, are reduced. It is acknowledged that further work should combine the economic optimisation methods with the environmental optimisation techniques outlined in works such as [112, 104, 71], but this would require overcoming the limitations of each study (for example by studying the impact of a broader range of species) and selecting weightings for the trade-off between optimal economics and environmental impacts.

Location based costs

In Section 2.2.2, expenditure is assumed to be a function of the number of turbines, but in practice is it likely to depend on their location too. Two of the most significant factors in tidal energy costs that vary with location are the depth and the distance to shore [99], and both have been demonstrated to be two of the main cost drivers in offshore wind [132]. As both increase the installation and maintenance of the turbines become harder to carry out, and the costs increase. They also affect the environmental loads to which the turbines are exposed, the cable costs and electricity losses.

There have been some studies which optimise the design tidal arrays based on the location dependent costs. On a macro-level Vazquez et al. [99] assesses the spatial distribution of capital costs, coupled with a Navier-Stokes flow solver, to balance the capital investment against the energy productions and find a map of the LCaOE (levelised capital cost of energy). This is used as a decision parameter to identify the best sites to install tidal stream arrays. This can be done as a precursor to the array optimisation methods where the number of turbines and their individual locations are optimised.

Studies in which the micro siting of tidal stream arrays is optimised with respect to location-varying costs include [100] and [105]. [100] and [105] focus on optimisation

of a given number of turbines, where the functional is based on an approximation to profit. [100] includes a model for cable costs per metre and support structure costs that depend on the nature of the seabed, the depth and the peak moment resistance required. [105] optimises the income as a function of power minus the cost as a function of cable length. Both use genetic algorithms to minimise the cable length.

While important, the costs that depend on the individual turbine locations make up a smaller variation in the overall costs than those due to changes in the number of turbines. Vasquez et al. [99] estimated that the cabling costs make up 13% of the CAPEX for a typical tidal stream array, whereas it accounted for 9% of the CAPEX and none of the OPEX breakdown reported by MeyGen Phase 1A [67]. Culley et al. demonstrated an optimisation of a tidal array in Orkney, where they optimised for power alone, maximisation of financial return including cable costs, as well as the maximisation of financial return where the cost of the cable per unit length is doubled; in each case the returned cable lengths of the optimal arrays were found to be 9.70km, 9.23km, and 8.71km respectively [105]. So even when optimising for an exaggerated cable cost, including the cabling in the functional in this case only reduced the cabling cost by around 10% and therefore the overall cost in the order of 1%.

Optimisation while accounting for location varying costs can be very computationally expensive, and usually comes at the sacrifice of other modelling capabilities. For example, [100] uses a genetic algorithm to optimise the locations while taking into account variations in cable and support structure costs with location, but only within the framework of a relatively simple 2D wake deficit based model, and only for uniform flow in one direction. Optimisation of the cable routes can produce savings that are significant, but are a lower priority compared to optimising the balance between power and number of turbines. It is therefore suggested in the following work that location varying costs need not be included as another variable in very computationally expensive micro-siting optimisation. Instead location based costs can be taken into account either at the macrositing stage, as demonstrated by [99], through exclusion zones, where a maximum depth or steepness requirement is enforced [133], or post micro-siting, for example where a genetic algorithm or travelling salesman type problem [105] is used to minimise the cable length for a given set of turbine locations.

Furthermore, currently there is not enough publicly available information to build a model that can predict the costs as a function of different distances to shore, depths and number of turbines, so this thesis just focuses on varying the latter.

Furthermore the sites selected for first-generation tidal turbine arrays are usually a relatively short distance to shore and require depths of 25–50m [114, 36]. It is anticipated that later generations of tidal stream will be designed for operation in deeper water, where modelling of location-varying costs will become more crucial [114].

2.3 Cost reduction pathways

Estimates from the Offshore Renewable Energy Catapult (OREC) in 2018 anticipated that tidal stream energy costs in the UK could come down by 70% from a representative LCOE of £300/MWh to £90/MWh as the installed operational capacity rises from 10MW to 1GW [12]. Part of this reduction in costs is due to saving time and cost through "learning rates", part is due to "economies of scale", such as moving to larger rotor and higher rated devices, and part is due to the move to larger scale arrays which benefit from "economies of volume". It is important to be aware of the distinction between the different types of cost reduction, because they present opportunities at different stages of array development to cut to cost of energy. Some cost reduction pathways can be exploited through optimal location and numbers of turbines and others cannot. Learning rates can only be exploited by delaying the deployment of an array to avoid the first mover disadvantage, and the latter two can be exploited by choosing the optimal turbine specification and the optimal number of turbines respectively. Learning cost reductions versus economies of volume can be distinguished between, as costs falling due to an increase in installed cumulative capacity versus costs falling due to increased number of turbines within one array [98]. The following work using the same terminology of each type of cost reduction as the OREC report on tidal stream and wave energy cost reduction [12] and a study by Coles et al. on mechanisms for reducing the cost of tidal stream energy, applied to the context of the expansion of the MeyGen tidal array from currently operational Phase 1A to the plans for Phase 1C [49].

2.3.1 Learning rates

Learning rates encompass all cost reductions where the costs of an industry fall with time due to increased knowledge. This will not be included in the following models as it is assumed that developers have a fixed level of experience at the time

they are optimising their array design. However, it is worth considering that the bounds for costs presented will likely become overestimates with time, and that sources for typical values to use in the following models will be more reflective of the current state of the industry if more recent. The extent to which learning rates will impact costs can be estimated by observing what has happened in other industries, such as wind power, where costs are decreasing as the cumulative installed capacity increases. They are typically represented by a percentage reduction in costs with each doubling in cumulative capacity. An Arup produced 'Review of Renewable Electricity Generation Cost and Technical Assumptions' estimates that the doubling of installed tidal capacity will result in a 13% CAPEX cost reduction and a 19% OPEX fall [134], whereas OREc assumed 13% for CAPEX but a more conservative learning rate of and 11% for OPEX [12]. The impact of learning rates are most significant in the near term for fledgling industries like tidal, because when the cumulative installed capacity is so low it is easier for it to double. Learning rates can be accelerated by collaboration, but hindered by protection of intellectual property preventing these opportunities. Cost reduction through learning can be grouped into two main categories; learning-by-doing and learning by innovation.

Learning-by-doing cost reduction relates to project developers repeating processes with each array that they install, thus learning how to optimise procedures and minimise costs. Examples of cost reductions through learning include better planning of operations and maintenance using operational and weather data, supply chain optimisation and automation, and familiarity with installation sites [12]. Standardisation of foundation and component design will become possible as the number of devices deployed increases, so costs for the industry will fall.

Repeat installations of tidal arrays can also lead to improved proof of concept, resulting in increased confidence from investors and a reduction in the cost of capital as projects are seen as less risky. The cost of capital is the required return for a project to be worthwhile, for internally financed projects it is the cost of equity (mostly comprising of dividends), and for externally finance projects it is the cost of debt (the effective interest rate paid on debts). The weighted average cost of capital (WACC) is used to combine the cost of equity and debt into one figure and it is often used as the discount rate for present value analysis of future cash flows, such as the NPV and LCOE models in (2.10) and (2.13) respectively. Currently tidal projects are financed through a combination of grant support and private finance, and tidal has a far higher cost of capital than the more established offshore wind industry. Increased confidence from financial institutions will see a rise in financing from

commercial debt too. OREC estimated the cost of capital for 10MW cumulative capacity is 10% and that it will fall to 8.4% by 100MW, 8.0% by 200MW and 7.1% by 1GW [12]. They believe that these reductions can be achieved through increasing the proportion of debt finance (which has a lower interest rate of around 4.5%) and reducing the rate of equity premiums (from around 10% to 8%). The more familiar and stable the technology is perceived to be, the greater the cost of capital reductions that can be obtained. OREC noted that each 1% reduction in WACC (and therefore discount rate) resulted in a 6% reduction in LCOE in their studies. MeyGen released their lessons learnt report from the 1A construction phase [21] which found that the turbines were exceeding their contractual key performance indicators such as average power coefficient (8% increase), capacity factor (20% increase) and lifetime energy yield estimate (18% increase). These substantial improvements demonstrate a reduced risk to investors and could lead to a reduction in the cost of capital for future tidal arrays.

Learning by innovation covers cost reductions due to technological improvements such as improved performance and reliability of individual components. Some of these innovations may arise from the experience gained in the more mature offshore oil, gas and wind industries, and will therefore reduce the level of perceived risk to investors. Innovation may reduce the operational costs or improve the structure or the availability of the turbines. For example, a consortium led by ITPEnergised, has designed a customised barge for installing turbines which may allow the industry to move away from hiring expensive dynamic positioning vessels. These barges are anticipated to be much cheaper for installation of larger scale arrays [135]. Leask Marine Ltd have successfully used multi-cat vessels to install and remove multiple tidal turbines and their subsea bases, demonstrating the potential for multi-cat vessels to replace the need for multi-million-pound large dynamic positioning drilling ships and jack-ups. Improved electrical connectors are also expected to reduce the cost of tidal in the short term. Wet mate connectors are a technological development that allow the cable connections to the turbines to be made sub-sea rather than on the vessel, thus simplifying the installation on operations. They allow turbines to be installed onto their foundations in less than 60 minutes, and reduce the installation cost by 65% compared to a turbine with a dry mate connector where the export cable must be brought onto the vessel to connect it to the turbine [49]. Again the following models will not include learning by innovation, because this work is aimed at developing a method to assist developers in optimising array design given the technology options currently available to them.

2.3.2 Economies of scale

The following work uses the same distinction between the economies of scale and volume as [12, 49]. Economies of scale is used to exclusively refer to the cost reductions gained from moving to larger rotor, higher wattage turbines (i.e. increased scale of the turbines themselves) and not to the effects of increasing the number of turbines.

Coles et al. [49] demonstrated the significant impact that economies of turbine scale could have, by investigating the predicted yield of the 1.5MW rated AR1500 device compared to the 2MW rated AR2000. The AR1500 is currently operational as part of the MeyGen Phase 1A, the AR2000 is the next generation device by SIMEC Atlantis Energy, which is expected to be deployed in future phases of the MeyGen project. Both devices are capable of accommodating a range of physical options, but Coles et al. assessed an 18m diameter AR1500 with a hub height of 14m to a 20m diameter AR2000 with a hub height of 15m. Coles et al. [49] estimated that economies of turbine scale could lead to a reduction in LCOE of 17%, 20% or 23% due to the 29% uplift in anticipated yield when progressing from the AR1500 to the AR2000, depending on whether the CAPEX increases by 10%, 5% or 0% between the two devices. It is difficult to predict how much CAPEX will increase between the turbine designs, because the costs are commercially sensitive. They are likely to increase due to higher loading from larger blades, increased generator size and hub height, but the AR1500 was designed to meet conservatively high loads, and through the proof of concept in MeyGen 1A, the AR2000 may not require as conservative a design. However, for each of the CAPEX scenarios investigated, it was shown that small achievable changes to the turbine specification can result in significant near-term reductions to the LCOE of tidal energy.

Foundation costs also make up a significant proportion of the lifetime costs of an array, so some developers plan to use several rotors on the same supports to spread the foundation costs over a higher rated power, and achieve economies of scale [136].

2.3.3 Economies of volume

Economies of volume are found when costs can be spread across more turbines in an array; when the installed capacity in MW for a potential tidal site is increased, the effective cost per MW decreases. For example, the cost of mobilising (preparing the vessel) and demobilising (unloading and returning of the vessel) for offshore

operations, installations and maintenance falls per turbine as the number of turbines increases. For small arrays these activities take up a significant proportion of the total vessel time. [49] demonstrated that in MeyGen 1C the anticipated number of mobilisation and demobilisation days per turbine falls from 1.13 to 0.83 if the number of turbines increases from the current 4 to a planned 36.

There are fixed costs in tidal array development, such as the site evaluation and substation costs, which lead to a reduced cost per MW when they are split across a greater number of turbines. Potential cost reductions due to economies of volume can also include bulk order discounts, reduced production costs per unit and savings due to serial production and standardisation of common components. For example, dedicated mass-manufacturing facilities for large-scale turbine orders will be more cost-effective, but this is not possible for smaller arrays. Also, inter-array cable costs may increase approximately linearly with the number of turbines but the costs of a substation and the much more expensive export cables to shore will be roughly fixed, so the more turbines generating power, the lower the total cable cost per MW.

To date tidal stream has only been demonstrated in arrays with small numbers of turbines; the world's first arrays being three turbines by Nova Innovation off the coast of Shetland and four turbines installed by Meygen in the Inner Sound of the Pentland Firth. Even without cost reductions due to experience or improved technology, substantial cost reductions could be seen in the immediate term, just by moving from these demonstrator sized arrays to commercially sized ones.

It is worth noting that while costs are expected to fall with time and volume, there are more significant cost reductions to be made while tidal energy is a relatively new industry. The cost reductions as the tidal industry advances from small demonstrator arrays to the first large-scale commercial arrays will be significant but as the industry develops the potential to reduce costs will diminish. Some aspects of tidal arrays are already well-established, building on what can be learnt from other offshore energies. For example, electrical connection to the grid (which makes up around 5% of the lifetime costs of tidal arrays) has less potential for dramatic cost reduction due to developments already being carried out by the offshore wind industry, so the learning reductions have to some extent plateaued [136]. However, there is still potential for significant economies of volume to be achieved on these costs through subsea hubs which will allow the electrical connection of multiple devices resulting in cheaper configurations.

Expenditure break down

The capital costs are split into fixed costs and turbine-dependent costs, to help include economies of volume into the model. There are some costs that need to be overcome no matter how many turbines are installed and some that increase linearly with number of turbines. For example, the inter-array cabling may be considered a turbine-dependent cost because the length of cables will be proportional to the number of turbines. However, the export cable will be a fixed cost, since there will always need to be a cable that transports power generated from the substation to shore, regardless of number of turbines. The CAPEX can therefore be written as

$$\mathrm{Ex}_{i=0} = \mathrm{CAPEX} = \mathrm{CA}_f + \mathrm{CA}_t \times n_t. \tag{2.18}$$

Similarly the operational expenditure are the costs incurred every year after installation and are assumed to linearly increase with number of turbines. Furthermore, this study assumes that the OPEX is the same year on year, for simplicity, however developers could use this model with costs that vary very easily. For example, some components of the array may need maintenance every year whereas others may need maintenance every few years, causing a routine increase in costs. By splitting the OPEX into fixed and turbine dependent costs it can be written as

$$\mathrm{Ex}_{i>0} = \mathrm{OPEX} = \mathrm{O}_f + \mathrm{O}_t \times n_t. \tag{2.19}$$

The basis for the linear relationship between costs and number of turbines assumed in (2.18) and (2.19) is that many components of the cost of a tidal energy array will be charged at a flat initial rate with a part that linearly increases with the number of turbines. For example vessels hired to install and maintain turbines may be charged at an initial flat rate, plus a multiple of the number of days or hours that it must be hired for, which increases approximately linearly with the number of turbines. Or to manufacture the turbines themselves the initial cost of designing and certifying a turbine may be independent of the number used, but the material and labour costs increases with the number of turbines. There are of course many non-linearity's in the costs, however these average out to an approximately linear relationship overall, especially at higher numbers of turbines. For example, some subsea substations can connect to seven turbines, so the substation cost per turbine is lowest when the number of turbines is a multiple of seven [30]. This non-linearity

is significant for lower numbers of turbines, i.e. the cost of two substations for eight turbines is substantially higher than the cost of one substation for seven turbines (a ratio of 0.25 vs 0.143), but the non-linearity diminishes for higher numbers of turbines i.e. the cost of 11 substations for 71 turbines is not much higher than the cost of 10 substations for 70 turbines (a ratio of 0.155 vs 0.143).

This expenditure break down results in a more realistic representation of economies of volume than modified break even power representation given in (2.8) because the costs per MW from (2.8) decrease linearly with number of turbines, whereas the costs per MW from (2.18) and (2.19) decrease reciprocally with the number of turbines, as shown in Fig. 2.3 and discussed in greater detail in Section 2.4.1. This reflects the fact that economies of volume causes the costs per MW drop the most significantly for small numbers of turbines and then the benefits of economies of volume diminish for larger scale arrays. This linear assumption is used in other tidal and wind energy cost models, including a notable study by Higgins and Foley, whose cost per MW model, which is demonstrated to be equivalent to a linear cost model in Section 2.4.2, is based on real-world cost data taken across the more mature wind energy industry [2].

2.3.4 Revenue

In order to build a complete financial model, income must be accurately predicted, as well as expenditure. For a tidal farm, income depends primarily on two factors – the net energy output and the tariff at which this energy is sold to the grid (which may well be higher than the market price due to subsidies and other government schemes).

Since early stage tidal energy deployments often receive a fixed price per MWh, through subsidy schemes described below, most hydrodynamic models used for optimisation of tidal array design produce an average power estimate for the array, P_{avg}, rather than a time varying prediction of the instantaneous power over the whole lifetime. Therefore, the energy generated in each year is assumed to be constant, such that $E_i = E \ \forall i = 1, \ldots, L$. In practice, even when evaluating metrics such as NPV and LCOE on an annual level, lunar nodal cycles cause variations in the yearly average yield over an 18.6 year cycle [115, 116]. Since the earlier years of generation count more towards these metrics, due to discounted cash flow, this could lead to an effective difference in the performance of the array depending on which stage of the tidal cycle it begins generating in.

Assuming a constant power, P_{avg}, year on year, the annual energy generation, E_i, can be found by multiplying the number of hours of generation each year, t_i, with the average power, to find the gross energy output in MWh;

$$E_i = t_i \times P_{\text{avg}}. \tag{2.20}$$

t_i can be approximated as the number of hours in a year minus the anticipated number of hours of downtime for maintenance. The MeyGen Phase 1A reported an average availability of 95% in 2020 (having entered its operational phase in 2018), with a higher availability of 98% in the summer compared to 90% in the winter [67]. Increased experience in planning and predicting operations and maintenance could see these downtime windows decrease and availability increase in future tidal projects. When used in industry the availability could be modelled to depreciate throughout an array's lifetime, to account for decreases in efficiency as devices age, e.g. due to component wear or bio-fouling. This effect has been well documented in the wind industry [119, 118]. However, for simplicity it can be kept constant for initial investigations. This is a reasonable assumption because there is limited information on the rate of degradation of tidal stream arrays, with few years of operational experience to date, and due to the high discount rate currently used in tidal the latter years of the array's generation (where degradation would be highest) contribute significantly less to the NPV and LCOE. Finally, the net energy output can be found from the gross energy output by a factor, C_E, to account for electrical efficiency losses.

The net energy output can be multiplied by the electricity tariff, T_e [£/MWh], to find the expected revenue of a tidal array in a year. The market price may fluctuate over days and years, however government schemes can often make this value more predictable and stable, the details of these schemes are discussed below in Section 2.4.3. In initial economic models it can be assumed that arrays receive a constant price per unit energy, however future models could estimate P_{avg} over smaller time scales and use this in conjunction with a fluctuating energy price to determine the impact on revenue, cf. related optimisation work in the context of tidal lagoons [137].

According to the simplifications of the economic model made in (2.18), (2.19) and (2.20), the model for LCOE from (2.13) can be rewritten as

$$\text{LCOE} = \frac{\text{CA}_f + \text{CA}_t \times n_t + \sum_{i=1}^{L} \frac{O_f + O_t \times n_t}{(1+r)^i}}{\sum_{i=1}^{L} \frac{C_E \times E_i}{(1+r)^i}}. \tag{2.21}$$

2.4 Estimate of inputs to economic models

The following section compiles a series of tidal energy cost estimates and reformats them appropriately for use in a LCOE model such as (2.21). The main inputs needed are CAPEX split up into fixed, CA_f, and turbine-dependent, CA_t, components, OPEX split up into fixed, O_f, and turbine-dependent, O_t, components, lifetime, L, and the discount rate, r. Data from different sources is discussed below along with the methods used to convert this into the format needed, where total CAPEX and OPEX can be broken down into the forms shown in (2.18) and (2.19) respectively. Some information from the offshore wind industry is used to guide estimates for tidal and to guide the relationship between estimated values.

2.4.1 Relationship between cost and size of array

Firstly, information on how CAPEX and OPEX in the wind industry varies in relation to number of turbines is used to justify the relationship assumed in (2.18) and (2.19). Wind is the more established industry and can therefore be used to help predict the cost reductions that can be realised through economies of volume for tidal. CAPEX and OPEX values are commercially sensitive and hard to establish, and while there have been a number of studies which have communicated with many different developers of varying sizes [12], they often anonymise this data by converting to a metric that is independent of array size, such as cost per MW installed capacity.

Much of the available information found in this literature review on the costs of tidal turbine arrays is given as a CAPEX/MW, for an array of a certain rated capacity. Figure 2.3 shows how the total CAPEX increases with number of turbines if the linear relationship given in (2.18) is assumed. This can be used to show the relationship between CAPEX/MW and number of turbines, by dividing (2.18) by the total capacity of the array (n_t turbines, each with a rated capacity of MW_t) to get

$$\text{CAPEX/MW} = \frac{\text{CA}_f + \text{CA}_t \times n_t}{n_t \times MW_t}. \tag{2.22}$$

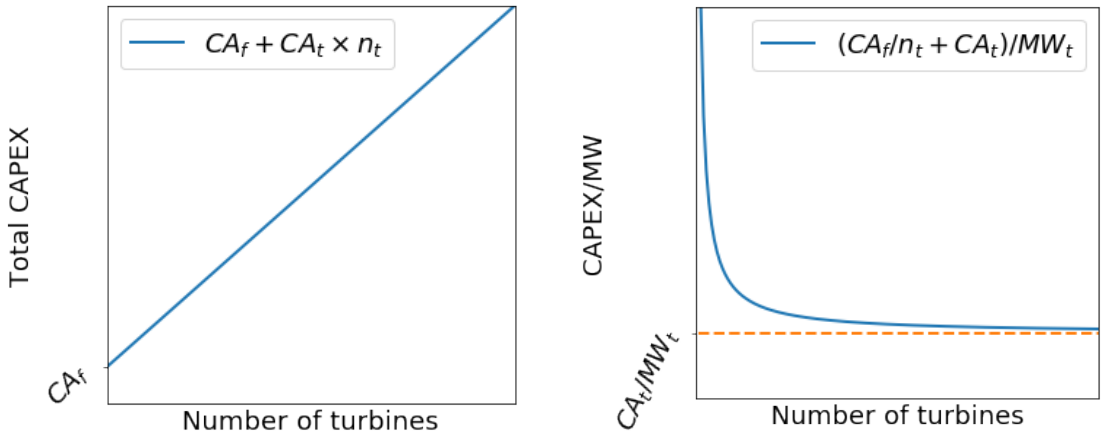

(a) (b)

Figure 2.3: Variation in the total CAPEX of an array and the CAPEX per MW installed capacity as functions of the number of turbines, according to (2.18).

Since there are two unknowns in each of (2.18) and (2.19), two simultaneous equations must be used to solve each in order to find CA_t, CA_f, O_t and O_f. In order to convert from the CAPEX/MW to CA_f and CA_t values, (estimates for) the CAPEX/MW for arrays of two different sizes is needed, allowing the conversion to total CAPEX, which would give two points on the line in Figure 2.3a) and allow the gradient (i.e. CA_t) and the intercept (i.e. CA_f) to be calculated. Alternatively, if the total CAPEX is only known at one array size then the ratio of the fixed component of CAPEX over the turbine-dependent component of CAPEX, $\mathrm{CA}_f/\mathrm{CA}_t$, must be known or estimated. The ratio can be used to split the total cost into each of its components, such that $\mathrm{CAPEX} = (\frac{\mathrm{CA}_f}{\mathrm{CA}_t} + n_t)\mathrm{CA}_t$. The same is needed for operational costs to find O_f and O_t, however limited OPEX data is available, since very few tidal arrays have been in operation and only for a relatively short period, so sometimes OPEX must be estimated as a percentage of CAPEX.

Method 1: Knowing two data points

If the total CAPEX is known for two values of n_t, e.g. n_{t_1}, n_{t_2}, $\mathrm{CAPEX}(n_{t_1})$ and $\mathrm{CAPEX}(n_{t_2})$, then the following simultaneous equations can be solved:

$$\mathrm{CAPEX}(n_{t_1}) = \mathrm{CA}_f + \mathrm{CA}_t \times n_{t_1}, \tag{2.23}$$

$$\mathrm{CAPEX}(n_{t_2}) = \mathrm{CA}_f + \mathrm{CA}_t \times n_{t_2}. \tag{2.24}$$

The difference of these two equations can be solved for CA_t, such that

$$\mathrm{CAPEX}(n_{t_2}) - \mathrm{CAPEX}(n_{t_1}) = \mathrm{CA}_t \times (n_{t_2} - n_{t_1}) \tag{2.25}$$

$$\Rightarrow \mathrm{CA}_t = \frac{\mathrm{CAPEX}(n_{t_2}) - \mathrm{CAPEX}(n_{t_1})}{n_{t_2} - n_{t_1}} \tag{2.26}$$

CA_f can then be found from (2.23) and the CA_t value just found.

The turbine-dependent and fixed components of the OPEX can be found similarly by evaluating (2.19) at two values of n_t and similarly rearranging.

Method 2: Knowing the ratio of fixed to turbine-dependent costs

Alternatively, if the ratio of the fixed costs to the turbine-dependent costs is known, such that

$$\mathrm{CA}_{ft} \coloneqq \frac{\mathrm{CA}_f}{\mathrm{CA}_t}, \tag{2.27}$$

then the total CAPEX only needs to be known for one value of n_t, e.g. n_{t_1} and $\mathrm{CAPEX}(n_{t_1})$. The turbine-dependent CAPEX, CA_t, can be found by solving

$$\mathrm{CAPEX}(n_{t_1}) = \mathrm{CA}_{ft} \times \mathrm{CA}_t + \mathrm{CA}_t \times n_{t_1} \tag{2.28}$$

$$\Rightarrow \mathrm{CA}_t = \frac{\mathrm{CAPEX}(n_{t_1})}{\mathrm{CA}_{ft} + n_{t_1}} \tag{2.29}$$

and CA_f is simply found from

$$\mathrm{CA}_f = \mathrm{CA}_{ft} \times \mathrm{CA}_t. \tag{2.30}$$

The same relationship can be applied for OPEX.

2.4.2 Cost data available in literature

Using the two methods described above, a literature review of publicly available cost information for tidal stream arrays has been performed. While there are many studies on the economics of tidal energy, not all of them are useful for building an economic model that is flexible to array size. For example, if given the cost of energy as an LCOE, there is rarely enough information to back calculate the raw CAPEX and OPEX values in order to predict how much impact changing the

number of turbines would have on the array economics. This would make it very difficult to model the cost reductions that can be found through economies of volume. Instead most studies collated in this work refer to raw CAPEX and OPEX values or CAPEX/MW and OPEX/MW estimates.

Higgins and Foley: The evolution of offshore wind power in the United Kingdom

Firstly the assumptions made in (2.18) and (2.19), and demonstrated in Figure 2.3, can be validated by comparing them to actual trends found in the wind industry. Higgins and Foley [2] performed a review of offshore wind power in the United Kingdom, where they aggregated cost data from multiple wind farms and presented anonymised cost information in the form of a normalised CAPEX/MW. Higgins and Foley [2] investigated how the costs of offshore wind farms increases with cost per device and distance from shore, and decreases with number of turbines. Figure 2.4(a) shows the relationship they found between number of turbines and normalised CAPEX/MW, and how this varies depending on the price of individual turbines. The costs are normalised by the CAPEX/MW of an array consisting of ten turbines each costing £2m, so for example these figures show that if there are ten turbines but they each cost £4m, the CAPEX/MW of the overall array is 36% higher.

Figure 2.4(b) shows that when multiplying this by the number of turbines to find normalised total CAPEX values, a linear relationship is obtained, further justifying the relationship defined in (2.18). The exact values of CA_f and CA_t cannot be found, since the information was normalised due to commercial sensitives. However, it can be shown that for arrays made of turbines which cost $£4$ million, $£3$ million and $£2$ million, the fixed component of CAPEX would be 2.6, 3.1 and 3.9 times the turbine-dependent component of CAPEX respectively. The cheaper the devices become the more important economies of volume are (since the fixed costs make up a bigger portion of the overall costs). These CA_{ft} values can be used in method 2 for calculating the cost components.

Higgins and Foley also presented how the CAPEX/MW would change with number of turbines for different distances to shore – 5km, 15km, 25km, 35km, 45km, 75km and 150km. The southern part of the Pentland Firth, which passes between Stroma Island and the Scottish mainland is only approximately 3km wide. By comparison the narrowest distance between Alderney and Cap de la Hague is 15km wide. Therefore only the $textCA_{ft}$ ratios from the CAPEX curves defined by data from

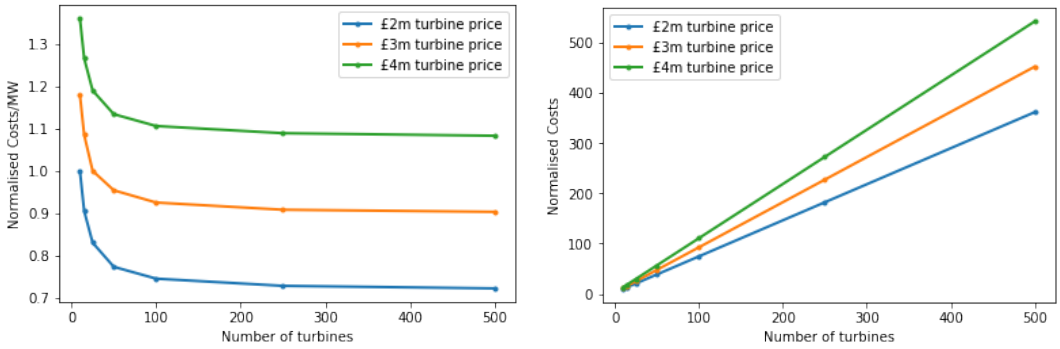

(a) (b)

Figure 2.4: (a) Variation of the normalised capital costs per MW installed capacity with the number of turbines from [2]. (b) The corresponding linear relationship between total CAPEX and number of turbines, for wind turbine arrays where each turbine costs £2, 3 or 4 million.

turbines 5 to 15km from shore are considered, which have a CA_{ft} value of 2.3 and 2.7 respectively. As the distance to shore increases the CA_{ft} ratio increases, since economies of volume become more important to overcome the fixed costs of long cable routing and shipping distances. At 150km to shore $CA_{ft} = 8.4$, however, this distance is very unlikely for a tidal energy site in the foreseeable future, since the required high energy flows are generally accelerated near islands and other coastal features. Therefore upper and lower bounds of $2.3 < CA_{ft} < 3.9$ were used in method 2, for calculating CA_f and CA_t separately when given one fixed CAPEX or CAPEX/MW value. There is limited information on OPEX varying with the size of the array so it is assumed that the ratio remains the same. i.e. $O_{ft} \coloneqq CA_{ft}$.

Culley et al.: Optimisation of Cable Costs

One easy-to-visualise example of how capital costs can be split into a fixed and turbine-dependent component is cable based costs. Culley et al. [105] investigated the optimisation of cable routing and array layout and used estimates for the total cabling costs of between £254.51 per meter with a fixed £5.16 million vessel mobilisation fee and £862.48 per meter with a fixed £6.22 million vessel mobilisation fee. These estimates were based on the costs given for wind energy from Green et al. [138] in 2007, adjusted for inflation to 2016 levels and with an assumed 51% rise in costs applied, in line with the 51% rise in wind energy costs between 2006 and 2010, as outlined by Heptonstall et al. [139]. Depending on the weighting of the cable cost in the functional they found optimised configurations of their model of eight turbines

with total cable lengths of 9.70km, 9.23km, and 8.71km. This leads to a total cost per metre of $254.51 \times 8.71 \times 1000 = £2.22$ million to $862.48 \times 9.7 \times 1000 = £8.37$ million, or a cost of £0.28 to £1.04 million per turbine. Therefore for the cable costs alone there is a fixed cost an order of magnitude higher than the per turbine cost. These cost estimates are not included in the calculation of CA_f and CA_t values, because they only cover cable costs, which account for approximately 10% of the total CAPEX. However, they do help demonstrate why the method of splitting CAPEX into CA_f and CA_t is appropriate.

OREC: Tidal Stream and Wave Energy Cost reduction and Industrial Benefit

A recent cost analysis was performed by the Offshore Renewable Energy Catapult (OREC) based on aggregated data from tidal developers working in the kW to MW scale [12]. They also forecast the costs and job creation of a potential deployment scenario for the UK, where 1GW of tidal stream is deployed by 2030 at a rate of 100MW per year from 2020. The predicted UK 2030 spend in this scenario was £307 million; with £227 million spent on CAPEX for a 100MW array and £80 million on cumulative OPEX for the existing 10 100MW arrays. The study investigated arrays with turbines in the 1–2MW range, so a turbine rating of 1.5MW is assumed in the following calculations. The CAPEX/MW of an 100MW array in the OREC report is £2.27 million, which combined with the ratio $2.3 < \mathrm{CA}_{ft}$ from [2] and using method 2 results in a fixed CAPEX of $£7.6\mathrm{m} \leqslant \mathrm{CA}_f \leqslant £12.8\mathrm{m}$ and a turbine-dependent CAPEX of $£3.26\mathrm{m} \leqslant \mathrm{CA}_t \leqslant £3.34\mathrm{m}$. The OPEX/MW of a 100MW array is £0.08 million/year, which can be similarly split into $£0.27\mathrm{m} \leqslant O_f \leqslant £0.45\mathrm{m}$ and $£0.113\mathrm{m} \leqslant O_t \leqslant £0.116\mathrm{m}$.

IEA Technology: International LCOE for ocean energy technology

An IEA Technology report estimated costs for different ocean technologies at different stages of their development [11]. Looking at the first commercial scale projects with a capacity of 3–90MW and assuming that the maximum project capacity corresponds to the minimum CAPEX/MW, and vice-versa, their minimum and maximum scenarios correspond to a small array with two 1.5MW turbines and a larger array of 60 turbines with a total CAPEX of $16.8m and $297m, respectively. These two points can be converted to GBP (assuming a rate of $1 = £0.79) and used in

Table 2.1: The CAPEX and OPEX components found by combining the optimistic (Opt), typical (Typ) and pessimistic (pes) estimates of Orbital Marine Power Ltd [9], with the upper and lower CA_{ft} limits found in [2].

	$CA_{ft} = 2.3$			$CA_{ft} = 3.9$		
	Opt	Typ	Pes	Opt	Type	Pes
CA_f (£m)	6.4	6.7	7.2	9.2	9.6	10.3
CA_t (£m)	2.4	2.5	2.6	2.8	2.9	3.1
O_f(£m/year)	0.41	0.49	0.60	0.59	0.71	0.87
O_t(£m/year)	0.15	0.18	0.22	0.18	0.21	0.26

method 1 to find a fixed CAPEX of $CA_f = £5.6m$ and a turbine-dependent CAPEX of $CA_t = £3.8m$.

Similarly, IEA Technology found a small (3MW) commercial array has an OPEX/year of $1.2m and the large array (90MW) is $8.1m/year. From this, method 1 can be use to calculate the fixed OPEX per year as O_f = £0.76m/year and the turbine-dependent OPEX per year as O_t = £0.094m/year.

Orbital Marine Power Limited: Technology Update

Orbital Marine Power Limited (formerly known as Scotrenewables Tidal Power) issued a cost analysis for a 10MW array, with their cost assumptions and methodology approved by the Carbon trust. It predicted a base CAPEX/MW of £2.60m with a pessimistic prediction of £2.80m and an optimistic one of £2.50m [9]. Furthermore they had a base OPEX/MW/year prediction of £0.1982m with a pessimistic value of £0.235m and an optimistic value £0.16m. Since this range of CAPEX and OPEX predictions were only for 10MW arrays, they can be combined via method 2 with the $2.3 < CA_{ft} < 3.9$ ratio from Higgins and Foley [2], which defines the shape of the cost reductions with economies of volume. This results in six estimates of each of CA_f, CA_t, O_f and O_t, which are summarised in Table 2.1. Taking the extremes for each value, the fixed CAPEX may lie in the range £6.3m $< CA_f <$ £10.4m, turbine-dependent CAPEX may be $£2.4m < CA_t < £3.1m$, fixed OPEX per year may be £0.41m $< O_f <$ £0.87m, and turbine-dependent OPEX per year may be £0.15m $< O_t <$ £0.26m.

Black & Veatch: Cost of and financial support for wave, tidal stream and tidal range generation in the UK

An executive summary by Ernst & Young and Black & Veatch [10] investigated the relative costs of wave and tidal energy in the UK, at different stages of deployment. They provided cost estimates for tidal arrays in both deep ($\leqslant 40m$) and shallow ($> 40m$) water for a 10MW tidal stream array at different stages of developer experience; for a developer's first 10MW demonstration project and for a 10MW commercial project where the developer has already deployed over 50MW in the past. Since these economic models are to be used to optimise large-scale tidal arrays, commercial figures are used, and because the likely locations of the UK's first commercial tidal arrays, e.g. in the Alderney Race and Pentland Firth, are approximately 30–40m in depth, the shallow water values are used in this work.

Black & Veatch estimated that the typical CAPEX/MW for a 10MW tidal stream array is £3.2m/MW, with a lower and upper bound of £2.7m/MW and £3.9m/MW, respectively. By comparison they estimated that a developer's first 10MW demonstrator array would have a CAPEX/MW of £4.3m/MW, showing the significant impact that learning-by-doing can have on the cost of tidal stream in the short term. A commercial array in deep water rather than shallow saw only a small increase in CAPEX/MW to £3.3m/MW, which was attributed to a different deployment method, structure foundations or mooring possibly being needed in greater depths, but otherwise the shallow and deep technologies may be largely the same, and can therefore benefit from learning from each other.

Similarly, Black & Veatch estimated that the typical OPEX/MW for a 10MW tidal stream array is £150k/MW, with a lower and upper bound of £120k/MW and £190k/MW, respectively. Demonstrator arrays are substantially more expensive with an OPEX/MW of £310k/MW. Deeper projects were predicted to have a lower OPEX/MW of £120k/MW. Black & Veatch noted that all costs were expected to decline due to the anticipated future global deployments and corresponding impact on learning in the industry.

These typical and lower/upper bounds can be converted into their separate fixed and turbine-dependent components using method 2 and the $2.3 < \mathrm{CA}_{ft} < 3.9$ ratio from Higgins and Foley [2]. The three values given for each of CAPEX/MW and OPEX/MW by Black & Veatch, along with the upper and lower values for CA_{ft} result in six estimates for each parameter, which are summarised in Table 2.2. The maximum and minimum values in this table provide the parameter ranges

Table 2.2: The CAPEX and OPEX components found by combining the optimistic (Opt), typical (Typ) and pessimistic (Pes) estimates of Black & Veatch [10], with the upper and lower CA_{ft} limits found in [2].

	$CA_{ft} = 2.3$			$CA_{ft} = 3.9$		
	Opt	Typ	Pes	Opt	Type	Pes
CA_f (£m)	6.9	8.2	10.0	10.0	11.8	14.5
CA_t (£m)	3.0	3.6	4.4	2.5	3.0	3.7
O_f(£m/year)	0.31	0.38	0.49	0.44	0.55	0.70
O_t(£m/year)	0.13	0.17	0.21	0.11	0.14	0.18

Table 2.3: A summary of the typical (Typ), optimistic (Opt) and pessimistic (Pes) estimates of CA_t, CA_f, O_t and O_f from IEA Technology [11], Orbital Marine Power Limited [9], Black & Veatch [10] and OREC 2018 report [12].

Source:	OREC		IEA	Orbital Marine Power Ltd		Black & Veatch	
Type:	Opt	Pes	Typ	Opt	Pes	Opt	Pes
CA_f (£m)	7.6	12.8	5.6	6.3	10.4	6.9	14.5
CA_t (£m)	3.26	3.34	3.8	2.4	3.1	2.5	4.4
O_f(£m/year)	0.27	0.45	0.76	0.41	0.87	0.31	0.70
O_t(£m/year)	0.113	0.116	0.094	0.15	0.26	0.11	0.21

that can be estimated using the Black & Veatch cost information for commercial arrays. The fixed CAPEX may lie in the range £6.9m $< CA_f <$ £14.5m, turbine-dependent CAPEX may be £2.5m $< CA_t <$ £4.4m, fixed OPEX per year may be £0.31m $< O_f <$ £0.70m, and turbine-dependent OPEX per year may be £0.11m $< O_t <$ £0.21m.

Summary of CA_t, CA_f, O_t and O_f estimates

This literature review sought to collate CAPEX/MW and OPEX/MW estimates from a range of sources and convert them to a format more suitable for modelling the impact of economies of volume, to enable the comparison of arrays of different sizes. Table 2.4 summarises the upper and lower bounds and the average of the different estimates for CA_t, CA_f, O_t and O_f found in each of the sources reviewed above.

Discount rate

The discount rate, r, is a key parameter when evaluating the economic success of a project over its lifetime as it determines the present value of future cash flows.

It is the interest rate used in discounted cash flow analysis. It reflects that future cash flow has less value than current cash flow to investors due to opportunity costs and risks. In general higher rates are applied to less developed technologies, to account for the greater risks and uncertainty associated with the novel design and speculative cost estimation. Determining an appropriate discount rate is important for any economic metrics such as net present value, LCOE and payback periods.

Ouyang and Lin [123] investigated the LCOE of different renewable energy technologies in China and the appropriate subsidies and policies to support them. They found the discount rates required for different forms of renewables varied through 5, 8 and 10%, with the higher rates being needed for novel renewable energy sources, such as tidal, which are seen as more risky compared to more established forms of renewables, such as onshore wind or solar PV. In general it can be shown that a transition to lower discount rates will help renewable energy become more cost competitive with fossil fuels. Khatib [140] performed a review of generation costs in OECD countries and found that as the discount rates fall from 10% to 5% more capital intensive forms of energy, such as nuclear, wind and tidal, become more cost competitive compared to coal and gas. Both papers used a common discount rate across the whole energy market due to limited data to distinguish the relative risks for different technologies. Common discount rates have been criticised for not reflecting these risks appropriately, and more recent studies have suggested specific values for the tidal other ocean energy industries, which are on the higher end of the spectrum due to their novelty and perceived risk.

A report on the cost of ocean energy, by SI Ocean for the European Commission [136], used a discount rate of 12% for both wave and tidal, but also investigated how changes in the rate chosen could have a significant impact on the LCOE. Reducing r from 12% to 6% results in a decrease in their predicted LCOE of demonstrator arrays, from 32.0c/kWh (£288/MWh) to 23.1c/kWh (£208/MWh).

The OREC 2018 report estimated a discount rate at 10MW cumulative tidal capacity of 10%, but their models predicted this would fall to 8.4% by 100MW, 8.0% by 200MW and 7.1% by 1GW global installed capacity, reflecting the potential that learning has to reduce the cost of capital. They also demonstrated that each percentage point reduction in discount rate leads to a significant LCOE reduction (of approximately 6%), for example the discount rate changing from 7.1% to 6.1% would reduce their 1GW cummulative capacity LCOE estimate from £91 per MWh to £80 per MWh[12]. This is consistent with SI Oceans's results, which fell by 6.4% on average per percentage point reduction in discount rate. Falls in r could be achieved

as the industry matures and investing in tidal energy is seen as less of a risk.

The Carbon Trust predicted that the first commercial marine energy schemes would have a discount rate of around 15%, which could fall to 8% as the technology matures [141]. Vazquez and Iglesias [99, 122] used a discount rate of 10% in their Levelised CAPEX of Energy tool. In another paper they argued that tidal stream energy projects have greater technological risks, due to their novelty compared to conventional types of energy generation, and high capital costs which results in a conservative discount rate being needed of between 10% and 12% [121].

Allan et al. [142] used a high and low discount rate of 15% and 6% respectively, with 10% used as the central value when finding the LCOE of wave and tidal, which is often used as a common rate across multiple different technologies [143, 144]. Allan et al. [142] noted that higher discount rates adversely affect technologies with longer lifetimes and high CAPEX as a proportion of the LCOE. Both of these factors apply to tidal, so it is anticipated to be highly sensitive to variation in the discount rate.

Culley et al. [105] also used a 10% discount rate for their study into cost modelling and micro-siting of tidal stream, and found that this amounted to a 35% reduction in income when compounded over an assumed 20 year array lifetime. Coles et al. [49] used a discount rate of 12% when investigating mechanisms for reducing the LCOE of tidal. Dalton et al. [145] suggested a discount rate of 8% to 15% is typical in UK ocean energy, however they noted that more in-depth economic studies could use multiple rates within one project to reflect the different risks of individual cash flows. Klaus et al. [146] assumed a financial discount rate of 10% but also tested the impact of varying it over the range 5–15%. They emphasised the importance of thorough investigation into the choice of discount rate, by demonstrating the the results of LCOE comparisons between technologies can be inverted as the discount rate is varied through its conventional range.

This present study therefore recommends using a discount rate of 5 to 15% with a typical value of 10%. However, due to the high sensitivity of LCOE to the discount rate, sensitivity analysis of the final LCOE prediction to the choice of r should be performed.

Lifetime of array

The lifetime of the array is the number of years that the tidal project is planned to operate for. It is normally determined by contracts and insurance based on the

assumed time an array can perform well before there is too much degradation due to environmental conditions. Vazquez and Iglesias [99, 121, 122] used an expected lifetime of installation of 20 years in their Levelised CAPEX of Energy tool. Likewise Dalton et al. [145] and the report by SI Ocean[136] assumed a lifetime of 20 years. The Department of Business, Energy and Industry Strategy (BEIS) assumed an operating period of 22 years for tidal stream in their 2016 generation costs report[144].

The world's largest currently operating, the MeyGen 6MW array in the Pentland Firth, announced in 2018 it had entered into its 25 year operations phase [147, 67]. Similarly Johnstone et al. [31] assumed a lifetime of 25 years in their techno-economic analysis of tidal energy, and as did Coles et al. [49]. As the technology becomes more tested and proven lifetimes are likely to increase even further. Therefore a typical value of 25 years with an upper and lower bound of 30 and 20 years respectively was used in this study.

Tidal energy is currently perceived as a relatively risky investment, and therefore has a high discount rate, this makes the NPV and LCOE less sensitive to the choice of array lifetime, because both revenue and costs many years into the future are heavily discounted. At a discount rate of 10% cashflows 20, 25 and 30 years into the future have a present value reduced by 85%, 91% and 94% respectively, so adding additional years to the project lifetime does not contribute much to the overall LCOE. If the discount rate falls to 5% then the present value reductions fall to 62% 70% and 77% respectively.

Summary of all cost model inputs

The maximum, minimum and mean values of the cost parameters and other economic inputs (discount rate and lifetime of an array) across all the sources discussed above are summarised in Table 2.4, as the Pessimistic, Optimistic and Typical values. It should be noted that the cost information summarised in this review is based on the limited publicly available information at the time of writing and that there is a significant difference between the optimistic and pessimistic values due to the high degree of variability in this relatively new industry. There is uncertainty in these estimates and they are only suitable for demonstration purposes in academic modelling and optimisation of tidal stream arrays, which will carry through to uncertainty in the predicted cost of energy and the economically extractable resource in the regions investigated in this thesis. In practice tidal developers should use their

Table 2.4: Estimates for the optimistic (Opt), typical (Typ) and pessimistic (Pes) parameters used in the economic models, and the amount they vary.

Symbol	Description	Value range			Units
		Opt	Typ	Pes	
CA_f	Fixed CAPEX	5.6	9.2	14.4	£m
CA_t	Turbine dependent CAPEX	2.4	3.3	4.4	£m/turbine
O_f	Fixed OPEX	0.27	0.32	0.87	£m/year
O_t	Turbine dependent OPEX	0.094	0.15	0.26	£m/year/turbine
r	Discount rate	0.05	0.10	0.15	N/A
L	Lifetime of an array	30	25	20	years

internal cost information for more accurate economic array design. Furthermore the costs inputs used in this thesis are just for demonstration purposes. The methods for array optimisation developed in the following chapters are specifically setup to allow the array developers to combine their own financial model with relative ease and a great deal of flexibility in the complexity of the model that can be used.

In the following sections the impact of the uncertainty in the input values on the predicted cost of energy is assessed using Monte Carlo analysis and assuming a rectangular distribution between the most pessimistic and optimistic value for each parameter. These give us insight into the impact that uncertainty in these parameters has on the final results, and can be used to find a confidence interval, where there is only a 10% chance of values being less than the P_{10} value and only a 90% chance of values being higher than the P_{90} value.

2.4.3 Revenue inputs

In all of the financial models above, the income must be estimated in order to analyse the cost-benefit balance of different array designs. Assuming that the main source of income for an array operator is from selling the energy generated, then the revenue, in year i, can be approximated from

$$\text{Revenue}_i = P_{\text{avg}} \times t_i \times T_e, \tag{2.31}$$

where P_{avg} is the average power generated, predicted using a hydrodynamic model of the array, and either used as an average over the whole lifetime of the array, or calculated over smaller time scales, for example to take into account variation due to the lunar cycle. t_i is the number of hours of generation each year, which

can be multiplied by the average power, to find the gross energy output in MWh. Below is a discussion on factors that affect the ratio of operational hours to hours of downtime. T_e [£/MWh] is the electricity tariff, i.e. the price per MWh the electricity generated is sold at. This price is greatly dependent on the subsidies and other schemes available to developers, and the schemes available in the UK are discussed in greater detail below.

Strike price of energy

Traditionally, large scale electricity generators sell their energy to suppliers at a time varying market price. In the UK, the wholesale electricity market price (or 'reference price') hovers between £40–£50/MWh. This market price changes throughout the day and the year in response to the balance of supply and demand.

Renewable energy sources often need subsidies and schemes for additional income support for a number of reasons. Firstly, many forms of renewables, especially the tidal industry, have a relatively high LCOE due to their relative infancy. Governments often seek to subsidise the expensive new forms of energy by paying higher than the market rate. This helps decarbonise the electricity grid and support in the early stages may help new technologies become cost competitive by the time they are deployed on a larger scale. Secondly, renewable energy technologies are often non-dispatchable, in that the production cannot be scaled up and down on demand easily. This means they cannot react to falls and rises in the market prices, which can lead to worsening problems as renewables account for increasingly high portions of the energy generation mix. The wind energy industry has already seen that times where the wind is high at one farm often correlates with times of high winds at other farms in the surrounding regions, and therefore the price falls and operators get a low return per unit during their periods of highest production. In the US this has led to a rise in the frequency of negative prices in areas with high levels of wind and solar and which have transmission constraints [148]. To address this problem governments can offer schemes that guarantee a fixed electricity tariff. These tariffs are not necessarily higher that the market price, but the guarantee reduces uncertainty for investors and can result in lower discount rates and protect the income of operators during times where supply is high. This is less likely to be a problem for tidal energy because it accounts for a far lower proportion of total energy generation than wind energy, and also it is possible to take advantage of phase differences across the country to smooth out the daily power production[63].

Improvements to the grid, such as increased storage, may reduce the need for these kind of subsidies in the future.

Power Purchase Agreements (PPAs) are contracts between the generators and the suppliers that outline how much generators will be paid for the power exported over the duration of the contract. PPAs enable generators to earn payments for the energy they export to the grid. These agreements can be long or short term, so could be negotiated to last the full lifetime of a tidal array. PPAs ca be negotiated to be market-varying price or fixed price, the latter being preferable for a predictable income for tidal projects. Similarly to ROCs, PPAs help remove exposure to price volatility and make cost planning more predictable. The advantages of PPAs from a supplier's perspective include fixed prices to reduce exposure to makret fluctuations and guarantees of renewable origin, to help meet the business's sustainability goals. MeyGen Phase 1A in the Pentland Firth signed a 10-year PPA with SmartestEnergy, to guarantee revenue on the power generated up to 2025. DeltaStream in Wales signed a PPA with EDF for their first tidal turbine in 2014.

The Renewables Obligation (RO) scheme incentivised large-scale ($\geqslant$ 5MW capacity) renewable electricity in the UK by requiring UK electricity suppliers to source a specified proportion of the electricity they provide to customers from eligible renewable sources. The scheme closed to new generators in March 2017, but electricity sources already accredited under ROs will receive their 20 year lifetime support until the final close of the scheme in 2037. Under this scheme, Renewable Obligation Certificates (ROCs) are issued to accredited renewable energy generators for the eligible electricity they generate. Generators can sell their ROCs to suppliers through the e-ROC auction, receiving a premium ontop of the wholesale electricity price. Suppliers present the ROCs bought from generators to Ofgem, and if they do not have enough ROCs to cover their obligation they must make a payment into the buy-out fund at a fixed price per MWh. Ofgem then redistributes the buy out funds proportionately to the suppliers who presented sufficient ROCs. When first introduced in 2002, one ROC is issued to the generators per MWh generated, to emphasise competition between technologies. However this favoured more established technologies, so in 2006 it was reformed to have different banding levels for different types of technology. Tidal stream projects accredited before the scheme closed in 2017 were issued 5 ROCs (the highest banding level), subject to a 30MW cap at each generating station. Power generated above the 30MW cap receives 2 ROCs. PPAs with a particular energy supplier can also guarantee the purchase of the ROCs issued to that generator over a specified period. The MeyGen Phase 1A was awarded

Ofgem accreditation as a five ROC project in 2017, meaning that their revenue was comprised of power generation sales (as agreed by a PPA) and a buy-out price of £44.77/MWh from each of five the ROCs (which has since risen to £50.80/MWh in 2021/22), which would bring the total T_e is circa £250 to £300/MWh, depending on the price agreed in the PPA.

As the ROC scheme was phased out in 2017 it was replaced with the Contracts For Difference (CfD) scheme, for guaranteeing low-carbon electricity generators a long-term energy price. A fixed "strike price" for each unit of energy produced is guaranteed, leading to a promise of steady returns for investors. During the contract period, typically 15 years, a low-carbon energy project is paid the difference between the market price and the strike price (or they pay back the difference, if the market price rises above the strike price). In the UK's most recent round (the third allocation in 2019), CfDs were allocated as low as £39.65/MWh, mostly for offshore wind. In its current state of deployment, the tidal industry cannot compete with these low prices. Alternative subsidy schemes, which allow developers of new forms of green energy greater funding until their costs can fall due to learning and economies of volume, are being investigated.

A recent Marine Energy Council report [149] proposed a number of different subsidy schemes to provide a route to market for the tidal energy industry and other innovative clean energy technology types, such as wave and Advance Combustion Technologies. An Innovation Power Purchase Agreement (IPPA) could support small-scale (up to 5MW) novel projects by starting at a guaranteed price, far above the market rate, at prices starting at £290/MWh and falling by 15% for every 30MW of deployment (where each individual technology type can only make use of 5MW out of every 30MW price band) down to £150/MWh by 120MW of net deployment. The idea would help enable each novel technology to demonstrate their performance and cost reduction potential, without having to compete against far more established technologies.

Marine Energy Council also proposed an Innovation Contract for Difference (iCfD) to allow for a new pot within the government's existing CfD framework for new technologies [149]. This would act as a bridging mechanism to allow projects of larger than 5MW but less than 100MW and exploit economies of volume until they can compete in open CfD rounds or other PPAs which could enable a higher revenue than the UK market price. It could be limited to projects of up to 100MW and could see the costs fall by 7% per 100MW from £150/MWh to £90/MWh, based on the predictions of the OREC 2018 report [12]. Marine Energy council anticipated that

these proposed schemes would support tidal energy to reach target costs of less than £100MWh after 1GW of deployment

These wide ranges of prices represent the highs and lows of what may be achievable through subsidy for tidal energy in different stages of global deployment. This study proposes a typical strike price of £150/MWh, chosen to represent the gap bridged between small scale demonstrator arrays and larger ones which can use iCfDs, with a lower bound of £40/MWh and an upper bound of £290/MWh to represent the market prices or open CfDs and the propose iPPA starting prices respectively. However it should be noted that there is a great deal of uncertainty in these prices and they will depend greatly on the state of the marine energy industry and government decisions at the time. Using LCOE for evaluating the economics of tidal arrays removes the need for assuming the strike price of energy in the calculations, so it can be a suitable metric until more information about the subsidy levels available are known.

Downtime and degradation

Availability is a measure of the time that an array is available for operation. Availability can be calculated from the number of hours downtime over a given period, such that

$$\text{Availability} = 1 - \frac{\text{hours downtime}}{\text{total hours}}, \tag{2.32}$$

therefore the number of hours of generation in year i, as used in the LCOE expression (2.13), can be predicted as $t_i = 365 \times 24$ multiplied by the anticipated availability in year i. In the wind industry it has been found that turbines often have lower availabilities during high-wind periods, where the production and loads are higher so faults are more likely to occur. To account for this effect, availability is sometimes calculated in two ways – as a time-based availability given in (2.32) or as a production-based availability, found as the percentage of actual energy produced over energy expected. The former is easier to calculate but the latter is a better representation of the energy lost. Downtime in high winds often results in the percentage energy lost being higher than the percentage of hours lost, with one study finding that a 3% non-availability in time resulted in an 11% reduction in energy generated in the Irish wind farm investigated [150], whereas DNV-GL found that the two metric differed by up to 2%[151]. The production-based availability can be improved by scheduling maintenance, where possible, during periods of low resource.

Hours of downtime, or non-availability, can have several causes; turbine availability can include scheduled or unscheduled maintenance or faults in the turbines causing periods of non-operation, grid availability can include periods of time where the grid is unable to accept electricity due to lack of capacity or grid failure, or balance of plant (BoP) availability, where electricity generated at the turbines is lost due to failure of supporting components and auxiliary systems [151].

Turbine suppliers will often guarantee a minimum turbine availability rate when they sell their turbines to operators and if turbine failures cause the availability to drop below that value the suppliers will pay compensation to the operators. This contractual availability is negotiated during the turbine supply agreement (TSA). In wind energy a typical value of 97% is used as the industry standard [150]. There is limited operational data to form conclusions about the typical time-based versus production-based availability in tidal, but the MeyGen Phase 1A guaranteed a contractual availability of 95%, and anticipated that the turbines would exceed their target performance in practice[152, 67].

When more data becomes available from operational tidal stream arrays, it may become possible to model the downtime as a function of time. There are likely to be cyclic patterns to the number of hours downtime needed a year for scheduled maintenance, as some operations may need to occur on a five year cycle for example. There is also evidence from the wind industry that failure rates vary greatly depending on the year in the operating lifetime [119]. Faulstich et al. [118] demonstrated that wind farms often follow a "bathtub curve" where there is a high failure rate in the early life due to teething problems or 'infant mortality', a period where the failure rate is approximately constant and low, with just intrinsic random failures occurring and a wear-out period near the end of an array's lifetime, where damage accumulates and the failure rate increases. This degradation could be due to increased component wear or bio-fouling impacts.

2.5 Conclusions and summary

There are a great number of metrics that can be used to evaluate the performance of tidal energy arrays. These include power alone (which results in array designs with too many turbines if the number is not pre-specified), as well as purely economic metrics such as break-even power analysis, NPV, LCOE, IRR and PP. Some studies have expanded upon performance metrics further to include the trade-off between

economic performance and environmental impacts of the arrays, however this requires decisions on the relative weightings of each criteria. This study proposes that many of these economic metrics can be estimated for large scale arrays by assuming a linear relationship between CAPEX and OPEX and the number of turbines, an therefore splits each of these expenditures into their fixed and turbine-dependent components, CA_f, CA_t, O_f and O_t respectively. The data collection study identifies a realistic range for each of the parameters needed in a simple economic model of a tidal stream array, summarised in Table 2.4. Additionally, the range of past, present and proposed subsidy schemes in the UK were examined, to identify possible upper and lower bounds on strike prices, however it is noted that the actual value will be highly dependent on the state of the industry and levels if government support at the time. It should be noted also that there is a great deal of uncertainty in each of the economic input estimates and they should be used for the purpose of providing a reasonable range for academic studies and may not reflect the real economic performance of a potential tidal site. These estimates are useful in the absence of real financial data from developers, which is often commercially sensitive, and can be used for proof of concept when demonstrating new techniques for optimising tidal array designs. In practice, array design studies should be repeated with a developers internally-validated financial models.

Chapter 3

Efficient economic optimisation of tidal stream arrays

Abstract

The content within this chapter is based on **Z. L. Goss**, S. C. Kramer, A. Avdis, C. J. Cotter, and M. D. Piggott, Economic optimisation of large scale tidal stream turbine arrays, in *13th European Wave and Tidal Energy Conference*, Naples, 2019, pp. 1598–1-18, and **Z. L. Goss**, D. S. Coles and M. D. Piggott. Efficient optimisation of economic functionals in large-scale tidal stream arrays, *Applied Energy*, 2021.

As the tidal energy industry moves from demonstrator arrays comprising just a few turbines to large-scale arrays made up of potentially hundreds of turbines, there is a need to optimise both the number of turbines and their spatial distribution in order to minimise cost of energy. Optimising array design manually may be feasible for small arrays, but becomes an impractically large approach when the number of devices is high, especially if taking into account both the cost effectiveness of each turbine and also the coupled nature of the turbine locations and the local as well as far-field hydrodynamics.

Previous work has largely focused on producing computational tools to automatically design the size and layout of large-scale tidal turbine arrays to optimise power.

There has been some limited preliminary work to incorporate costs into these models, in order to improve the economic viability of tidal arrays. This chapter provides the first in depth implementation and analysis of economic functionals, based upon metrics such as break even power and levelised cost of energy, used for design of explicit array sizing and spatial variation.

The addition of these new economic functionals introduces complexity by increasing the number of inputs to the model, each of which are subject to their own uncertainty in value. For this reason, sensitivity analysis becomes both more important as well as more difficult to undertake. This chapter presents a novel rapid methodology for deriving the optimal array design (number of turbines and their spatial distribution throughout the farm area) to minimise cost functionals, and its sensitivity to variations in the economic inputs. Importantly, the new aspects of this method introduced here do not rely on repeated model runs and iterative optimisation, two aspects that typically prove to be impractically expensive computationally. This more readily allows for the impact of changes in investor priorities to be investigated. It is also shown that, while the optimal solution varies greatly with uncertainty in the input parameters, this uncertainty is reduced significantly through Monte Carlo analysis.

3.1 Introduction

In recent years the price of offshore wind has fallen dramatically, with record-low prices of £39.65/MWh seen in the UK's third Contracts for Difference auction [111]. Currently, tidal stream and other ocean energies must compete against offshore wind for subsidies and other forms of government support, however tidal stream is at a much earlier stage of development. As a result of this, tidal energy is currently a higher cost technology and needs further development pathways to remove this barrier to market penetration [153]. Commercial-scale tidal stream energy arrays have yet to be deployed, and so the emerging industry needs to rely on models to help understand the factors affecting array performance, including coupled interactions to the hydrodynamics. Laboratory experiments have practical limitations and have only tested limited configurations, e.g. comprising two to ten three-bladed rotors,

notably by Stallard et al. [46] and Mycek et al. [154], so computational models must be relied on as the number of turbines in an array increases. This motivates the need for innovative tools, which can be used to optimise the array design to reduce the cost of tidal energy [82, 81, 105, 112, 155].

As the tidal energy industry develops, cost reductions are anticipated to come in many forms, some from improved technological solutions such as cheaper or easier to install foundations or higher rated rotors [49]. In order to achieve commercial viability in an open market, reductions in the cost of energy must also come through improved array design using existing technology. Many tools have been created which can predict and maximise the yield of tidal stream arrays. Optimal array design can take advantage of the economies of volume that result from larger scale arrays and can lead to higher yields from intelligent micro-siting of the turbines to minimise negative blockage effects. For example [81] found that the yield of an optimised array layout in an open channel increased by up to 38%, compared to a regular grid layout, and that in a strait between an island and a landmass the yield increased by 22%. Similarly, [82] demonstrated optimisation of layout within a square basin and found the power production of 152 turbines in a regular non-staggered grid layout increased by 104% from 41.4MW to 84.5MW when using an irregular optimised layout.

More recently, hydrodynamic models of potential tidal array sites have been implemented in *Thetis* — coastal ocean modelling software which allows the array design to be coupled with the flow and enables gradient-based optimisation through the availability of an adjoint mode [82, 81, 156, 157]. Earlier iterations of these tools focused on optimising with respect to power alone [105, 112, 104]. However, modelling array power alone does not take into account the diminishing returns in yield per device as the number of turbines in an array increases. This decrease in the average power per device is due to both blockage effects and turbine spacing requirements which lead to additional turbines being placed in lower flow areas. Therefore there is a need to incorporate the balance of costs associated with adding turbines to an array against the additional yield gained from them, to decide on both an optimal number of turbines and suitable locations.

Later adaptations of these tools incorporated costs by introducing a break even power, P_{BE}, to the optimisation functional, such that there is an effective capacity factor that turbines must achieve in order to be cost efficient to install [3, 4]. Introducing a break even power into the functional is a simple way to bring the balance of maximising power vs minimising costs into the optimisation of array de-

sign. However, this approach relies on a lot of assumptions, and does not account for many factors which may make one array design more advantageous over another. For example, in the form used in previous work, break even power is assumed to be independent of the number of turbines. In practice there may be economies of volume, such that the effective costs of turbines, and therefore P_{BE}, decreases as the number of turbines increases. This chapter provides a new understanding of how economies of volume impacts upon optimal array design by applying a factor to decrease the break even power with the number of turbines. Choosing an appropriate value for this factor and the break even power itself relies on a complex balance of metrics not explicitly included, such as the lifetime of array, discounted cash flow analysis and the balance of CAPEX and OPEX.

This chapter furthers these investigations into break even powers, by using more holistic economic indicators as the optimisation functional. It advances on previous array optimisation studies, through a novel approach to explicit array sizing and spatial distribution with respect to a realistic model for profitability. There are a number of different ways to express the profitability of a tidal stream array, including the Net Present Value (NPV), Internal Rate of Return (IRR), Return on Investment (ROI), Payback Period (PP) and Levelised Cost of Energy (LCOE). All of these metrics take into account the sum of energy generated over an array's lifetime, and the sum of costs incurred over the lifetime. These metrics each have different advantages and times when they may be more appropriate to use. Policy makers often use LCOE as a simple metric to enable like-for-like comparisons of the performance of different energy technologies. This is the most common metric used by institutions such as the Offshore Renewable Energy Catapult (OREC), the Centre for Climate Finance & Investment (CCFI) and Green Investment Bank (GIB) [12, 158, 159], and thus is investigated in Section 3.6.3.

More holistic economic indicators bring in many more parameters for a better representation of true array financing, however this large parameter space also adds uncertainty. It becomes intractable to perform optimisations over all possible sets of costs inputs. To overcome this problem, this chapter describes the development of a new emulator approach which enables rapid testing of the functional over a large range of parameters. The construction of the novel emulator method is based on the realisation that despite the many forms the economic models and their associated functional(s), they can typically be reduced to a bi-objective trade-off between number of turbines and realisable power output with the optimal result for any given functional being Pareto efficient. The emulator is then combined with Monte Carlo

based sensitivity analysis to allow for better understanding of the uncertainty by defining a P10 to P90 confidence interval.

Section 3.2 describes the inputs for the financial models and the ways that costs of tidal energy may fall. Section 3.3 presents the model for break even power and LCOE. Section 3.4 gives the details of the idealised model used as a simple representation of a typical tidal site. Section 3.5 shows the results of optimising a farm within this simple channel, over different break even powers. Section 3.6 describes how the results from optimising over a range of break even powers can be used to build an emulator for the rapid evaluation of the LCOE (or other economic models) over many different combinations of cost inputs. Section 3.6.1 outlines the process that can be used to apply the developed emulator method to real-world array design. An application of the methodology developed in this chapter appears in Chapter 4, showing that it can be used to predict the LCOE that can be achieved in the Alderney Race for different levels of deployment. This shows that the methods developed and validated in this chapter can be applied for assessment of the economic viability of real-world tidal sites.

3.2 Inputs and cost reduction pathways

Chapter 2 identified a range of cost parameter estimates, outlined in Table 2.4, by reviewing publicly available information on tidal energy costs. The pessimistic, typical and optimistic value for each parameter, are used to estimate the economic performance of array designs in the following work and assess the uncertainty in these predictions. All economic models used in this chapter are evaluated using a typical year, where the revenue is assumed to be constant year-on-year and can be found from 2.31. Similarly to power generation, OPEX is assumed to be constant each year in this model, however in practice it could be adjusted to increase with time, assuming failure rate increases. A more detailed review of tidal costs and the methods used to obtain the estimates in Table 2.4 was given in Chapter 2.

The MeyGen project reports a project-wide availability of 95% [152]. However, this assumption was made before the array was operational and it was anticipated that the turbines would exceed their target performance in practice. Due to the lack of publicly available and validated estimates, this chapter assumes 100% availability, so in 2.31 $t_i = 365 \times 24$ hours, however the model user can replace this with their own, potentially commercially sensitive values in practice. The electricity tariff,

T_e, is likely to remain constant because in its early stages tidal energy will rely on fixed-price subsidies such as Contracts for Difference (CfDs). However, the power generation is time varying and even if yield is averaged on a yearly basis it will fluctuate due to the 18.6 year lunar nodal cycle [115, 116]. The number of generating hours will also vary because the number of faults and need for maintenance will likely increase as the devices age, as has been seen in the offshore wind industry [118, 119]. This study assumes a constant value of generating hours to reflect the 'average' year because when demonstrating the methods on an idealised test case, the year the array goes into production is not known. Also at the time of writing, tidal arrays have not yet been in production long enough to build an accurate model of the anticipated increase in downtime with time.

The three main categories for cost reduction described in Section 2.3 are economies of scale, economies of volume and learning rates. In this chapter, only economies of volume will be explicitly investigated. Economies of volume are implemented through the distinction between fixed and turbine-dependent costs outlined in Section 2.3.3 and defined by (2.18) and (2.18). Economies of scale cannot be considered in the following investigations, because it is assumed that at the start of the design optimisation process that the size and rating of the turbines is specified. This is necessary because the optimisation method used accounts for the coupled effect of the array design and the hydrodynamics, and therefore the size and rating must be known so that the power and drag can be calculated from the appropriate power and thrust curves. Learning rates will be subject to the cumulative installed capacity, and developers will have no influence over this at the point of designing an array. Furthermore it is hard to predict the extent to which technology innovation and decreased cost of capital can be achieved. While not explicitly calculated in this work, the three scenarios in Table 2.4 are investigated and it is likely that learning rates will be the mechanism by which costs within the industry fall from the pessimistic and typical range towards the optimistic scenarios.

Typically CAPEX and OPEX are modelled as a cost per MW installed, which falls as the number of turbines in an array increases [160, 11]. In Chapter 2 it was demonstrated how the trends observed in cost per MW data from industry studies are equivalent to assuming that each expenditure type linearly increases with the number of turbines, as shown in (2.18) and (2.19). The use of this linear relationship helps to model economies of volume. In real arrays the relationship is not likely to be exactly linear but it is a good approximation and can be used to demonstrate the effectiveness of the following array optimisation methods. If used in practice

tidal developers could easily replace these cost assumptions with their own internal financial models.

3.2.1 Turbine specifications

The cost inputs in Table 2.4 are all from calculations made in Chapter 2, which were calculated using the assumption that the turbines are 16m in diameter and 1–2MW rated power. This is based on the amount of cost information available for different turbine sizes, and an average of the most common turbine specifications [161, 98, 49, 162]. In this chapter it is assumed that the turbines have a rated power of 2MW.

The turbines are assumed to have a thrust coefficient below rated of $C_T = 0.8$ [76] and a power coefficient below rated of $C_P = 0.41$ [98]. Again this is based on commonly found values in the literature, however all these parameters could be readily updated in order to optimise an array of turbines with different specifications.

3.3 Economics modelling methods

In the following section discusses the increasingly detailed methods used in this Chapter to bring economic considerations into the array optimisation process. Initially break even power is added as a proxy for the costs of the turbines, then the break even power is adapted to account for economies of volume. Finally a model of the Levelised Cost of Energy (LCOE) of the array is implemented as the functional instead. A more detailed description of the models and their assumptions is given in Section 2.2.

3.3.1 Break even power

The break even power, P_{BE}, is the average power over all turbines that needs to be generated in order for the array to break even over its lifetime, such that

$$\max_{P,n_t} J(P, n_t) = P - P_{\mathrm{BE}} \times n_t, \tag{3.1}$$

where P_{avg} is the average power generated by the whole array in MW, and n_t is the number of turbines. If an appropriate P_{BE} is chosen to reflect all of the costs that comprise Ex_i in (2.1), this choice of functional effectively maximises the profit and penalises the addition of turbines which do not generate enough power to outweigh their costs.

Section 3.5.1 demonstrates the impact of varying the break even power from $P_{\text{BE}} = 0$, such that the functional optimises power alone, increasing to find the maximal value of P_{BE}, such that the turbines become so expensive that the optimal array design contains no turbines.

Break even power with economies of volume

The functional shown in (3.1), would result in a design with the optimal number of turbines if the break even power were constant over arrays of all sizes. However, in practice economies of volume, which are discussed in greater detail in Chapter 2, would result in a lower P_{BE} required to break even for large-scale arrays than for small scale arrays. For simplicity this chapter investigates a P_{BE} that linearly decreases with the number of turbines, at a rate of EV. EV is varied through 0.00005, 0.0001, 0.00015 and 0.0002 MW. For example, if an array of 2MW turbines has a P_{BE} of 0.8MW, the minimum required capacity factor for one turbine to be economically viable is 40% (=0.8MW/2MW). However, with an EV of 0.0001MW an array with 100 turbines would have a reduced the break even power of 0.6MW (=0.8MW-100×0.0001MW) and the capacity factor would need to be just 30% (=0.6MW/2MW). This results in the following functional

$$\max_{P,n_t} J(P, n_t) = P_{\text{avg}} - (P_{\text{BE}} - EV \times n_t) \times n_t, \tag{3.2}$$

where P_{BE} and EV are the break even power and economies of scale to be specified in the functional, J, and P and n_t are the power and number of turbines in the array design being optimised. The EV values chosen are picked somewhat arbitrarily, in order to reflect a reasonable range of the rates at which the costs of tidal arrays can fall as their size increases. $EV = 0.0002$ was chosen to represent the higher end of the spectrum, which could reduce the break-even power of a 600 turbine array by $0.12MW$, whereas $EV = 0.00005$ was chosen to represent the lower end of the spectrum where the break even power of a 600 turbine array would reduce by just $0.03MW$. This is a simplified approach and is limited due to the lack of data available on what the appropriate choice of EV rate should be, and due

to assuming that the costs per installed MW capacity decrease linearly with the number of turbines, when in reality the costs would drop far faster for lower numbers of turbines than higher ones due to the economical inefficiencies of bespoke array designs.

Section 3.5.2 investigates how adding different extents of economies of volume to the break even power impacts upon optimal array design.

3.3.2 LCOE

A more robust way to include economies of volume in the functional is to calculate the levelised cost of energy (LCOE), while using the fixed and turbine-dependent breakdown of CAPEX and OPEX, defined in (2.18) and (2.19). The LCOE is a proxy for the average price of energy, T_e [£/MWh], that an array must receive in order to break even over its lifetime, and can be used as a functional to optimise, such that

$$\min_{P,n_t} J(P,n_t) = \text{LCOE} = \frac{\text{CA}_f + \text{CA}_t \times n_t + \sum_{i=1}^{L} \frac{O_f + O_t \times n_t}{(1+r)^i}}{\sum_{i=1}^{L} \frac{E_i}{(1+r)^i}}. \tag{3.3}$$

In the following work the estimates summarised in Table 2.4 are used as the inputs to this functional. A full comparison of LCOE to other metrics such as Net Present Value, Internal Rate of Return and Payback Period is given in Chapter 2. The linear assumption made on the relationship between total cost and number of turbines, in (2.18) and (2.19), results in a reciprocally decreasing costs per installed MW capacity that drops sharply for low numbers of turbines, then has a reduced affect for higher numbers of turbines, as demonstrated in Fig. 2.4. This is much more realistic than the simple break even power model which decreases linearly with economies of volume, because it follows the trends observed in the more mature wind industry [2], shown in Fig. 2.4.

3.4 Idealised model set-up

In this work, the above economic optimisation methods are applied to an idealised channel set-up. Draper et al. [1] characterised coastal sites that are especially suitable for tidal stream energy extraction due to accelerated flow via four generic

coastline configurations. These sites are a strait between two infinite ocean basins, a headland, an enclosed bay, and a strait between an island and a semi-infinite landmass.

Many tidal energy resource studies focus on the Alderney Race as a potential site, due to it's highly concentrated energy potential [163]. SIMEC Atlantis and the Development Agency for Normandy have a joint venture plan to install up to 2GW of tidal capacity in the Race. Much like the generic idealised site of flow between an island and a semi-infinite landmass, the flow is accelerated as it is confined between the Isle of Alderney and Cap de la Hague in France. The velocities can reach up to $5\,\mathrm{m\,s^{-1}}$, resulting in an estimated maximum average power potential of 5.1 GW [34]. Since the Alderney Race is most similar to Draper et al.'s final idealised case, this study focuses on the optimisation of a tidal arrays within the strait between an island and a landmass. Peréz-Ortiz et al. [5] recently investigated power extraction by narrow arrays (similar to tidal fences) spanning across such a strait. This work extends upon that by optimising array design and studying large-scale arrays rather than tidal fences, so there is more freedom in where the turbines can be placed. The following sections describe the setup of this idealised model. UK wide resource assessments have identified that 'first generation' tidal-stream sites require peak spring tidal velocities in excess of $2.5\,\mathrm{m\,s^{-1}}$ and depths between 25 and 50 m [114, 36]. Both the Alderney Race and this idealised setup satisfy those conditions.

3.4.1 Numerical model in *Thetis*

A flexible finite-element based coastal ocean model, *Thetis*, is used to solve the shallow water equations on an unstructured triangular mesh [157]. *Thetis* is built using the *Firedrake* framework (`https://www.firedrakeproject.org/`), which automates the generation of optimised low level application code from high level descriptions of finite element discretisations specified using the domain-specific Unified Form Language (UFL) [164]. *Thetis* is the coastal ocean modelling package chosen for use here since it is open-source and the adjoint mode allows the array design process to be coupled with the hydrodynamic model [82, 81, 156, 157], enabling optimisation of the functionals defined in (3.1), (3.2) and (3.3).

Flow through the channel is modelled here using the nonlinear shallow water equations in their non-conservative form (1.3). The kinematic viscosity of the fluid, ν, is set to a value of $10^{-4}\,\mathrm{m^2\,s^{-1}}$, and C_d the dimensionless quadratic drag coefficient

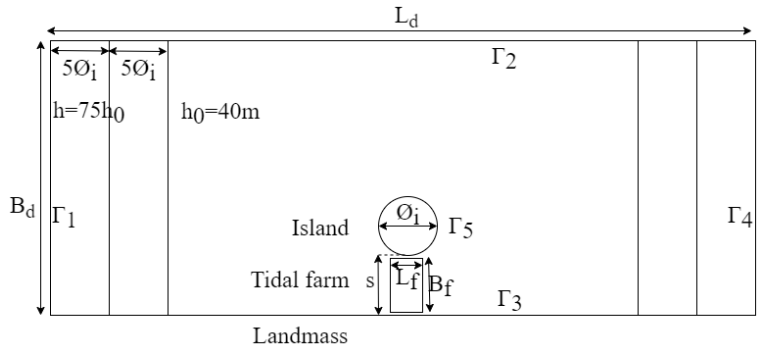

Figure 3.1: Idealised geometry for a model of flow through a channel with an island of diameter $\emptyset_i = 2\,\text{km}$ and a tidal site of area $A_f = B_f \times L_f$ where turbines can be added. The depth is increased linearly from h_0 to $75h_0$ to mimic the conditions at the continental shelf. $L_d = 140\,\text{km}$ is the length of the channel and $B_d = 40\,\text{km}$ is the width. $s = 2\,\text{km}$ is the minimum distance from the island to the southern landmass. This matches the setup used used in [3] (not to scale).

for seabed friction, is set to 0.0025. Due to simplifying assumptions Coriolis, wind and wave conditions, and atmospheric pressure are not included in this chapter.

3.4.2 Simplified model parameterisation

The geometry of the channel and the island is adapted from [5], and uses the same values as their setup where the channel in this domain is is $L_d = 140\,\text{km}$ long and $B_d = 40\,\text{km}$ wide, with a circular island of diameter $\emptyset_i = 2\,\text{km}$ located in the middle of the channel. It has a minimum distance from the island to the southern landmass of $s = 2\,\text{km}$. This is shown is Fig. 3.1.

The farm area, A_f, is $L_f = 1\,\text{km}$ long and $B_f = 1.92\,\text{km}$ wide, as shown Fig. 3.2. This is to approximately represent the dimensions of the Alderney Race tidal lease plots available to build on, spanning across about half of the length of the island and the whole width of the strait, with a 0.4 km buffer to the edge of the southern land mass and the island. In the region between 20 km and 10 km from from the eastern and western boundaries, the water depth is linearly increased in the streamwise direction from $h_0 = 40\,\text{m}$, which is the depth throughout the majority of the domain, to $75h_0$ in the band within 10km of the boundaries. This depth profile, shown alongside the computational mesh in Fig. 3.2, was chosen by [5] to mimic the conditions at the edge of the continental shelf and help prevent spurious reflections at the boundary.

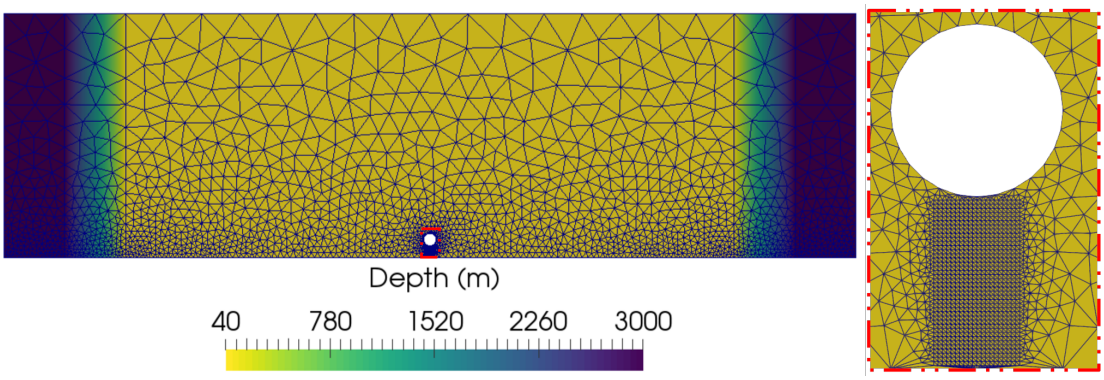

Figure 3.2: Multi-scale triangular computational mesh across the idealised domain. This is overlaid on a map of depths which increase from 40m to 3000m at the open boundaries. An enlarged view of the regular isosceles triangular mesh used within the farm area is shown on the right. This domain and mesh are identical to those used in [4] and are adapted from the setup used in [5].

3.4.3 Tidal forcing and boundaries

The domain shown in Fig. 3.1 has solid boundaries which correspond to a semi-infinite landmass, at the northern and southern sides of the domain, Γ_2 & Γ_3, on which a free slip boundary condition is applied. A free slip boundary condition is also applied to the solid boundary of the circular island, Γ_5. There are open boundaries on the western and eastern side of the channel, Γ_1 & Γ_4 respectively. Here M2 tidal forcing is applied to the free surface perturbation variable, which has an amplitude of $a = 3\,\mathrm{m}$ and a frequency of $\omega_t = 1.41 \times 10^{-4}\,\mathrm{rad\,s^{-1}}$, such that

$$\eta = a_0 a \sin(\omega_t t). \tag{3.4}$$

The multiplier $a_0 = 0.5(1 - \cos(\omega_t t/4))$ is used to ramp up the tidal signal over the first two tidal cycles. The model is run for seven tidal cycles in total, with the third and fourth being excluded to allow for spin up once the model has fully ramped up and time averages are only taken over the final three tidal cycles.

3.4.4 Discretisation of the model

Many discretisation options are available in *Thetis* due to the flexibility afforded by the use of the *Firedrake* mesh generation framework. In this work piecewise-linear, discontinuous basis functions are used to represent both the velocity and the free surface fields (the $\mathrm{P_{1DG}} - \mathrm{P_{1DG}}$ velocity-pressure finite element pair). The shallow

water equations are solved on an unstructured triangular mesh, which is generated by defining the element edge length on each boundary region.

The element edge length used in the unstructured part of the mesh is coarsest on the northern landmass, Γ_2, to a value of $\pi\emptyset_i = 6.28km$. It is set finer along the southern landmass, Γ_3, at $\pi\emptyset_i/6 = 1.05km$ due to proximity to the array area. The finest resolution in the unstructured part of the mesh is specified around the island boundary, Γ_5, at a value of $\pi\emptyset_i/28 = 0.22km$. A regular grid of 20 by 40 right isosceles angled triangles is used in all meshes for the tidal farm area, corresponding to an edge length of 48m by 50m. This results in a mesh with 5010 elements overall. The boundaries, $\Gamma_1 : 5$, are specified in Fig. 3.1 and tidal farm area and resultant mesh are shown in Fig. 3.2. As far as the hydrodynamics are concerned, the numerical setup is identical to the model used in [4] and [3] and therefore the mesh convergence study used to decide on this mesh resolution is not repeated here.

For the temporal discretisation a Crank-Nicolson time stepping method is used, with $\Delta t = 800\,\text{s}$. This was also chosen as an appropriate time step size in a previous study [4], through a time step independence test for Δt varying from 1600 s down to 100 s.

3.4.5 Turbine representation

This work uses a continuous approach for turbine representation, as proposed in [82], where a spatially varying turbine density field $d(\mathbf{x})$, defined in (1.9), is optimised. This approach, which does not attempt to represent individual turbines rather their 'concentration', is suitable for coarser mesh resolutions. It optimises the total number of turbines and their location (in an averaged sense) together within one optimisation loop. This greatly reduces the computational cost, which is important for modelling large-scale arrays.

The swept area of the turbines used in this study, A_T, is based on the 16 m diameter 2 MW OpenHydro turbines or 1.5 MW turbines installed in the MeyGen project. The turbine density is given a maximum allowable upper limit which is chosen to represent a high but still plausible, upper bound density of turbines. It corresponds to a minimum inter-device spacing of 2.5 turbine diameters centre-to-centre laterally and 5 turbine diameters in the stream-wise direction, or equivalently a 1.25 diameter lateral spacing and 10 diameter downstream spacing. The turbines have a cut in speed of $1m/s$ and a cut out speed of $4.5m/s$. C_T, the turbine thrust coefficient,

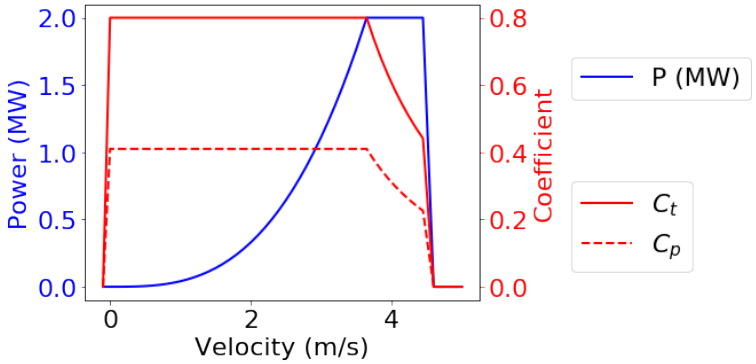

Figure 3.3: Power curve of a typical generic tidal turbine assumed for this work.

which corresponds to the idealised thrust curve shown in Fig. 3.3, is 0.8 below rated and is scaled by $\frac{u^3_{rated}}{u^3}$ above rated speed. In reality the drag force will be increased partly due to the rotor thrust represented in (1.8) and in part due to the drag of the turbine structure system. The latter is not included explicitly in this work, because the drag of the structure is relatively small compared to the rotor thrust and this work considers a highly idealised example to demonstrate this new method of economic optimisation. Furthermore, the calculation of the support structure drag depends on design chosen by manufacturers, so this chapter remains generalised by simply using a high C_T [84]. The implications of this assumption and a method for handling the turbine structure drag is discussed in Section 3.7.

The total number of turbines is found from the array density using (1.10), and the time-averaged power is found similarly using (1.11). These two parameters are combined in the functionals discussed in Section 3.3 to help quantify the financial success of the array. In this chapter, C_P, the turbine power coefficient, is 0.41 below rated [98] and is scaled by $\frac{u^3_{rated}}{u^3}$ above rated speed, as also show in in Fig. 3.3.

Experiments were carried out in [165], to investigate the validity of using a depth-averaged continuous drag method of representing turbines for tidal resource analysis. Porous fences spanning the width of a recirculating flume were used to simulate the added drag of a large, multi-row, uniformly-distributed array of tidal turbines. Load cells were used to measure the thrust force on each porous fence, and these measurements were compared to the results of the continuous drag method. The level of agreement between the depth-averaged flow speeds used in (1.8) and the local flow through the turbine rotor (represented by the porous fences) determines the accuracy of the depth-averaged continuous drag method for representing turbines. This agreement was shown to be dependent on the level of wake recovery and longitudinal spacing between rows and the magnitude of the ambient turbulence, which

aids the mixing between the wakes and the accelerated bypass flow. Bed mounted ADCPs have shown that while the turbines are operational the turbulence intensity at the MeyGen 1A site is 10–12% [166]. Actuator disc experiments have found these turbulence intensities to correspond to an approximately 40% wake deficit at 5 diameters downstream and an approximately 20% deficit at 10 diameters downstream [167].

Further studies [168, 169, 47] demonstrate that wake impingement on downstream turbines in relatively dense arrays causes depth averaged flow speeds to overestimate the true flow speeds through the turbine rotor. The maximum array density has been specified to allow for sufficient longitudinal spacing between rows, to address this effect and allow for wake recovery. The European Marine Energy Centre (EMEC) recommend a greater spacing of 2.5 turbine diameters centre to centre and 10 diameter downstream, however they acknowledge that this can be shown to be a conservative spacing requirement once detailed wake effect modelling is undertaken [170]. The maximum allowable turbine density is therefore chosen to be slightly higher than this guideline, and to allow for designs with decreased lateral spacing between turbines. Numerical simulations in idealised channel flows by Consul et al. [171] showed that yield increases of up to 23% could be achieved by increasing blockage ratios and the recently developed Orbital O2 tidal device consists of two 1MW 20m diameter turbines mounted either side of a floating superstructure, with a 25m distance centre-to-centre. This is equivalent to a 1.25 diameter spacing laterally, so the upper limit on the turbine density used in this chapter in that case would be equivalent to imposing a minimum spacing of 10 turbine diameters downstream. This work demonstrates the method of optimising arrays to minimise the LCOE on an idealised domain. When applying this method to modelling real tidal sites the limitations on the turbine spacing can be updated as relevant information becomes available for a given site. An appropriate upper limit on the turbine density for any given site can be chosen once site specific ambient turbulence has been characterised, since turbulence intensity and length scales relative to rotor diameter have been shown to have a significant impact on wake recovery rate [167].

3.4.6 Adjoint-based optimisation

Optimisation of the array design, with respect to the different economic functionals outlined above, is performed using $d(\mathbf{x})$ as the control parameter. The optimisation procedures begins with zero turbines everywhere, then on each itera-

tion the forward model is run (solving the shallow water equations coupled with the turbine friction to find the power and other array characteristics, as described above), then the functional values are recalculated. The adjoint is calculated (via `http://pyadjoint.readthedocs.io/` library), to find the sensitivity of the functional to changes in the turbine density, while coupled to changes in the hydrodynamics. This information is fed into a L-BFGS-B based optimisation algorithm, to update the turbine density field in such a way so as to optimise the economic functional of choice. An optimal design is converged upon and the algorithm is completed, typically for this scenario within 5 to 20 iterations.

3.5 Array optimisation

An idealised set-up is used to test the impact of different functionals, which account for economic factors in increasing levels of detail, on optimal array design. First, the impact of varying break even power is investigated, followed by an optimisation where the break even power depends on the number of turbines employed through economies of volume. Similar studies that vary break even power [4] and economies of volume [3] are extended here over a greater range, to form the basis of the new optimisation procedure developed in the next section.

3.5.1 Varying break even power

The array design is optimised within the farm area, A_f, where the flow is accelerated in the vicinity of the island in the constricted channel setup shown in Fig. 3.1. Fig. 3.4 shows how the optimal array design varies as the break even power increases, using the functional described in (3.1). In Fig. 3.5 it is shown that as the break even power increases the net average power of the array and the number of turbines in the optimal array design decreases, because turbines are effectively more expensive to install, while the power per device increases, because fewer turbines result in lower blockage.

The break even power is varied from P_{BE} = 0MW to 1.3MW. $1.3MW$ is the highest break even power that can be specified before the optimal design consists of no turbines because the flow is not high enough for any one turbine in any location within A_f to generate more than 1.3MW. The optimisation is also performed in the other extreme for P_{BE} = 0MW. While this is possible numerically, in reality the

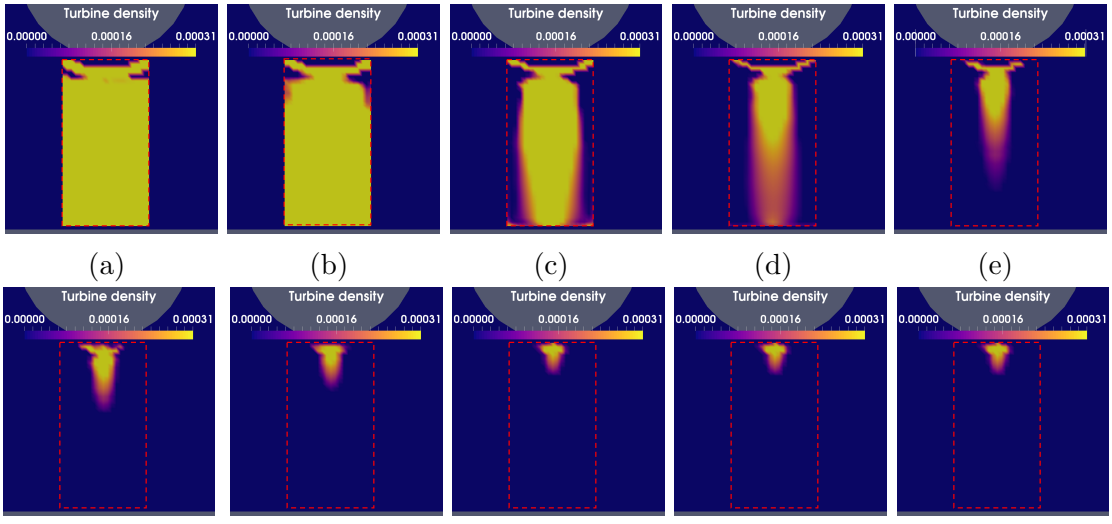

Figure 3.4: Array designs optimised for $J = P - P_{BE} \times n_t$, with a break even power of (a) 0, (b) 0.1, (c) 0.2, (d) 0.3, (e) 0.4, (f) 0.5, (g) 0.6, (h) 0.7, (i) 0.8 and (j) 0.9 MW. The farm boundary is shown in red, areas with maximum turbine density are shown in yellow and no turbines shown in blue.

break even power would never be zero, because that would mean that the turbines are free. Setting the break even power to zero thus changes the functional from an economic one to one that optimises for power alone. This is commonly used in some array optimisation studies ([81, 57, 83]) and is sensible if there is already a fixed number of turbines chosen. However, having a non-zero and appropriately chosen break even power becomes crucial if the number of turbines varies, because this allows the right balance between maximising power and minimising costs to be found. Including this as a case has two benefits, firstly to demonstrate the limit of no economic penalty and investigate financial models over a broad range of sample points, even extreme ones.

Secondly it helps demonstrate the impact of global blockage. In Fig. 3.4a, even though there is no cost associated with the turbines because $P_{BE} = 0$MW, there are no turbines added in the semi-circular region around the island. Adding turbines here creates so much blockage that the power generated by the additional turbines is offset by the losses experienced by the other turbines. This array design represents a hypothetical maximum of how much power could be extracted if cost were not an issue, but in reality would never be economically practical.

A qualitative shift can be observed for $0.2 \leqslant P_{BE} \leqslant 0.4$MW, where the optimal array design paradigm shifts between a barrage or fence-like design that spans across the whole width of the channel (to exploit the benefits of channel-scale blockage control)

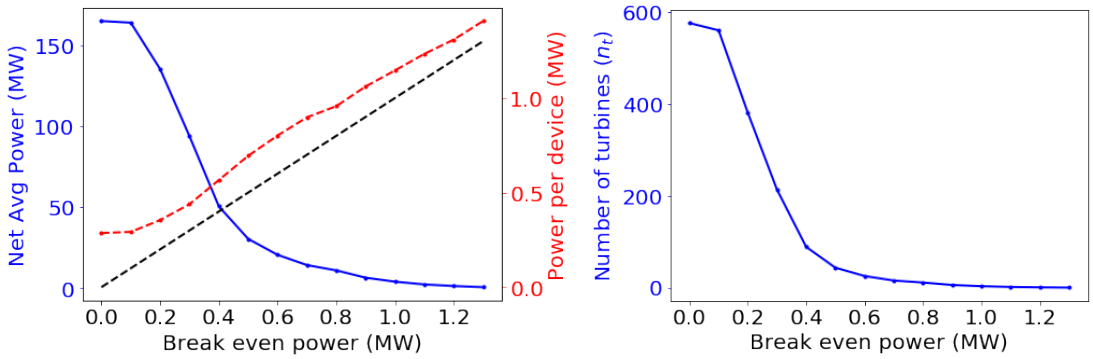

Figure 3.5: Variations in the total array power generated and the number of turbines for the optimal design as P_{BE} is increased, adapted from [4]. The black line shows that the average power per device (in red) always stays higher than the P_{BE} chosen in the functional.

to a cluster of turbines close to the island just taking advantage of the locally high flow velocities. This can be seen clearly though the sharp drop in net average power and optimal number of turbines, shown in Fig. 3.5. In this region small changes to the functional result in large changes to the optimal array design. This is problematic for array design, because there may be uncertainty in the appropriate choice of P_{BE} and it may vary with array size due to economies of volume. These results are discussed in more detail in [4].

3.5.2 Break even power with economies of volume : results

Next, realism is added to the functional, by making the break even power decrease linearly with number of turbines, such that $P_{\mathrm{BE}} \Rightarrow P_{\mathrm{BE}} - \mathrm{EV} \times n_t$, where EV is a parameter representing economies of volume. Fig. 3.6 shows how the macro array parameters, such as optimal number of turbines, total array power and average power per device, vary with the break even power and economies of volume.

Fig. 3.6 demonstrates that as the economies of volume are increased, the optimal number of turbines increase and therefore the total array power increases, since higher numbers of turbines result in lower costs per turbine. However, the power per device decreases, because through economies of volume the turbines are effectively cheaper and therefore do not need to generate as much power to be worth installing.

A key result of both of these pieces of work is that the optimal array design is greatly dependent on the choice of functional, and especially sensitive to small changes in the break even power for mid range values in the region $0.2 \leqslant P_{BE} \leqslant 0.4$. Changes

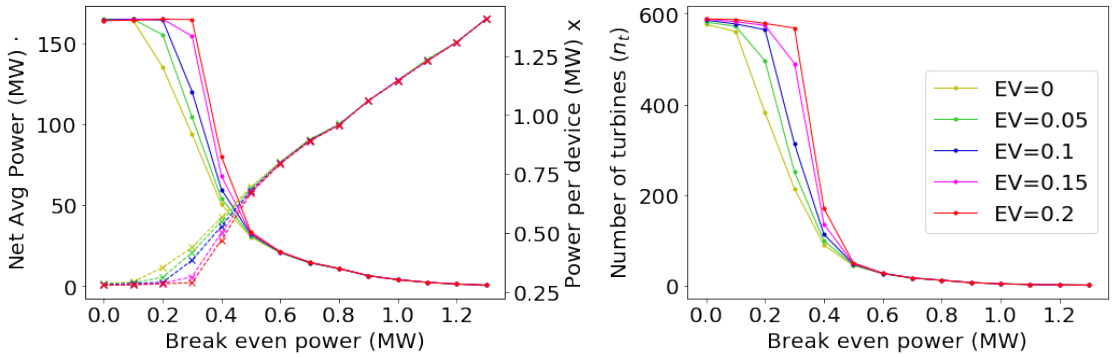

Figure 3.6: Variations in the average power generated and the number of turbines for the optimal design as P_{BE} and ev are increased.

to the scaling parameter EV, make relatively little impact on the optimal array design outside of this range and a significant impact within it. This shows that the optimal array design is very sensitive to changes in P_{BE} at mid-range values (for more details see [3]). Since both functionals used are a simplification of the true profitability of an array, there is a need to optimise for a more complete financial model.

3.6 Economic Emulator

Each of the optimisation scenarios presented in Section 3.5 are obtained through running the full hydrodynamic model in a computationally expensive optimisation loop. This chapter presents an original method, where those optimisation runs can be performed in order to generate data to construct an emulator. The emulator can be used for the rapid assessment of optimal array parameters (such as number of turbines, array power and power per device) over a large range of functionals. This emulator is demonstrated by optimising LCOE over a variety of cost inputs. In order to validate the emulator predictions of optimal LCOE and number of turbines, the LCOE formula defined in (3.3) is used as the functional in a fully coupled hydrodynamic model and optimisation in *Thetis*. This is the first instance of coupling a hydrodynamic model of an array design in *Thetis* with a complex financial model of the array, such as LCOE, used as the functional of interest.

3.6.1 Schema of emulator-based methodology for the economic analysis of array design

The following sections present, in detail, the development and validation of an emulator method, which is demonstrated to be fast and flexible at identifying optimal array characteristics. The process developed can be applied to real world array design. A simplified summary of the steps to optimise a tidal array design in practice is as follows:

1. Build and validate a hydrodynamic model of the region of interest in *Thetis*.
2. Perform adjoint optimisation of the array design with respect to $J = P_{avg} - P_{BE} \times n_t$ over a range of sufficiently many (approximately ten to twenty here) different values of P_{BE}. This yields a set of turbine densities and corresponding optimal power versus number of turbines data points.
3. Interpolate between those data points to build an emulator to predict the optimal power that can be achieved over all possible numbers of turbines.
4. Use the emulator to feed P_{avg} and n_t values into an economic model of choosing, such as LCOE, Net Present Value, Internal Rate of Return or Payback Period. Choose the array size which optimises the metric of interest.
5. Perform Monte Carlo sensitivity analysis over the full range of uncertainty in the cost inputs used in the economic model, obtain P50, P10 and P90 values, which translate to the median value and 80% confidence interval.
6. Use this more detailed analysis to decide on an array size that keeps the P10, P50 and P90 predictions within a desirable range.
7. Perform a final full adjoint optimisation of the array size chosen to produce a map of the spatial distribution of turbines and validate the predictions of the emulator.

3.6.2 Building an emulator by finding the Pareto frontier

In Section 3.5.1 three parameters appear in the functional for break even power alone; P, n_t and P_{BE}, where in this work both P are n_t are found as a function of the turbine density field $d(\mathbf{x})$ and are obtained through the optimisation process.

This is true for the extended scenario in Section 3.5.2 also, with the addition of a fourth parameter for economies of volume, EV. There are therefore one or two parameters (P_{BE} or P_{BE} and EV) in each of the previous sections, which need to be decided upon before running the optimisation, each of which has uncertainty involved in the choice of parameter value. When there are only one or two input parameters to vary it is relatively easy to investigate the impact of this uncertainty. The optimisation process can simply be run repeatedly so that the impact that changes in parameter values over their plausible range make on the optimal design can be investigated.

However, when optimising for LCOE or other economic models which are derived from Net Present Value (NPV) analysis there are a large number of uncertain input parameters. NPV calculations require not only P and n_t to be known, but also r, L, T_e and all of the costs across all of the years of the array's lifetime. In this work those costs are simplified to be represented by only four parameters, C_t, C_f, O_t and O_f, by the assumptions made in (2.18) and (2.19). Even with this simplification, this would still require varying the chosen input parameters within a seven dimensional space to test the impact of uncertainty. This reduces to six dimensional space when using LCOE models instead of NPV, by removing the need to specify T_e — the input with arguably the most uncertainty [106] — through optimising at the break even point, NPV = 0. Full uncertainty quantification via the variation of all input parameters, would be prohibitively expensive because it would require an optimisation to be performed for every set of parameters.

This creates a need for a simpler, computationally cheaper proxy model, with which the uncertainty analysis can be performed through consideration of a great range of parameter values. In all of the economic models considered in this work, the costs are assumed independent of the turbine locations. Therefore, for the scenario considered here there will be an optimal array design which achieves maximal power for each possible number of turbines – from 0 to 576 (the number of turbines at which maximal power can be generated). With the maximum density, $d(\mathbf{x})$ and farm area, A_f, specified in Fig. 3.1, up to 600 turbines could be installed, but any more than 576 would generate less power than the optimal solution for $P_{BE} = 0$, from Fig. 3.4a. While there are no location-based costs, the optimisation procedure can be reduced to a bi-objective optimisation problem of choosing the optimal balance between number of turbines (corresponding to the costs of the array) and net average power (corresponding to the revenues of the array). Further work could include location-based costs at the site-scale by adjusting the CAPEX and OPEX appropriately for

the average distance to shore and depth, using the spatial tool developed by Vazquez and Iglesias [99].

Therefore, the optimal power that can be achieved for a given number of turbines can be plotted against number of turbines, as shown in Fig. 3.7 (a). If a curve can be fitted between these points, each of which is found through the *Thetis* optimisation of the spatially-varying turbine density, then a bi-objective trade-off curve is found, where improving either the power or number of turbines deteriorates the other parameter. Any formulation of the functional, which monotonically increases with power for a fixed n_t and, reversely, monotonically decreases with n_t for a fixed power, will have an optimal solution which falls somewhere along this trade-off curve. In multi-objective optimisation, this is known as a Pareto frontier, where the points on the trade-off curve form the set of all Pareto efficient solutions. Pareto efficiency is a condition where no performance criterion can be improved upon without a trade-off making at least one other criterion worse. In this case, each optimal solution shown in Fig. 3.7 (a) is Pareto efficient because the power can not increase without the number of turbines (and therefore the cost) increasing, and vice versa. The different economic models and choice of input parameters values just shift the weighting between the two.

The values from the break even power study are just used as an example of how the Pareto frontier can be explored using a simple functional and by varying one parameter. Increasing P_{BE} from 0 to rated power ensures that there are samples distributed across the Pareto frontier. Once the sample points are obtained, for example from the break even power study, an emulator for the optimal achievable power for each number of turbines can be created, here through the use of quadratic (cubic giving essentially the same result) spline interpolation between each successive pair of points. Quadratic spline interpolation is sufficient to produce a smooth curve between the optimal points found from the break even power study and increasing to cubic spline interpolation had little impact on the shape of the curve fitted. This curve can be used to predict the optimal net power that can be achieved as a function of the number of turbines in an array, i.e. $P \equiv P(n_t)$. Therefore, the optimisation can be considered a problem in just one dimension – choosing the optimal number of turbines for the economic functional chosen.

Fig. 3.7 (a) demonstrates how this interpolation, for the fourteen data points obtained from optimisation runs when break even power varies from 0 to 0.8 MW, can be used to build an emulator to predict the net average array power and other related characteristics such as power per device. The emulator is used to produce the curve

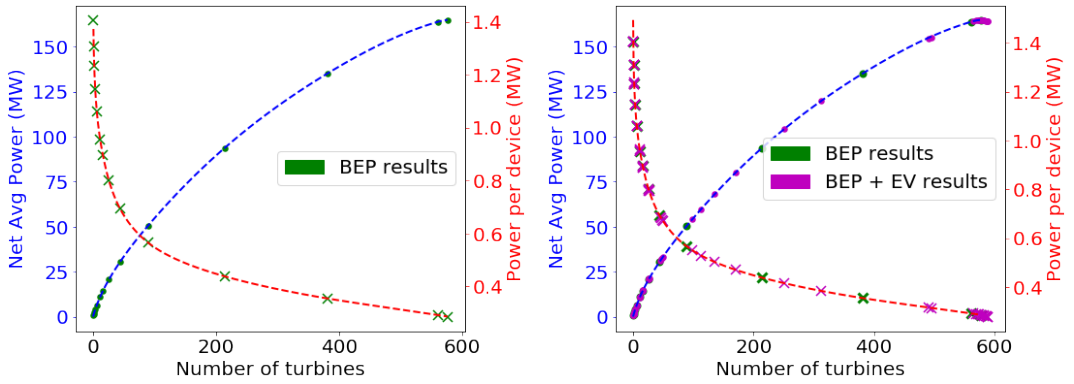

Figure 3.7: (a) The fourteen data points from the break even power study (shown in green) and the emulator for optimal power that can be generated from these as a function of the number of turbines. (b) The emulator compared to the optimised array parameters from 36 simulations optimising for break even power with economies of volume added (shown in magenta). For both studies the optimised array power is marked by a dot and the optimised power per device is marked by a cross.

of predicted net powers, shown in blue, and predicted average powers per device, shown in red. The predictions generated by this emulator are compared in Fig. 3.7 (b) to the results obtained when optimising for break even power with economies of volume, based on the functional (3.2). This testing demonstrated that quadratic spline interpolation is more than sufficient to match the *Thetis* model data. It can be seen that running the computationally expensive *Thetis* optimisation model only fourteen times is enough to obtain good predictions for these 84 optimisation scenarios. A user may be able to reduce the number of optimisation model runs needed if some minimum array power level is required to make a significant energy contribution, which would allow the minimum number of turbines considered to be increased above the low numbers included in this example, for example.

3.6.3 LCOE Results

Once the emulator has been generated, instead of re-running the expensive optimisation loop in *Thetis*, the LCOE can be estimated across all possible n_t values, with the corresponding $P(n_t)$ values found from the emulator. The n_t which minimises the LCOE can then be obtained. Fig. 3.8 shows this approach for finding the optimal LCOE and corresponding number of turbines for three different sets of parameter values. The first set uses the typical values shown in Table 2.4, the second set uses the highest L values and the lowest values for all other parameters

in order to find the optimal LCOE in the best case scenario given the uncertainty in parameter values, and the final set uses the reverse to find the optimal LCOE in the worst case scenario.

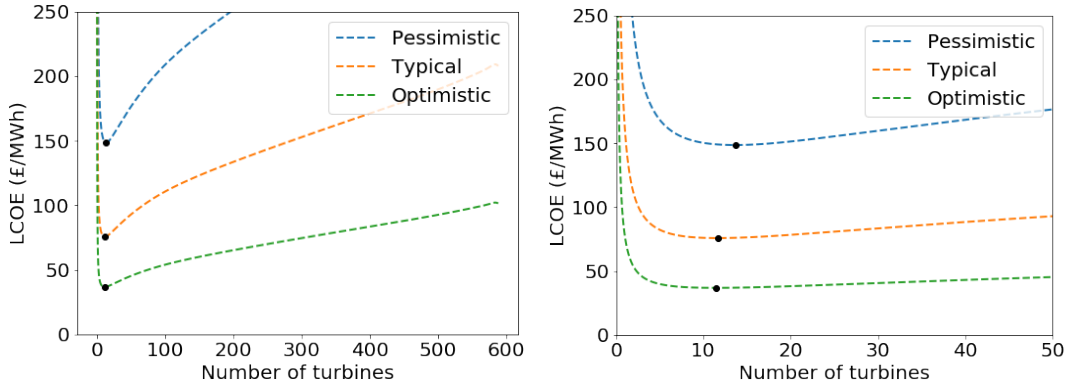

Figure 3.8: The emulator prediction for LCOE across all n_t values from 0 to 600 and a snapshot around the optimal values. The optimal LCOE for each set of parameter values is shown as a black dot, and the input parameters are chosen to match the pessimistic, typical and optimistic values shown in Table 2.4.

Results presented in Sections 3.6.4 and 3.6.5 demonstrate how the emulator can be used to enable the prediction of the optimal array design for LCOE under a large range of parameter values. The main findings are that the CAPEX has more influence on the LCOE and optimal array features than the OPEX, due to CAPEX accounting for a higher percentage of the lifetime costs, especially when a high discount rate is applied. The turbine-dependent components of the costs, CA_t and O_t, have more impact on the LCOE than the fixed components. This is despite the fixed components having a greater uncertainty range to vary over (the pessimistic estimate for CA_f is 2.5 times the optimistic estimate, whereas the pessimistic estimate for CA_t is 1.8 times the optimistic estimate) and the fixed components being approximately three times the size of their respective turbine dependent components (CA_f is 2.3, 2.8 and 3.2 times the size of CA_t in the optimistic, typical and pessimistic cases respectively. Similarly O_f is 2.9, 2.1 and 3.3 times the size of O_t in the optimistic, typical and pessimistic cases). This is because the turbine dependent components of the costs are multiplied by the number of turbines, so becomes more dominant as the number of turbines increases. The results presented in Sections 3.6.4 and 3.6.5 also demonstrate that when the cost parameter values change the LCOE varies a lot more than the optimal number of turbines. Overall it demonstrates that the variability of the optimal solution with different parameter choices is interconnected with other parameter choices. This is an example of in depth sen-

sitivity analysis that would be computationally prohibitive to perform using direct optimisation over a vast number of different functionals.

Emulator validation for LCOE results

Fig. 3.9 shows how the number of turbines and LCOE for the final iterations of the *Thetis* optimisation procedure compare to the curve found using the emulator for the optimal LCOE that can be achieved for each number of turbines in the array. The optimal LCOE and corresponding number of turbines from the emulator is marked as a black dot, with the final iteration of the *Thetis* optimisation marked with a black cross. Three scenarios are compared – when all the parameters are set to their typical value from Table 2.4 and when all are set to their typical value except CA_t, which is set to the maximum and minimum value.

This comparison demonstrates how the selection of the optimal design differs between the two methods; the emulator starts by estimating the LCOE for the optimal design for each number of turbines, then selects the number of turbines that minimises this, the *Thetis* model starts with an initial turbine density field then optimises it until the LCOE improves no more. The final iterations are included in Fig. 3.9 to make the point that each iteration will always be on or above the curve from the emulators. This is because the *Thetis* model starts with a non-optimal turbine configuration and improves the density field until it ends up on the configuration that optimises the given functional, whereas the emulator starts with the Pareto frontier, where the turbine configuration maximises the power generation for any given number of turbines, and from this information selects the n_t which optimises the functional.

Fig. 3.10 compares the optimal solution obtained via the *Thetis* model to the predictions of the emulator. Since the emulator is much cheaper to run, predictions across the whole range of parameters from max to min are shown, whereas only the max, min and typical values are shown for the *Thetis* model. These results show that the predictions for LCOE are quite accurate and the emulator is suitable for predicting LCOE. However, they also show that the predictions for the optimal number of turbines has a much greater error. Inspection of Fig. 3.9 shows that the LCOE curves are relatively flat and very insensitive to changes in the number of turbines near to the optimal solution. This shows that the optimal solution may be a robust one, however accuracy in n_t predictions may be harder to obtain because of this. Furthermore the magnitude of the error is approximately one turbine or less,

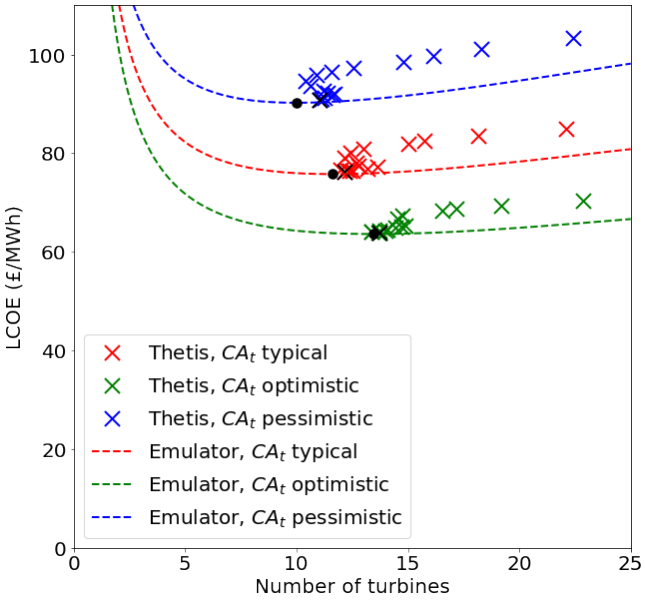

Figure 3.9: The emulator prediction for how LCOE varies with n_t, shown as a dashed line, compared to the final iterations of the *Thetis* optimisation, shown as coloured crosses. The optimal LCOE from the final iteration of the *Thetis* optimisation for each set of parameter values is shown as a black cross. The optimal LCOE from the emulator is marked as a black dot. The results for where CA_t is set to its max, min and typical values are shown, while all other parameters set to their typical values.

except for the optimistic CA_f scenario, where it is almost two turbines.

Fig. 3.11 shows how each of the solutions obtained via the *Thetis* model lie on (or very close to) the Pareto frontiers for optimal array power and power per device, obtained from the emulator. This further supports the conclusion that the emulator can be used to accurately find the set of array designs with an optimal trade-off between number of turbines and power.

Monte Carlo evaluation of LCOE predictions

Since there is a significant degree of uncertainty in the input parameters from Table 2.4, there is a drastic difference between the LCOE predictions in the optimistic and pessimistic scenarios shown in Fig. 3.8. This LCOE variation is so large partly due to the fact that the costs are commercially sensitive so it is hard to obtain an academic prediction of them. They are also subject to change with time, because costs in the industry will fall due to learning rates. However, variation is also exaggerated due to the pessimistic and optimistic scenarios being the combination of all inputs at their most extreme values, when in practice this is very unlikely.

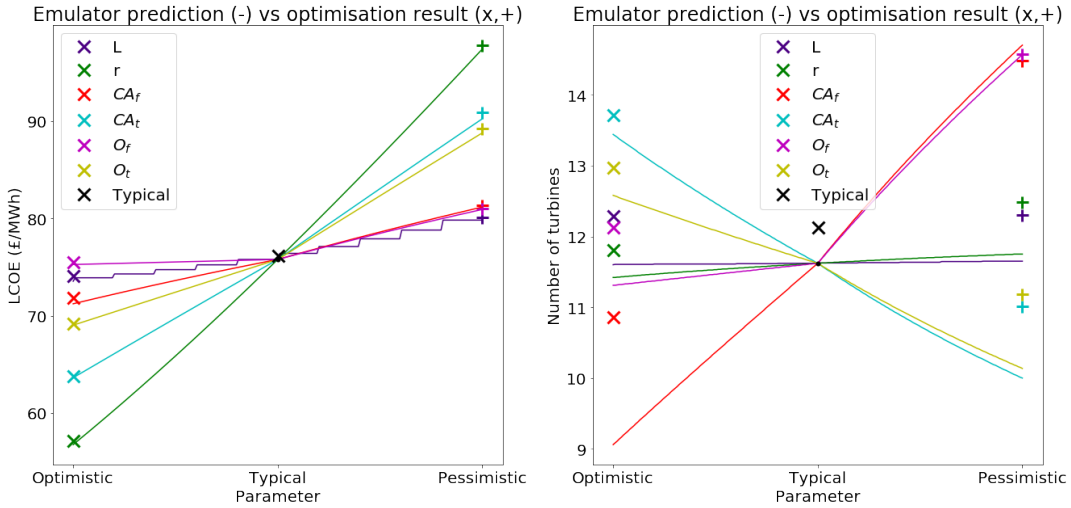

Figure 3.10: The impact that varying each of the input parameters, from the optimistic (x) to pessimistic (+) value given in Table 2.4, has on the optimal LCOE and number of turbines. This demonstrates the small errors between the optimal solution obtained through the emulator, shown as a line evaluated over all intermediate values too, and from the *Thetis* optimisation, shown as crosses. The line for L decreases in steps because the years increase discretely.

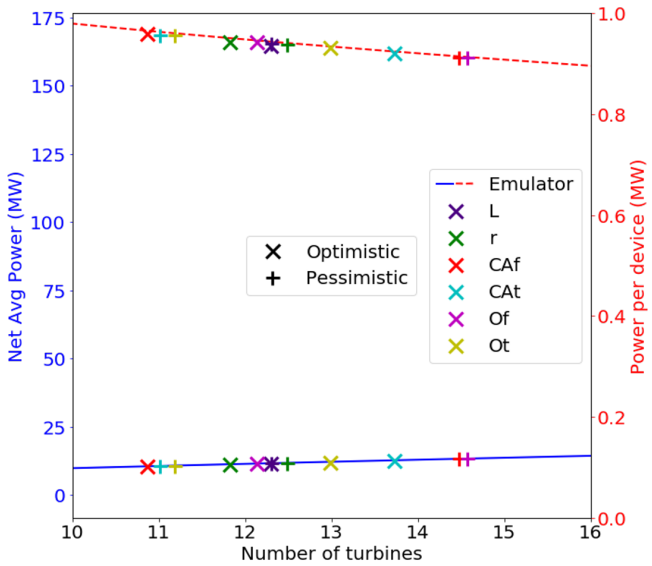

Figure 3.11: The net time-averaged array power and the average power per device generated in each of the optimal array designs obtained in *Thetis* as each of the input parameters are varied from their optimistic (×) to pessimistic (+) value, as given in Table 2.4. This demonstrates that all optimal solutions lie on the line of emulator predictions for the relationship between number of turbines and optimal power that can be achieved.

The traditional static and deterministic financial models, such as that described in (3.3), produce a single value of LCOE or NPV for each energy project. Stochastic

methods, such as Monte Carlo analysis, can capture the impact that uncertainty in the input variables has on the economic viability [172]. Monte Carlo simulations consist of repeated random sampling and statistical analysis of the results to capture sensitivities to the inputs. Monte Carlo simulations take all uncertain variables and assign a random variable to each according to an assumed distribution. In this case the uncertain variables are the inputs in Table 2.4 and a uniform distribution is assumed between their most pessimistic and optimistic values. The result (in this case the LCOE) is then re-calculated with the new random variables and this process is repeated many times with new random sampling each time. Ten thousand re-samplings of the LCOE within a Monte Carlo simulation ensures here that the mean and median across samples are stable each time the Monte-Carlo analysis is re-run, and is computationally practical due to the efficiency of the new emulator method. This is a novel feature of the emulator method developed in this chapter, compared to other numerical methods of optimising array design which would be too computationally expensive to generate a sufficient number of samples for Monte Carlo analysis to be stable. The LCOEs found in each of the resamples can then be ordered so that the 10th, 50th (i.e. the median) and 90th percentile can be found, these are termed the P_{10}, P_{50} and P_{90} values. 90% of the resampled LCOE predictions are better (lower) than the P_{90} values, whereas only 10% of the resampled LCOE predictions are better than the P_{10} values.

This gives a much more realistic representation of how much the LCOE is likely to vary with respect to uncertainty in the inputs from Table 2.4. The results of such analysis are shown in Fig. 3.12. In practice the uncertainty in the input values is more likely to follow a Gaussian distribution, with greater weight given to the values around the mean, typical value and lower weight given to those nearer the optimistic and pessimistic ends of the spectrum. This would result in even less variation between the P_{10} and P_{90} results and more certainty in the LCOE predictions in the following results. However, a Gaussian distribution would need to be defined with a standard deviation of the uncertainty in the inputs based on published values. There are currently not enough publicly available data points for each of the cost inputs in Table 2.4 to derive a standard deviation and define an appropriate Gaussian distribution. Therefore a more conservative uniform distribution is assumed instead. In practice however, tidal developers using this approach may have a far more detailed and accurate range of cost estimates, based on discussions with their suppliers. They would therefore be able to use this approach combined with their internally held financial information to generate LCOE predictions with far lower P_{10} to P_{90} uncertainty ranges, than those given in this thesis.

As discussed in Chapter 2, the variability between the Optimistic, Typical and Pessimistic costs scenarios likely reflects the great rate at which costs have already fallen from the first demonstrator projects and are anticipated to fall with learning in the industry [12]. It is likely that as the cumulative installed capacity for tidal increases further the LCOE will fall from the P90 to P50 to P10 values. It is also noticeable that in the optimistic, typical and pessimistic cases, once the optimal number of turbines is exceeded, the LCOE increases, but slowly. A developer may see modest increases in LCOE as acceptable in order to produce more energy.

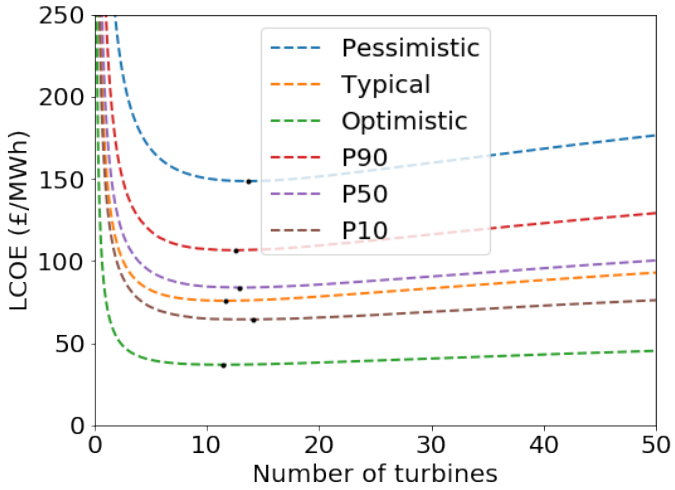

Figure 3.12: Predictions for the optimal LCOE that can be achieved for each number of turbines, and the resultant array design that minimises it, for the pessimistic, typical and optimistic scenarios outlines in Table 2.4, as well as the P_{10}, P_{50} and P_{90} values obtained through a Monte Carlo simulation assuming uniform distributions of uncertain parameters.

The optimal LCOE found in the pessimistic, typical and optimal scenarios are £149/MWh, £76/MWh and £37/MWh respectively. Applying Monte Carlo analysis reduced this range to a P_{90}, P_{50} and P_{10} value of £107/MWh, £83/MWh and £64/MWh respectively. The optimal number of turbines always remained between 11 and 14, highlighting that optimal array design lies between the $P_{BE} = 0.7$ and 0.8MW designs shown in Fig. 3.4h and 3.4i. In all scenarios it can be seen that increasing the number of turbines past the optimal number does not increase the LCOE dramatically. Therefore there is a lot of flexibility for developers hoping to install an array of a larger size, while keeping the LCOE below a maximal acceptable value.

3.6.4 Sensitivity with respect to cost estimates

This section considers the sensitivity of the LCOE, number of turbines and power generation of the optimal array design to changes in the capital and operational cost parameters that it was designed for. This level of sensitivity analysis where multiple parameters are varied together, to analyse their interacting effect on the optimal design, would be prohibitively computationally expensive without the use of the new emulator method.

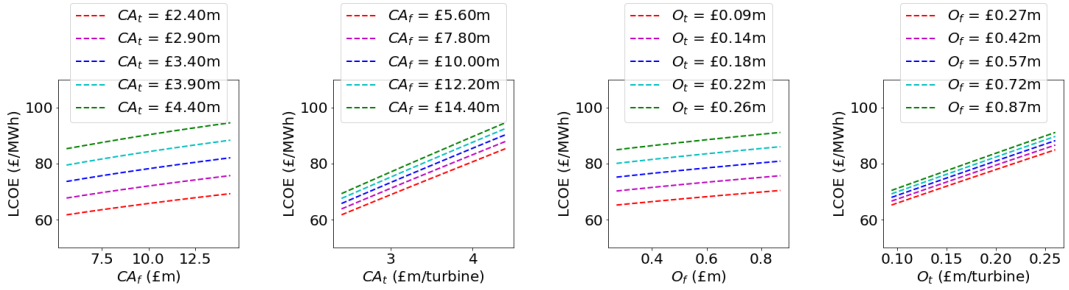

Figure 3.13: The optimal LCOE that can be achieved changes as each of the cost parameters are varied.

Fig. 3.13 shows how the LCOE of the optimal array design varies as different values of CA_t, CA_f, O_t and O_f are tested in the economic (LCOE) model used for the optimisation functional. The parameters which are not being varied are set to their average values from Table 2.4, with the lifetime of the array set to 20 years and the discount rate set to 10%. CA_t, CA_f, O_t and O_f are all varied from their minimum to maximum estimates supported by the literature review, in Chapter 2. As expected, it can be seen that as each of the cost parameters is increased the optimal LCOE also increases, as energy becomes more expensive to produce.

Since Capital costs make up a higher percentage of the lifetime costs than Operational ones, especially once discounting is taken into account, varying the CAPEX parameters has more impact on the optimal LCOE than varying the OPEX parameters. This is seen despite the greater relative range of uncertainty in the OPEX parameter estimates than in the CAPEX ones. For both CAPEX and OPEX, varying the turbine-dependent component has more impact on the optimal LCOE than varying the fixed component of the costs. This is again despite the fact that the range of uncertainty in the fixed component parameter estimates is much greater than the range of uncertainty in the turbine-dependent parts. This is because although CA_f is approximately three times the size of CA_t, CA_t is multiplied by

the number of turbines in an array, so it soon becomes the dominant factor as n_t increases.

Depending on the combination of input cost parameters the optimal LCOE that could be achieved varied from around £60/MWh to £100/MWh. By comparison the OREC 2018 analysis [12], predicted that tidal stream in the UK has the potential to reach an LCOE of £150/MWh at 100MW cummulative capacity and £80/MWh by 2GW cummulative capacity. While this model is of an idealised channel, it has velocities similar in magnitude to potential tidal sites such as the Alderney Race and Pentland Firth, so it seem promising that the LCOE predictions are of a similar magnitude, although slightly optimistic.

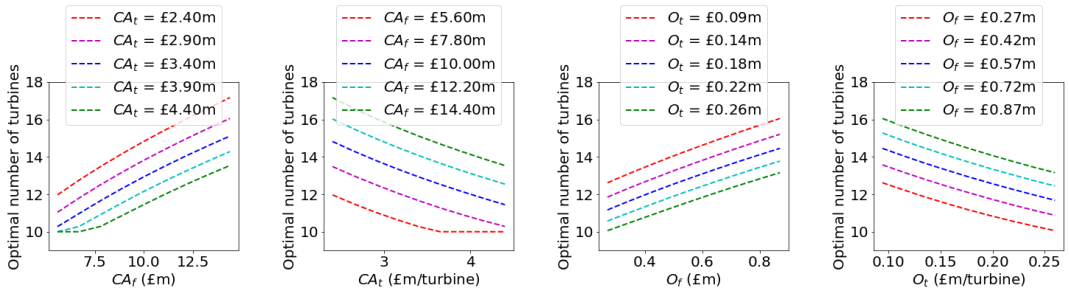

Figure 3.14: The number of turbines, n_t, in the array design that results in the optimal LCOE, as each of the cost parameters are varied.

Fig. 3.14 shows how the corresponding number of turbines in the optimal array design varies as different values of CA_t, CA_f, O_t and O_f are considered. Predictably, as the turbine-dependent costs are increased the optimal number of turbines decreases, since they are more expensive to install. However, as the fixed costs increase the optimal number of turbines increases. As CA_f becomes larger with respect to CA_t, the impact of economies of volume becomes more significant and more turbines are required to spread the initial fixed costs over. Similarly, the optimal n_t increases as O_f increases with respect to O_t. Again, the uncertainty in OPEX estimates have less impact on the optimal number of turbines than the uncertainty in CAPEX estimates. This is despite there being greater variation in OPEX, due to CAPEX being a higher factor in the lifetime discounted costs of an array. However, the optimal number of turbines varies by a similar very amount over the minimum to maximum range of fixed costs compared to turbine-dependent costs, despite the LCOE being more sensitive to variation in turbine-dependent costs.

Fig. 3.15 and Fig. 3.16 show how the total array power and the average power

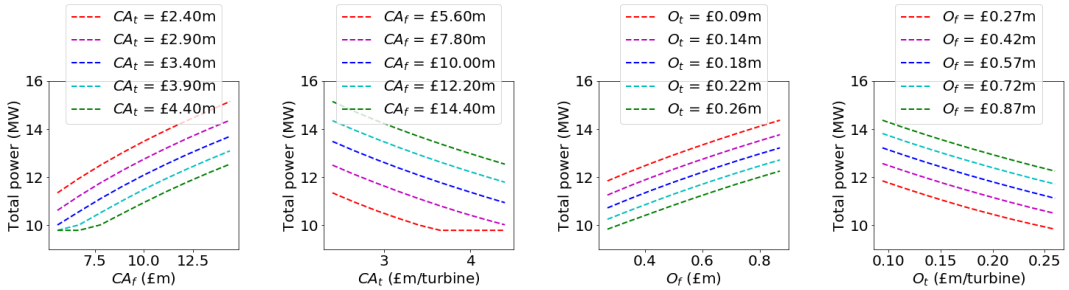

Figure 3.15: The total array power of the design that results in the optimal LCOE as the cost parameters are varied.

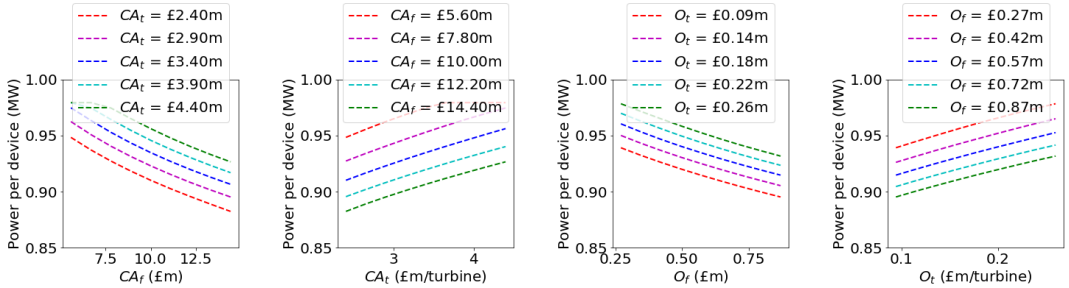

Figure 3.16: The average power per device in design that results in the optimal LCOE as the cost parameters are varied.

per device of the optimal array designs vary with different values of CA_t, CA_f, O_t and O_f, respectively. They show that as the fixed costs increase (for both CAPEX and OPEX), the total array power increases, but the average power per device decreases. This corresponds to the increase in the number of turbines with increased fixed costs shown in Fig. 3.14. The higher the fixed costs the more power needs to be generated to compensate for it, even if this comes at the expense of more turbines and a lower return per turbine. Conversely, as the turbine-dependent costs increase the total power decreases but the average power per device increases. As the turbines become the more costly part of the array expenses, fewer turbines should be installed, allowing a higher percentage of them to fit in the fastest flowing locations. Similarly to LCOE and n_t, varying the CAPEX has a greater impact on the total array power and average power per device than varying the OPEX.

3.6.5 Sensitivity with respect to array lifetime and discount rate

Similarly, the sensitivity of the optimal design to change in L and r with respect to one another can be investigated. Fig. 3.17 shows how varying both parameters impacts the optimal LCOE and the number of turbines at which the optimal LCOE is found. Varying the discount rate is found to have a bigger impact on the optimal LCOE than varying the lifetime of the array, and as the discount rate increases the impact of the lifetime on both the LCOE and the number of turbines decreases. This is because discounting minimises the impact of the revenue and expenditure in the final years of the array on the LCOE and the greater the discount rate the less impact increasing the lifetime will have.

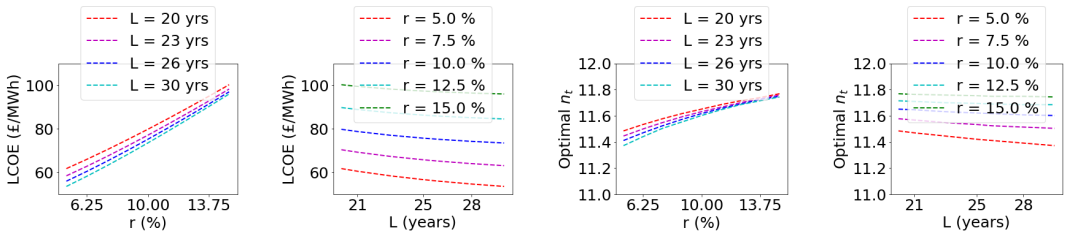

Figure 3.17: The total LCOE and number of turbines in the array design that results in the optimal LCOE as the lifetime of the array, L, and the discount rate, r, are varied.

While lifetime has relatively little impact on the LCOE, the discount rate has an impact of similar magnitude to varying the cost inputs, shown in Fig. 3.13. However both the discount rate and the lifetime of the array have very little impact on the optimal number of turbines, compared to the costs shown in Fig. 3.14. This is because the balance of fixed to turbine-dependent costs changes the extent to which there are economies of volume, and therefore moves the optimal number of turbines more, whereas L and r shift the LCOE vs n_t curve (such as that shown in Fig. 3.8) up and down, but do not change its shape much.

Fig. 3.18 shows how the total array power and the average power per device of the optimal array designs vary with different values of L and r. Again it can be seen that the discount rate has more impact than the lifetime on the total and average power generation, but both have much less impact than varying CA_t, CA_f, O_t and O_f, as shown in Fig. 3.15 and Fig. 3.16. Since varying these parameters has very little impact on the number of turbines, it is not changing the array design, and therefore

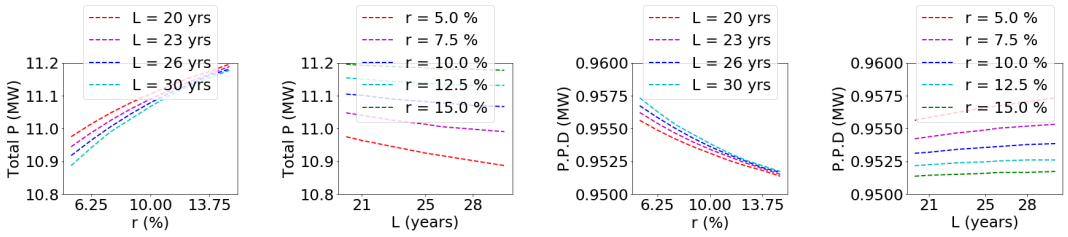

Figure 3.18: The total array power and the average power per device in the design that results in the optimal LCOE as the lifetime of the array, L, and the discount rate, r, are varied.

the power generated by much, it is just changing the profitability (and therefore LCOE) of the array. Throughout the whole range of L and r values found in Table 2.4, the optimal number of turbines remains between 11 and 12, corresponding to the array design shown in Fig. 3.4i and thus the power generated remains roughly the same.

3.7 Limitations and applications

This chapter presents the optimisation and in depth economic assessment of large-scale tidal arrays as well as a new method enabling rapid assessment of the LCOE for arrays of different sizes, through the use of an emulator. A number of assumptions and simplifications are made in this work to demonstrate the development of this method, without focusing on the specifics of any particular real world tidal site. This work is presented on a highly idealised domain, with very simplified tidal forcing that could be considered an approximation of an M2 tide. As such the LCOE values presented in this chapter should not be taken as a prediction the cost of energy that can be achieved for tidal deployments, but instead as a demonstration of how this method can be used to predict LCOE when applied in more detail to real tidal domains.

Future work should apply this approach to the assessment of real world tidal sites with more complex bathymetry and flow. The rapid emulator method will help to increase the scope of economic analysis that can be performed without scaling up the computational expense, which will be especially important in more complex models. A more complex application of the methodology developed in this chapter appears in Chapter 4. There it is used to predict the LCOE that can be achieved

in the Alderney Race as the installed capacity is increased; this demonstrates that the process works for more complex realistic sites.

The modelling approach employed here does not distinguish between the force of the rotor thrust given in (1.9) and the drag due to the turbine structure system. A simple approach to include this, which is compatible with the depth-averaged continuous turbine modelling approach used in this chapter, is presented in [84]. The total drag force is found via

$$F(\mathbf{u}) = \frac{1}{2}\rho(A_T C_t(||\mathbf{u}||) + A_{\text{support}} C_{\text{support}})||\mathbf{u}||\mathbf{u}, \tag{3.5}$$

where A_{support} is the cross-sectional area of the support structure and C_{support} is its drag coefficient. Various different support structure designs are available, but taking a 3m diameter monopile installation as an example, on a 16m diameter turbine with a tip to seabed clearance of 4m, the cross sectional area is $A_{support} = 3\times(4+8) = 36m^2$. [84] assumed a drag coefficient for a pylon structure of $C_{support} = 0.7$, a typical value for flow past a cylinder at high Reynolds numbers. At the maximum turbine density allowed in this chapter, this additional support drag term results in a dimensionless drag coefficient of 0.0039, which is small compared to the equivalent rotor drag coefficient of 0.025 (below rated for $C_T = 0.8$) but a notable increase on the standard physical bottom friction term's value of 0.0025. When applied to a real array the drag term should be updated to include the support structure of the turbine design chosen. This will result in a higher drag added by the presence of the turbines, leading to a greater impact of global blockage effects, with few turbines installed at each break even power and more significant diminishing returns as the number of turbines increases.

Another limitation and scope for further study is that this work only tests one maximum turbine density and one turbine diameter and rated power. Studies should be carried out to test the impact of varying the maximum allowable turbine density on the optimal design. This is especially important because the wakes of each turbine are not modelled explicitly, so it may be necessary to increase the spacing requirements enforced to ensure accuracy of the depth-averaged continuous drag method [165]. Modelling the impact of changes in the turbine scale (rotor diameter and rated power) on the economics is also an important extension on this work, because it has been shown that the LCOE could reduce significantly even with small increases in turbine scale [49].

There is potential to extend this approach from continuous representation to discrete

modelling of individual turbines. This would allow for the effects of accelerated bypass flow and local blockage to be investigated, which can have a substantial impact on the yield of an array [171]. The emulator based approach could substantially reduce the number of iterations needed to find the optimal number of turbines in a discrete approach, but resolving the turbines individually still requires requires a much finer mesh and is much more computationally expensive. To reduce this expense a two stage optimisation as described in [82] could be used, where the continuous optimisation provides a good initial layout, so that the discrete turbine micro-siting optimisation requires overall fewer iterations to converge. However, the emulator method would need to be validated again for testing it's accuracy at predicting the optimal power and LCOE in a discrete model.

3.8 Conclusions and further work

It has been shown that an emulator can be built for rapid prediction of optimal array characteristics, with respect to many different economic models. It can be built using the results of computationally expensive adjoint optimisations over a simple functional, such as $J = P - P_{BE} \times n_t$. Only a small number of these results spread across a range of different n_t values enables us to accurately emulate a Pareto frontier between the two dominant criterion affecting the success of an array design; minimising cost, i.e. reducing n_t and maximising revenue, i.e. increasing Power generation.

The emulator that approximates this Pareto frontier has been shown to be effective at quickly evaluating a large number of functionals based on different economic metrics and different input parameters. Validation has shown this method accurately produces very similar optimal array characteristics to performing the relatively computationally expensive adjoint optimisation within *Thetis*. The fact that this emulator can accurately predict the n_t, P, LCOE and other parameters of the optimal array design very quickly enables the evaluation of the functional over a large range of input parameters and uncertainty analysis which would be unfeasibly computationally expensive otherwise. This includes the calculation of P_{10} and P_{90} confidence parameters over 10,000 Monte Carlo samples. Without building the emulator, each sample would have taken days to complete using an adjoint Thetis optimisation and Monte Carlo analysis would have been impossible. Although the underlying hydrodynamic model configuration in this chapter is idealized, it should be noted that once constructed the cost of evaluating the emulator is independent

of the complexity of the hydrodynamic model. Thus this approach makes it feasible to apply the same analysis to more realistic cases based on model setups with high levels of detail and accuracy.

In order to effectively test this method the LCOE was the main economic metric evaluated, however it can be applied to a vast range of other functionals including Internal Rate of Return, Payback Period and Net Present Value. Economic inputs estimates from Chapter 2 were used to give an prediction of how the LCOE of large-scale tidal energy arrays could be reduced with costs which fall with experience, time, economies of volume and smart array design.

The presence of turbines in the flow can have unintended negative environmental and ecological impacts on the surrounding area. Neil et al. demonstrated that commercial-scale arrays in the vicinity of a headland could have significant impact on nearby sandbanks through disrupting the sediment transport [173]. Studies by du Feu et al. [112, 104] demonstrate how environmental impact can be incorporated into an array optimisation functional through the addition of a penalty term to the array profit. This approach could easily be combined with the revenue given in (2.31) to optimise the trade-off between economic performance and environmental impact, but this chapter focused on economics alone.

Chapter 4

A study on the economic viability of tidal stream in the Alderney Race

Abstract

This chapter is heavily based on [108]. **Z. L. Goss**, D. S. Coles and M. D. Piggott. Identifying economically viable tidal sites within the Alderney Race through optimisation of LCOE, *Royal Society, Philosophical Transactions A*, 2020.

Costs of tidal stream energy generation are anticipated to fall considerably with array expansion and time. This is due to both economies of volume, where arrays comprising of large numbers of turbines can split fixed costs over a greater number of devices, and learning rates, where the industry matures and so arrays of the same size become cheaper through the lessons learnt from previous installations. This chapter investigates how tidal energy arrays can be designed to minimise the levelised cost of energy (LCOE), by optimising not only the location but also the number of devices, to find a suitable balance between decreased costs due to economies of volume and diminishing returns due to global blockage effects. It focuses on the Alderney Race as a case study site due to the high velocities found there, making it a highly suitable site for large scale arrays. It is demonstrated that between 1 and 2 GW could be feasibly extracted as costs in the tidal industry fall, with the LCOE

depending greatly on the assumed costs. A Monte-Carlo analysis is undertaken to account for variability in capital and operational cost data used as inputs to the array optimisation. Once optimised, the estimated P50 LCOE of an 80 MW array is £110/MWh. This estimate aligns closely with the level of subsidy considered for tidal stream projects in the Alderney Race in the past.

4.1 Introduction

The Alderney Race contains a significant tidal energy resource, with a maximum average power potential of 5.1 GW and large regions of the Race exhibiting velocities of up to 5 m/s [34]. In order to develop tidal stream energy projects in the Alderney Race, there is a need to understand how the resource can be harnessed most cost effectively. Through phased array development, the cost of energy can be reduced as the industry matures and array deployments within the Alderney Race expand.

Newly developed methods for optimising the placement of tidal stream turbines within arrays have demonstrated potential to increase array efficiency (energy yield per turbine) by up to 100% in some cases, thereby providing an avenue for further cost of energy reduction [82]. This gradient-based optimisation approach is implemented within a full hydrodynamics solver in order to link the changes to the hydrodynamics caused by the iterative movement of turbines within the optimisation to the resulting power of the array. This is a critical requirement when optimising large arrays in order to account for array scale blockage, as has been demonstrated in [91].

In this chapter, we implement array optimisation in the Alderney Race to minimise the Levelised Cost of Energy (LCOE). We implement a proxy for learning rates and economies of volume based on information in the literature in order to propose optimal phased array development in the Alderney Race, where these cost reductions unlock ongoing array development. The array optimisation is implemented within the *Thetis* hydrodynamic model, which is described in Section 4.2. The model is validated using four bed mounted ADCP datasets and tidal gauge data from around the model domain (Section 4.3). The optimisation approach is described in Section 4.4.1. Results from the optimisation are presented and discussed in Section 4.4.2.

4.2 Hydrodynamic model

The nonlinear shallow water equations are discretised using the finite element method, via the flexible coastal ocean modelling software *Thetis* [174, 175], implemented within the *Firedrake* [164] finite element code generation framework. The $P_{1DG} - P_{1DG}$ velocity-pressure finite element pair is used for spatial discretisation. The semi-implicit Crank-Nicolson time stepping method is used for temporal discretisation, with a constant time step of $\Delta t = 600s$. These discretisation options are second order accurate in space and time, as verified for the three-dimensional version of the *Thetis* model in [157] and for the two-dimensional depth-averaged version (which is the one used in this work) in [176]. The model domain, which covers the majority of the English Channel, is shown in Figure 4.1. The model is forced by Q1, O1, P1, K1, M2, S2, N2, K2 and M4 constituent elevation forcing at the open boundaries, implemented via the *Uptide*[1] package using data extracted from the OSU Tidal Prediction Software (OTPS) [75]. *Thetis* solves the non-conservative form of the nonlinear shallow water equations, given in 1.3.

Over the majority of the domain the kinematic viscosity, ν, is set to a value of 10 m^2s^{-1}. This artificially increased value acts primarily as a stabilisation mechanism and accounts for scales of motion not resolved at the mesh resolutions utilised. At the open boundaries, the viscosity is increased to a value of 1000 m^2s^{-1}, over a region extending 50km from the open boundaries. This acts as a further stabilisation mechanism for any spurious flow behaviour that can be generated through minor inconsistencies (e.g. due to different resolution and bathymetry data employed) between the model and set-up, and the configuration used to generate the tidal harmonic forcing data. This has negligible impact on the flow speeds within areas of interest for energy extraction. The location of the open boundaries are also chosen, in part, to be far enough away from the array location such that changes in hydrodynamics do not propagate significantly back to the open boundaries, which would invalidate the assumption of unchanged boundary forcing. Justification of the selection of the time step and kinematic viscosity described above, is given through a sensitivity test in Section 4.3.2.

In this chapter the bottom friction, τ_b, is calculated using the Manning formulation;

$$\frac{\tau_b}{\rho H} = gn^2 \frac{||\mathbf{u}||\mathbf{u}}{H^{\frac{4}{3}}}, \tag{4.1}$$

[1] https://github.com/stephankramer/uptide

where n is the Manning coefficient, which is uniformly applied over the whole domain and tuned during model calibration in Section 4.3.2.

The Coriolis forcing, $f\mathbf{u}^{\perp}$, is represented by the beta-plane approximation, due to the size of the domain, such that;

$$f = f_0 + \beta y, \tag{4.2}$$

where the Coriolis and Rossby parameters are given by;

$$f_0 = 2\omega \sin(\zeta), \qquad \beta = \frac{1}{R} 2\omega \cos(\zeta), \tag{4.3}$$

respectively, where ω is the angular frequency of the Earth's rotation, ζ the latitude and R is the earth's radius.

Additional meteorological forcings such as wind and atmospheric pressure have not been included here. Some studies have found that the effects of wind-driven waves can have a notable impact on the tidal power extraction, especially in extreme and winter conditions [177, 178]. However, tide-induced currents are the dominant forcing for tidal current estimation, especially at the depths concerned for tidal energy extraction [179]. For this reason, the exclusion of these additional meteorological forcings is common in regional scale hydrodynamic modelling work, such as [32, 34, 37, 180].

Bathymetry data was obtained from the Marine Digimap database [7], with 1 arc-second resolution ($\approx$ 30 m) over the Northern half of the Channel and 6 arc-second resolution ($\approx$ 180 m) over the Southern half of the Channel. There is a small region around Normandy that is not covered by the Marine Digimap database. For this region bathymetry was obtained from the General Bathymetric Chart of the Oceans (GEBCO) 2014 dataset with 30 arc-second resolution ($\approx$ 900 m) [8].

Coastlines were adapted from the Global Self-consistent, Hierarchical, High-resolution Geography Database (GSHHG) [181]. Coastline geometry has been simplified to remove estuaries and islands (except for the islands closest to Alderney). This was done to reduce computational expense as it enables lower mesh resolution to be used around the coastlines of the domain while having minimal impact on the region of interest[110].

The model employs an unstructured triangular mesh, allowing variable mesh resolution across the domain, as shown in Figure 4.1. A mesh independence study

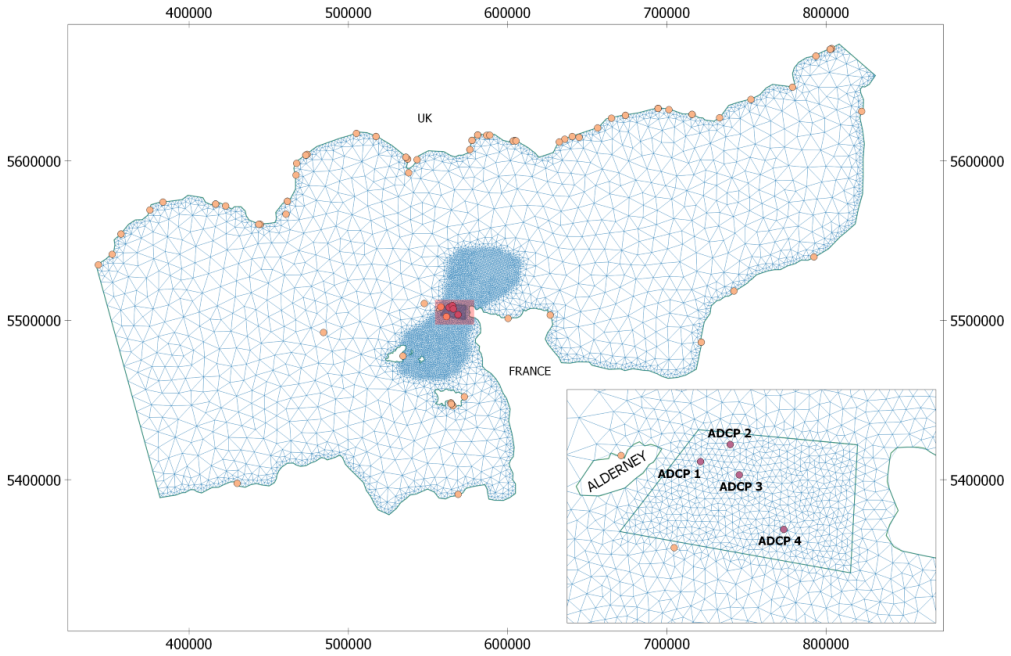

Figure 4.1: The unstructured triangular mesh used in the shallow water English Channel model, with the locations of the four ADCPs (purple pointers) and the 68 tide gauges (yellow pointers) used to validate the model [6]. The farm area considered is also shown within the Alderney Race.

was carried out to establish the most suitable mesh resolution to achieve accurate ambient flow results at acceptable computational expense. Table 4.1 summarises the resolution and number of nodes/elements in the four meshes considered in the mesh independence study. Results from the mesh independence study are presented in Section 4.3.2, demonstrating that mesh independence was achieved with Mesh 3. Mesh 3 has a resolution of 500 m within the tidal energy plots in the Alderney Race, 2,000 m around coastlines and 10,000 m within the rest of the domain. The mesh comprises of 14,260 unstructured triangular elements and 7,126 nodes.

Table 4.1: Resolution and node/element count of meshes used in the mesh independence study.

	Tidal Plot	Alderney Race	Shorelines	Rest of domain	Nodes	Elements
Mesh 1	1000m	2000m	4000m	10000m	2876	5760
Mesh 2	750m	1500m	3000m	10000m	4086	8180
Mesh 3	500m	1000m	2000m	10000m	7126	14260
Mesh 4	375m	750m	1500m	10000m	11485	22978

4.3 Calibration and Validation

4.3.1 Methods

The *Thetis* model was calibrated by varying the bed drag to establish the value of Manning coefficient that achieves the highest level of agreement with field measurements of flow speed and tidal elevation. In similar tidal calibration studies (e.g. [182]) non-dimensional quadratic drag coefficients, c_D, typically in the range 0.0025 to 0.0075 have been considered. The quadratic drag coefficient can be converted to a Manning coefficient using [183];

$$c_D = gn^2 h^{-1/3}, \tag{4.4}$$

where g is acceleration due to gravity, n is the Manning coefficient and $h = 35m$ is the representative depth in the Alderney Race. This results in a Manning coefficient range of approximately 0.03 to 0.05 $sm^{-1/3}$. In this study five values of Manning coefficient were considered: 0.02, 0.025, 0.03, 0.035 and 0.04 $sm^{-1/3}$. Section 4.3.1 provides a description of the methods used to carry out the model calibration and validation. Results from the calibration and validation studies are presented in Sections 4.3.2 and 4.3.3.

Flow speeds

An industry partner provided data from three bed mounted ADCP campaigns within the Alderney Race, which were used to calibrate the model. The ADCP datasets provide 10 minute averages of flow speed and direction within 1 m vertical bins spanning the majority of the water column. The datasets cover a 1 month period. The flow speed and directions obtained from the ADCPs were depth averaged to compare against simulated results.

Five separate simulations were run using the aforementioned Manning coefficients. The model accuracy was quantified using three different metrics. The Normalised Root Mean Squared Error (NRMSE) provides a comparison between simulated and measured flow speeds;

$$NRMSE = \frac{1}{\max(mes_i)} \sqrt{\frac{1}{N} \sum_{i=1}^{i=N} (mod_i - mes_i)^2} \tag{4.5}$$

where mes_i is the measured data obtained from the bed mounted ADCPs at time step i and mod_i is the model prediction at time step i.

The Index of Agreement (IA), also known as the Willmott Index [184], is used as a relative covariability of the model predictions and ADCP observations about an estimate of the 'true' mean. Bias (B) and Relative Bias (RB) are also used to quantify the systematic error of the model in simulating the flow. This is consistent with the approach taken in [185] and [186]. These quantities are defined mathematically as;

$$IA = 1 - \frac{\sum_{i=1}^{i=N}(mod_i - mes_i)^2}{\sum_{i=1}^{i=N}(|mod_i - \bar{mes_i}| + |mes_i - \bar{mes_i}|)^2}, \tag{4.6}$$

$$B = \bar{mod_i} - \bar{mes_i}, \qquad RB = 100\frac{B}{\bar{mes_i}}, \tag{4.7}$$

The model was validated against an additional sea bed mounted ADCP dataset (ADCP 4) obtained in the Alderney Race [187]. This dataset covered a period of 14.6 days, providing flow speeds and directions at hourly intervals. The location of the four ADCP deployments in the Alderney Race are shown in Figure 4.1.

Tidal elevations

Free surface elevation data was extracted from 68 locations around the domain to compare against tide gauge data. The tide gauge locations are shown in Figure 4.1[6]. For each of the Manning coefficients used to tune the model, the *Thetis* simulation was run over a two month period and the elevation predictions at each of the tide gauge and ADCP locations were extracted. Least squared regression was performed on the η time signal, via the *Uptide* python package, to calculate the model phase and amplitude for each of the harmonic constituents in the tidal forcing. These were then compared either directly to the tide gauge phase and amplitude readings or to phase and amplitudes calculated in the same manner from elevation time series readings at the location of each of the ADCPs. The model amplitude error, $100 \cdot (amp_{mod} - amp_{mes})/amp_{mes}$, and phase error, $(pha_{mod} - pha_{mes})^\circ$, for the two most dominant constituents in the region, M2 and S2, are presented below.

The time period of the signal must be long enough to distinguish each pair of constituents, and this required period can be calculated in *Uptide* using the Rayleigh

Criterion. Most pairs can be resolved within a month, however S2 & K2 and P1 & K1 require much longer to resolve, and so, for the purpose of harmonic validation, the latter of each pair (the constituent which is smaller in magnitude in the region) was removed. All nine constituents were included in models for all other purposes except harmonic validation.

4.3.2 Calibration results

Model stability

The impact of varying both the kinematic viscosity and time step were investigated using a Manning coefficient value of $0.03sm^{-1/3}$. Increasing the time step through $\Delta t = 30, 60, 300, 600, 1200$ seconds resulted in a velocity magnitude NRMSE for ADCPs 1–3 of 11.7%, 11.5%, 11.8%, 11.8% and 12.5%, respectively. A time step of 600 seconds was selected for future runs since (a) it was computationally prohibitive to use a smaller time step within the adjoint optimisation loop, and (b) only minor changes in model results where exhibited for the time step range considered when compared to ADCP data.

ADCP 4 was used to test the sensitivity of the model to changes in the kinematic viscosity, using $\nu = 1, 10, 100, 1000$ m^2s^{-1}. The $\nu = 1$ m^2s^{-1} case resulted in model instability. The remaining kinematic viscosity cases resulted in a velocity magnitude NRMSE of 10.2 %, 10.8 % and 12.3 %, respectively. A viscosity of $\nu = 10$ m^2s^{-1} was selected since it provided the lowest NRMSE in velocity whilst also providing model stability.

Mesh sensitivity

Figure 4.2a compares the flow speed time series obtained from model simulations (using Meshes 1-4) and the ADCP measurements. The difference in peak flow speeds obtained by Meshes 1 and 2 is approximately 0.2 m/s. Further refinement of the mesh reduces the difference in peak flow speeds (obtained by Mesh 3 and 4) to 0.1 m/s.

Table 4.2 shows the NRMSE for each combination of mesh and Manning coefficient tested. There was on average a 0.66% improvement in NRMSE between Meshes 3 and 4 across the range of Manning coefficients tested. Mesh 1 took under 2 hours

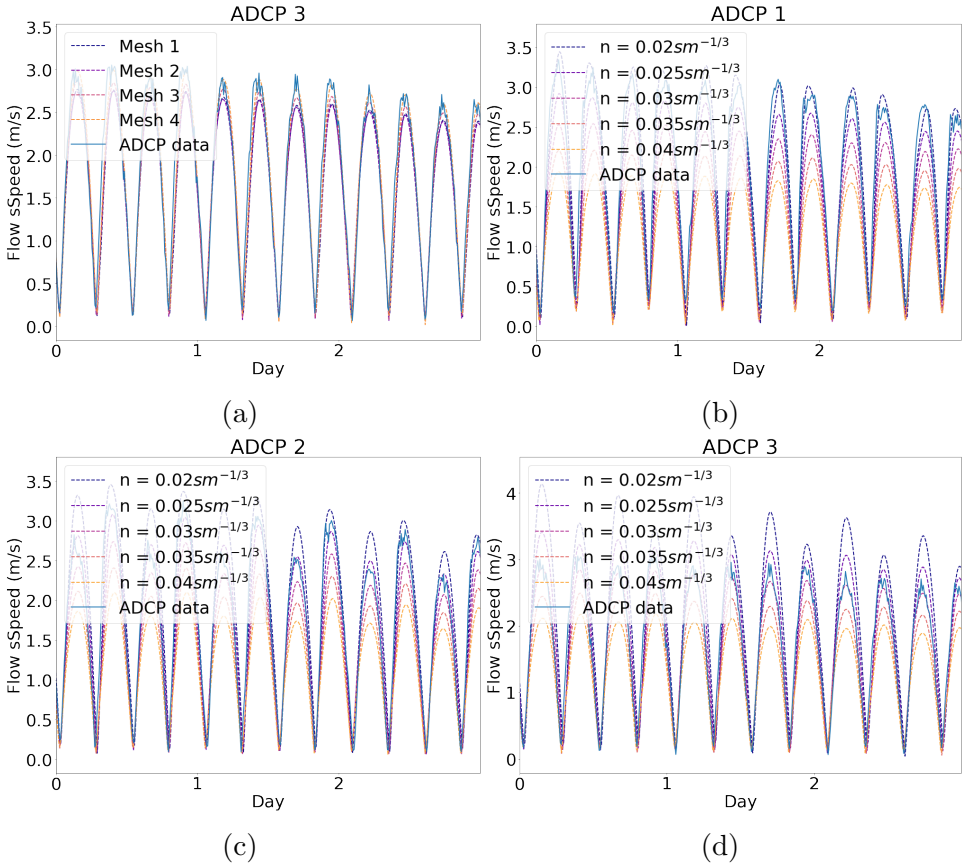

Figure 4.2: The sensitivity of the *Thetis* model velocity magnitude predictions to (a) changes in the mesh resolution for a Manning coefficient of $0.03sm^{-1/3}$, at ADCP 3, and to changes in the Manning coefficient, at (b) ADCP 1, (c) ADCP 2 and (d) ADCP 3, all while using Mesh 3.

to model 60 days, Mesh 2 took under 4 hours, Mesh 3 took just over 5 hours and Mesh 4 took just over 11 hours. This is a significant increase in the computational expense for a relatively small difference between models. The computational expense for a single model run is of key importance as the array optimisation aspect of the modelling is fully coupled to the hydrodynamics – for every iteration of the optimisation algorithm, the forward model needs to be re-run to calculate the updated hydrodynamics. Therefore Mesh 3 was chosen for the following work.

Table 4.2: The *Thetis* model NRMSE, averaged over ADCP's 1–3

	Manning coefficient ($sm^{-1/3}$)				
	0.02	0.025	0.03	0.035	0.04
Mesh 1	13.7 %	11.8 %	12.6 %	15.2 %	18.6 %
Mesh 2	13.7 %	11.8 %	12.3 %	14.9 %	18.5 %
Mesh 3	13.5 %	11.2 %	11.8 %	14.2 %	17.7 %
Mesh 4	14.5 %	11.0 %	10.4 %	12.9 %	16.3 %

Calibration – flow speed

Figures 4.2b–4.2d compare the flow speed time series obtained using Mesh 3 for each of the Manning coefficients considered. These results are compared against field data obtained from the ADCPs. To protect the confidential nature of the ADCP data, a start date is not specified and instead the time is shown in days from the start of the model. The time series data demonstrates that the flow speeds are relatively sensitive to the Manning coefficient, as there is approximately a 0.5 m/s difference in peak flow speeds across the range of Manning coefficients used.

Table 4.3 provides the error metrics achieved for each of the Manning coefficients considered at each ADCP location. Closest agreement between simulated and measured NRMSE velocities was achieved using a Manning coefficient of $0.025sm^{-1/3}$ and $0.03sm^{-1/3}$, depending on location within the Alderney Race. Closest agreement with ADCP 1 and 2 was achieved using $n = 0.025sm^{-1/3}$, resulting in an average NRMSE across the three ADCPs of 12.4 and 9.7%) respectively. Reasonable agreement was also achieved using $n = 0.03sm^{-1/3}$, which achieved an NRMSE of 15% and 11% respectively). Closest agreement with ADCP 3 was achieved with $n = 0.03sm^{-1/3}$ (9.4%), with $n = 0.035sm^{-1/3}$ (11.1%) and $n = 0.025sm^{-1/3}$ (11.6%) also having close levels of performance. The biases show that for Manning coefficients of $0.03sm^{-1/3}$ and above, the model underestimates the flow speeds at all ADCP locations. For a Manning coefficient of $n = 0.02sm^{-1/3}$, flow velocities at ADCP 3 are overestimated. For a Manning coefficient of $n = 0.025sm^{-1/3}$, flow velocities at ADCP's 2 and 3 are overestimated.

Calibration – free surface elevation

Table 4.4 provides a comparison of modelled vs. actual M2 and S2 elevation amplitudes and phases at the ADCP locations. Closest agreement was achieved using a Manning coefficient of 0.03 $sm^{-1/3}$, where M2 and S2 phase were predicted very well (0.1–1.0° and 0.5–2.1° error respectively) and the M2 and S2 amplitudes had errors ranging between 9.7–17.7% and 1.3–10.2% respectively.

Table 4.5 shows the M2 and S2 elevation amplitude errors from the *Thetis* model relative to the tide gauge readings. Closest agreement was achieved for $n = 0.025sm^{-1/3}$. However, $n = 0.03sm^{-1/3}$ achieved very similar performance. For a Manning coefficient of $0.03sm^{-1/3}$, the M2 and S2 normalised phase errors were 16.7% and 16.4% respectively, whereas for a Manning Coefficient of $0.025sm^{-1/3}$, they were 13.8%

Table 4.3: The *Thetis* velocity amplitude model error metrics at ADCPs 1–3 for different Manning coefficients.

	Manning coefficient ($sm^{-1/3}$)				
	0.02	0.025	0.03	0.035	0.04
NRMSE 1	11.7 %	12.4 %	15.0 %	18.4 %	21.9 %
NRMSE 2	11.4 %	9.7 %	11.0 %	13.2 %	16.4 %
NRMSE 3	17.4 %	11.6 %	9.4 %	11.1 %	14.7 %
NRMSE (Avg)	13.5 %	11.2 %	11.8 %	14.2 %	17.7 %
IA 1	0.938	0.926	0.885	0.826	0.762
IA 2	0.944	0.954	0.936	0.902	0.843
IA 3	0.895	0.946	0.960	0.938	0.884
IA (Avg)	0.925	0.942	0.927	0.889	0.830
Bias 1 (m/s)	-0.06	-0.22	-0.36	-0.50	-0.62
Bias 2 (m/s)	0.10	-0.06	-0.21	-0.32	-0.44
Bias 3 (m/s)	0.27	0.09	-0.08	-0.24	-0.38
Relative Bias 1	-3.4 %	-12.7 %	-21.3 %	-29.2 %	-36.4 %
Relative Bias 2	6.1 %	-3.6 %	-13.2 %	-20.9 %	-28.5 %
Relative Bias 3	16.6 %	5.7 %	-5.1 %	-14.8 %	-23.6 %

Table 4.4: The *Thetis* model prediction and error in the M2 and S2 phase and amplitude, for each Manning coefficients tested. Harmonic analysis is performed on η readings taken at the locations of ADCPs 1–3.

	Manning coefficient ($sm^{-1/3}$)				
ADCP	0.02	0.025	0.03	0.035	0.04
			M2 Amplitude		
1	1.82 (-13.3%)	1.86 (-11.3%)	1.90 (-9.7%)	1.90 (-9.3%)	1.90 (-9.6%)
2	1.78 (-14.0%)	1.82 (-11.9%)	1.85 (-10.5%)	1.86 (-10.0%)	1.86 (-10.2%)
3	1.90 (-20.0%)	1.94 (-18.5%)	1.96 (-17.7%)	1.96 (-17.5%)	1.96 (-17.9%)
			S2 Amplitude		
1	0.75 (-3.9%)	0.76 (-3.3%)	0.76 (-3.3%)	0.75 (-4.3%)	0.74 (-5.9%)
2	0.74 (-2.0%)	0.74 (-1.2%)	0.74 (-1.3%)	0.74 (-2.2%)	0.72 (-3.7%)
3	0.79 (-9.5%)	0.79 (-9.5%)	0.78 (-10.2%)	0.77 (-11.4%)	0.76 (-13.1%)
			M2 Phase		
1	197.23 ° (-1.2 °)	198.52 ° (0.1 °)	199.38 ° (1.0 °)	199.78 ° (1.4 °)	200.01 ° (1.6 °)
2	198.79 ° (-1.8 °)	199.98 ° (-0.6 °)	200.74 ° (0.1 °)	201.01 ° (0.4 °)	201.14 ° (0.5 °)
3	198.58 ° (-0.6 °)	199.56 ° (0.4 °)	200.20 ° (1.0 °)	200.47 ° (1.3 °)	200.62 ° (1.5 °)
			S2 Phase		
1	254.47 ° (-3.7 °)	256.41 ° (-1.7 °)	257.60 ° (-0.5 °)	258.27 ° (0.1 °)	258.82 ° (0.7 °)
2	255.87 ° (-5.1 °)	257.70 ° (-3.2 °)	258.81 ° (-2.1 °)	259.34 ° (-1.6 °)	259.80 ° (-1.1 °)
3	255.75 ° (-3.5 °)	257.32 ° (-1.9 °)	258.30 ° (-0.9 °)	258.84 ° (-0.4 °)	259.33 ° (0.1 °)

and 13.4%, respectively. This suggests that further work could use a variable bed friction throughout the channel, based on maps of bed type such as the "Service Hydrographique et Océanographique de la Marine Service" (SHOM) [188], as used

in [185], since a coefficient of $0.03sm^{-1/3}$ generally produced better results for ADCPs and gauges within the Race, whilst a coefficient of $0.025sm^{-1/3}$ produced better results for tide gauges spread throughout the wider Channel.

Table 4.5: The *Thetis* model M2 and S2 amplitude errors over the 68 tide gauge locations.

	Manning coefficient ($sm^{-1/3}$)				
Error type	0.02	0.025	0.03	0.035	0.04
M2 RMSE	0.219 m	0.233 m	0.281 m	0.347 m	0.416 m
M2 NRMSE	13.0 %	13.8 %	16.7 %	20.6 %	24.7 %
S2 RMSE	0.081 m	0.078 m	0.096 m	0.123 m	0.152 m
S2 NRMSE	13.8 %	13.4 %	16.4 %	21.2 %	26.1 %

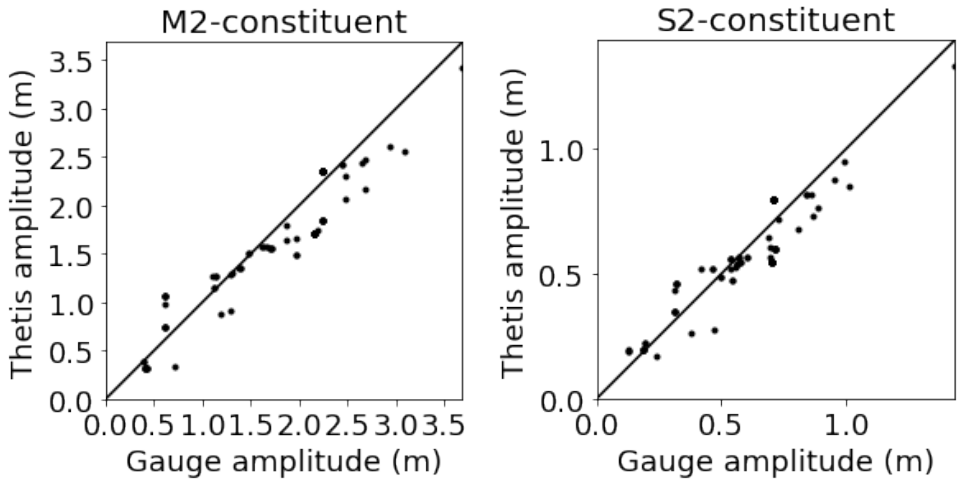

Figure 4.3: The M2 and S2 amplitude of the 68 tide gauges across the English Channel against the *Thetis* model predictions, for a Manning coefficient of $n = 0.03sm^{-1/3}$.

Inspection of the ADCP 1–3 velocity time series data against the *Thetis* model and harmonic analysis of the M2 and S2 elevation phase and amplitude have shown that closest agreement was achieved with a Manning coefficient $0.03sm^{-1/3}$. The NRMSE of ADCP 1–3 velocity time series data and the harmonic analysis of the elevation at the 68 tide gauges showed slightly better results for $0.025sm^{-1/3}$ (11.2% v.s. 11.8%). On balance, for this work a Manning coefficient of $0.03sm^{-1/3}$, applied uniformly over the domain, was established as the most suitable value to take forward to the array optimisation study.

4.3.3 Validation

The model was calibrated with ADCPs 1–3, leaving ADCP 4 from [187] for independent validation. Table 4.6 provides a comparison of the NRMSE, Bias, Relative Bias and Index of Agreement at the location of ADCP 4, obtained from the five bed drag coefficient cases.

The NRMSE and Index of Agreement results suggest that the $n = 0.03sm^{-1/3}$ case provides best agreement with ADCP 4 data, reinforcing the choice of the Manning coefficient from the calibration tests. However, the difference between these results and those obtained with $n = 0.025sm^{-1/3}$ is small and the bias is lowest at $n = 0.025sm^{-1/3}$. For comparison, the RMSE at ADCP 4 with $n = 0.03sm^{-1/3}$ is 0.243 m/s, whereas [185] achieved a RMSE of 0.15–0.26 m/s, a relative bias of between -1% and -8%, and an IA of 0.962–0.990 using a model with 100 m resolution and a time step of 10 seconds.

Table 4.6: The *Thetis* velocity amplitude model error at ADCP 4 for different Manning coefficients.

	Manning coefficient ($sm^{-1/3}$)				
	0.02	0.025	0.03	0.035	0.04
NRMSE	21.8 %	11.3 %	10.2 %	15.7 %	21.5 %
Bias (m/s)	0.19	-0.01	-0.16	-0.31	-0.44
Relative Bias	13.8 %	-0.6 %	-11.7 %	-22.9 %	-32.3 %
IA	0.859	0.956	0.960	0.898	0.809

4.4 Economic resource assessment

4.4.1 Method

Turbines were introduced into the *Thetis* model via the inclusion of a turbine drag coefficient, c_t, which appears within an additional sink term, (1.8), in the shallow water momentum equation (1.3). The additional turbine drag coefficient is added to the existing sea-bed drag coefficient at the location of the turbines. The added turbine drag coefficient is applied continuously over the array area, and is allowed to vary spatially depending on the local density of turbines. This continuous approach for parameterising array drag was favoured over the more computationally expensive discrete approach, where each individual turbine is allocated its own drag term [81]. The discrete approach requires a mesh with element sizes constrained to be

below the turbine rotor diameter to allow individual turbines to be resolved. The continuous approach is particularly well suited to the problem at hand because it allows for the number of turbines as well as their positions to be simultaneously optimised for. In [82] flow modelling from the continuous and discrete turbine representations are compared, showing that the farm wake and bypass flow modelled by both methods are largely consistent. However, the continuous method does not resolve the individual wakes within the farm area. Inter-array flow effects such as the impingement of wakes on downstream turbines are mitigated to an extent in this work by constraining the minimum longitudinal spacing between turbines to ten rotor diameters. This turbine spacing constraint is informed by guidelines published by the European Marine Energy Centre (EMEC) [170]. In taking this approach, this work provides a valid approach to modelling large scale arrays in order to model the impacts of array scale blockage on energy yield.

The swept area and rated power of the turbines used in this work are assumed to be 16 m and 2 MW respectively. This is informed by (a) the scale of turbines in operation currently and (b) the depths within the Alderney Race. Typically, turbines in operation at present have rotor diameters and rated capacity ranging between 9 m – 18 m and 100 kW – 1.5 M respectively, e.g. such as the Nova Innovation turbines at the Shetland Tidal Array [161] and the SIMEC Atlantis Energy and Andritz Hydro Hammerfest turbines at the MeyGen array [98]. Studies suggest that increasing the rotor diameter and rated power can be key drivers for reducing the cost of tidal stream energy in the future [49], and SIMEC Atlantis Energy have developed a 2 MW turbine with 20–24m rotors for the next phase of the MeyGen project [162]. However, the rotor diameter of the turbines are limited here in regions of the East Race since it is relatively shallow. On balance, 16 m diameter 2 MW turbines were chosen to be representative of future commercial turbines that may be deployed in this region. It is acknowledged that in reality, a variety of turbine sizes may be needed given the spatial variation in depth across the Race, as demonstrated in [91], and this is an area identified for further work.

Below the rated speed the thrust and power coefficient are assumed equal to $C_T = 0.8$ [76] and $C_P = 0.41$ [98] respectively. Above rated speed, the coefficients are scaled by $\frac{u_{rated}^3}{u^3}$ to maintain constant drag and power. The turbine density is set to zero outside of the farm area, A_f, shown in Figure 4.1, and within the array it is allowed to vary continuously up to a density value which corresponds to a spacing of 2.25 diameters laterally (centre-to-centre) and 10 diameters longitudinally [170].

To optimise the array, a gradient-based optimisation algorithm is employed which

utilises *Thetis*'s adjoint to obtain the required gradient, where c_t is the control parameter for evaluating the sensitivity of the optimisation functional, and is the quantity that is updated at every optimisation iteration. Further details may be found in [82]. The array design, including the number of turbines (obtained via the integral of the turbine density field) and their spatial distribution, is optimised with respect to a functional J which here takes the form;

$$J = P_{\text{avg}} - P_{\text{BE}} \times n_t. \tag{4.8}$$

where P_{avg} is the average power generated by the whole array and n_t is the number of turbines in the array. P_{BE} is the break even power, which is the time-averaged power that a turbine must generate to be economically viable for the project. In this work the break even power is varied between 0 to 700 kW. A 2 MW turbine that achieves a time averaged power of 700 kW is performing with a capacity factor of 35%. An increase in break even power results in a decrease in the optimal number of turbines in the array. In this case adding additional turbines has a detrimental impact on the power generated per turbine, because the added turbines increase array blockage, slowing the flow velocities and hence reducing the available power to the array, so that the break even power cannot be achieved. This is overcome within the optimisation by reducing the number of turbines in the array.

The optimisation was run over a representative 14.5 day spring-neap cycle, ensuring a sufficient duration to capture the dominant tidal variations whilst also achieving acceptable computational time for the optimisation to converge. The model was spun up for one day before each optimisation iteration.

Once the optimisation completed for each of the break even powers considered, the Levelised Cost Of Energy (LCOE) of each optimal array was calculated. The Levelised Cost of Energy (LCOE) describes the fixed price per MWh that needs to be received by the developer for an array to break even over its lifetime. In this chapter, it is calculated using the fixed and turbine-dependent breakdown of CAPEX and OPEX, defined in (2.18) and (2.19) to give;

$$\text{LCOE} = \frac{\text{CA}_f + \text{CA}_t \times n_t + \sum_{i=1}^{L} \frac{\text{O}_f + \text{O}_t \times n_t}{(1+r)^i}}{\sum_{i=1}^{L} \frac{E_i}{(1+r)^i}}. \tag{4.9}$$

where CA_f and CA_t are the fixed and turbine dependent components of the Capital Expenditure (CAPEX), defined below. L is the operational lifetime of the array in years, where each year is denoted by i. O_f and O_t are the fixed and turbine de-

pendent components of the Operational Expenditure (OPEX) per year, also defined below. E_i is the energy generated in year i and r is discount rate applied annually. In this model the simplifying assumption is made that the annual energy generation, E_i, is constant year on year. In practice the yield is likely to vary annually due to the 18.6 year lunar nodal cycle and degradation of the turbine performance for example, however this is not considered at this stage of investigation.

The inputs used for each of these fixed/turbine costs were calculated in Chapter 2 by drawing together inputs from multiple sources [189, 9, 10, 190] and are summarised in Table 2.4. We consider a range of values for each cost, ranging between pessimistic and optimistic values quoted in literature. We also carry out a Monte Carlo analysis to find the P10, P50 and P90 values of LCOE, by assuming a uniform distribution over each of the cost inputs in Table 2.4 with the 'pessimistic' and 'optimistic' values as their upper limits to randomly vary between. P10, P50 and P90 are the values for which 10%, 50% and 90% of the LCOE estimates are better (lower) than, respectively. This uses the same approach for optimising arrays to minimise LCOE, as was first presented in Chapter 3 for idealised array cases.

4.4.2 Results

Figure 4.4 shows the optimal array designs for the range of break even powers considered. In general, the optimal array layouts span the Alderney Race in fence-like structures orientated perpendicular to the flow direction. This is consistent with findings in [191]. Orientating the turbines in these fence-like structures maximises power generation by preventing the flow from passing around the array as a result of the added turbine drag.

At high levels of break even power, the optimal array contains a low number of turbines in order to mitigate against array blockage effects that detrimentally impact upon power generation. This is synonymous with the early stages of tidal energy development, where the relatively high CAPEX/OPEX and discount rate only permit turbines to be installed in the highest resource areas, otherwise the cost of energy becomes unacceptably high. As the break even power decreases, larger scale arrays become more viable, as it becomes economically acceptable to install turbines in lower energy regions of the Race. It is only once the break even power reduces below £300/MWh that the array contains turbines in the West Race (i.e. in Alderney territorial waters). This result suggests that to minimise cost of energy, early stage development should take place in French territorial waters, however this

may not be the case once different turbine designs (i.e. rotor diameter and rated speed) are considered, as the deeper West Race (Alderney territorial waters) may be more suitable for turbines with a larger rotor diameter, for example.

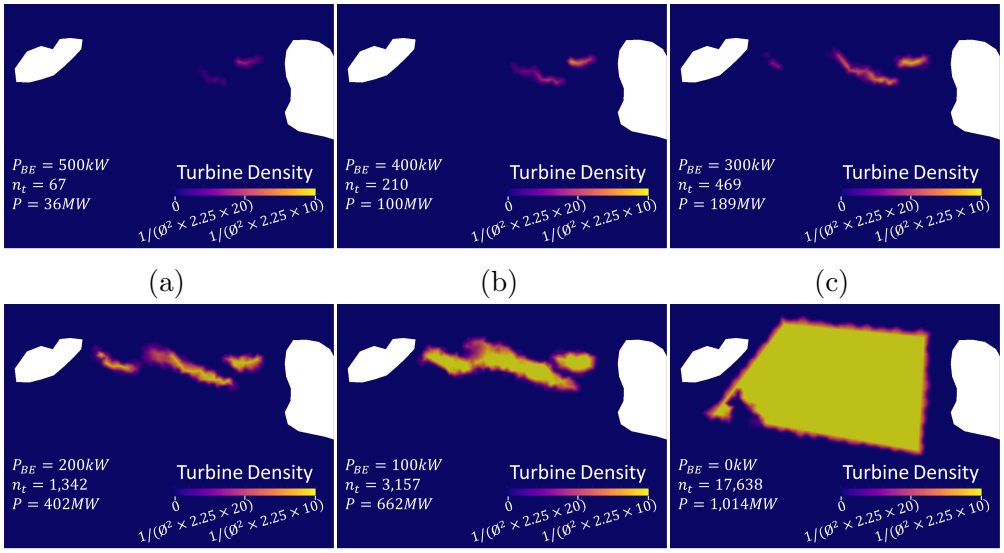

Figure 4.4: Optimal array design for break even power of (a) 500 kW, (b) 400 kW, (c) 300 kW, (d) 200 kW, (e) 100 kW and (f) 0 kW. The number of turbines and net average power for the optimal array design can be seen for each break even power.

Figure 4.5 shows the relationship between the break even power and (a) net average array power and corresponding average power per device and (b) number of turbines. Decreasing the break even power reduces the acceptable level of power generation per turbine, so that larger scale arrays become more viable. This has the same impact as reducing CAPEX and/or OPEX, where reductions in CAPEX/OPEX mean that turbines can generate less power to achieve the same LCOE. Mechanisms that enable these CAPEX/OPEX cost reductions include learning taken from previous projects as the industry develops, and cost reduction unlocked by development of the supply chain, for example [49, 190]. Economies of volume are inherently modelled as a cost reduction mechanism in this chapter through the distinction of the fixed and turbine dependent components of both CAPEX and OPEX. Learning rates as a cost reduction mechanism can be investigated by comparing the impact of moving from the pessimistic to typical to optimal scenarios presented in Table 2.4.

Increasing the number of turbines increases the total array drag, slowing the flow in the region of the array and thus reducing the available power. When the reduction in CAPEX/OPEX costs achieved from economies of volume outweigh the negative impacts of array blockage, it becomes economically viable to install more turbines.

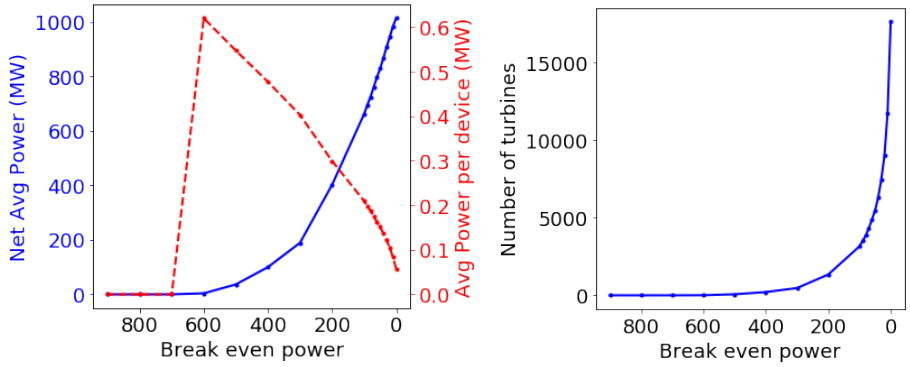

Figure 4.5: Variation of the macro parameters of the optimal array design with the break even power used in the functional.

However, the detrimental impacts of array blockage result in a diminishing return on array power as the array size increases. This is illustrated in Figure 4.6, which shows the relationship between the number of turbines and (a) net average array power, and (b) net average power per device. As the number of turbines increases to very high levels (¿2,000 turbines), the net average array power begins to plateau, leveling out to an upper bound of approximately 1 GW by 15,000 turbines.

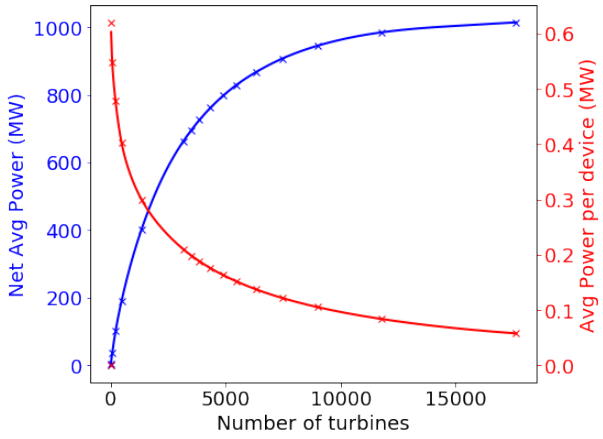

Figure 4.6: A prediction for the power generated in the optimal array design for all numbers of turbines, achieved by curve fitting between the results of each P_{BE} optimisation.

Figure 4.7 shows the relationship between the number of turbines in the array and the minimum estimated LCOE. The optimal relationship between number of turbines and LCOE is shown for the 'pessimistic', 'typical' and 'optimistic' scenarios outlined in Table 2.4, as well as the P10, P50 and P90 estimates obtained from the Monte Carlo analysis. The optimal LCOE estimates are also presented in Table 4.7. As the number of turbines increases from 0, there is a steep decrease in LCOE, which is enabled through economies of volume. As the number of turbines

approaches the optimal value there is a turning point, where the impact of economies of volume vs. diminishing returns from adding more turbines balance out. As the number of turbines increases further the diminishing returns due to blockage have a dominant effect and cause the LCOE to increase. Based on the P50 estimate, a minimum LCOE of £110/MWh is achieved with 38 turbines and an installed capacity of 81 MW. Increasing the installed capacity to 1 GW and 2 GW increases the estimated LCOE to £150/MWh and £180/MWh respectively.

The optimal LCOE obtained from the 'optimistic' and 'pessimistic' cases is £37/MWh and £209/MWh respectively. This disparity between the LCOE estimates is caused as a result of all input parameters being set to their most extreme values. In practice, while there is uncertainty in the associated costs, it is unlikely that all parameters will be at their best or worst at once. This was investigated by estimating the LCOE based on a Monte Carlo analysis, so that a range of CAPEX, OPEX and discount rates could be considered simultaneously. Results in Table 4.7 show that the P10, P50 and P90 minimum LCOE estimates are £78/MWh, £110/MWh and £146/MWh respectively. Whilst this still provides a broad range, it is significantly reduced in range relative to the pessimistic and optimistic cases. This disparity in estimated LCOE is likely to reduce further once more cost information becomes available.

Whilst the minimum estimated LCOE can vary widely depending on the cost inputs, the number of turbines required to achieve the minimum LCOE remains largely the same, in the region of 33 to 43 turbines. This is equivalent to a break even power of approximately 550 kW, or a layout with slightly fewer turbines than shown in Figure 4.4a.

In this work the cost reductions due to learning with time are not explicitly modelled, however the 'pessimistic' scenario would likely correspond to the costs at a very low cumulative installed capacity, and as more arrays are deployed the industry would move towards the increasingly optimistic scenario curves. The further the costs drop, towards the P10 and 'optimistic' scenarios, the flatter the increase in LCOE projection becomes when the number of turbines exceeds the optimal amount to minimise LCOE. The Offshore Renewable Energy Catapult has predicted that learning rates will cause costs to fall by 7% per 100 MW of cumulative deployed capacity[190]. If it is assumed that the 'optimistic' cost inputs can be achieved through learning, as many as 500 turbines, with a total install capacity of 1 GW could be installed whilst still keeping LCOE below £50/MWh.

The typical cost case achieves an optimal LCOE of £110/MWh with 34 turbines. This agrees closely with the P50 estimate, which achieves the same minimum LCOE of £110/MWh with 38 turbines. This estimate falls within 15% of the level of subsidy support proposed by the French government for 'marine hydraulic energy', of £130/MWh (=€150/MWh)[192]. Furthermore, a recent Marine Energy Council report [149] proposed a number of different subsidy schemes to provide a route to market for the tidal energy industry and other innovative clean energy technology types. The typical LCOE predictions are in line with its conclusion that an Innovation Contract for Difference (iCfD) set at an initial level of £150/MWh and falling to £90/MWh could support novel projects in the 5 to 100 MW installed capacity range.

This 'typical' LCOE prediction of £110/MWh falls just below the strike price of £115-120/MWh won by offshore wind farm projects at the Contract for Difference (CfD) auctions in 2014–15 in the UK [193]. Since the time of the 2014–15 CfD auctions in the UK, the LCOE of offshore wind projects in the UK have reduced to around £40/MWh [111], facilitated by the CfD scheme that has enabled economies of volume, economies of scale and technology innovation to drive down costs [190]. This supports the argument that with similar subsidy support, the cost of tidal energy could move from the pessimistic to optimistic levels set out in Table 2.4.

After 10 MW of installed capacity, the pessimistic LCOE estimate is £295/MWh. The Offshore Renewable Energy Catapult has published figures indicating the LCOE achieved by tidal stream energy was approximately £300/MWh after 10 MW of total installed capacity worldwide (based on 2012 pricing), aligning closely with the pessimistic LCOE approximation in this chapter [190]. Likewise this model prediction is in line with the Marine Energy Council report [149] proposal for an Innovation Power Purchase Agreement (IPPA) set at a level of £290/MWh to support novel small-scale projects.

Table 4.7: Optimal LCOE and corresponding array parameters for different scenarios: optimal, pessimistic and typical scenarios and the P10, P50 and P90 generated using a Monte Carlo based analysis with a uniform distribution and upper and lower limits of the optimistic and pessimistic values.

	Optimistic	Typical	Pessimistic	P10	P50	P90
LCOE (£/MWh)	36.6	109.5	209.0	77.7	110.0	146.2
n_t	42.0	34.0	39.0	46.0	38.0	33.0
P_{avg} (MW)	24.0	19.7	22.4	26.1	21.9	19.2
P_{avg}/n_t (kW)	541	554	546	534	547	556
P_{BE} (kW)	541	554	546	534	547	556

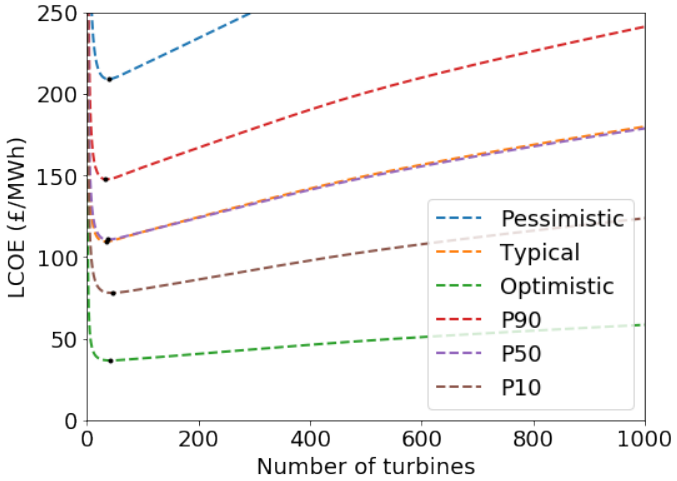

Figure 4.7: Prediction of optimal LCOE that can be achieved as a function of number of turbines, for the optimistic, pessimistic and typical scenarios outlined in Table 2.4, and the P10, P50 and P90 values obtained through a Monte Carlo simulation assuming uniform errors.

4.5 Conclusion

A new, validated *Thetis* model set-up for the English Channel with non-uniform mesh resolution has been used to minimise the LCOE of tidal stream turbine arrays in the Alderney Race. This work considers arrays using turbines with a rated power of 2 MW and a rotor diameter of 16 m. In general, the optimal array solutions consist of 'fence-like structures' of turbines orientated perpendicular to the flow. These array layouts help prevent the flow from diverting around the array as a result of the added array drag and is consistent with previous array optimisation studies [191]. Results demonstrate that in the early stages of array development in the Race (0 – 100 MW of installed capacity), steep reductions in LCOE are achievable through optimisation of turbine placement, and economies of volume. Based on the turbine specification considered in this chapter, the optimal location for turbines at this early stage of development is in the East Race.

Given the early stage of tidal stream energy industry development, cost information that provides the inputs to the array optimisation is limited, with a wide range of estimated CAPEX/OPEX and discount rates found in the literature. This uncertainty in associated costs is reflected in the LCOE estimates presented in this work, where the minimum LCOE based on assuming 'pessimistic', 'typical' and 'optimistic' cost scenarios is £36.60/MWh, £109/MWh and £209/MWh respectively. A Monte Carlo analysis is conducted to reflect that it is unlikely that all costs will

be at their most extreme (i.e. pessimistic or optimistic) values. Results from this study yield P10, P50 and P90 minimum LCOE estimates of £78/MWh (with 46 turbines), £110/MWh (with 38 turbines) and £146/MWh respectively (with 33 turbines) respectively. This provides a significantly reduced range of LCOE estimates, where the number of turbines required to achieve the minimum LCOE are closely aligned.

There are some notable similarities between the LCOE estimates presented in this work and published data from industry. For example, in this chapter, the pessimistic LCOE estimate after 10 MW of installed capacity (i.e. when economies of volume are limited) is £295/MWh. This aligns closely with information published by the Offshore Renewable Energy Catapult, who estimate that the LCOE after 10 MW of installed capacity worldwide was £300/MWh, based on 2012 prices and aggregated data from multiple tidal stream turbine developers.

Additional cost reduction mechanisms such as learning rates are not considered explicitly in this work, because developers will need to optimise their array designs based on the current costs in the industry, unless they plan to significantly delay production to avoid potential first-mover disadvantages. However, it could be argued that learning will allow costs to drop from the more pessimistic end towards the optimistic levels found in the literature. If this is possible, it is estimated that a 1 GW array could achieve an LCOE of £49/MWh, based on optimistic cost inputs. The cost inputs used in this thesis were based on the publicly available data at the time, analysed in Chapter 2, however as the industry gains more experience the costs are likely to fall. Therefore if developers use this approach in practice they should use updated cost inputs that reflect the current state of the industry.

4.6 Limitations and further work

Aspects of the work presented in this chapter can be developed further to reduce uncertainty in the results. This includes improvement to model validation in order to reduce error in modelled velocities, owing in part to the coarseness of the mesh required to provide acceptable run times when using the model within an optimisation loop. This can translate into large errors in power. At the settings used in this model the mean velocity is generally underestimated, so it is likely that the conclusions are conservative relative to what can be achieved in reality. However wave effects, which have been shown to lead to a net reduction in tidal power, have

not yet been included in this work. Since wave effects can have a notable impact, especially in sites more exposed to waves, they should be included in future studies [177, 178].

The LCOE calculations should be updated once additional cost information becomes available. Additional cost information will also be important to validate the assumptions made in this chapter, such as the linear increase in OPEX with number of turbines, for example.

Another area of further work is consideration for a suitable range of turbine scales for the Alderney Race. The current work considers 16m rotors only, however it has been shown that LCOE could reduce significantly if turbine diameter is increased, even by a few metres [49]. It will be important in future array optimisation work to identify the rotor diameter limits within different regions of the Race to establish how best to harness the resource with different turbine sizes. This also requires an understanding of any constraints that would prevent turbines from being installed in specific regions of the Alderney Race. For example, local areas with uneven bathymetry may prevent turbines from being installed [133]. The impact of different turbine diameters could be studied in a number of ways. The analysis carried out in this chapter could be repeated for a number of different turbine diameters, and their results compared to find the most suitable turbine design for the site. Or it is possible that final array designs may include turbines with multiple different diameters, which may be made economically viable by modular designs where the rotor sizes are varied but otherwise the drive train is identical [194]. This could be studied by including a turbine density field for each of the different turbine designs, with the maximum turbine density enforced on the sum of these parameters at each location. The functional could be set to the sum of the powers generated across all devices, minus the sum of the number of each device multiplies by its break even power, which may vary between devices to reflect the relevative increase in cost of greater rotor sizes.

The impacts of local blockage and accelerated bypass flow on the yield of tidal stream turbines in large-scale arrays should also be considered [171]. These are not represented using the continuous optimisation approach and therefore all optimised array designs obtained in this thesis do not reflect the potential yield uplift that could be achieved by strategic placement of turbines in the accelerated bypass flow of upstream rows of turbines, nor does it account for the potential losses due to the wakes of upstream turbines. Therefore the accuracy of the predicted yields and optimal layouts is limited, and the extent of the error depends on the extent to which

optimising the micro-siting of the discrete turbine positions, to use the accelerated bypass flow, offsets the losses due to local blockage. However comparisons between the continuous and discrete turbine representations in [82] showed that the farm wake and bypass flow modelled by both methods are largely consistent.

Given that resolving turbines individually requires a much finer mesh and is computationally very expensive, a number of approaches for discrete representation of the turbines would need to be investigated. A two stage optimisation as described in [82] could be implemented, such that continuous optimisation provides a good initial layout, so that the discrete turbine micro-siting optimisation requires overall fewer costly iterations to converge. Alternatively, this emulator method could be potentially be combined with a fully discrete optimisation approach. Discrete optimisation is currently computationally prohibitive for a non-fixed number of turbines, because optimisation of the layouts would need to be nested within a loop for optimising the number of turbines. Using the emulator method would greatly reduce the number of expensive optimisations that would need to be run to find the optimal number of turbines. However, each optimisation would still be very computationally expensive compared to the continuous method due to the high mesh resolution needed to resolve individual turbines.

Another avenue to explore further is to combine this economic optimisation with further terms in the functional to minimise potentially detrimental environmental impact. Environmental impact assessment [129, 70, 130] and optimisation [112, 104] of tidal energy has been addressed in numerous studies and is discussed in further detail in Section 2.2.8. One method of including environmental impact in the optimisation algorithm would be to penalise the functional by the amount that the turbines impact the flow in the surrounding regions, with a heavier weight given to regions of environmental interest, such as notable habitats for marine life. This environmental penalty term could be set up in a mathematically similar way to how the break even power term penalises the functional for increase the number of turbines and therefore the cost, except that it uses the turbine density field to calculate a measure of the change in flow rather than the number of turbines. Such optimisation is possible because the continuous turbine representation still couples the array presence with the regional hydrodynamics. This would likely result in optimal solutions with a decreased array yield, to reduce the effect on the surrounding flow. The optimal array layouts would likely look very similar in shape to those presented in Fig. 4.4, but with fewer turbines for a given break even power. For example, if the break even power is 200kW, the optimal layout based on break

even power alone is shown in Fig. 4.4d, but if impact on the flow was also penalised in the functional then the optimal layout would move in the direction of Fig. 4.4c or Fig. 4.4b. This hypothesis is based on the observations that the turbines which are removed first as the break even power is increased tend to be those which have the greatest negative impact on the yield through increasing the global blockage, and therefore would also have the most impact on the surrounding flow. However some of the best locations for energy extraction also have a notable impact on the flow in the surrounding regions.

Further work also needs to be done to investigate the impact of varying the maximum turbine density on the optimal solutions and therefore the guidance on how much energy can be economically extracted from a given tidal site. Since both the longitudinal and latitudinal spacing are combined into the one density parameter for this continuous turbine representation, the impact of halving one spacing or another cannot be separated or compared, unless a discrete optimisation method is used instead. Decreasing the turbine density would increase the predicted economic performance of the array and increase the optimal number of turbines to be installed, because more turbines could be fitted in the areas with higher flow speeds. However in practice local blockage effects would be much more significant at higher turbine densities, and since there are not represented in the continuous model of arrays, the model accuracy would be reduced.

Chapter 5

An array specification design method, applied in the Pentland Firth

Abstract

The work presented in this chapter was carried out in collaboration with SIMEC Atlantis. The author would like to thank SIMEC Atlantis for their provision of data, guidance and industrial motivation for this project.

MeyGen Phase 1A is at the time of writing the world's largest tidal stream turbine array, with an installed capacity of 6MW. From this array many valuable lessons have been learnt about the construction, installation, operation and maintenance of a tidal stream project. SIMEC Atlantis has plans to expand this array to 86MW capacity as part of Phase 1C of the site's development, with the necessary consent and grid capacity already arranged. This would be the world's first commercial scale tidal array, and therefore is used here as a case study to investigate the impact of varying consents, in terms of turbine rated power and rotor diameter, as well as turbine placement within the consented area.

The array is designed here through the use of a greedy optimization algorithm to find a configuration of turbines which meets the consents envelope specified in each

scenario and achieves a high average annual yield. This yield is predicted using an ADCP validated ambient flow model for the array and surrounding areas. A series of array designs based on current consents and variations on them are presented, to investigate how requests to extend the consents could improve the commercial viability of this and future large scale arrays. Practical constraints such as depth and steepness of the seabed, to constrain the regions in which turbines can be placed, are also taken into account.

It is found that for arrays of 2MW 20m diameter turbines, with current spacing consents applied, up to 266GWh in a typical year could be extracted by the array. However, if these choices and constraints were all expanded to allow closer spacing and smaller seabed clearances then up to 307GWh/year could be extracted. It is found that increasing the allowable turbine diameter and tip-to-tip cross flow spacing had the greatest positive impact on the overall yield, whereas the seabed clearance had a much less significant impact. Increasing the rated power of each turbine had the biggest positive impact on the average power generated per device, but it had a negative impact on the overall array yield, since fewer turbines are allowed within the 86MW expansion capacity.

5.1 Introduction

MeyGen Phase 1A is currently the world's largest tidal stream turbine array, with an installed capacity of 6MW, and plans to expand this array to 86MW capacity, under the so-called Phase 1C of the site's development, with the necessary consent and grid capacity already arranged. Before this expansion is installed, decisions about the array design need to be made, including the turbine specifications and their spacing requirements. Limitations are placed on some of these specifications, either due to physical constraints, such as minimum depths or maximum seabed steepness so as to allow for safe installation of the turbines, or due to licensing guidelines imposed in a consents envelope, issued by the Marine Scotland - Licensing Operations Team, MS-LOT.

These constraints are often imposed for environmental or safety reasons. There may be some potential to negotiate a relaxation of some of these constraints, if they can

be shown to have a significant impact on improving the array yield and not be a notable detriment to the surrounding environment. For example, if environmental studies show the overall impact on marine life is the same, then the crossflow spacing between turbines could be decreased while the downflow spacing is increased, or vice-versa. Array developers may wish to be able to quantify how significant each of the array specifications are in relation to one another, to determine which areas of the consents envelope and turbine design to push in order get the best improvements in anticipates annual array yield.

To address these questions, a custom greedy optimisation tool is proposed. This method can provide a quick first estimate of a suitable and feasible layout and the yield obtainable for each combination of settings specified. A map of the flow distribution across the site must be provided as an input to this optimisation tool. In this work, estimates of the ambient hydrodynamic conditions across the site are obtained using the *Thetis* model, once validated with ADCP data, and the results are post-processed to obtain a map of the flow distributions within the site boundary. The optimisation tool then uses this to predict the yield of turbines in each location, and combines this with a map of feasible locations, e.g. by identifying whether each location meets geometric requirements for the turbine specified and the clearance required. Ultimately a greedy optimisation algorithm is run to place turbines in the areas of highest yield concurrently identified as feasible locations. Upon selection of each turbine location, an exclusion zone is imposed to prevent a subsequent device from being installed in close proximity. This method enables very rapid assessment of the potential yield for each combination of input settings, since at the design stage the hydrodynamic model only needs to be run once and is not repeated with each new optimisation run. Follow up simulations of the final array design should be performed to affirm the yield predictions produced.

The expansion of the MeyGen array, from Phase 1A to 1C, is used as a case study here for investigating the trade-off between environmental consent conditions and their impact on array yield. In practice many arrays will need to make similar decisions as developers will often have a choice between multiple turbine designs and specifications, and these decisions will need to be made before detailed hydrodynamic modelling of the array design and more computationally costly optimisation of the site is carried out. For tidal array design tools to provide accurate annual energy production (AEP) estimates, the array design must be coupled with the flow model, so that effects of blockage are appropriately taken into account. However, many of these tools require the turbine specifications and limits on array spacing

to be given as inputs. Running more accurate optimisation models for all possible combinations of design options would be prohibitively computationally expensive. The tool presented here provides a first-pass estimate for AEP, which may not be as accurate as a fully coupled model, but is still useful for narrowing down the set of options to investigate, before a more complete model can be tested to assess the final design. This novel tool allows for broad parameter sweeps to be made, and is computationally light, making it suitable for array developers in the early stages of their project design, where their scope needs to be narrowed, but there is not yet access to significant computational resource and complex models.

5.2 Varying deployment consents

This section summarises the different array specifications that a tidal array developer may need to make a decision on in the early stages of array design, before in-depth array modelling and optimisation may be carried out. The current consents for MeyGen Phase 1C and the aspirational range to be investigated in this case study are summarised in Table 5.1

Table 5.1: The current consents envelope outlined by MS-LOT versus the upper limits of what SIMEC Atlantis could be interested in changing the consents to.

Consent	Symbol	Current	Aspirational
Turbine diameter	Ø	16–20m	18–26m
Turbine rated power	P_{rated}	1–2.4MW	1.5–3MW
Clearance: tip-to-seabed	s_{seabed}	4.5m	2m
Clearance: tip-to-LAT	s_{LAT}	8m	8m
Cross flow spacing	$s_{\text{crossflow}}$	45m centre-to-centre [1]	4m tip-to-tip
Down flow spacing	s_{downflow}	10Ø	10Ø

5.2.1 Existing turbines

The existing turbines are 18m in diameter, are rated at 1.5MW, and their locations are shown in Figure 5.1. Figure 5.1 also shows the site boundary, which is the outer limits of where turbines are allowed to be placed in Phase 1C of the MeyGen project, as well as detailed bathymetry data (0.2m resolution) at the site, provided by MeyGen. This bathymetry data is used for calculating whether the depth is sufficient to satisfy the clearance constraints for a given turbine diameter, rather

[1] The 45m centre-to-centre spacing was defined with the 16-20m diameter turbines in mind.

than the coarser bathymetry data which covers the wider region and is used in the hydrodynamic model.

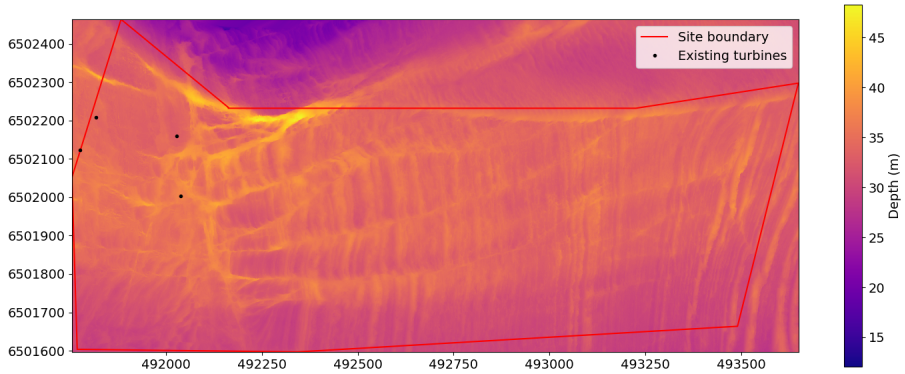

Figure 5.1: The detailed bathymetry data provided by MeyGen (0.2m resolution), and a map of the site boundary and the locations of the existing turbines from Phase 1A of the MeyGen project. Locations given in Eastings and Northings using the UTM 30 projection.

The results presented below are the anticipated yield for the additional 80MW which will be installed in Phase 1C, not including the generation of the existing four turbines in Phase 1A. The new turbines are allowed to be placed anywhere within the array boundary, subject to practical constraints such as depth and steepness, and to spacing constraints. Exclusion zones are drawn around the existing turbines, depending on the spacing requirements specifies by the user of the optimisation tool. This is discussed in greater detail below. Exclusion zones help prevent new turbines being directly in the wake of the existing turbines and vice versa, but in practice adding a substantial number of turbines will influence the surrounding flow through array scale blockage. Once this method is used for a preliminary indication of appropriate design choices, in-depth hydrodynamic modelling, which accounts for the local and global blockage effects of the array, should be performed and the impact of the new turbines on the yield on the existing turbines should be assessed.

This study aims to investigate how much increasing these parameters increases the yield at a real tidal site, like the Pentland Firth, where practical depth limitations and realistic upper limits to flow velocities must be taken into account. It aims to quantify the benefit of each marginal increase in turbine scale, so that developers can evaluate the trade-off between yield and cost and achieve a balanced decision.

5.2.2 Turbine specifications

The first two consents given in Table 5.1, typically referred to together as the turbine scale, relate to the choice of turbine design to deploy in the array. This method has been developed to allow the investigation of arrays with a single rotor diameter and rated capacity or mixed size arrays, in which the consent is imposed as an upper limit to the diameter or rated capacity of any one turbine in the array. This functionality has been developed for use by developers with modular designs, where the turbines can be mass produced and fitted with different sized blades depending on the flow conditions and depths. For example the Schottel device, which is designed for 4m and 6.3m diameter rotors with an otherwise identical drive train [194]. Generally it is assumed to be preferable to choose a single diameter and rated capacity across the whole array, because this will simplify construction and exploit economies of volume in manufacturing.

SIMEC Atlantis produce turbines to a number of different specifications. The rated capacity can range from the least powerful AR500, a 500kW rated device that has recently been deployed in a demonstrator project in Japan, to the most powerful AR3000, a concept for a 3MW device, which is currently in the design phase and has yet to be deployed at a test site. Currently the consents are agreed for up to 2.4MW rated turbines, but SIMEC Atlantis is investigating whether this new higher rated turbine concept is suited to the flows at the Pentland Firth site, and whether this consent should be renegotiated. Likewise, the existing turbines in Phase 1A are 18m in diameter, but SIMEC Atlantis are developing turbine designs of up to 26m in diameter, and would like to choose the most appropriate size for the site.

There are anticipated cost reductions that come with economies of turbine scale [12], so it is generally assumed that the turbines installed in Phase 1C will be at least as big and powerful as the four turbines already deployed, if not more so (at least 18m diameter and 1.5MW rating). Economies of turbine scale are generally anticipated because greater turbine diameters produce more power at lower flow velocities and greater rated turbines produce more power at higher flow velocities and it is believed that these power gains will offset the marginal cost increases for these greater devices. Coles and Walsh [49] assessed the economic impact of increasing the rotor design from 18m to 24m and the rated power from 1.5MW to 3MW under three possible cost scenarios; an optimistic case which assumed no increase in CAPEX as a result of the changes to turbine specification, a base case assuming a 5% increase in CAPEX and a pessimistic case assuming a 10% increase

in CAPEX and predicted LCOE reductions of 23%, 20% and 17% respectively.

However there will be a limit to the cost reductions that can be achieved. For increasing diameters there will be practical limits due to the number of suitable locations deep enough to allow for sufficient overhead clearance. Furthermore, there are cost limitations as greater diameters will increase the loading a turbine must withstand and the amount of material within a design, thus driving up the price. For increasing rated powers, the rated speed of the devices increases too, this means the yield increases in flow conditions which exceed the current rated speed of the turbine, but these benefits diminish to nothing as the rated speed of the turbine approaches the peak velocity at the site. There becomes a point where these diminishing yield gains do not outweigh the extra costs of larger diameter and higher rated devices.

5.2.3 Clearance

The second two consents specified in Table 5.1 specify the vertical clearance from the lowest point that the tip of the blades pass through to the seabed (the *bottom clearance*) and the highest point that the tip of the blades pass through to the lowest astronomical tide (LAT) (the *top clearance*). These clearances largely depend on the hub height, turbine diameter and local water depth.

A review of tidal energy by the European Marine Energy Centre (EMEC) in 2009 [170], recommended a bottom clearance of 25% of the water depth, or 5m, whichever is greater, to allow materials carried by the currents that could potentially damage the turbines to move along the seabed below them, and to minimise the turbulence and shear loading caused by bottom boundary layer effects. However, these clearances are now considered over-conservative. The Nova Innovation array in Bluemull sound has a bottom clearance of 4.5m, with a 9m hub height and 9m diameter turbines. The AR1500 turbines installed in MeyGen 1A have a hub height of 14m and diameter of 18m, making the bottom clearance 5m. A bottom clearance of 25% of the water depth would be much greater than the clearances used for these two arrays. Currently the agreed upon minimum bottom clearance for Phase 1C is 4.5m, this study investigates the benefits of negotiating a decrease in this value, to potentially as low as 2m, to increase the number of locations suitable for larger diameter turbines.

EMEC also generally recommended a minimum top clearance of 5m to allow for recreational activities, and to minimise turbulence and wave loading effects[170].

At the MeyGen site and even greater top clearance of 8m is needed to allow for local shipping activities. MeyGen consider it unlikely that the minimum surface clearance of 8m will be reduced, due to marine traffic transiting the Pentland Firth, and therefore this study does not consider varying s_{LAT}.

5.2.4 Turbine spacing

The impact of varying the minimum spacing constraints between the turbines is considered in this study. The current consents require at least ten turbine diameters spacing downflow between rows of turbines and at least 45m in the crossflow direction, from the centre of one turbine to the next.

By comparison, EMEC recommend a conservative crossflow spacing of at least ten turbine diameters downstream and two-and-a-half turbine diameters centre-to-centre, however they acknowledge that these spacing may be reduced once modelling of wake effects is undertaken [170]. These limits were based on the maximum rotor sizes considered at the time of 20–25m, so the crossflow spacing corresponds to 50–62.5m centre-to-centre and 30–37.5m tip-to-tip. EMEC also recommend a staggered layout between rows of turbines however this is often impractical for non-idealised site conditions.

This study investigates the benefits of decreasing the tip-to tip crossflow spacing, especially since some studies have found yield uplifts that can be gained from array designs with higher blockage ratios [171]. The downflow spacing remained fixed, to allow space for the turbine wakes to regenerate, with significant wake deficits observed at shorter distances in actuator disc experiments [167]. SIMEC Atlantis conducted a boat-mounted ADCP campaign at the site after the installation of Phase 1A. They found that, due to the high levels of turbulent mixing at the site, the wake effects diminished notably from four to seven turbine diameters downstream of their devices and velocities were significantly regenerated by ten diameters downstream (MeyGen, pers.comm.).

Furthermore, the current crossflow spacing requirements are specified from the centre-to-centre of adjacent devices. This requirement would likely need to be re-evaluated and renegotiated for turbines with an increased rotor diameter anyway, because a 45m centre-to-centre spacing is equivalent to a 29m tip-to-tip spacing for 16m diameter turbines and a 19m tip-to-tip spacing for 26m diameter turbines.

Ultimately the final crossflow and downflow spacing should be decided on balance of three things:

- The benefits of decreasing spacing allowing for greater flexibility in where the turbines are placed, such that the turbines can be placed in higher flow areas.
- The ecological safety impacts of decreasing the spacing.
- The possible yield gains or losses due to accelerated by pass flows or turbine wakes.

Exclusion zone shape

The spacings specified in the consents envelope are easily interpreted when applied to regular rows of turbines in a rectangular or staggered layout and when the flood and ebb are aligned. But in practice it may be beneficial to install turbines in irregular layouts, such as sideways 'U' shapes facing the flow and funnelling it into the back row of turbines, as found in [81], or due to certain regions being infeasible for installation, pushing the turbines out of a perfect row-based layout. This study addresses this point by investigating two types of exclusion zone, areas around each turbine that future turbines cannot be placed in, to prevent additional turbines being directly in each others wakes and too close to satisfy the spacings imposed by the consents. Both types of exclusion zone extend downstream of the turbine, so that subsequent turbines will not be placed in the wake of existing turbines, as well as upstream of the turbine, so that subsequent turbines will not create a wake immediately upstream of existing turbines.

Figure 5.2a shows the first of the two types of exclusion zone used in this work. When a turbine is added to the array design, the grey ellipse is drawn around its centre and the centre of all subsequent turbines must be placed outside of this ellipse. The ellipse has a minor axis diameter of $2Ø + 2s_{\text{crossflow}}$, ensuring that the minimum distance from the centre of one turbine to the next nearest turbines is $Ø + s_{\text{crossflow}}$, giving a tip-to-tip spacing of $s_{\text{crossflow}}$. The ellipse has a major axis of $20Ø$, ensuring a minimum downflow spacing of $s_{\text{downflow}} = 10Ø$. In the example plotted, the ellipse is aligned with flow in the East-West direction, but the major axis should always be chosen to allign with the dominant direction of the flow. A blue ellipse with both axes halved is also drawn to represent the spacing allowance per turbine. The blue ellipses may touch but never overlap in the final array designs produced.

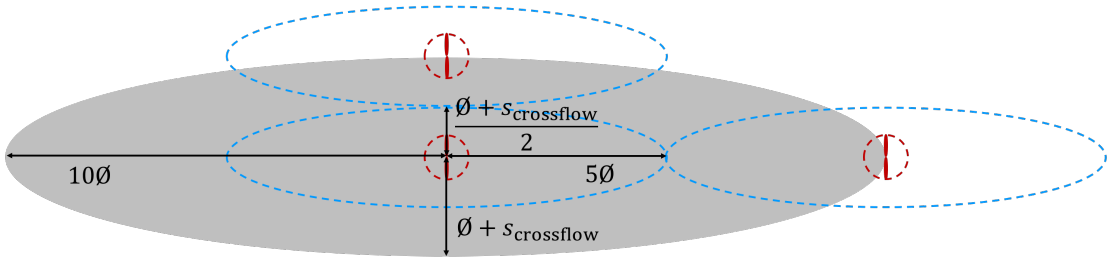

(a) The *ellipse* shaped exclusion zone tested in this work. The grey exclusion ellipse has a minor axis diameter of $2Ø + 2s_{crossflow}$ and a major axis of $20Ø$, ensuring a minimum downflow spacing of $s_{downflow} = 10Ø$. A blue ellipse with both axes halved is also drawn to represent the spacing allowance per turbine, and examples of how close subsequent turbines can be placed are shown.

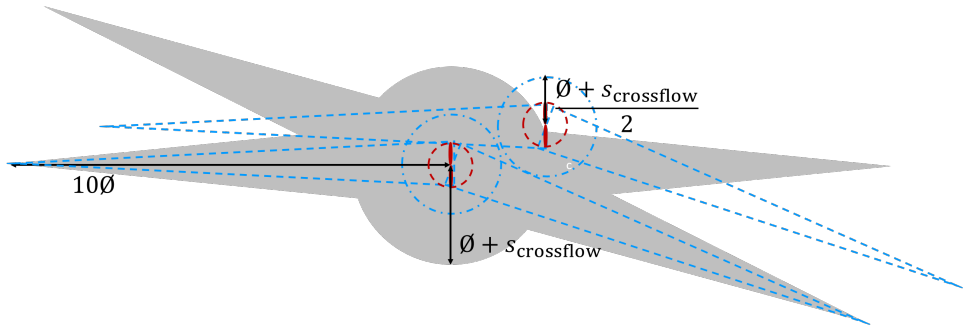

(b) The *directional* shaped exclusion zone tested in this work. The grey exclusion shape consists of two triangles aligned with the ebb flow at 270° clockwise from North and two triangles aligned with the flood flow at 111°, and a circle of diameter $2Ø + 2s_{crossflow}$. The triangles have a length of $Ø + s_{crossflow}$ each, and a height of $2Ø$. A blue shape of half the width is also drawn around each turbine to visualise the wake region and crossflow requirements per turbine.

Figure 5.2: The two exclusion zone types tested in this chapter, shown in grey. Subsequent turbines have been drawn to demonstrate that the exclusion zone enforces the required $s_{crossflow}$ and $s_{downflow}$.

An advantage of the ellipse-based spacing type is that it is easy to visualise and understand. A drawback of the ellipse-based spacing type is that it assumes that both the flood and the ebb are in the same direction. In practice it is found that the flow in flood is typically aligned at 111° clockwise from North, and the flow in ebb is aligned at 270° from North, as shown in Figure 5.3, in data obtained from MeyGen site studies. When applied to the example of the MeyGen site, the ellipse is aligned with the ebb flow, because the flow through the MeyGen tidal plot is ebb-dominant.

Figure 5.2b shows an alternative means to define an exclusion zone around each turbine, that accounts for the difference in dominant direction of the flood and ebb flow. When a turbine is added to the array design, the grey shape is drawn around its centre and the centre of all subsequent turbines must be placed outside

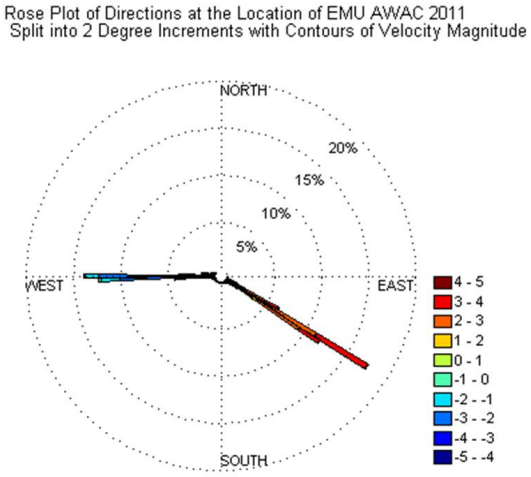

Figure 5.3: A rose plot showing the dominant flow directions at the MeyGen tidal site, plot courtesy of MeyGen.

of this shape. The shape consists of two triangles aligned with the ebb flow at 270° clockwise from North and two triangles aligned with the flood flow at 111°, and a circle of diameter $2Ø + 2s_{\text{crossflow}}$, ensuring that the minimum distance from the centre of one turbine to the next nearest turbines is $Ø + s_{\text{crossflow}}$, giving a tip-to-tip spacing of $s_{\text{crossflow}}$. The triangles have a length of $Ø + s_{\text{crossflow}}$ each, and a height of $2Ø$. For visualisation purposes, the algorithm also draws a blue circle around each of the turbines of radius $\frac{Ø+s_{\text{crossflow}}}{2}$, these circles may touch but never overlap, and show the the crossflow spacing requirement is always satisfied. A blue triangle in the flood and ebb direction of each turbine is also drawn, with length $10Ø$ and height $Ø$, to show that turbines are never placed in this immediate wake region of other turbines.

The directional spacing does not allow turbines to be placed in each other's wakes in the dominant directions, but it otherwise allows turbines to be placed a little closer diagonally. However, this current work assumes that the flood and ebb directions are at the same angle throughout the site (currently set to 111° in flood and 270° in ebb, based on the directionality of the existing turbines and site studies) and that the turbines yaw to face the flow direction. In practice the flow direction changes slightly with location. Further work should be conducted to create directional spacing by feeding in a map of ebb and flood directions at each location to create an array design where the turbine orientation varies with location to face the dominant directions of the flow. The yield losses that result from yaw and flow misalignment could also be assessed, to determine the importance of yawing over fixed-axis turbines.

5.3 Hydrodynamic model setup and validation

A depth-averaged ambient flow model of the MeyGen site was setup in *Thetis*. This model was used to provide the input data needed to make yield predictions in the optimisation tool developed in this work. The model solves the shallow water equations over a discretised domain, shown in Figure 5.4. The finite-element mesh is comprised of 31,144 nodes and 62,486 elements. The element size increases from 50m around the MeyGen site boundary, to 1000m further out in the North Sea. The bathymetry used is a combination of measurements taken from Edina Digimap Service [7] and the General Bathymetric Chart of the Oceans (GEBCO) 2014 dataset[8], with a resolution of $1/3600^\circ$ applied where possible and $1/600^\circ$ otherwise. The semi-implicit Crank–Nicolson method of temporal discretisation is used for stepping forward in time, with a constant time step of $\Delta t = 100s$. The model is forced at the open boundaries Q1, O1, P1, K1, M2, S2, N2, and K2 constituent elevation forcing functions, implemented via *Uptide*[2]. The bottom friction is calculated using the Manning formulation and the Coriolis forcing is represented using the beta-plane approximation.

The model was calibrated by tuning the Manning coefficient, as shown in Figure 5.5, for which a value of 0.04 $sm^{-1/3}$ provided the best results. It was calibrated by comparing to ADCP data from 3 locations, provided by MeyGen, and tidal gauges spread throughout the site, and a good agreement was found with an R squared score of 0.989 and NRMSE of 11.4%. Extensions of this study are improving on this through a finer spatial resolution, smaller timestep and spatially varying bottom friction, but the preliminary results are presented here.

The calibrated and validated tidal model is then run over a 2-week period that is representative of the tidal dynamics averaged over the 18.6 year lunar cycle, using a similar approach to [195], where a 20 year tidal signal is built up using constituent data and harmonic reconstruction, then a period representative of typical conditions which has the lowest error to the mean high water spring, mean high water neap, mean low water spring and mean low water neap found over an 18.6 year lunar nodal cycle. The elevations and depth-averaged tidal velocities are captured over the whole domain over the simulation period, and the velocities within the MeyGen site boundary are passed as an input to the new rapid optimisation tool developed in this work.

[2]https://github.com/stephankramer/uptide

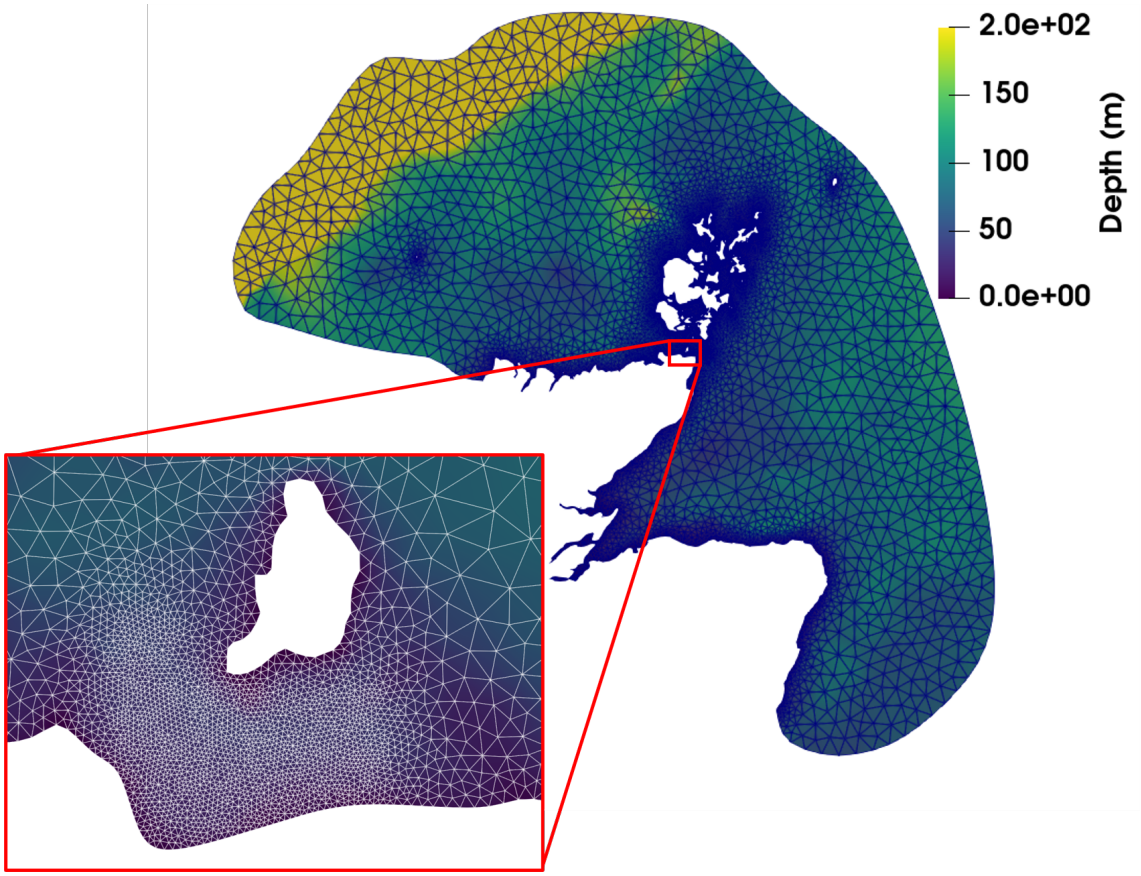

Figure 5.4: A map of the domain modelled in *Thetis*, showing the unstructured triangular mesh used to solve the shallow water model, overlaid over the bathymetry in the region, with data taken from a combination of the Marine Digimap database [7] and the General Bathymetric Chart of the Oceans (GEBCO) 2014 dataset[8].

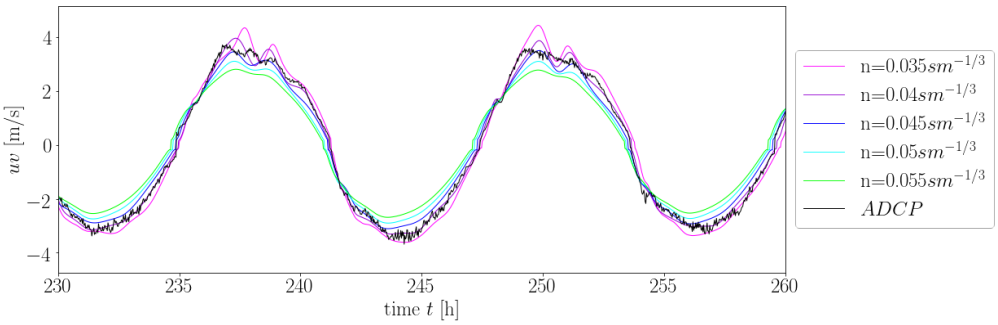

Figure 5.5: An example of the calibration of the *Thetis* tidal model, by comparing depth averaged velocities against ADCP data provided by MeyGen, for Manning Coefficients from 0.035 $sm^{-1/3}$ to 0.055 $sm^{-1/3}$.

Figure 5.6, shows a snapshot of the instantaneous velocities from this tidal model, demonstrating how the peak velocities can reach as high as 5m/s in the region, and how the Pentland Firth is an ideal location for tidal energy extraction, with among the most powerful tidal currents in the Orkneys and the Pentland Firth

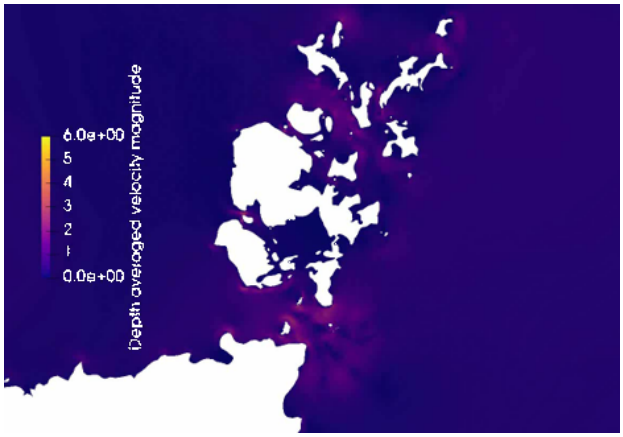

Figure 5.6: A snapshot of the *Thetis* model of the flows around the Pentland Firth region, demonstrating high instantaneous velocities through the MeyGen tidal site and past nearby islands.

region [32, 33].

5.4 Optimisation Tool

The following section describes the development and implementation of a novel optimisation tool used to provide an early-stage assessment of the ideal array specifications. An outline of the process used in the optimisation tool is given in Figure 5.7 but a more detailed description of each stage follows. The optimisation method is computationally cheap, allowing the tool to be run over a wide ranging combination of input settings.

5.4.1 Flow distribution adjusted to hub height

Velocity time series data is obtained at points on a finite element mesh from a *Thetis* model, as described in Section 5.3. The velocity time-series data at each location within the site boundary is summed over all time steps into velocity bins with an interval of 0.05m/s, an example of which is shown in Figure 5.8. Convergence tests were performed and it was found that the size of the velocity bin had no impact on the time-averaged power estimate for bin widths of around 0.1m/s or lower.

The power calculation assumes that the velocity and power coefficient are uniformly distributed across the swept area of the rotor. In reality drag from the sea bed creates a velocity profile that approximately logarithmically increases with height, and an

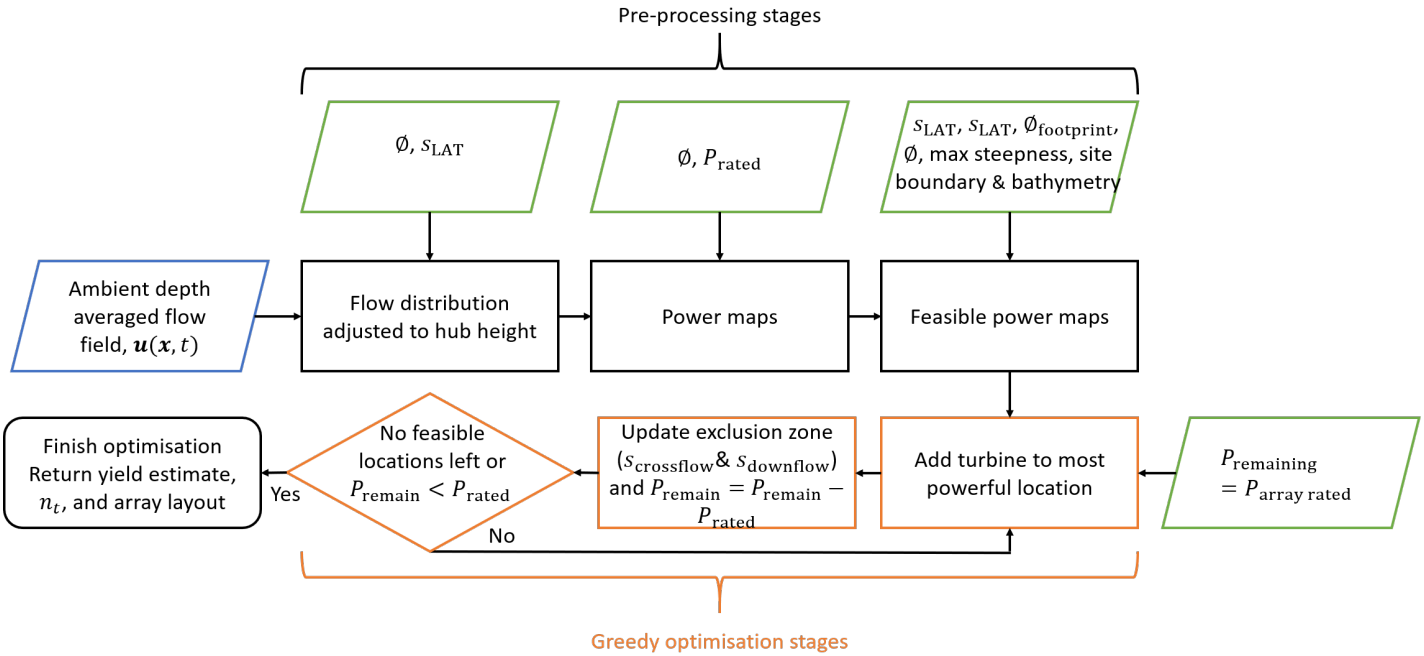

Figure 5.7: A schematic of the process used for providing yield estimates and array designs with the novel optimisation tool.

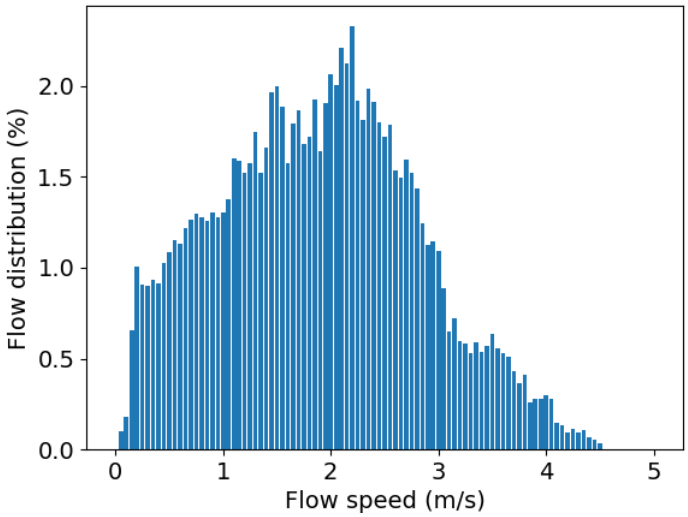

Figure 5.8: A flow distribution of time spent within each 0.05m/s velocity bin at an example location taken within the MeyGen site boundary.

idealised profile is shown in Figure 5.9. Therefore a correction factor is applied to the depth averaged velocities in the flow distribution, to adjust them to the average flow speed across the swept area of the rotor. It is assumed that, regardless of the choice of turbine diameter, the upper tip of each turbine is always 8m below the lowest astronomical tide, and therefore the hub height is always positioned at

$\varnothing/2 + 8$m below the LAT level. Therefore a different correction factor is applied for each turbine diameter investigated.

The flow is adjusted by the log law shown in Figure 5.10 to find the average speed across the turbine rotor. Since the flow is fastest higher in the water column, it is assumed at all locations that the turbine is placed as high as possible in the water columns, such that the highest tip is 8m below LAT.

The correction is calculated by assuming a depth-varying velocity profile of

$$\frac{\mathbf{u}}{\mathbf{u}_\infty} = \left(\frac{z}{h}\right)^{1/n_l}, \tag{5.1}$$

where $\mathbf{u}$ is the velocity at height z, $\mathbf{u}_\infty$ is the free stream velocity, where the boundary effects have diminished to zero, h is the local total water depth. n_l is the power law exponent that defines the shape of the logarithmic velocity profile, and $n_l = 7$ is found to provide a good fit against bed mounted ADCP data from the site. If $\mathbf{u}^*$ is the depth-averaged velocity, then the equation can be solved to find the height at which $\mathbf{u}(z^*) = \mathbf{u}^*$. It is found that $z^* = 0.34875 \times h$ and this can be used to find the depth varying velocity $\mathbf{u}(z)$ from the depth averaged velocity provided by the *Thetis* model, such that

$$\mathbf{u}(z) = \mathbf{u}^* \left(\frac{z}{z^*}\right)^{1/n} . \tag{5.2}$$

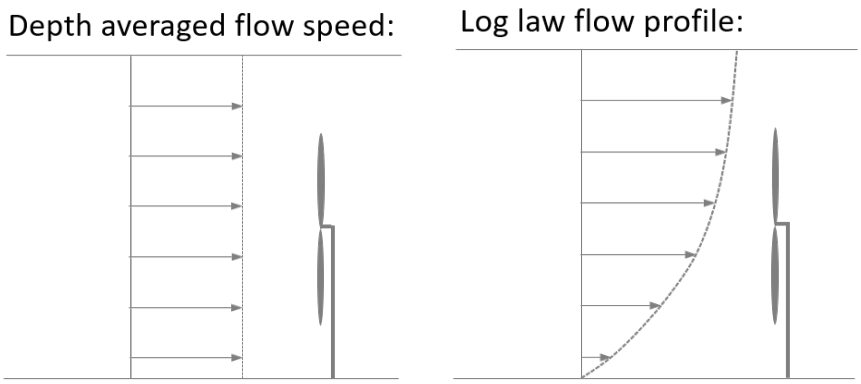

Figure 5.9: Shallow water models produce a depth-averaged flow speed, that are assumed to be constant over the whole water column. The design tool assumes the flow profile has a logarithmic shape due to boundary layer effects from the seabed friction.

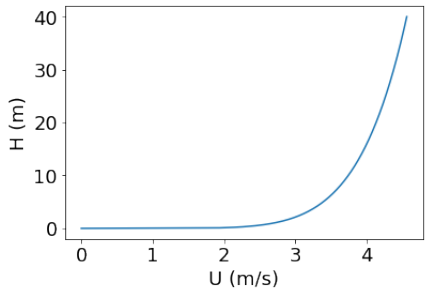

Figure 5.10: An example of log-law model of flow speed variation with depth, given a depth averaged speed of 4m/s.

5.4.2 Creating power maps

The optimisation tool allows the user to test array designs over a range of turbines of different P_{rated}, u_{rated} and $\emptyset$, and the combination of these two parameters affects the power curve. Figure 5.11 shows the idealised power curves for a range of the different rotor diameters and rated powers tested. A power coefficient of $C_P = 0.41$ is used below rated speed and $C_P = 0.41(\mathbf{u}_{\text{rated}}/\mathbf{u})^3$ above rated [98]. A cut in speed of 1.0m/s and a cut out speed of 4.5m/s is applied, based on power curves published by SIMEC Atlantis.

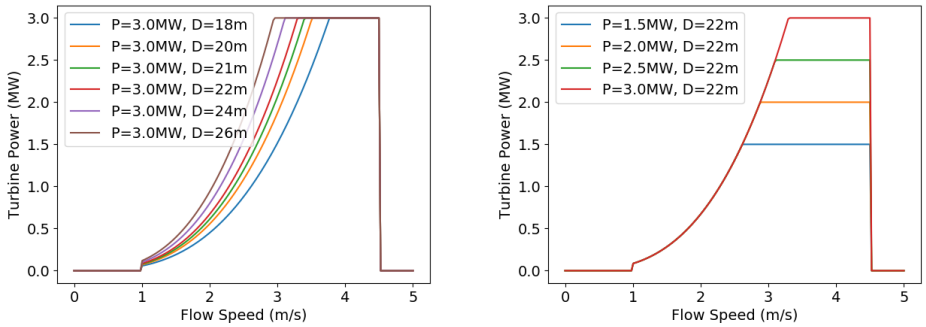

Figure 5.11: The impact that the choice of rotor diameter and rated power can have on an idealised power curve of a device.

Increasing the rotor diameter increases the power generation at low flow speeds and decreases the speed at which rated power is met, u_{rated}. Increasing the rated power increases the power generation at high flow speeds and increases u_{rated}. Both increases to the turbine scale are likely to result in an increase in the cost per device, so it is important to establish whether each improvement to the power curve results in a substantial enough increase in AEP to offset the costs.

The array design tool combines the flow distribution at each location with the choice

of rated power and rotor diameter to produce a set of maps of the predicted time-averaged power generation of a turbine at that location. One map is produced per each combination of rated power and rotor diameter to be tested. Figure 5.12 shows examples of these maps for an 18m diameter and 1.5MMW rated turbine and a 26m diameter 3MW rated turbine. The former can achieve an average power of 0.72MW (corresponding to a 48.2% capacity factor) in the best possible location and the latter can achieved average power of 1.43MW (corresponding to a 47.7% capacity factor).

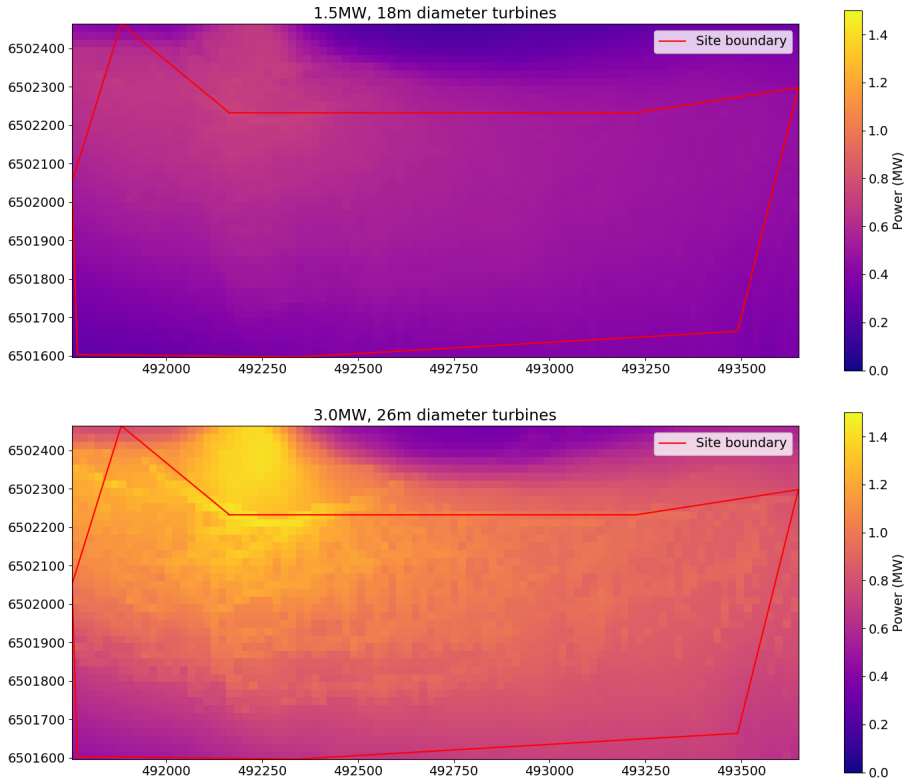

Figure 5.12: Estimates for the time-averaged power generation of (a) an 18m diameter 1.5MW rated turbine and (b) a 26m diameter 3MW rated turbine, centred at each location on the map.

The C_P value has been chosen to reflect the anticipated water-to-wire efficiency, however the power predictions are not yet adjusted in this study for anticipated turbine availability and maintenance losses. It is assumed that these effects will have an approximately proportionate impact on the yield across all array designs found, and that they do not need to be modelled at this stage given that this tool is primarily used to make relative comparisons between designs, rather than provide a final and accurate power estimate.

Because larger diameter turbines generate more power at lower flow speeds they can

generate enough thrust to have a lower cut in speed. Therefore some of the larger devices are likely to have an cut in speed of less than 1m/s and a higher availability during neap tides. However, since the power generation is very low at these speeds the different cut in speeds between different diameter turbines have very little impact on the overall yield and therefore are not modelled in this study. For example, given the flow distribution from the MeyGen site shown in Fig. 5.8, if the cut in speed for a 26m diameter turbine decreases from 1m/s to 0.9m/s or 0.8m/s the predicted yield increases by only 0.25% and 0.43%, respectively. Small changes at the top of the power curve have far more impact on the yield than changes at the bottom of the power curve. The important changes in power curve with rotor diameter are already accounted for in the following results by the changes shown in Fig. 5.11.

5.4.3 Physical constraints and feasible locations

Once a power estimate in each location is calculated, the site is filtered based on steepness and clearance constraints.

Steepness

The MeyGen site is characterised by lots of steep ridges along the sea floor, with flatter regions in between. Figure 5.13a shows the seabed angle at all locations across the MeyGen site, calculated from detailed bathymetry data provided by SIMEC Atlantis. Currently monopiles are the intended foundation design for MeyGen 1C [52], so it is assumed that all the turbines will have a footprint diameter, $\emptyset_{\text{footprint}}$, of 3m and require a seabed steepness of less than 5° for installation. This steepness requirement remains the same in this study, regardless of turbine specifications. Monopiles have a far smaller footprint than the tripod gravity-based foundations currently used on the Phase 1A turbines, so alternative foundation choices could restrict the feasible locations for installation even further. Figure 5.13b, shows the same data filtered subject to a 5° angle limit, outlining any non-compliant sites.

Clearance

Whether it is too shallow will depend on the tip to LAT clearance, the bottom clearance and the turbine diameter parameters. Figure 5.14 shows an example of

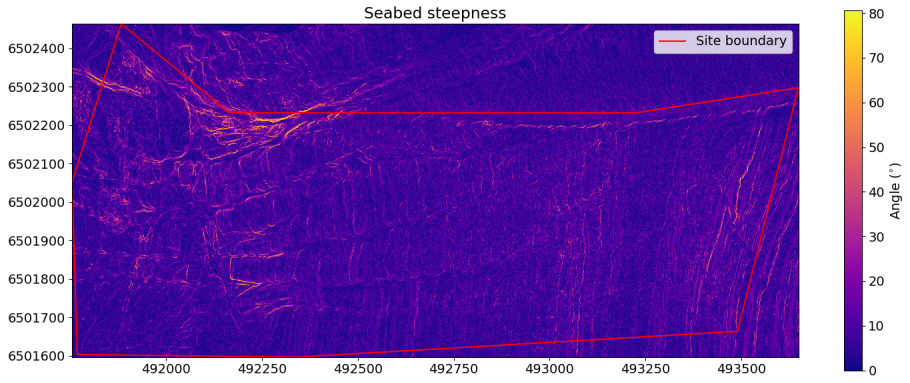

(a) The angle of the seabed in each location.

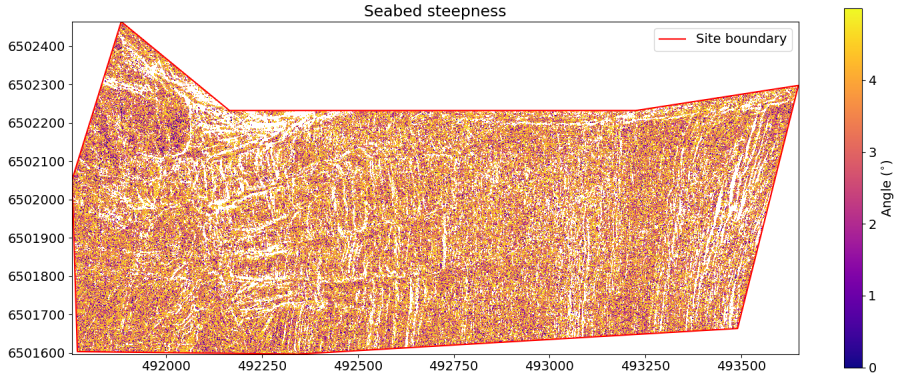

(b) The unfeasible locations, either outside of the site boundary or too steep for installation, are shown in white and filtered out.

Figure 5.13: Map of MeyGen tidal site, demonstrating the approach to identifying regions too steep to install turbines. It is assumed that the seabed angle needs to be less than 5° within the 3m footprint to safely install a monopile turbine.

how the three parameters are combined to test if a turbine will fit at a given location or not.

Figure 5.14: An example of how the depth at a given location is combined with the tip to LAT and bottom clearance, to determine which rotor diameters can fit there.

The steepness and clearance criteria are combined to generate maps of maximum feasible turbine diameter in each location. Figure 5.15 shows that if the seabed clearance required is decreased from 4.5m to 3m, or even further to 2m, it can be seen how the number of suitable locations for larger turbine diameters increases. With the current consents of $s_{\text{bottom}} = 4.5m$ there are a number of locations on the Southern border of the MeyGen site which are too shallow for even 18m diameter turbines to be installed.

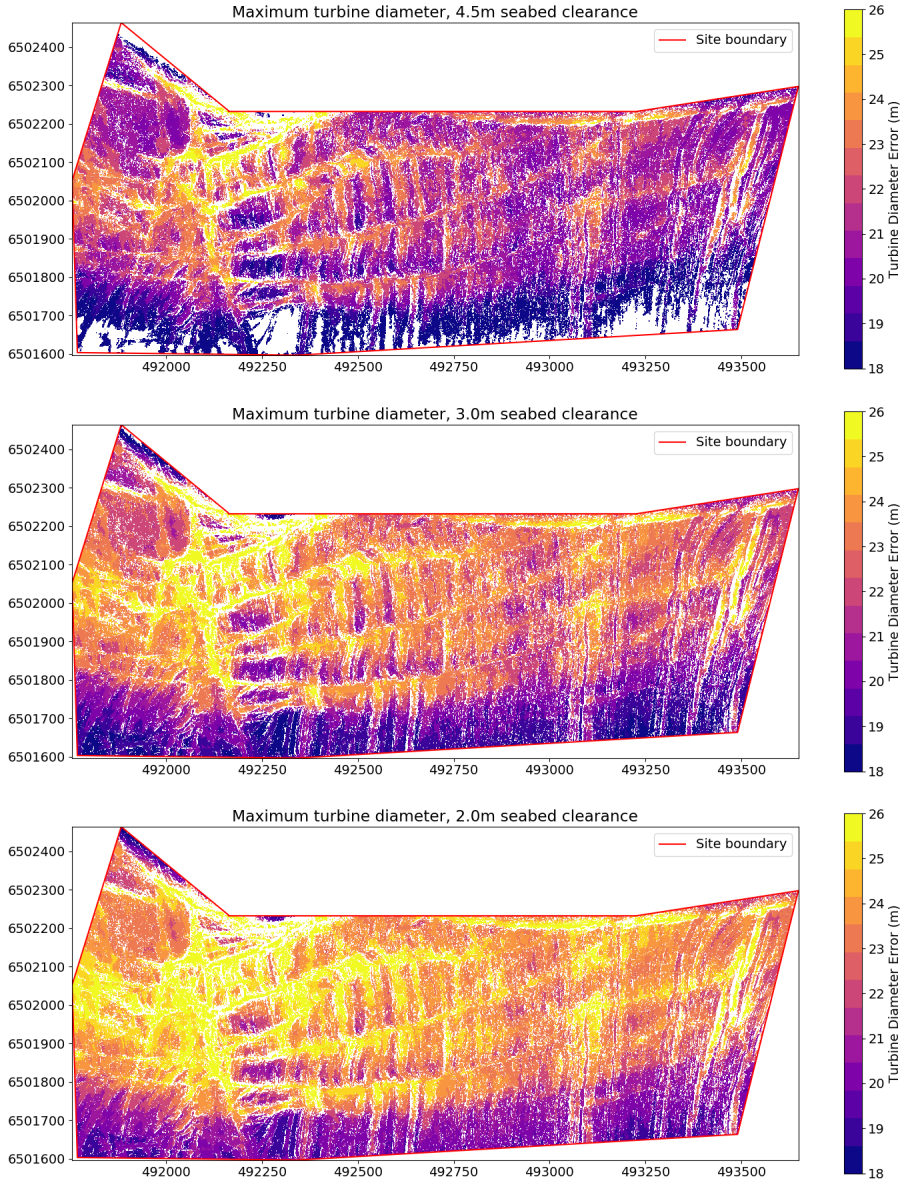

Figure 5.15: The maximum turbine diameter that can be installed in each location for a bottom clearance of (a) 4.5m, (b) 3m and (c) 2m. The regions that are too steep or too shallow for any of the turbine diameters tested are filtered out.

The maps shown in Figure 5.15 allow the optimisation tool to find array designs

which feature multiple rotor sizes, if the user allows. Or the user can specify an exact rotor size at the start of the optimisation algorithm. If this is the case the tool uses a power map of the site using the power curve relating to the rated power and diameter chosen, with a filter of feasible locations applied relating to the diameter and clearance requirements chosen. Examples of these final power maps used as a starting point for the optimisation algorithm are shown in Figure 5.16.

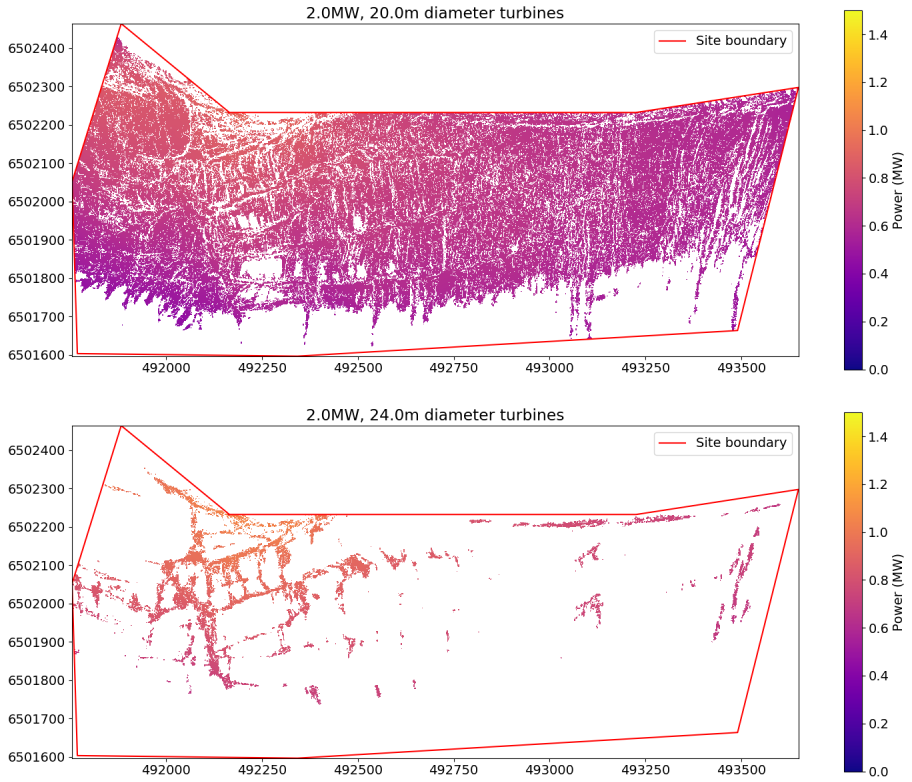

Figure 5.16: Examples of the maps of the time-averaged power predictions for a 2MW (a) 20m or (b) 24m diameter turbine, with the feasible locations filtered using a 4.5m bottom clearance requirement.

5.4.4 Greedy optimisation process

The user gives the tool a list of all the rated powers, rotor diameters, spacings and clearances they are interested in testing and the tool obtains a feasible power map, such as the ones shown in Figure 5.16, for each possible combination of these settings. Once those power maps are obtained the user can specify a combination of interest, for example a rated power of 2MW, rotor diameter of 20m, bottom clearance of 4.5m and centre-to-centre spacing of 45m with an ellipse exclusion zone shape. The greedy optimisation algorithm selects the power map that corresponds

to the clearance, rating and diameter specified, then performs a greedy optimisation algorithm that iteratively adds a turbine to the location with the highest feasible power prediction, then applies an exclusion zone based on the spacing specified from Table 5.1 and shape specified in Figures 5.2a or 5.2b. It then repeats this process, adding turbines to the next highest generating feasible location an drawing an exclusion zone around it until one of two conditions is met. Either adding another turbine would increase the array capacity over the total capacity allowed, i.e. the remaining capacity, which is initially set to $P_{\text{array rated}}$, falls to $P_{\text{remain}} < P_{\text{rated}}$. Or there are no remaining feasible locations left within the site boundaries.

Figure 5.17 shows an example of the first few iterations of this algorithm, for the example specifications given above. First the four existing turbines in MeyGen 1A are drawn with exclusion zones around them, then a turbine is added at each step. The exclusion zone is shown as a white ellipse of locations now filtered out as unfeasible. The blue ellipse has a minor axis diameter equal to the turbine diameter plus the tip-to-tip crossflow spacing, and a major axis diameter equal to the downflow spacing; it is drawn on to represent the buffer zone around each turbine mat touch but may not cross.

If the user specifies that a combination of multiple rotor diameters is allowable, the algorithm selects the best location across multiple maps. In some cases the next best location may be for the largest possible rotor diameter in other cases the fastest flow may be in regions too shallow for the largest rotors, and therefore a location from the map of a smaller rotor is chosen. The functionality could be useful for developers with modular designs, with multiple blade size options.

5.5 Optimisation results

Firstly the impact that the exclusion zone shape has on the array yield and design is investigated. Figure 5.18 shows the array layouts that result from using the ellipse and directional exclusion zone shapes defined in Figures 5.2a and 5.2b. These designs result in a predicted annual yield of 266.0 GWh and 290.7 GWh, respectively, with an average capacity factor of 38.0% and 41.5%. There is a notable difference in both yield and array layout. In the directional spacing the turbines are packed closer together, due to the narrower exclusion shape used. This may increase blockage effects, which are not yet modelled in this stage of the array design. However, some of the turbines forms rows together and others are staggered in positions which may

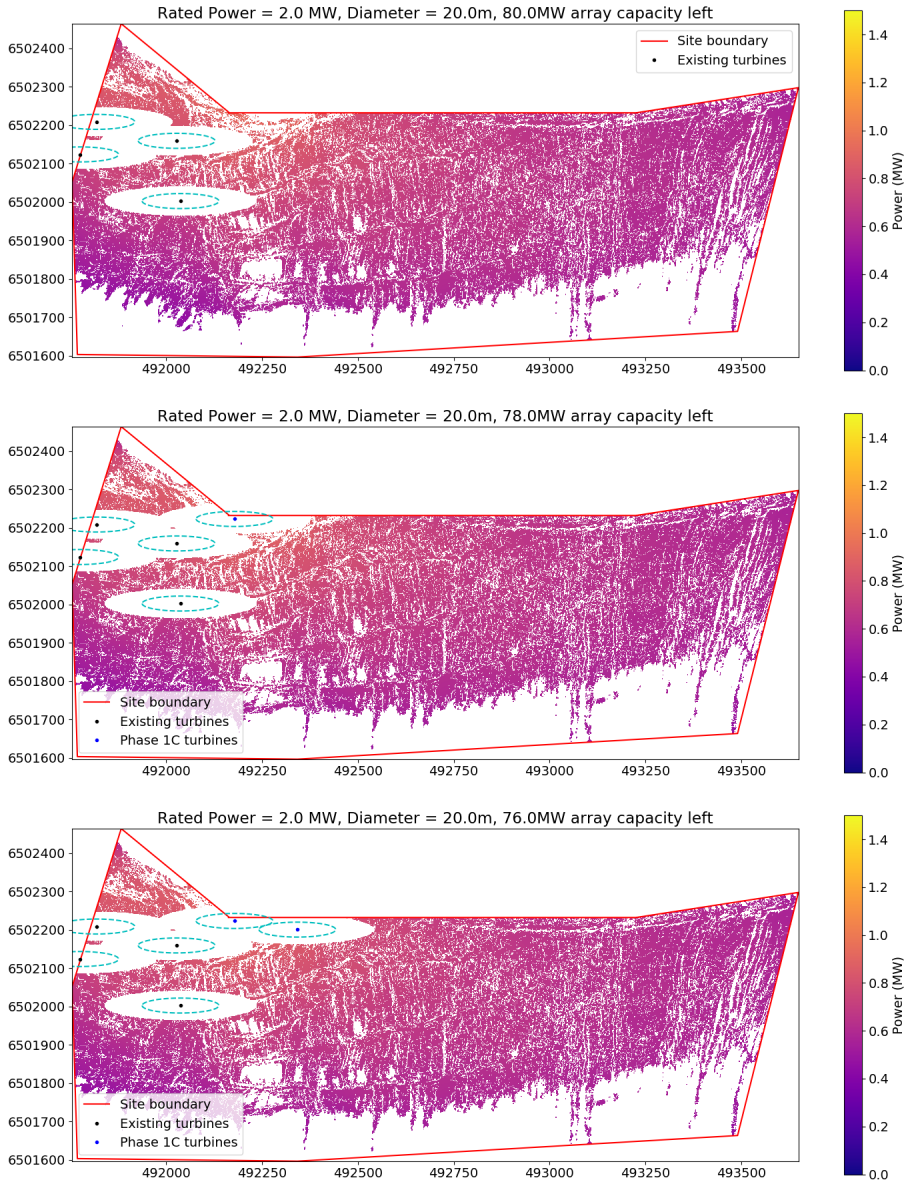

Figure 5.17: The first three iterations of the greedy optimisation algorithm for a rotor diameter of 20m, rated power of 2MW, bottom clearance of 4.5m and crossflow spacing of 45m centre-to-centre.

be able to exploit the accelerated bypass flow between the turbines in the previous rows, as demonstrated in [87, 88, 89, 83]. It has been shown in other optimisation studies that layouts formed of staggered fence-like rows of turbines are favourable for power generation, and they are also known to be easier for array installation and cable routing [191, 90]. The directional spacing is used in the following results because it takes into account the difference between flood and the ebb directions.

This optmisation process allows the comparison of array designs using the current consents envelope to the aspirational consents envelope. The results presented in

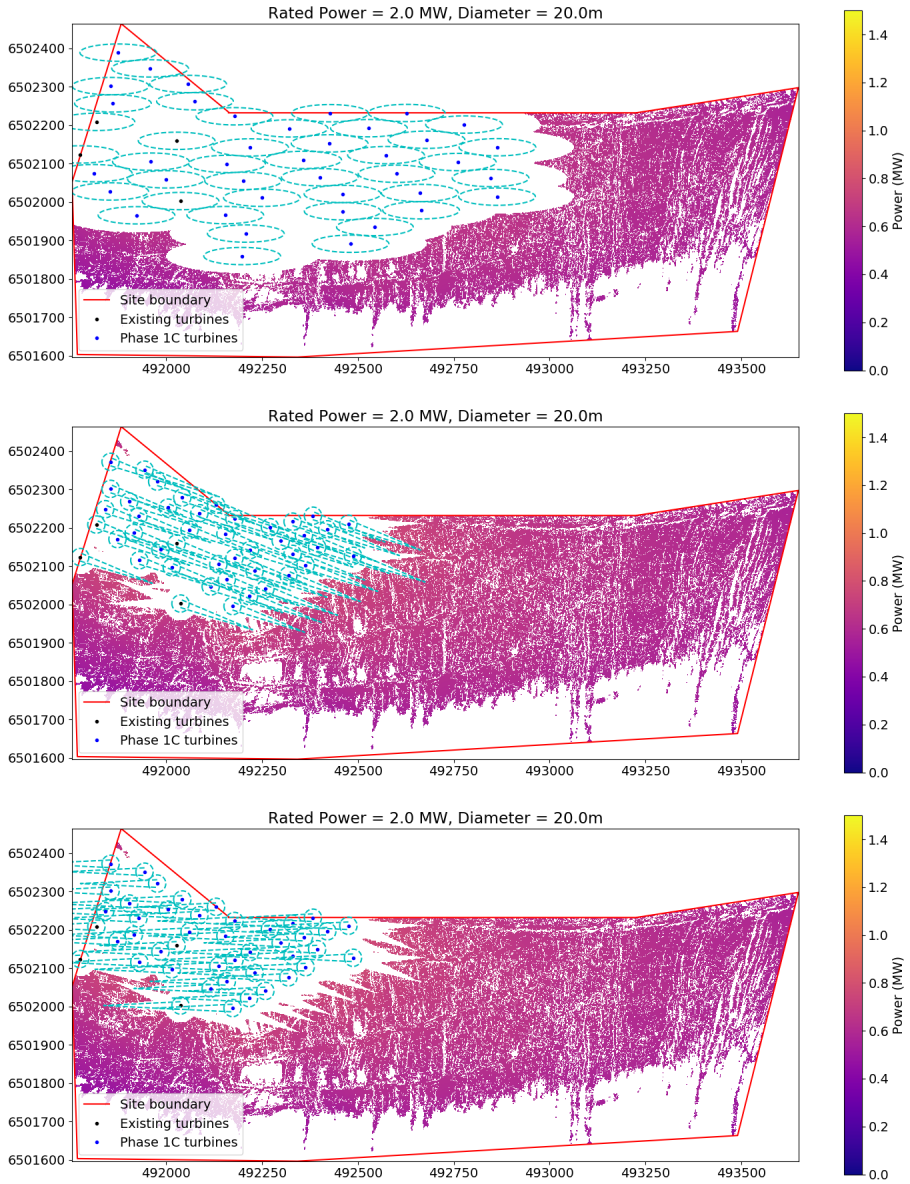

Figure 5.18: The array layouts obtained using the current consents (20m diameter, 2MW rated, 4.5m seabed and 8m LAT, 25m tip-to-tip), with (a) ellipse exclusion zones and directional exclusion zones tested, disallowing turbines to be places in the path of the wake in the (b) flood and (c) ebb directions, resulting in a predicted annual yield of 266.0 GWh and 290.7 GWh, respectively.

Table 5.2 show the impact of adjusting each of the consents on the array parameters. Current consents are specified in Table 5.1, with a diameter of 20m and a rated power of 2MW chosen. The array layout produced by the optimisation tool for these settings is shown in Figure 5.18 (b).

Increasing the turbine diameter to 24m had the biggest impact on improving the array yield (+11.3% compared to current consents). However, increasing it further

Consent change	Annual Yield	n_t	p.p.d	CF	% diff
Current consents	290.7 GWh	40	0.83 MW	41.5%	–
Ø =26m	209.3 GWh	25	0.96 MW	47.8%	-28.0%
Ø =24m	323.5 GWh	40	0.92 MW	46.2%	+11.3%
P_{rated} = 3MW	227.5 GWh	26	1.00 MW	33.3%	-21.7%
P_{rated} = 2.5MW	259.4 GWh	32	0.93 MW	37.0%	-10.8%
s_{seabed} = 2m	291.2 GWh	40	0.83 MW	41.6%	+0.2%
s_{seabed} = 3m	291.2 GWh	40	0.83 MW	41.6%	+0.2%
$s_{\text{crossflow}}$ = 4m tip-to-tip	294.1 GWh	40	0.84 MW	42.0%	+1.2%
$s_{\text{crossflow}}$ = 8m tip-to-tip	294.1 GWh	40	0.84 MW	42.0%	+1.2%

Table 5.2: The impact of varying each of the consents individually on the annual array yield, the number of turbines, average power per device and capacity factor, using a directional spacing shape. The current consents are Ø = 20m, P_{rated}=2MW, s_{seabed} = 4.5m, s_{LAT} = 8m, $s_{\text{crossflow}}$ = 45m centre-to-centre, and s_{downflow} = 10Ø.

to 26m diameter decreases the array yield drastically (-28.0%), because it is only deep enough to fit 25 out of 40 additional turbines in. This shows that increasing the rotor diameter without also negotiating a decreased rotor clearance has limited benefits past a certain point. The full 40 26m diameter turbines could be fitted in if the seabed clearance is simultaneously decreased to 3m or 2m, and this would result in an annual yield of 333.4GWh (+14.7%) and 340.9GWh (+17.3%).

Increasing the rated power to 3MW results in a trade-off between a higher power generation per turbine, and therefore greater returns on each device, against lower overall annual yield. This is because the 1C expansion is capped at 86MW total capacity, which would only allow for 26 more 3MW turbines, compared to 40 more 2MW turbines. This causes the annual yield to decrease by 21.7% and the number of turbines decreases by 35%, corresponding to an increase in the power per device of 20.5%. If the array expansion size was limited to 40 additional turbines, rather than 80MW additional capacity, then increasing the rated power to 2.5MW would increased the array yield by 9.6% to 318.5GWh, and increasing to 3MW would increased the array yield by 16.2% to 337.6GWh. This would make increasing the turbine rated power the second most beneficial change, after increasing the rotor diameter. However, the total array capacity for MeyGen Phase 1C is likely to be limited to 86MW based on the gird connection capacity.

Changing the seabed clearance had very little impact for 20m diameter turbines. However it would have a much bigger impact for 26m diameter turbine arrays, because it would greatly increase the amount of feasible locations and allow the array to meet the 86MW capacity.

Decreasing the tip-to-tip spacing to 8m increased the annual yield by 1.2%. This is because the closer the turbines are allowed the more turbines fit in the fastest flowing regions of the site. Reducing it further however, to 4m tip-to-tip, had a negligible impact on the annual yield. This preliminary assessment needs to be evaluated with a model which resolves the individual turbine wakes, because there is likely to be a trade-off due to greater wake interference and potential to exploit accelerated bypass flow, neither of which are not demonstrated in this model.

Consent change	Annual Yield	n_t	p.p.d	CF	% diff
Current consents	290.7 GWh	40	0.83 MW	41.5%	–
24m diameter, 2MW rated	334.4 GWh	40	0.95 MW	47.7%	+15.0%
26m diameter, 2MW rated	342.4 GWh	40	0.98 MW	48.9%	+17.8%
24m diameter, 3.5MW rated	249.5 GWh	22	1.29 MW	37.0%	-14.2%
26m diameter, 3.5MW rated	264.2 GWh	22	1.37 MW	39.2%	-9.1%

Table 5.3: The impact of varying the consents from their current values (20m diameter, 2MW rated, 4.5m seabed and 8m LAT, 25m tip-to-tip) to their aspirational values (2m seabed and 8m LAT, 4m tip-to-tip) with various choices of turbine diameter and rated power).

Next the impact of changing all of the consents to their most aspirational values together are presented in Table 5.3. As could be seen with the relationship between increasing the turbine diameter and decreasing the bottom clearance, often array design solutions can be improved by varying the multiple consents in unison. Firstly, when comparing arrays of 2MW rated devices, decreasing the seabed clearance to 2m, and decreasing the tip-to-tip spacing to 4m, allows the installation of up to 40 26m diameter turbines, which is not possible at the current consents. This leads to the greatest annual yield increases of the simulations tested in this study; 15.0% increase for 24m diameter turbines and 17.8% increase for 26m diameter turbines. If the rated power per device is also increased, to 3.5MW, the annual yield decreases (14.2% for 24m diameter turbines and 9.1% for 26m diameter turbines) compared to the array design at the current consents, but the yield decrease is small compared to the substantial reduction in number of turbines that are installed, and the corresponding reduction in costs of the array. The average power generation per device is the highest of all the scenarios observed in this study for 3.5MW turbines (at 1.33MW for 24m diameter turbines and 1.40MW for 26m diameter turbines). If an estimate of the relationship between the costs of the devices and the increased diameter and rated power is known, these yield estimates could be combined with a Levelised Cost of Energy model, to compare the overall economic efficiency of an array with the current consents to an array of fewer but more efficient turbines.

5.6 Conclusions and further work

In summary, a simple method of assessing many different array designs and consents choices has been developed. It makes a number of assumptions, which impact the accuracy of the yield predictions, and does not attempt to provide a globally optimal design. However, it can be used for rapid assessment of a wide range of array design parameters, and can be used to assess the relative importance of each change to these. This tool is useful for the early stages of tidal array design, and is particularly suitable when there are still many unknowns and when available computational resource is too limited to allow for expensive coupled hydrodynamic optimisation. This tool can allow developers to narrow down the choice of options and test a smaller number of array designs with a computationally expensive model, e.g. one that is able to resolve individual turbine wakes.

This new tool is applied to the expansion of the MeyGen array to 86MW installed capacity, and is used to identify the main drivers for improving array yield out of the current consents envelope. Overall increasing the turbine diameter is found to have the biggest impact on increasing the predicted yield, followed by reducing the crossflow spacing. Seabed clearance is found to have very little impact, except for designs with large turbine diameters which cannot fit in much of the site. Increasing the rated power leads to a trade off between lower overall yield but a higher power per device, which needs to be investigated further by combining with a financial model.

A limitation of this study is that it is based on hydrodynamic data from a single ambient flow model run, and therefore does not currently include the impact that turbines will have on the flow themselves (e.g. in terms of both local and global blockage effects). There may be potential uplift obtained through careful placing of turbines in the accelerated flow caused by other turbines, however there are likely to be wake losses once this is sufficiently modelled too. These counteracting effects may be studied in detail by testing a subset of the designs using a more computationally expensive model which can model the individual turbines, such as the currently being tested discrete turbine version of *Thetis*. Therefore these results should be interpreted as a guideline for how varying each aspect of the array design will affect the array yield and not a reliable estimate of array yield. The relative speed of this ambient flow model allows the rapid testing of far more scenarios than a more accurate model which can resolve individual wakes, which is useful for early stage assessment, but needs further validation.

This work performed initial comparisons into the impact the the two exclusion shapes have on the predicted yield. The directional exclusion shape was shown to have a higher yield due to the ability to pack the turbines in closer within the higher flow regions of the site. However, these estimates are based on an ambient flow model that does not account for blockage effects, which would could be significant for these tighter packed array layouts. Future work should investigate the impact of the exclusion zone shape further by coupling the greedy optimisation with an analytical model to approximate the wake effects. The relative yield of different exclusions shapes should be compared again and these results could be validated by testing the optimised layouts in a numerical model that resolved the turbines explicitly.

This work is based on the assumption that all turbines will use a monopile foundation with a 3m footprint diameter that requires the seabed to be under 5° steep. Future work could investigate how different choices of foundation limit the size and structure of the feasible regions for installing turbines, for example by modelling gravity bases as an alternative, increasing the footprint diameter or varying the 5° requirement. This could be used to assess how significant the resultant impact on AEP is due to the reduced set of practical locations.

Chapter 6

Conclusion

6.1 Summary of thesis

This Thesis investigates the optimisation of tidal stream arrays, particularly as the industry moves towards large-scale deployments for the first time. The focus is on using holistic economic modelling to account for the trade-off between increased power and increased costs, and using simplified and efficient models to help reduce the parameter space for optimal array design, before focusing on high fidelity, computationally expensive hydrodynamic models to fine tune array design and validate yield predictions.

Chapter 1 provides a general introduction into the tidal energy industry and its current state. The challenges of moving from relatively small-scale demonstrator arrays to large-scale commercial arrays provides motivation for the development computational models that can aid array design. Chapter 2 reviews the existing literature on the optimisation of tidal array design and the advantages of different types of objective functional, that incorporate various features of the array design into the optimisation. A particular focus on economic functionals, which find an optimal balance in the trade-off between array yield and costs, is made. Different pathways for reducing the costs of tidal stream energy are discussed, including learning by doing, economies of volume that can be attained by moving to arrays which consist of greater numbers of turbines, and economies of scale that can be found by moving to devices with larger rotor diameters or higher rated power. Cost estimates available in the literature are reviewed and collated to provide a typical range of values for use in an LCOE model of tidal arrays, which in turn is suitable for use in the

economic optimisation methods developed this thesis.

Chapter 3 presents the development of a novel economic optimisation method, that uses a set of computationally expensive adjoint optimisation runs to produce an emulator model that produces time-efficient estimates of the economic performance and yield across all possible numbers of turbines. This method can be used to rapidly evaluate the optimal array characteristics using different economic metrics as the functional and over a vast range of economic inputs. This allows for detailed uncertainty analysis to be applied such as using the Monte-Carlo method to find a P90, P50 and P10 percentile estimates of the yield and cost. This can reduce the number of times a computationally expensive optimisation loop with coupled hydrodynamics needs to be run in order to find an array design that is robust. Chapter 4 demonstrated the application of this new method to the real-world tidal site of the Alderney Race. It demonstrates the potential to feasibly extract between 1 and 2 GW at this powerful tidal site, in line with the current plans of the Normandie Hydrolienne project. It estimates that an initial commercial scale deployment of 80 MW could achieve an LCOE of £110/MWh, which aligns closely with the level of subsidy considered for tidal stream projects in the Alderney Race in the past [192, 149, 190].

In Chapter 5 a method was developed to assess the relative yield gains that can be achieved by changing a variety of array design parameters such as rotor diameter, turbine rated power, spacing between turbines and clearance above and below turbines. This work was carried out in collaboration with SIMEC Atlantis and applied to a case study of the expansion of the MeyGen array from 6MW currently deployed to 86MW planned. A greedy-based optimisation algorithm is developed to obtain an array layout and yield estimate, while adhering to practical constraints imposed by the depth and the steepness of the seabed, and legal constraints that depend on the consents negotiated with a licensing organisation. The potential yield gains that can be achieved through negotiating changes to the consents is investigated, with the most notable improvements being found by increasing the turbine diameter and, for diameters of over 24m, decreasing bottom clearance requirements to increase the number of viable locations. This method makes a number of simplifying assumptions, and the impact of this on the validity of the yield estimates needs to be investigated through comparison to hydrodynamic models of the array designs produced. However, it is useful at the early stages of tidal stream array design, where the design parameter space needs to be reduced before more complex models can be applied.

This work has shown that substantial cost reductions can come from optimised array design, rather than significant technological advances. While many designs were presented in Chapter 1, often intelligent deployment of existing technologies can lead to substantial advances. The different cost reduction pathways were outlined in Chapter 2, and the following chapters present computational methods that can be used by developers to guide array design and actualise those cost reductions. Both Chapters 3 and 4 demonstrate how economies of volume can be best exploited to reduce the cost of tidal energy. The method developed in Chapter 5 can be used to assess how economies of turbine scale can be best exploited to increase the array yield and reduce the cost of energy, while taking account of the practical constraints at a real tidal site.

6.2 Future Work

The limitations of the results and the possible avenues for future work are discussed in their relevant chapters. The key points of which are summarised below.

6.2.1 Improved model calibration and validation

The hydrodynamic models of the Alderney Race and Pentland Firth, presented in Chapters 4 and 5, were limited based on available computational resource as well as limited access to ADCP data to calibrate the model with. The computational resource limits the resolution that the model can be run at, whereas a developer applying these methods to design a real world array may be able to expend more time and computational power to produce a more accurate tidal model. Furthermore there are limits to the amount of ADCP data and even the detail of the bathymetry that is academically available. This reduces the amount of data that can be used to successfully calibrate the model. In practice tidal developers will take many measurements and readings from their sites when they lease them, so real-world applications of the methods developed in this thesis have potential for improved model accuracy.

6.2.2 Accounting for local and global blockage

Modelling tidal stream arrays is a highly multi-scale problem, with each of the length-scales coupled to its adjacent scales, making modelling complex and computationally expensive. Simplifying assumptions, such as applying the shallow water equations to solve a 2-dimensional approximation to the flow, are often employed. All three of Chapters 3, 4 and 5 use depth-averaged models to reduce the computational expense. Further simplifications in the way the turbines are represented help to reduce the computational expense, but at the cost of mis-representing certain blockage effects.

Chapters 3, 4 used a continuous turbine density function to represent the arrays of turbines. The approach is used as a cheaper alternative to methods that resolve each turbine individually, for example, modelling turbines via a bump function that locally increases bed friction[81] or as a porous disc [196], each with the same diameter as the turbine. This continuous density method was first developed by Funke et al. [82] to reduce the mesh resolution needed to resolve a tidal array and remove the need for an expensive nested optimisation approach when optimising the number of turbines as well as their layout. This approach accounts for the effects of global blockage, and reflects the diminishing returns as more turbines are added to a channel and the flow is diverted around the array due to the increased friction. But it does not account for local blockage and only produces an optimal array shape through the density function, rather than an explicit layout of locations of each individual turbine, which can be optimised to minimise wake effects and exploit accelerated by-pass flows caused by local blockage where possible. The emulator method developed in this thesis allows the number of turbines to be optimised using information from only a small number of adjoint optimisation runs. This emulator could be used to replace the expensive outer loop needed to optimise the number of discretely modelled turbines, as well as their location. Further work could combine this emulator method with the discrete adjoint optimisation of tidal arrays shown in [81], to produce relatively computationally efficient optimal array designs that account for both global and local blockage and optimise economic metrics of choice, such as LCOE.

Chapter 5 simplifies the modelling even further by basing yield estimates on a model of the ambient flow at a tidal site, and assuming that the exclusion zones applied to satisfy spacing requirements between turbines are sufficient to avoid negative local blockage or wake effects. Validation needs to be carried out to assess whether

the wake has sufficiently regenerated outside of the downstream exclusion zones for the assumption to holds true. This method does not currently account for the potential gains that can be found from exploiting the accelerated bypass flow around upstream rows of turbines through using staggered layouts, although the shape of the exclusion zones often forces the array design into an approximately staggered layout. It also does not account for the increasing detrimental effects of global blockage as increasingly large-scale arrays are deployed. Future work is currently investigating whether analytical wake models, such as an adaption of the Jensen wake model often used in wind turbine array design [197], can be incorporated into this method to account for local blockage effects. This analysis could be further developed by investigating whether an analytical penalty for increasing the array size and therefore the global blockage can also be applied.

6.2.3 Variable electricity tariff

The LCOE model used in Chapters 3 and 4 assumes a fixed electricity tariff for simplicity and to reflect the setup of the currently most likely funding scenario; Contracts for Difference. If different forms of subsidy become more likely this could easily be changed such that the tariff, T_e is a function of time. Mackie et al [198] investigated the ability to optimise tidal lagoon operation with respect to a time varying price signal, this could be expanded upon to optimise tidal stream array design when subject to a spot price rather than a fixed one.

6.3 Hierarchy of array design approaches

Section 6.2 outlines some of the limitations of the approaches used in this thesis and potential paths to improve them. But it is important to note that these methods can be useful for developers even with the limitations to their accuracy, provided they are used as part of a wider array design context, and supported by complimentary models and methods. This thesis does not attempt to provide design methods that holistically optimise all aspects of tidal array design to a high level of fidelity, but instead to provide methods that fit within a hierarchy of models, where each method within the hierarchy can be used to narrow down the scope of array design options to allow for a higher fidelity modelling of a smaller set of options at the next stage.

In the earliest stages of array design, regional scale models and global maps of

average current velocities can be used to identify regions in the world with sufficient depths and powerful enough flow for tidal stream energy extraction. Developers can then identify ideal sites in the region to lease for a tidal plot by using spatial methods that assess the trade off between spatially and temporally varying energy potential and the spatially varying capital costs (which increase with depth and distance to shore), such as [99, 122]. These methods can use depth-averaged ambient flow models and spatially varying cost estimates to identify the best sites to install tidal stream arrays and help developers find an appropriate site boundary to lease for a deployment.

Once the tidal plot is identified the developer has a wide range of choices from type of device to install, where to install it and at what spacing. To narrow these options down, the consents varying method developed in Chapter 5 can be used choose a turbine specification that is suitable for the flow characteristics at the site and the physical constraints. This tool can be used to compare the changes to the yield prediction for different design choices and therefore narrow the scope, but is based on an ambient flow model, so yield predictions may not be reflective of the true array potential and suggested array layouts are only first iterations.

The economic optimisation approach developed in Chapters 3 and 4 can be used to estimate the LCOE and the optimal number of turbines, taking into account the balance of energy generation against array costs, along with global blockage effects. However, at this stage the flow model is still depth-averaged and the turbines are represented by a spatially varying turbine density field. This approach requires the turbine power curve (which depends on the rotor diameter and rated power) to be specified already, because varying these along with the number of turbines and the layout would be too computationally expensive to solve. The continuous turbine approach in a shallow water model can be applied at single or multi-farm scales, for example earlier work by Goss et al. used this approach in *Thetis* to assess the impact that adjacent tidal arrays within the Alderney Race would have on each other [57]. The outputs of this stage are an optimal number of turbines and an array layout design in terms of the spatially varying density. This can be used to create a discrete set of turbine locations for use as an initial layout to reduce the number of iterations required in an adjoint optimisation of the discrete array layout. Such optimisations include the shallow water discrete layout optimisation, where turbines are represented as local friction bumps, presented in [81].

Finally, when a discrete optimisation provides a set of turbine locations and specifications, full three-dimensional models can be used to improve the array yield

estimates and model the operation of the turbines and the loading experience by them. These models are very computationally expensive, so only a limited set of array designs can realistically be tested. Ideally the array design is optimised through the early stages of the array design hierarchy and these models are only used to validate the final array design and not to optimise it. Within three-dimensional models there are a range of different fidelity representations of the tidal turbines than can be used, from a porous disc that can be used for power predictions, to a fully resolved rotating hub, blades and support structure, that requires a much higher resolution computational mesh, but can be used to predict the temporally varying forces experienced by the turbines, and model the turbulent wakes behind them.

Appendix A

Permissions table

Page No.	Name	Image reproduced with permission of the Copyright holder	Permission granted on
5	Figure 1.1	Aqua-RET, aquatt@aquatt.ie	12/05/2021
7	Figure 1.2	Aqua-RET, aquatt@aquatt.ie	12/05/2021
11	Figure 1.3	SIMEC Atlantis Energy, ir@simecatlantis.com	25/05/2021
12	Figure 1.4	SIMEC Atlantis Energy, ir@simecatlantis.com	25/05/2021
15	Figure 1.5a	SIMEC Atlantis Energy, ir@simecatlantis.com	25/05/2021
15	Figure 1.5b	Aqua-RET, aquatt@aquatt.ie	12/05/2021
15	Figure 1.5c	Aqua-RET, aquatt@aquatt.ie	12/05/2021
15	Figure 1.5d	Image reproduced with permission of the rights holder, Aqua-RET, aquatt@aquatt.ie	12/05/2021
16	Figure 1.6a	Ortbital Marine Power, webenquiries@orbitalmarine.com	27/05/2021
16	Figure 1.6b	Sustainable Marine, info@sustainablemarine.com	07/06/2021
56	Figure 2.2	Leask Marine Ltd, info@leaskmarine.com	06/05/2021
160	Figure 5.3	SIMEC Atlantis Energy, ir@simecatlantis.com	24/06/2021

Table A.1: Permissions table

Bibliography

[1] S. Draper, *Tidal Stream Energy Extraction in Coastal Basins*. PhD thesis, St Catherine's College, Oxford, 2011.

[2] P. Higgins and A. Foley, "The evolution of offshore wind power in the united kingdom," *Renewable and Sustainable Energy Reviews*, vol. 37, pp. 599–612, 9 2014.

[3] Z. L. Goss, S. C. Kramer, A. Avdis, C. J. Cotter, and M. D. Piggott, "Variations in the optimal design of a tidal stream turbine array with costs," in *Oxford Tidal Energy Workshop*, (Oxford), pp. 33–34, 2019.

[4] Z. L. Goss, S. C. Kramer, A. Avdis, C. J. Cotter, and M. D. Piggott, "Economic optimisation of large scale tidal stream turbine arrays," in *13th European Wave and Tidal Energy Conference*, (Naples), pp. 1598–1598, 2019.

[5] A. Pérez-Ortiz, A. G. Borthwick, J. McNaughton, H. C. Smith, and Q. Xiao, "Resource characterization of sites in the vicinity of an island near a landmass," *Renewable Energy*, vol. 103, pp. 265–276, 4 2017.

[6] N. O. Centre, "Harmonic constituents at several gauge locations." Personal Communication with J. Eric Jones., 2011.

[7] Edina Digimap Service, "Hydrospatial one, gridded bathymetry." `http://digimap.edina.ac.uk/marine/`, 2014. , SeaZone Solutions Ltd, Online; accessed 2017.

[8] D. C. Kapoor, "General bathymetric chart of the oceans (GEBCO)," *Marine Geodesy*, vol. 5, no. 1, pp. 73–80, 1981.

[9] M. Hamilton, "Technology Update," tech. rep., Scotrenewables Tidal Power Ltd, 2012.

[10] Ernst & Young, "Cost of and financial support for wave, tidal stream and tidal range generation in the UK," tech. rep., 2010.

[11] Ocean Energy Systems, "International LCOE for Ocean Energy Technology," tech. rep., 2015.

[12] G. Smart and M. Noonan, "Tidal stream and wave energy cost reduction and industrial benefit," *Offshore Renewable Energy Catapult*, 2018.

[13] G. T. Pecl, M. B. Araújo, J. D. Bell, J. Blanchard, T. C. Bonebrake, I. C. Chen, T. D. Clark, R. K. Colwell, F. Danielsen, B. Evengård, L. Falconi, S. Ferrier, S. Frusher, R. A. Garcia, R. B. Griffis, A. J. Hobday, C. Janion-Scheepers, M. A. Jarzyna, S. Jennings, J. Lenoir, H. I. Linnetved, V. Y. Martin, P. C. McCormack, J. McDonald, N. J. Mitchell, T. Mustonen, J. M. Pandolfi, N. Pettorelli, E. Popova, S. A. Robinson, B. R. Scheffers, J. D. Shaw, C. J. Sorte, J. M. Strugnell, J. M. Sunday, M. N. Tuanmu, A. Vergés, C. Villanueva, T. Wernberg, E. Wapstra, and S. E. Williams, "Biodiversity redistribution under climate change: Impacts on ecosystems and human well-being," *Science*, vol. 355, 3 2017.

[14] Department of Energy & Climate Change, "The Carbon Plan: Delivering our low carbon future," tech. rep., 2011.

[15] H. Ritchie, "Electricity Mix - Our World in Data." `https://ourworldindata.org/electricity-mix`, 2021.

[16] M. Rubio-Varas and B. Muñoz-Delgado, "Long-term diversification paths and energy transitions in Europe," *Ecological Economics*, vol. 163, pp. 158–168, 9 2019.

[17] A. Stirling, "Multicriteria diversity analysis. A novel heuristic framework for appraising energy portfolios," *Energy Policy*, vol. 38, pp. 1622–1634, 4 2010.

[18] Black & Veatch, "UK Tidal Current Resource & Economics," *Carbon Trust*, 2011.

[19] M. J. Hannon, J. Griffiths, A. Vantoch-Wood, M. Carcas, S. Bradley, R. Boud, and S. Wyatt, "World Energy Resources, Marine Energy," *World Energy Council*, 2016.

[20] UK Gov., "Wave and tidal energy: part of the UK's energy mix," 2013.

[21] The Crown estate, "UK Wave and Tidal Key Resource Areas Project," 2013.

[22] P. Gleizon, F. Campuzano, P. Carracedo, A. Martinez, J. Goggins, R. Atan, and S. Nash, "Wave energy resources along the European Atlantic Coast," in *Marine Renewable Energy: Resource Characterization and Physical Effects*, pp. 37–69, Springer International Publishing, 5 2017.

[23] S. P. Neill, A. Angeloudis, P. E. Robins, I. Walkington, S. L. Ward, I. Masters, M. J. Lewis, M. Piano, A. Avdis, M. D. Piggott, G. Aggidis, P. Evans, T. A. Adcock, A. Židonis, R. Ahmadian, and R. Falconer, "Tidal range energy resource and optimization – Past perspectives and future challenges," *Renewable Energy*, vol. 127, pp. 763–778, 11 2018.

[24] A. Angeloudis, N. Hawkins, S. Kramer, and M. Piggott, "Comparison of twin-basin lagoon systems against conventional tidal power plant designs," in *Advances in Renewable Energies Offshore - Proceedings of the 3rd International Conference on Renewable Energies Offshore*, pp. 159–168, CRC Press/Balkema, 2018.

[25] A. Angeloudis, S. C. Kramer, A. Avdis, and M. D. Piggott, "Optimising tidal range power plant operation," *Applied Energy*, vol. 212, pp. 680–690, 2 2018.

[26] J. Xia, R. A. Falconer, and B. Lin, "Impact of different tidal renewable energy projects on the hydrodynamic processes in the Severn Estuary, UK," *Ocean Modelling*, vol. 32, pp. 86–104, 1 2010.

[27] C. Retiere, "Tidal power and the aquatic environment of La Rance," *Biological Journal of the Linnean Society*, vol. 51, pp. 25–36, 1 1994.

[28] C. Hendry, "The role of tidal lagoons," tech. rep., 12 2016.

[29] F. O. Rourke, F. Boyle, and A. Reynolds, "Tidal energy update 2009," *Applied Energy*, vol. 87, pp. 398–409, 2 2010.

[30] N. Hopley, "Innovation in Tidal Energy - The Subsea Hub," *SIMEC Atlantis Energy*, 11 2020.

[31] C. M. Johnstone, D. Pratt, J. A. Clarke, and A. D. Grant, "A techno-economic analysis of tidal energy technology," *Renewable Energy*, vol. 49, pp. 101–106, 1 2013.

[32] S. Draper, T. A. Adcock, A. G. Borthwick, and G. T. Houlsby, "Estimate of the tidal stream power resource of the Pentland Firth," *Renewable Energy*, vol. 63, pp. 650–657, 3 2014.

[33] R. Vennell, S. W. Funke, S. Draper, C. Stevens, and T. Divett, "Designing large arrays of tidal turbines: A synthesis and review," *Renewable and Sustainable Energy Reviews*, vol. 41, pp. 454–472, 2015.

[34] D. S. Coles, L. S. Blunden, and A. S. Bahaj, "Assessment of the energy extraction potential at tidal sites around the Channel Islands," *Energy*, vol. 124, pp. 171–186, 2017.

[35] M. Piano, S. P. Neill, M. J. Lewis, P. E. Robins, M. R. Hashemi, A. G. Davies, S. L. Ward, and M. J. Roberts, "Tidal stream resource assessment uncertainty due to flow asymmetry and turbine yaw misalignment," *Renewable Energy*, vol. 114, pp. 1363–1375, 12 2017.

[36] M. Lewis, S. P. Neill, P. E. Robins, and M. R. Hashemi, "Resource assessment for future generations of tidal-stream energy arrays," *Energy*, vol. 83, pp. 403–415, 4 2015.

[37] R. A. Walters, M. R. Tarbotton, and C. E. Hiles, "Estimation of tidal power potential," *Renewable Energy*, 2013.

[38] G. Sutherland, M. Foreman, and C. Garrett, "Tidal current energy assessment for Johnstone Strait, Vancouver Island," *Proceedings of the Institution of Mechanical Engineers, Part A: Journal of Power and Energy*, vol. 221, pp. 147–157, 3 2007.

[39] J. Blanchfield, C. Garrett, A. Rowe, and P. Wild, "Tidal stream power resource assessment for Masset Sound, Haida Gwaii," *Proceedings of the Institution of Mechanical Engineers, Part A: Journal of Power and Energy*, vol. 222, pp. 485–492, 8 2008.

[40] R. Campbell, A. Martinez, C. Letetrel, and A. Rio, "Methodology for estimating the French tidal current energy resource," *International Journal of Marine Energy*, vol. 19, pp. 256–271, 9 2017.

[41] J. Zheng, P. Dai, and J. Zhang, "Tidal stream energy in China," in *Procedia Engineering*, vol. 116, pp. 880–887, Elsevier Ltd, 1 2015.

[42] R. Collombet, "Ocean Energy Key trends and statistics 2020," tech. rep., Ocean Energy Europe, 2 2021.

[43] R. Collombet, A. Parsons, and R. Gruet, "Ocean Energy Key trends and statistics 2018," tech. rep., Ocean Energy Europe, 2019.

[44] R. Collombet, A. Parsons, and R. Gruet, "Ocean Energy: Key trends and statistics 2019," tech. rep., Ocean Energy Europe, 2020.

[45] C. A. Douglas, G. P. Harrison, and J. P. Chick, "Life cycle assessment of the Seagen marine current turbine," *Proceedings of the Institution of Mechanical Engineers Part M: Journal of Engineering for the Maritime Environment*, vol. 222, pp. 1–12, 2 2008.

[46] T. Stallard, R. Collings, T. Feng, and J. Whelan, "Interactions between tidal turbine wakes: experimental study of a group of three-bladed rotors," *Phil. Trans. R. Soc. A.*, vol. 371, no. 20120159, 2013.

[47] S. Waldman, S. Yamaguchi, R. O'Hara Murray, and D. Woolf, "Tidal resource and interactions between multiple channels in the Goto Islands, Japan," *International Journal of Marine Energy*, vol. 19, pp. 332–344, 9 2017.

[48] Low Carbon Innovation Coordination Group, "Technology Innovation Needs Assessment (TINA) Marine Energy Summary Report," tech. rep., 2012.

[49] D. S. Coles and T. Walsh, "Mechanisms for reducing the cost of tidal stream energy," in *13th European Wave and Tidal Energy Conference*, (Naples), pp. 1836–1, 2019.

[50] P. J. Schubel and R. J. Crossley, "Wind turbine blade design," *Energies*, vol. 5, pp. 3425–3449, 9 2012.

[51] R. W. Thresher and D. M. Dodge, "Trends in the Evolution of Wind Turbine Generator Configurations and Systems," *Wind Energy*, vol. 1, pp. 70–85, 1998.

[52] D. S. Coles, "MeyGen update," in *Supergen Annual Assembly*, (Glasgow), 11 2019.

[53] G. Cornelis Van Kooten, "Wind power: the economic impact of intermittency," *Lett Spat Resour Sci*, vol. 3, pp. 1–17, 2010.

[54] E. Denny, "The economics of tidal energy," *Energy Policy*, vol. 37, pp. 1914–1924, 5 2009.

[55] P. Coker, J. Barlow, T. Cockerill, and D. Shipworth, "Measuring significant variability characteristics: An assessment of three UK renewables," *Renewable Energy*, vol. 53, pp. 111–120, 5 2013.

[56] L. Hirth, "The market value of variable renewables. The effect of solar wind power variability on their relative price," *Energy Economics*, vol. 38, pp. 218–236, 7 2013.

[57] Z. L. Goss, M. D. Piggott, S. C. Kramer, A. Avdis, A. Angeloudis, and C. J. Cotter, "Competition effects between nearby tidal turbine arrays-optimal design for Alderney Race," in *3rd International Conference on Renewable Energies Offshore*, (Lisbon), pp. 255–262, 2018.

[58] J. A. Clarke, G. Connor, A. D. Grant, and C. M. Johnstone, "Regulating the output characteristics of tidal current power stations to facilitate better base load matching over the lunar cycle," in *Renewable Energy*, vol. 31, pp. 173–180, Pergamon, 2 2006.

[59] I. G. Bryden and D. M. Macfarlane, "The utilisation of short term energy storage with tidal current generation systems," *Energy*, vol. 25, pp. 893–907, 9 2000.

[60] E. Barbour and I. G. Bryden, "Energy storage in association with tidal current generation systems," in *Proceedings of the Institution of Mechanical Engineers, Part A: Journal of Power and Energy*, vol. 225, pp. 443–455, SAGE PublicationsSage UK: London, England, 6 2011.

[61] S. Manchester, B. Barzegar, L. Swan, and D. Groulx, "Energy storage requirements for in-stream tidal generation on a limited capacity electricity grid," *Energy*, vol. 61, pp. 283–290, 11 2013.

[62] D. S. Coles, A. Angeloudis, Z. L. Goss, and J. R. Miles, "Tidal Stream vs. Wind Energy: The Value of Cyclic Power When Combined with Short-Term Storage in Hybrid Systems," *Energies*, vol. 14, p. 1106, 2 2021.

[63] S. P. Neill, M. R. Hashemi, and M. J. Lewis, "Optimal phasing of the European tidal stream resource using the greedy algorithm with penalty function," *Energy*, vol. 73, pp. 997–1006, 8 2014.

[64] P. L. Fraenkel, "Power from marine currents," *Proceedings of the Institution of Mechanical Engineers, Part A: Journal of Power and Energy*, vol. 216, pp. 1–14, 12 2002.

[65] R. Vennell and T. A. Adcock, "Energy storage inherent in large tidal turbine farms," *Proceedings of the Royal Society A: Mathematical, Physical and Engineering Sciences*, vol. 470, 6 2014.

[66] R. Vennell, "Exceeding the Betz limit with tidal turbines," *Renewable Energy*, vol. 55, pp. 277–285, 7 2013.

[67] Black & Veatch, "Lessons Learnt from MeyGen Phase 1A: Final Summary Report," 2020.

[68] T. A. Adcock, S. Draper, and T. Nishino, "Tidal power generation - A review of hydrodynamic modelling," in *Proceedings of the Institution of Mechanical Engineers, Part A: Journal of Power and Energy*, vol. 229, pp. 755–771, SAGE Publications Ltd, 11 2015.

[69] M. A. Shields, D. K. Woolf, E. P. Grist, S. A. Kerr, A. C. Jackson, R. E. Harris, M. C. Bell, R. Beharie, A. Want, E. Osalusi, S. W. Gibb, and J. Side, "Marine renewable energy: The ecological implications of altering the hydrodynamics of the marine environment," 1 2011.

[70] R. Ahmadian and R. A. Falconer, "Assessment of array shape of tidal stream turbines on hydro-environmental impacts and power output," *Renewable Energy*, vol. 44, pp. 318–327, 8 2012.

[71] K. Nelson, S. C. James, J. D. Roberts, and C. Jones, "A framework for determining improved placement of current energy converters subject to environmental constraints," *International Journal of Sustainable Energy*, pp. 1–15, 6 2017.

[72] R. du Feu, M. Piggott, and B. Halpern, *Advanced computational modelling of large-scale tidal energy systems: optimising the trade-off between environmental impacts and power generation*. PhD thesis, 2019.

[73] R. Mazumder and M. Arima, "Tidal rhythmites and their implications," *Earth-Science Reviews*, vol. 69, pp. 79–95, 2 2005.

[74] M. Grabbe, E. Lalander, S. Lundin, and M. Leijon, "A review of the tidal current energy resource in Norway," *Renewable and Sustainable Energy Reviews*, vol. 13, pp. 1898–1909, 10 2009.

[75] G. D. Egbert, S. Y. Erofeeva, and R. D. Ray, "Assimilation of altimetry data for nonlinear shallow-water tides: Quarter-diurnal tides of the Northwest European Shelf," *Continental Shelf Research*, vol. 30, pp. 668–679, 4 2010.

[76] A. S. Bahaj, A. F. Molland, J. R. Chaplin, and W. M. J. Batten, "Power and thrust measurements of marine current turbines under various hydrodynamic

flow conditions in a cavitation tunnel and a towing tank," *Renewable Energy*, vol. 32, pp. 407–426, 3 2007.

[77] A. Bahaj, L. Myers, and G. Thompson, "Characterising the wake of horizontal axis marine current turbines," *Seventh European Wave and Tidal Energy Conference*, 2007.

[78] J. Connell and R. George, "Wake of the MOD-0A1 wind turbine at two rotor diameters downwind on December 3, 1981," tech. rep., Pacific Northwest National Laboratory (PNNL), Richland, WA (United States), 11 1982.

[79] M. D. Piggott, G. J. Gorman, C. C. Pain, P. A. Allison, A. S. Candy, B. T. Martin, and M. R. Wells, "A new computational framework for multi-scale ocean modelling based on adapting unstructured meshes," in *International Journal for Numerical Methods in Fluids*, vol. 56, pp. 1003–1015, John Wiley & Sons, Ltd, 3 2008.

[80] M. A. Abolghasemi, M. D. Piggott, J. Spinneken, A. Viré, C. J. Cotter, and S. Crammond, "Simulating tidal turbines with multi-scale mesh optimisation techniques," *Journal of Fluids and Structures*, vol. 66, pp. 69–90, 10 2016.

[81] S. W. Funke, P. E. Farrell, and M. D. Piggott, "Tidal turbine array optimisation using the adjoint approach," *Renewable Energy*, vol. 63, pp. 658–673, 3 2014.

[82] S. W. Funke, S. C. Kramer, and M. D. Piggott, "Design optimisation and resource assessment for tidal-stream renewable energy farms using a new continuous turbine approach," *Renewable Energy*, vol. 99, pp. 1046–1061, 2016.

[83] T. Divett, R. Vennell, and C. Stevens, "Optimization of multiple turbine arrays in a channel with tidally reversing flow by numerical modelling with adaptive mesh," *Philosophical Transactions of the Royal Society A: Mathematical, Physical and Engineering Sciences*, vol. 371, p. 20120251, 2 2013.

[84] R. Martin-Short, J. Hill, S. C. Kramer, A. Avdis, P. A. Allison, and M. D. Piggott, "Tidal resource extraction in the Pentland Firth, UK: Potential impacts on flow regime and sediment transport in the Inner Sound of Stroma," *Renewable Energy*, vol. 76, pp. 596–607, 4 2015.

[85] G. Vallis, *Atmospheric and Oceanic Fluid Dynamics*. Cambridge University Press, 1 2006.

[86] I. G. Bryden, T. Grinsted, and G. T. Melville, "Assessing the potential of a simple tidal channel to deliver useful energy," *Applied Ocean Research*, vol. 26, pp. 198–204, 7 2004.

[87] T. Nishino and R. H. Willden, "The efficiency of an array of tidal turbines partially blocking a wide channel," *Journal of Fluid Mechanics*, vol. 708, pp. 596–606, 10 2012.

[88] S. R. Turnock, A. B. Phillips, J. Banks, and R. Nicholls-Lee, "Modelling tidal current turbine wakes using a coupled RANS-BEMT approach as a tool for analysing power capture of arrays of turbines," *Ocean Engineering*, vol. 38, pp. 1300–1307, 8 2011.

[89] S. Draper and T. Nishino, "Centred and staggered arrangements of tidal turbines," *Journal of Fluid Mechanics*, vol. 739, pp. 72–93, 2014.

[90] C. Garrett and P. Cummins, "The efficiency of a turbine in a tidal channel," *Journal of Fluid Mechanics*, vol. 588, pp. 243–251, 10 2007.

[91] D. S. Coles, L. S. Blunden, and A. S. Bahaj, "The energy yield potential of a large tidal stream turbine array in the Alderney Race: Energy yield estimate for Alderney Race," *Philosophical Transactions of the Royal Society A: Mathematical, Physical and Engineering Sciences*, vol. 378, 8 2020.

[92] A. Segalini and J.-Å. Dahlberg, "Global Blockage Effects in Wind Farms," *J. Phys*, 2019.

[93] J. Schneemann, F. Theuer, A. Rott, M. Dörenkämper, and M. Kühn, "Offshore wind farm global blockage measured with scanning lidar," *Wind Energ. Sci*, vol. 6, pp. 521–538, 2021.

[94] A. S. Bahaj, L. E. Myers, R. I. Rawlinson-Smith, and M. Thomson, "The effect of boundary proximity upon the wake structure of horizontal axis marine current turbines," *Journal of Offshore Mechanics and Arctic Engineering*, vol. 134, 12 2011.

[95] D. M. Culley, S. W. Funke, S. C. Kramer, and M. D. Piggott, "A surrogate-model assisted approach for optimising the size of tidal turbine arrays," *International Journal of Marine Energy*, vol. 19, pp. 357–373, 9 2017.

[96] J. Schluntz and R. H. Willden, "The effect of blockage on tidal turbine rotor design and performance," *Renewable Energy*, vol. 81, pp. 432–441, 9 2015.

[97] R. Vennell, "Realizing the potential of tidal currents and the efficiency of turbine farms in a channel," *Renewable Energy*, vol. 47, pp. 95–102, 11 2012.

[98] MeyGen, "Lessons Learnt from MeyGen Phase 1A Part 2/3: Construction Phase," 2018.

[99] A. Vazquez and G. Iglesias, "Capital costs in tidal stream energy projects – A spatial approach," *Energy*, vol. 107, pp. 215–226, 7 2016.

[100] P. Sullivan and P. McCombie, "Optimisation of tidal power arrays using a genetic algorithm," *Proceedings of the Institution of Civil Engineers - Energy*, vol. 166, pp. 19–28, 2 2013.

[101] J. Xue, R. Ahmadian, and O. Jones, "Genetic Algorithm in Tidal Range Schemes' Optimisation," *Energy*, vol. 200, p. 117496, 6 2020.

[102] H. S. Huang, "Distributed genetic algorithm for optimization of wind farm annual profits," in *2007 International Conference on Intelligent Systems Applications to Power Systems, ISAP*, 2007.

[103] M. Bilbao and E. Alba, "Simulated annealing for optimization of wind farm annual profit," in *2009 2nd International Symposium on Logistics and Industrial Informatics, LINDI 2009*, 2009.

[104] R. J. du Feu, S. W. Funke, S. C. Kramer, J. Hill, and M. D. Piggott, "The trade-off between tidal-turbine array yield and environmental impact: A habitat suitability modelling approach," *Renewable Energy*, vol. 143, pp. 390–403, 12 2019.

[105] D. M. Culley, S. W. Funke, S. C. Kramer, and M. D. Piggott, "Integration of cost modelling within the micro-siting design optimisation of tidal turbine arrays," *Renewable Energy*, vol. 85, pp. 215–227, 2016.

[106] Z. Goss, D. Coles, and M. Piggott, "Economic analysis of tidal stream turbine arrays: a review," 5 2021.

[107] Z. Goss, D. Coles, S. Kramer, and M. Piggott, "Efficient economic optimisation of large-scale tidal stream arrays," *Applied Energy*, vol. 295, p. 116975, 8 2021.

[108] Z. L. Goss, D. S. Coles, and M. D. Piggott, "Identifying economically viable tidal sites within the Alderney Race through optimization of levelized cost of energy," *Philosophical Transactions of the Royal Society A: Mathematical, Physical and Engineering Sciences*, vol. 378, p. 20190500, 8 2020.

[109] Z. L. Goss, M. D. Piggott, and S. C. Kramer, "An English Channel Model for the Optimisation of Tidal Turbines in the Alderney Race," in *Oxford Tidal Energy Workshop*, (Oxford), pp. 10–11, 2018.

[110] Z. L. Goss, S. C. Warder, A. Angeloudis, S. C. Kramer, A. Avdis, and M. D. Piggott, "Tidal modelling with Thetis: preliminary English Channel benchmarking," tech. rep., Imperial College, 2019.

[111] UK Gov., "Contracts for Difference Allocation Round 3 Results," tech. rep., 2019.

[112] R. J. du Feu, S. W. Funke, S. C. Kramer, D. M. Culley, J. Hill, B. S. Halpern, and M. D. Piggott, "The trade-off between tidal-turbine array yield and impact on flow: A multi-objective optimisation problem," *Renewable Energy*, vol. 114, pp. 1247–1257, 12 2017.

[113] D. M. Culley, S. Funke, M. Piggott, and A. Peter, *The modelling and design optimisation of tidal stream turbine arrays*. PhD thesis, Imperial College London, 2016.

[114] A. S. Iyer, S. J. Couch, G. P. Harrison, and A. R. Wallace, "Variability and phasing of tidal current energy around the United Kingdom," *Renewable Energy*, vol. 51, pp. 343–357, 3 2013.

[115] J. Thiébot, S. Guillou, and E. Droniou, "Influence of the 18.6-year lunar nodal cycle on the tidal resource of the Alderney Race, France," *Applied Ocean Research*, vol. 97, p. 102107, 4 2020.

[116] I. D. Haigh, M. Eliot, and C. Pattiaratchi, "Global influences of the 18.61 year nodal cycle and 8.85 year cycle of lunar perigee on high tidal levels," *Journal of Geophysical Research: Oceans*, vol. 116, 6 2011.

[117] S. Song, W. Shi, Y. K. Demirel, and M. Atlar, "The effect of biofouling on the tidal turbine performance," *Applied Energy Symposium: MIT A+B*, 2019.

[118] S. Faulstich, B. Hahn, and P. J. Tavner, "Wind turbine downtime and its importance for offshore deployment," *Wind Energy*, vol. 14, pp. 327–337, 4 2011.

[119] L. Ziegler, E. Gonzalez, T. Rubert, U. Smolka, and J. J. Melero, "Lifetime extension of onshore wind turbines: A review covering Germany, Spain, Denmark, and the UK," *Renewable and Sustainable Energy Reviews*, vol. 82, pp. 1261–1271, 2 2018.

[120] N. Lewis, T. Eschenbach, and J. Hartman, "Real Options And The Use Of Discrete And Continuous Interest Rates," *American Society for Engineering Education*, no. 2009 Annual Conference & Exposition, pp. 1–14, 2009.

[121] A. Vazquez and G. Iglesias, "Device interactions in reducing the cost of tidal stream energy," *Energy Conversion and Management*, vol. 97, pp. 428–438, 6 2015.

[122] A. Vazquez and G. Iglesias, "LCOE (levelised cost of energy) mapping: A new geospatial tool for tidal stream energy," *Energy*, vol. 91, pp. 192–201, 11 2015.

[123] X. Ouyang and B. Lin, "Levelized cost of electricity (LCOE) of renewable energies and required subsidies in China," *Energy Policy*, vol. 70, pp. 64–73, 7 2014.

[124] Marine Scotland, "Review of Approaches and Cost of Decommissioning Small Scale Offshore Renewable Energy Developments," tech. rep., 2018.

[125] B. S. Halpern, S. Walbridge, K. A. Selkoe, C. V. Kappel, F. Micheli, C. D'Agrosa, J. F. Bruno, K. S. Casey, C. Ebert, H. E. Fox, R. Fujita, D. Heinemann, H. S. Lenihan, E. M. Madin, M. T. Perry, E. R. Selig, M. Spalding, R. Steneck, and R. Watson, "A global map of human impact on marine ecosystems," *Science*, vol. 319, pp. 948–952, 2 2008.

[126] J. E. Eckman, C. H. Peterson, and J. A. Cahalan, "Effects of flow speed, turbulence, and orientation on growth of juvenile bay scallops Argopecten irradians concentricus (Say)," *Journal of Experimental Marine Biology and Ecology*, vol. 132, pp. 123–140, 11 1989.

[127] J. Firestone and C. Jarvis, "Response and responsibility: Regulating noise pollution in the marine environment," *Journal of International Wildlife Law and Policy*, vol. 10, pp. 109–152, 4 2007.

[128] J. T. Zimmerman, "The tidal whirlpool: A review of horizontal dispersion by tidal and residual currents," *Netherlands Journal of Sea Research*, vol. 20, pp. 133–154, 8 1986.

[129] R. Ahmadian, R. Falconer, and B. Bockelmann-Evans, "Far-field modelling of the hydro-environmental impact of tidal stream turbines," *Renewable Energy*, vol. 38, pp. 107–116, 2 2012.

[130] A. E. Mccluskie, L. R. H. W. . Wilkinson, and N. I. Rspb, *Birds and wave & tidal stream energy: an ecological review.*

[131] R. E. S. Steven J. Phillips, Miroslav Dudík, "MaxEnt software for modeling species niches and distributions (Version 3.4.1)." `http://biodiversityinformatics.amnh.org/open_source/maxent/`, 2018.

[132] N. Ederer, "Evaluating capital and operating cost efficiency of offshore wind farms: A DEA approach," *Renewable and Sustainable Energy Reviews*, vol. 42, pp. 1034–1046, 2015.

[133] T. Schwedes, D. A. Ham, S. W. Funke, and M. D. Piggott, *Mesh Dependence in PDE-Constrained Optimisation*. Springer International Publishing, 2017.

[134] O. Arup, "Review of Renewable Electricity Generation Cost and Technical Assumptions," *Department of Energy and Climate Change*, 2016.

[135] ITPEnergised, "Dynamically Positioned Barge Set to Revolutionise Tidal Energy Installation."

[136] SI Ocean, "Ocean Energy: Cost of Energy and Cost Reduction Opportunities," 2013.

[137] F. Harcourt, A. Angeloudis, and M. D. Piggott, "Utilising the flexible generation potential of tidal range power plants to optimise economic value," *Applied Energy*, vol. 237, pp. 873–884, 3 2019.

[138] J. Green, A. Bowen, L. J. Fingersh, and Y. Wan, "Electrical Collection and Transmission Systems for Offshore Wind Power," *Offshore Technology Conference*, 2007.

[139] P. Heptonstall, R. Gross, P. Greenacre, and T. Cockerill, "The cost of offshore wind: Understanding the past and projecting the future," *Energy Policy*, vol. 41, pp. 815–821, 2 2012.

[140] H. Khatib, "Review of OECD study into "Projected costs of generating electricity-2010 Edition"," *Energy Policy*, vol. 38, pp. 5403–5408, 10 2010.

[141] Entec, "Cost estimation methodology," *The Carbon Trust*, 2006.

[142] G. Allan, M. Gilmartin, P. McGregor, and K. Swales, "Levelised costs of Wave and Tidal energy in the UK: Cost competitiveness and the importance of "banded" renewables obligation certificates," *Energy Policy*, vol. 39, pp. 23–39, 1 2011.

[143] IEA NEA, *Projected Costs of Generating Electricity 2015*. 2015.

[144] Department for Business Energy & Industrial Strategy, "Electricity generation costs," tech. rep., 2016.

[145] G. Dalton, G. Allan, N. Beaumont, A. Georgakaki, N. Hacking, T. Hooper, S. Kerr, A. Marie O'hagan, K. Reilly, P. Ricci, W. Sheng, and T. Stallard, "Economic and socio-economic assessment methods for ocean renewable energy: Public and private perspectives," *Renewable and Sustainable Energy Reviews*, vol. 45, no. 850-878, 2015.

[146] S. Klaus, "Financial and Economic Assessment of Tidal Stream Energy—A Case Study," *International Journal of Financial Studies*, vol. 8, p. 48, 8 2020.

[147] SIMEC Atlantis Energy, "MeyGen Phase 1A completes construction phase and officially enters 25 year operations phase."

[148] A. D. Mills, D. Millstein, R. Wiser, J. Seel, J. P. Carvallo, S. Jeong, and W. Gorman, "Impact of Wind, Solar, and Other Factors on Wholesale Power Prices An Historical Analysis-2008 through 2017," *Electricity Markets and Policy Group*, 2019.

[149] "UK Marine Energy 2019 - A new industry," tech. rep., Marine Energy Council, RenewableUK and Scottish Renewables, 2019.

[150] N. Conroy, J. P. Deane, and B. P. O Gallachoir, "Wind turbine availability: Should it be time or energy based? - A case study in Ireland," *Renewable Energy*, vol. 36, pp. 2967–2971, 11 2011.

[151] DNV GL, "Definitions of Availability Terms for the Wind Industry," tech. rep., 2017.

[152] MeyGen, "Lessons Learnt from MeyGen Phase 1a Part 1/3: Design Phase," 2017.

[153] S. Astariz and G. Iglesias, "The economics of wave energy: A review," *Renewable and Sustainable Energy Reviews*, 2015.

[154] P. Mycek, B. Gaurier, G. Germain, G. Pinon, and E. Rivoalen, "Experimental study of the turbulence intensity effects on marine current turbines behaviour. Part II: Two interacting turbines," *Renewable Energy*, vol. 68, pp. 876–892, 8 2014.

[155] P. Stansby and T. Stallard, "Fast optimisation of tidal stream turbine positions for power generation in small arrays with low blockage based on superposition of self-similar far-wake velocity deficit profiles," *Renewable Energy*, 2016.

[156] S. C. Kramer and M. D. Piggott, "A correction to the enhanced bottom drag parameterisation of tidal turbines," *Renewable Energy*, vol. 92, pp. 385–396, 2016.

[157] T. Kärnä, S. C. Kramer, L. Mitchell, D. A. Ham, M. D. Piggott, and A. M. Baptista, "Thetis coastal ocean model: discontinuous Galerkin discretization for the three-dimensional hydrostatic equations," *Geosci. Model Dev*, vol. 11, pp. 4359–4382, 2018.

[158] C. D. R. Donovan and C. Corbishley, "The cost of capital and how it affects climate change mitigation investment," *Grantham Institute*, no. 15, 2016.

[159] S. A. Morse, "The Green Investment Bank," *National Audit Office*, 2017.

[160] P. Higgins and A. M. Foley, "Review of offshore wind power development in the United Kingdom," in *2013 12th International Conference on Environment and Electrical Engineering*, pp. 589–593, IEEE, 5 2013.

[161] Nova Innovation, "Europe Case Study - Shetland Tidal Array," 2016.

[162] SIMEC Atlantis Energy, "SIMEC Atlantis Energy Unveils World's Largest Single Rotor Tidal Turbine, the AR2000," 2018.

[163] J. Thiébot, D. S. Coles, A.-C. Bennis, N. Guillou, S. Neill, S. Guillou, and M. Piggott, "Numerical modelling of hydrodynamics and tidal energy extraction in the Alderney Race: a review," *Philosophical Transactions of the Royal Society A: Mathematical, Physical and Engineering Sciences*, vol. 378, p. 20190498, 8 2020.

[164] F. Rathgeber, D. A. Ham, L. Mitchell, M. Lange, F. Luporini, A. T. T. Mcrae, G.-T. Bercea, G. R. Markall, P. H. J. Kelly, . D. A. Ham, and . P. H. J. Kelly, "Firedrake: Automating the finite element method by composing abstractions," *ACM Transactions on Mathematical Software*, vol. 43, no. 3, p. 24, 2016.

[165] D. S. Coles, L. S. Blunden, and A. S. Bahaj, "Experimental validation of the distributed drag method for simulating large marine current turbine arrays using porous fences," *International Journal of Marine Energy*, 2016.

[166] D. Coles, C. Greenwood, A. Vogler, T. Walsh, and D. Taaffe, "Assessment of the turbulent flow upstream of the Meygen Phase 1A tidal stream turbines," *AWTEC*, 2018.

[167] T. Blackmore, W. M. J. Batten, and A. S. Bahaj, "Influence of turbulence on the wake of a marine current turbine simulator," *Proc. R. Soc. A*, vol. 470, 2014.

[168] C. R. Vogel, R. H. Willden, and G. T. Houlsby, "Power available from a depth-averaged simulation of a tidal turbine array," *Renewable Energy*, vol. 114, pp. 513–524, 12 2017.

[169] A. J. Goward Brown, S. . Neill, and M. . Lewis, "Tidal energy extraction in three-dimensional ocean models," *Renewable Energy*, vol. 114, pp. 244–257, 2017.

[170] C. Legrand, "Assessment of Tidal Energy Resource," tech. rep., European Marine Energy Centre Ltd, 2009.

[171] C. A. Consul, R. H. Willden, and S. C. McIntosh, "Blockage effects on the hydrodynamic performance of a marine cross-flow turbine," *Philosophical Transactions of the Royal Society A: Mathematical, Physical and Engineering Sciences*, vol. 371, 2 2013.

[172] S. Raychaudhuri, "Introduction to monte carlo simulation," in *Proceedings - Winter Simulation Conference*, pp. 91–100, 2008.

[173] S. P. Neill, J. R. Jordan, and S. J. Couch, "Impact of tidal energy converter (TEC) arrays on the dynamics of headland sand banks," *Renewable Energy*, vol. 37, pp. 387–397, 1 2012.

[174] T. Kärnä, B. de Brye, O. Gourgue, J. Lambrechts, R. Comblen, V. Legat, and E. Deleersnijder, "A fully implicit wetting-drying method for DG-FEM shallow water models, with an application to the Scheldt Estuary," *Computer Methods in Applied Mechanics and Engineering*, vol. 200, pp. 509–524, 1 2011.

[175] C. V. Vouriot, A. Angeloudis, S. C. Kramer, and M. D. Piggott, "Fate of large-scale vortices in idealized tidal lagoons," *Environmental Fluid Mechanics*, vol. 19, pp. 329–348, 4 2019.

[176] W. Pan, S. C. Kramer, and M. D. Piggott, "Multi-layer non-hydrostatic free surface modelling using the discontinuous Galerkin method," *Ocean Modelling*, vol. 134, pp. 68–83, 2 2019.

[177] M. J. Lewis, S. P. Neill, M. R. Hashemi, and M. Reza, "Realistic wave conditions and their influence on quantifying the tidal stream energy resource," *Applied Energy*, vol. 136, pp. 495–508, 12 2014.

[178] M. R. Hashemi, S. P. Neill, P. E. Robins, A. G. Davies, and M. J. Lewis, "Effect of waves on the tidal energy resource at a planned tidal stream array," *Renewable Energy*, vol. 75, pp. 626–639, 3 2015.

[179] J. Thiébot, P. Bailly du Bois, and S. Guillou, "Numerical modeling of the effect of tidal stream turbines on the hydrodynamics and the sediment transport - Application to the Alderney Race (Raz Blanchard), France," *Renewable Energy*, vol. 75, pp. 356–365, 3 2015.

[180] R. H. Karsten, J. M. Mcmillan, M. J. Lickley, and R. D. Haynes, "Assessment of tidal current energy in the Minas Passage, Bay of Fundy," *Proc. IMechE*, vol. 222, pp. 493–507, 2008.

[181] P. Wessel and W. H. F. Smith, "A global, self-consistent, hierarchical, high-resolution shoreline database," *Journal of Geophysical Research: Solid Earth*, vol. 101, pp. 8741–8743, 4 1996.

[182] T. A. Adcock, S. Draper, G. T. Houlsby, A. G. Borthwick, and S. Serhadlioğlu, "The available power from tidal stream turbines in the pentland firth," *Proceedings of the Royal Society A: Mathematical, Physical and Engineering Sciences*, vol. 469, 9 2013.

[183] Marine Species Wiki, "Bed roughness and friction factors in estuaries," 2016.

[184] C. I. Willmott, "On the validation of models," *Center for Climatic Research*, 1981.

[185] J. Thiébot, N. Guillou, S. Guillou, A. Good, and M. Lewis, "Wake field study of tidal turbines under realistic flow conditions," *Renewable Energy*, 11 2020.

[186] N. Guillou, G. Chapalain, and S. P. Neill, "The influence of waves on the tidal kinetic energy resource at a tidal stream energy site," *Applied Energy*, vol. 180, pp. 402–415, 2016.

[187] A. Sentchev, T. D. Nguyen, L. Furgerot, and P. Bailly Du Bois, "Underway velocity measurements in the Alderney Race: Towards a three-dimensional representation of tidal motions: Underway velocity measurements," *Philosophical Transactions of the Royal Society A: Mathematical, Physical and Engineering Sciences*, vol. 378, 8 2020.

[188] "Bathymetric DTM Atlantic facade (Homonim Project)," tech. rep., SHOM, 2015.

[189] "International levelised cost of energy for ocean energy technologies," tech. rep., IEA Technology Collaboration Programme for Ocean Energy Systems (OES), 2015.

[190] G. Smart and M. Noonan, "Tidal stream and wave energy cost reduction and industrial benefit, Summary Analysis," tech. rep., Catapult Offshore Renewable Energy, 2018.

[191] D. Coles, S. C. Kramer, M. D. Piggott, A. Avdis, and A. Angeloudis, "Optimisation of tidal stream turbine arrays within Alderney Race," *European Wave and Tidal Energy Conference*, 2018.

[192] International Renewable Energy Agency, "Tidal Energy Technology Brief," tech. rep., 2014.

[193] Department of Energy & Climate Change, "Contracts for Difference (CFD) Allocation Round One Outcome," tech. rep., 2015.

[194] N. Kaufmann, T. Carolus, and R. Starzmann, "Turbines for modular tidal current energy converters," *Renewable Energy*, vol. 142, pp. 451–460, 11 2019.

[195] L. Mackie, S. C. Kramer, M. D. Piggott, and A. Angeloudis, "Assessing impacts of tidal power lagoons of a consistent design," *In preparation*, 2021.

[196] S. Gant and T. Stallard, "Modelling a Tidal Turbine in Unsteady Flow," *Proceedings of the Eighteenth (2008) International Offshore and Polar Engineering Conference: Proceedings of the Eighteenth (2008) International Offshore and Polar Engineering Conference; 2008. p. 473-479.*, pp. 473–479, 1 2008.

[197] R. Shakoor, M. Y. Hassan, A. Raheem, and Y. K. Wu, "Wake effect modeling: A review of wind farm layout optimization using Jensen's model," *Renewable and Sustainable Energy Reviews*, vol. 58, pp. 1048–1059, 5 2016.

[198] L. Mackie, F. Harcourt, A. Angeloudis, and M. D. Piggott, "Income optimisation of a fleet of tidal lagoons," *13th European Wave and Tidal Energy Conference*, 2019.